Composition-structure-property relation of oxide glasses

insight from an extended topological approach

Hermansen, Christian

DOI (link to publication from Publisher):
10.5278/vbn.phd.engsci.00014

Publication date:
2014

Document Version
Publisher's PDF, also known as Version of record

COMPOSITION-STRUCTURE-PROPERTY RELATION OF OXIDE GLASSES: INSIGHT FROM AN EXTENDED TOPOLOGICAL APPROACH

BY
CHRISTIAN HERMANSEN

DISSERTATION SUBMITTED 2014

AALBORG UNIVERSITY
DENMARK

Ph.D. Dissertation

Composition-structure-property relation of oxide glasses: insight from an extended topological approach

by

Christian Hermansen

Department of Chemistry
and Bioscience
Aalborg University, Denmark

AALBORG UNIVERSITY
DENMARK

Date of Defense:
February 6th, 2015

Assessment Committee

Vittorio Boffa
Associate Professor
Aalborg University, Denmark

Steve Warthen Martin
Professor
Iowa State University, USA

Matthieu Micoulaut
Professor
Université Pierre et Marie Curie, France

Supervisor

Yuanzheng Yue
Professor
Aalborg University, Denmark

Thesis submitted: December, 2014

PhD supervisor: Professor, Yuanzheng Yue
Aalborg University, Denmark

PhD committee: Associate Professor, Vittorio Boffa
Aalborg University, Denmark

Professor, Steve Warthen Martin
Iowa State University, USA

Professor, Matthieu Micoulaut
Université Pierre et Marie Curie, France

PhD Series: Faculty of Engineering and Science, Aalborg University

ISSN: 2246-1248
ISBN: 978-87-7112-205-3

Published by:
Aalborg University Press
Skjernvej 4A, 2nd floor
DK – 9220 Aalborg Ø
Phone: +45 99407140
aauf@forlag.aau.dk
forlag.aau.dk

Printed in Denmark by Rosendahls, 2015

Preface and acknowledgements

This thesis has been submitted for assessment in partial fulfillment of the Ph.D. degree. The thesis is based on the submitted or published scientific papers which are listed in Section 0. Parts of the papers are used directly or indirectly in the extended summary of the thesis. As part of the assessment, co-author statements have been made available to the assessment committee and are also available at the Faculty. The thesis is not in its present form acceptable for open publication but only in limited and closed circulation as copyright may not be ensured.

I would like to thank my supervisor, Yuanzheng Yue, for his enthusiasm and encouragement throughout the project. He encouraged me to work independently, while sharing his great insight into glass science and suggesting new perspectives. My thanks also go to thank Morten M. Smedskjaer from Aalborg University, and John C. Mauro from Corning Inc., who always had time to discuss the theory and application of constraint theory. It has been a joy and an inspiration to work with you all.

My kind acknowledgements go to Randall E. Youngman from Corning Inc. for measuring and analyzing the NMR spectra in this thesis. Thanks also to John Wang from the National University of Singapore for kindly letting me join his lab for four months, and thank you to Henche Kuan for his kind assistance in helping with the XPS measurements. A special thanks goes to Morten M. Smedskjaer for sponsoring the stay.

My colleagues at Aalborg University, especially members of the glass group, have provided an ambitious, supportive, and fun working environment. Jonas H. Kjeldsen, Rasmus R. Petersen, and Thuy T. Do have been colleagues for 8 years, and will continue to be friends for much longer.

Finally, very special thanks go to my wife Baoyun Wang. She patiently endured a long-distance relationship, while continuously providing support, encouragement, and even proof-reading. This thesis is dedicated to her.

Abstract

Accurate prediction of material properties from composition has long been the “holy grail” of the material science community. Such prediction has hitherto been impossible for glasses owing to their complicated non-crystalline structure and non-equilibrium nature. The properties of glasses are determined from their composition (constituent elements) and structure (spatial arrangement of atoms). The goal of this thesis is to quantify the relation between composition, structure, and properties of oxide glasses.

The structure of glasses can be described on different length scales: the short-range order corresponds to the first coordination shell and defines a coordination polyhedron; the topology is the way the polyhedra are linked together; and the intermediate range order is ordering in the second and third coordination shells. Structural models that describe all three length scales are developed in order to understand the structure-property relation.

The rheological properties are very important in glass production, as they determine the temperatures at which melting, forming, and annealing must be performed. Two parameters can in general describe the rheological properties of oxide glasses: the glass transition temperature and the liquid fragility. These two material properties can be related to the structure by temperature dependent constraint theory, which has proven a powerful method of understanding glass formation and dynamics.

Constraints are chemical bonds and bond angles around the atoms in the glassy network. The total number of possible constraints is determined from the type and number of coordination polyhedra in the glass, but their strengths depend on the type of elements and topology. The glass transition temperature is related to the number of intact constraints at this temperature, and the liquid fragility is related to how fast the number of intact constraints changes with temperature. In this thesis an extended constraint model is developed, which successfully explains the effect of the type and concentration of network modifiers and the mixed network former effect. Perspectives and challenges in using temperature dependent constraint theory for property prediction are presented in this thesis.

The number of constraints at room temperature is found to relate to the hardness of oxide glasses. Hardness is a measure of the ability of a material to resist surface damage, such as scratching, and has become an important material property with the advent of touchscreen devices. The quantitatively best theoretical model of hardness is the Yamane & Mackenzie model, which relates hardness to macroscopic material properties such as the elastic constraints. It is found that the theoretical derivation of the Yamane & Mackenzie model is inconsistent with experimental data for the permanent deformation occurring in glass subjected to surface damage, and the model therefore is empirical.

Resume (Danish abstract)

Den “hellige gral” for materiale videnskab har længe været evnen til at præcist kunne forudsigelse materiale egenskaber fra komposition alene. Desværre har sådan en forudsigelse indtil nu været umulig for glas, idet glas har en kompliceret ikke-krystallinsk struktur og ikke er i kemisk ligevægt. Egenskaberne af glas skyldes komposition (kemiske elementer) samt struktur (rumligt arrangement af atomer). Målet med denne afhandling er at kvantificere sammenhængen imellem komposition, struktur og egenskaberne af oxidglas.

Strukturen af glas kan beskrives på forskellige længde-skalaer: den første koordinations-skal af et atom definerer et koordinations-polyeder; netværkstopologien er måden at polyedre er sat sammen på; og mikrostrukturen er hvordan anden og tredje koordinations-skal er ordnet på. Der er blevet udviklet strukturmodeller der beskriver strukturen af glas på alle tre længde-skalaer for at kunne forstå sammenhængen imellem struktur og egenskaber.

Reologiske egenskaber er vigtige i produktionen af glas, idet de bestemmer temperaturerne hvor smeltning, formgivning og afstresning skal udføres. To parameter er normalt nok til at beskrive de reologiske egenskaber af oxidglas: glas overgangs temperaturen og skrøbeligheden. Disse to materiale egenskaber kan kædes til strukturen af glas igennem teorien of temperatur-afhængige bindingsbegrænsninger, som kan bruges til at forstå glas formation og dynamik.

Bindingsbegrænsninger er kemiske bindinger og bindingsvinkler omkring atomerne i glas netværket. Det totale antal mulige bindingsbegrænsninger kan bestemmes ud fra typen og antallet af koordinations-polyedre, men deres styrke afhænger typen af grundstoffer og netværkstopologien. Glas overgangs temperaturen afhænger af antallet af intakte bindingsbegrænsninger ved denne temperatur, og skrøbeligheden er et mål for hvor hurtigt disse bindingsbegrænsninger ændrer sig med temperatur. En udvidet bindingsbegrænsnings-model udvikles i denne afhandling, som kan forklare effekten af typen og koncentrationen af netværksmodifikatorer samt netværksdannere. Perspektiver og udfordringer for anvendelsen af teorien of temperatur-afhængige bindingsbegrænsninger for forudsigelse af materiale egenskaber præsenteres.

Vi har fundet ud af at antallet af netværksbegrænsninger ved stuetemperatur også bestemmer hårdheden af oxidglas. Hårdhed er et mål for modstandsdygtigheden af et materiale overfor kontaktskade, såsom ridser, og er blevet en vigtig materialeegenskab for glas til smartphones. Den kvantitativt bedste teoretiske model af kompositions-afhængigheden af hårdhed er Yamane & Mackenzie modellen, som relaterer hårdhed til makroskopiske materiale egenskaber som de elastiske moduli. Vi har påvist at den teoretiske udledning af modellen ikke er konsistent med eksperimentelt data for den permanente deformation i glas under kontaktskade, og kan derfor konkludere at modellen er empirisk.

Table of contents

1 Introduction

Glass is an important material in modern society, it is not only an irreplaceable part of such traditional products as windows, windshields and light bulbs, but it is also essential for hi-tech applications in biomaterials, liquid crystal displays, touch screen devices and optical fibers for telecommunication. Glass is ideally suited for these applications because it possesses a unique combination of optical transparency with ease of forming and good mechanical properties.

The mechanical properties of glass have two aspects; the elastic properties and fracture mechanics. Ideally glass is a purely elastic solid, which means that all deformation is reversible, and there is a linear relationship between stress and strain. Linear elasticity predicts that failure first occurs when the stress exceeds the strength of the chemical bonds in the glass [1]. However, failure often occurs at a much lower stress, which can be explained by fracture mechanics [2]. Fracture mechanics consider the stress to be intensified by flaws in the glass. This effect causes the local stress to exceed the theoretical strength at the tip of a flaw at a relatively low average stress, and is known as crack propagation. The ease of crack propagation in glass is the cause of catastrophic brittle fracture occurring on sharp impact. Many commercial glasses suppress the tendency for brittle fracture by undergoing treatment such as thermal strengthening of windshields, chemical strengthening for display glasses, and cladding of optical fibers that prevent crack formation or propagation. The advent of touchscreen devices has also caused hardness to be an important mechanical property of glass. Hardness is a measure of the ability of a material to resistant to surface damage, such as scratching. Scratches compromise the transparency of touchscreens and also lower the strength of the device by promoting brittle fracture.

All the commercial glass products listed above are oxide glasses, meaning that they are made from metal oxides. Traditionally three metal oxides are renowned for glass formation in their native state, namely silica (SiO_2), boron oxide (B_2O_3) and to a lesser extent phosphorous pentoxide (P_2O_5). These three metal oxides are referred to as network formers, due to their ability to form a glassy network. Silica is commercially the most important network former, for example window glass consists of approximately 73 wt% SiO_2, 14 wt% Na_2O (soda) and 9 wt% CaO (lime) and some other minor components [3]. Soda and lime are prototypical network modifiers, which disrupt the network created by the network formers. In general, network modifiers are added to SiO_2 in order to reduce the melting temperature to a practical range, and to improve chemical and physical properties.

Glass is commonly produced by quenching a melt of the raw materials. The melt is degassed and homogenized during melting. This homogeneous melt is cooled to the

1 Introduction

working point and formed into the desired shape, and then cooled further to the annealing point where internal stress caused by thermal shrinkage is relieved. The melting, working and annealing points all correspond to specific viscosities of the glass melt, and to produce a glass the viscosity-temperature relationship must therefore be known. The viscosity-temperature relationship can in general be modeled by two parameters, the glass transition temperature and the liquid fragility [4].

The glass transition temperature is the temperature which demarcates the glassy solid and liquid states of matter. The liquid to glass transition appears to be a second order phase transition with discontinuous changes in the second derivatives of the free energy in respect to its natural variables. These second order derivatives are for example the coefficient of thermal expansion and the constant volume or constant pressure heat capacity. However, observing these properties has never revealed a true thermodynamic second order phase transition from liquid to glass. Twenty years ago Nobel laureate Philip W. Anderson wrote that "t*he deepest and most interesting unsolved problem in solid state theory is probably the theory of the nature of glass and the glass transition*." [5]. The current understanding is that the glass is a non-equilibrium solid with broken ergodicity [6], and equilibrium thermodynamics cannot be applied [7].

The glass transition is a kinetic phenomenon. The liquid becomes a glass when the average relaxation time of the liquid becomes higher than the time-scale of observation. For this reason, glass has almost the same structure as the liquid it is derived from [8]. However, the first researchers tried to understand glass structure in the framework of crystal structure [3]. Zachariasen began his seminal paper with "*It must be frankly admitted that we know practically nothing about the atomic arrangement in glasses*", but what followed was a brilliantly insightful into the structural and topological rules for glass formation in oxides [9]. For example, Zachariasen discounted glass formation in metal oxides where the metal-oxygen coordination number is higher than four, which explains why B_2O_3 is a glass former *par excellence*, but Al_2O_3 is not a native glass former.

Structural characterization techniques have greatly improved since Zachariasen's time, and today the short-range order and topology of many binary glass forming systems are well characterized [10]. The short-range order is the structure of the metal-oxygen coordination polyhedra, and topology is how these polyhedra are linked to each other. Similar structural information of the network modifiers in the glass can also be obtained, which led Greaves to propose that modifiers are not always homogeneously distributed, but can cluster in chains or layers as they do in some crystal structures [10].

1 Introduction

A theory that accurately links the composition to the properties has long been the “holy grail” of the materials science community [11]. An important link between composition and properties is the structure and topology, as evidenced by some minerals having very different properties from glasses of the same composition [12]. However, despite having developed an understanding and experimental database of the structure and topology of many glass-forming systems [10], there is no consensus on how the structure is quantitatively related to the properties of the glass.

1.1 Background and challenges

A promising general theory of providing a structural basis for glass formation and certain glass properties is the topological constraint theory. Topological constraint theory is derived from Maxwell’s considerations on the rigidity of mechanical trusses [13]. Topological constraint theory was originally applied to chalcogenide glasses by Phillips, who considered glasses as an atomic-scale mechanical trusses [14]. Phillips argued that the glass forming ability should be maximized for compositions that are isostatic, meaning that the number of constraints on the movement of the atoms is equal to the available degrees of freedom per atom (equal to 3 in three dimensions):

$$N_c = N_f = 3 \tag{1.1}$$

The constraints are the chemical bonds and bond angles around the atoms in the glassy network. These are denoted as linear bond stretching constraints and angular bond bending constraints, and their number for a given atom *i* depend on the coordination number (CN) as:

$$n_{c,i,linear} = \frac{1}{2}\mathrm{CN}_i\Big|_{\mathrm{CN}_i \geq 2} \tag{1.2}$$

$$n_{c,i,angular} = \left(2\mathrm{CN}_i - 3\right)\Big|_{\mathrm{CN}_i \geq 2} \tag{1.3}$$

For a system with *N* types of atoms, the total number of constraints per atom (N_c) can be calculated as:

$$N_c = \sum_{i=1}^{N_{atoms}} \left(n_{c,i,linear} + n_{c,i,angular}\right) \Big/ N_{atoms} \tag{1.4}$$

By combining Eq. (1.4) with Eq. (1.1) then the isostatic condition is found to occur at an average coordination number CN = 2.4. This condition describes the exceptional glass

formation of $GeSe_4$ and As_2Se_3 compositions [14]. The applicability of Eq. (1.2) and (1.3) to chalcogenide glasses has recently been confirmed by molecular dynamics simulation [15].

Boolchand and co-workers have argued that a range of compositions should be isostatic, because the glass will self-organize to a degree in order to prevent the percolation of stress [16]–[19]. This compositional range is known as the intermediate phase. The primary experimental evidence for the intermediate phase is a minimum in non-reversing heat flow by temperature modulated differential scanning calorimetry (TM-DSC). The intermediate phase is also found to have very low fragility in chalcogenide glasses [20]–[22]. However the existence of the intermediate phase is still under debate [23]–[25].

An intermediate phase has also been observed for modified silicate glasses [26], [27], but describing the intermediate phase in silicate using topological constraint theory is not so straightforward. For example, the prototypical glass-former SiO_2 has $N_c = 3.67$ by Eq. (1.2) and (1.3), and should be stressed rigid, but a good glass-former is expected to have $N_c \approx 3$. The reason for the discrepancy between model and experiment is that bond bending constraints around oxygen are ineffective at the glass transition temperature [15]. When a modifying oxide is added to SiO_2 the glass transition temperature decreases, and the bond bending constraints around oxygen become intact again [28]. The intermediate phase is generally accounted for by assuming that oxygen bond bending constraints are intact for modified silicates, and considering modifying cations to have CN equal to their valence. These assumptions have also been used to predict the composition of window glass in the soda lime silica ternary system [29]. Despite that, a recent molecular dynamics simulation study for this system shows that the constraints on the modifying cations cannot be accounted for just by their valence, instead the number of constraints per modifying cation is somewhere between the valence and the actual coordination number [30].

Temperature dependent constraint theory is a theoretical framework that considers the effect of temperature on the intactness of the constraints [31], [32]. Each constraint is associated with an activation energy for breaking it, which corresponds to a particular onset temperature where a significant fraction of the constraints are broken. This is a measure of the strength of the chemical bonds and bond angles in the glass. By accounting for the chemistry in this manner, it has been possible to describe glass properties such as the glass transition temperature, fragility and hardness in the framework of topological constraint theory [31]–[34].

1.2 Objectives

The overall objective of this Ph.D. thesis is to study the universality of topological constraint theory and its ability to predict important glass properties such as glass transition temperature, fragility and hardness.

The major issue with applying constraint theory to oxide glasses is how to account for the topological role of modifying oxides, which cannot be described by Eq. (1.2) and (1.3) because of the ionic nature of their bonding. This problem is dealt with by studying binary phosphate glasses. Glasses easily form from binary phosphates with high modifier contents and their properties are strongly affected by the concentration and species of modifying oxide.

The universality of the results is tested by introducing other kinds of network forming oxides (B_2O_3 and SiO_2) into the phosphate glasses. The structures of these mixed-network former glasses are characterized and modeled, and their structure-property relations explained by topological constraint theory.

The complicated features of indentation hardness in silicate glasses are studied in order to clarify the factors that determine these features and the cause of a relation to the network constraints. The crack formation is studied for similar reasons.

The specific objectives of the Ph.D. thesis are summarized as follows:

1. Account for the effect of the concentration of network modifiers on the properties of oxide glasses.
2. Account for how properties of oxide glasses depend on the species of network modifier, such as alkali and alkaline earth oxides.
3. Model the structure and topology of mixed network former glasses and describe the structure-property relations in such glasses.
4. Clarify what determines the hardness of a glass, and relate this property to glass composition.
5. Characterize the degree ease of crack formation in silicate glasses, and relate this to other glass properties.

1.3 Thesis content

This thesis is presented as an introduction to glass structure, properties, and their relation in oxide glasses, followed by an overview of the journal papers (in which I act as the first author). These papers constitute the main body of the thesis, and are appended after the bibliography. The papers will be referred to by their roman numerals:

I. C. Hermansen, J. Matsuoka, S. Yoshida, H. Yamazaki, Y. Kato and Y.-Z. Yue, "Densification and plastic deformation under microindentation in silicate glasses and the relation to hardness and crack resistance," *Journal of Non-Crystalline Solids* **364**, 40-43 (2013). DOI: 10.1016/j.jnoncrysol.2012.12.047

II. C. Hermansen, J.C. Mauro and Y.-Z. Yue, "A model for phosphate glass topology considering the modifying ion sub-network," *Journal of Chemical Physics* **140**, 154501 (2014). DOI: 10.1063/1.4870764

III. C. Hermansen, J.C. Mauro and Y.-Z. Yue, "Response to comment on "A model for phosphate glass topology considering the modifying ion sub-network" [J. Chem. Phys. 140, 154501 (2014)]," *Journal of Chemical Physics* (2014) (under review)

IV. C. Hermansen, B.P. Rodrigues, L. Wondraczek and Y.-Z. Yue, "An extended topological model for binary phosphate glasses," *Journal of Chemical Physics* (2014) (in press).

V. C. Hermansen, R.E. Youngman, J. Wang and Y.-Z. Yue, "Structural and topological aspects of borophosphate glasses and their relation to physical properties," *Journal of Chemical Physics* (2014) (under review)

VI. C. Hermansen, X. Guo, R.E. Youngman, J.C. Mauro, M.M. Smedskjaer and Y.-Z. Yue, "Structure-Topology-Property correlations of phosphosilicate glasses," *Journal of Chemical Physics* (2015) (under review)

2 Glass structure: Theory and models

There are many structural characterization methods available for studying glass structure at varying length scales. The short-range order (SRO) of network formers can be probed by nuclear magnetic resonance (NMR), infrared and Raman spectroscopy [10], [35], [36]. These methods can in some cases also give information about the next-nearest neighbors or topology of the glass. Of these methods, magic angle spinning MAS-NMR stands out as the preeminent method for characterizing SRO of network formers because of its resolution and easily interpreted spectra.

The SRO of network formers is characterized by the network forming cation in well-defined coordination polyhedra with its anions, usually with a coordination number (CN) equal to 3 or 4, or in special cases up to 5 and 6 [37], [38]. The coordination polyhedron is denoted as a network forming unit (NFU), and is considered the rigid backbone of a glass [14], [39].

In oxide glasses, the oxygen in the NFU may bridge to another NFU, or be terminated by a network modifier. The first case is denoted as bridging oxygen (BO), and the second case as non-bridging oxygen (NBO). Traditionally, NFU species are denoted as Q^n species, where superscript n denotes the number of BO in the NFU. In this thesis NFUs will be denoted by the network forming cation and the number of BO. For example, the four-coordinated silicon with four BO in SiO_2 is denoted as a Si^4 NFU, not to be confused with the Si^{4+} cation.

The topology (*i.e.* NFU bonding) in oxide glasses can be probed by two-dimensional NMR techniques such as double-quantum (DQ), radio frequency dipolar recoupling (RFDR) and rotational echo double resonance (REDOR) [35], [40]. Another method is to measure O 1s electron binding energy by using X-ray photoelectron spectroscopy (XPS), as the binding energy is sensitive to the electronegativity of the nearest neighbors. This implies that XPS cannot distinguish the n of the neighboring Q^n NFUs, only the network former element [40].

The intermediate range order (IRO) is on a length-scale starting from the third coordination shell up to roughly 10 Å. The characterization of the IRO is in general more difficult than SRO, and is often accomplished by simulating X-ray and neutron diffraction data by Monte Carlo or molecular dynamics and analyzing the computed structure [41]. The IRO is often quantified by ring statistics [41]. Rings of NFU units occur in crystals and glasses. There is often a single ring size in crystals, such as 6 for ambient pressure forms of SiO_2, but a distribution for glasses [41], [42]. Borate crystals and glasses have very well-defined IRO based on three NFU membered rings [43]. For example glassy B_2O_3 has

approximately 75% of the boron atoms occurring in boroxol rings, which is a planar ring consisting of three B^3 NFUs [43].

The SRO and IRO of the network modifiers in oxide glasses are very difficult to determine. The primary methods are X-ray absorption spectroscopy and X-ray and neutron diffraction, but some information can also be gained from NMR [44], [45]. The SRO of the network modifiers are primarily characterized by an average coordination number, though the coordination environment is not as well-defined as for the network formers. The IRO is often characterized by the modifier-modifier pair distribution function derived from diffraction data [10]. According to the modified random network theory proposed by Greaves the IRO of the modifiers is characterized by the formation of modifier-rich channels or sheets in the glass [46].

In the following subsections the SRO and topology of phosphate-based glasses are characterized. Structural models that can account for the experimentally determined structure and topology are developed. The structural models are topological models, meaning that they are based on topological rules for which NFUs can bond together, and which cannot. They are idealized models that do not directly take into account physical and chemical properties.

2.1 Modified phosphate glasses

The SRO in P_2O_5 glass consists of P tetrahedra with three BO and one double-bonded terminal oxygen (TO). The neutron scattering factor shows IRO at length scales of 3.0Å and 4.8Å [35]. This IRO is similar to the intermolecular distance in the H-P_2O_5 crystal form, consisting of discrete P_4O_{10} molecules [47]. On the other hand, the IRO in P_2O_5 glass has also been argued to be due to voids and sheets lined with TO, similar to the polymeric O'-P_2O_5 crystal form [35].

When P_2O_5 is alloyed with a modifying oxide the P^3 NFUs are progressively depolymerized to P^2, P^1 and finally P^0 NFUs [35]. This occurs because the modifying cation requires charge-balancing by anions, and therefore forces the BO to convert to negatively charged NBO. When a P^3 NFU is converted to P^2, the TO shares the negative charge on the NBO due to π-bonding resonance [48]. This means that the TO and NBO are equivalent in the P^2, P^1 and P^0 NFUs. The SRO of each NFU in phosphate glasses is shown in Figure 2.1.

2 Glass structure: Theory and models

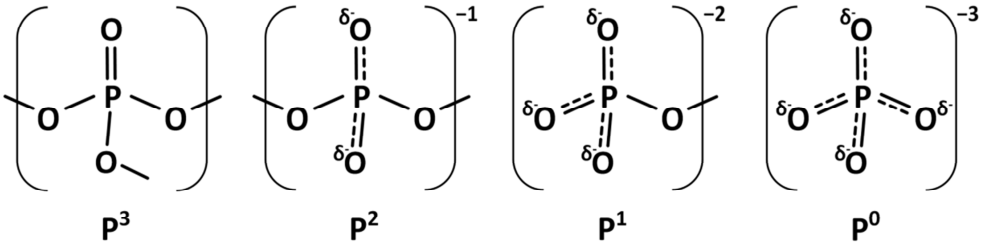

Figure 2.1: The possible structural units in modified phosphate glasses.

The concentration of NFUs in modified phosphate glasses are reasonably accounted for by the chemical depolymerization model suggested by Van Wazer [35], [49]. The model assumes that the phosphate network is sequentially depolymerized in order to charge-balance the modifying oxide, and that a maximum two NFU species can exist at any given composition.

The composition of a modified phosphate glass can be generally given as $x\mathrm{R}_{2/v}\mathrm{O}$ $(1-x)\mathrm{P}_2\mathrm{O}_5$, where $\mathrm{R}_{2/v}\mathrm{O}$ is a generic network modifying oxide with a cation of valence v. The mathematical expression for the concentration of each NFU of modified phosphate glasses are given in Eqs. (2.1)-(2.4). The square brackets indicate that the concentration of each NFU is given by a per total NFU basis (*i.e.* per mole of $\mathrm{P}_2\mathrm{O}_5$).

$$\left[\mathrm{P}^3\right]=\begin{cases}1-\dfrac{x}{1-x}, 0\le x<\dfrac{1}{2}\\ 0, \dfrac{1}{2}\le x<\dfrac{3}{4}\end{cases} \tag{2.1}$$

$$\left[\mathrm{P}^2\right]=\begin{cases}\dfrac{x}{1-x}, 0\le x<\dfrac{1}{2}\\ \dfrac{2-3x}{1-x}, \dfrac{1}{2}\le x<\dfrac{2}{3}\\ 0, \dfrac{2}{3}\le x\le\dfrac{3}{4}\end{cases} \tag{2.2}$$

$$\left[P^1\right] = \begin{cases} 0, 0 \le x < \frac{1}{2} \\ \frac{2x-1}{1-x}, \frac{1}{2} \le x < \frac{2}{3} \\ \frac{3-4x}{1-x}, \frac{2}{3} \le x \le \frac{3}{4} \end{cases} \tag{2.3}$$

$$\left[P^0\right] = \begin{cases} 0, 0 \le x < \frac{2}{3} \\ \frac{3x-2}{1-x}, \frac{2}{3} \le x \le \frac{3}{4} \end{cases} \tag{2.4}$$

The model by Van Wazer in Eq. (2.1) to (2.4) is compared to NFU fractions in anhydrous sodium ultraphosphate ($x \le 0.5$) glasses determined by ^{31}P MAS-NMR spectroscopy in Figure 2.2.

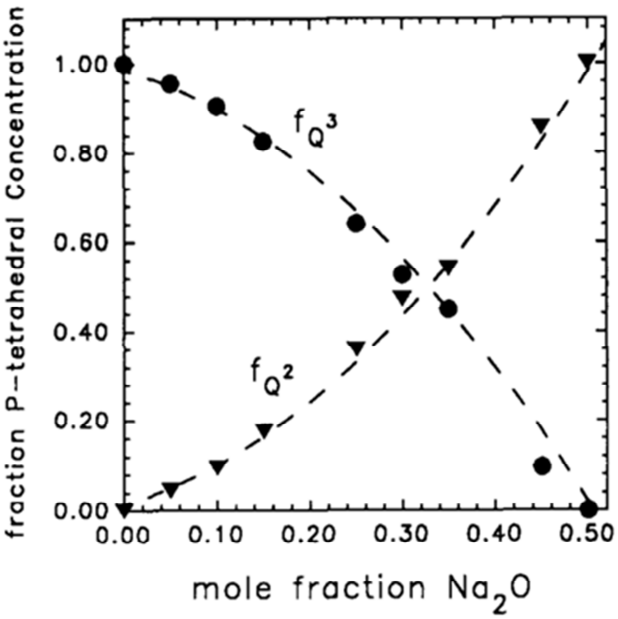

Figure 2.2: The concentration of P^3 and P^2 in anhydrous $x$$Na_2O$ (1-x)P_2O_5 glasses as determined by ^{31}P NMR-MAS spectroscopy (points) and Van Wazer's model (lines) from Eq. (2.1) and (2.2). Figure from [50].

2 Glass structure: Theory and models

The topology of alkali phosphate glasses is best described by a random distribution of linkages between the different NFUs, and there is no preference for bonding together of either similar or dissimilar NFUs [35].

The bonding character of modified phosphate glasses can be investigated by Raman spectroscopy. Raman spectra of anhydrous xNa$_2$O (1-x)P$_2$O$_5$ glasses are shown in Figure 2.3.

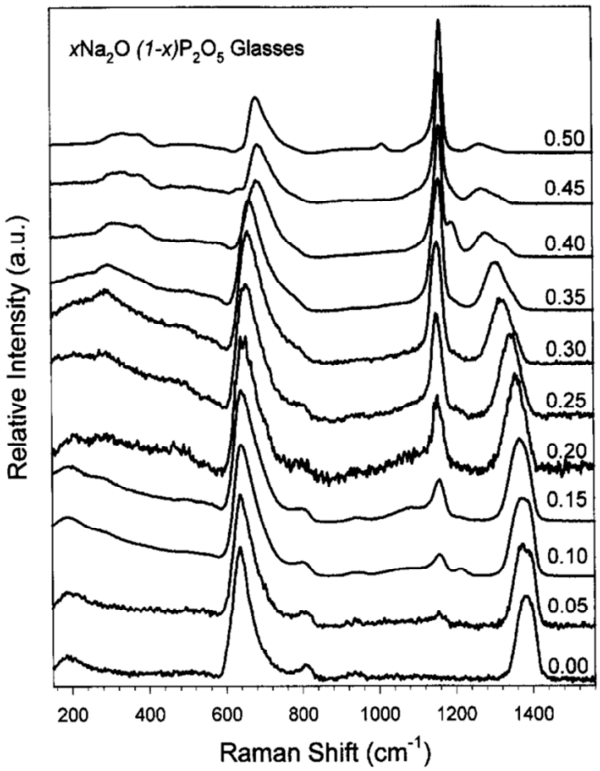

Figure 2.3: Raman spectra of anhydrous xNa$_2$O (1-x)P$_2$O$_5$ glasses. Figure adopted from [48].

The major peaks for the pure network former P_2O_5 glass are located at approximately 640 cm^{-1} and 1390 cm^{-1}. The 640cm^{-1} peak is assigned to the symmetrical stretching of P-O-P, that is a BO with two P NFU nearest neighbors [48]. The frequency of this vibration increases to about 690cm^{-1} in the metaphosphate (x = 0.5) composition.

The 1390 cm^{-1} peak is assigned to the symmetrical stretching of PO_2 in a P^3 NFU, and near the metaphosphate composition shifts to 1280 cm^{-1}, and is indistinguishable from the

asymmetric stretching vibration of PO_2^- in a P^2 NFU. This indicates a lengthening of the TO bond length with network modifier concentration [48]. The change in Raman shift with composition is larger for compositions with $x > 0.2$, and is thought to be caused by changes in the location of the network modifiers in the network [35].

Hoppe has developed a structural model of the SRO and IRO of network modifiers in modified phosphate glasses [51]. The model is based on the coordination number (CN) of alkaline earth cations in phosphate glasses decreasing with the content of network modifier. The CN decreases until a critical concentration and then becomes constant. This critical concentration occurs at the composition where the number of TO and NBO per modifying cation equals the lowest CN. For a generic network modifier with valence v in a modified phosphate glass of composition $x R_{2/v}O\ (1-x)P_2O_5$ the critical concentration x_{crit} can be determined as:

$$x_{crit} = \frac{v}{\mathrm{CN}} \tag{2.5}$$

For sodium phosphates, v is 1 and CN is approximately 5, and $x_{crit} = 0.2$ as seen in Paper I. This composition corresponds to the onset of more rapid change in the Raman shift of the asymmetric stretching vibration of PO_2^- in a P^2 NFU as discussed previously. When $x < x_{crit}$, the TO and NBO available for coordination is high and the network modifiers are expected to occur in isolated coordination environments with a significant number of TO in their coordination shell. But for compositions where $x > x_{crit}$, there are not enough NBO and TO available to coordinate each R^{v+}, and the modifier coordination polyhedra must share corners, edges or faces in order to satisfy their individual coordination requirements.

In Paper I, a specific SRO and topology of the alkali coordination polyhedra is suggested, where the modifiers occur in isolated sites below x_{crit}, and cross-linking sites above x_{crit}. This structural motif is denoted the ‘modifying ion sub-network’, and is illustrated in Figure 2.4. The modifying ion sub-network is useful for describing the glass formation and properties of modified phosphate glasses.

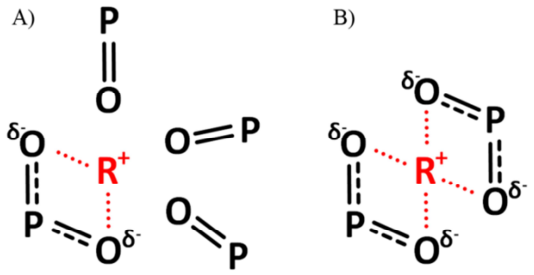

Figure 2.4: The SRO of a) the isolated modifier polyhedra occurring at $x < x_{crit}$ and b) cross-linking modifier polyhedra occurring for $x > x_{crit}$.

2.2 Borophosphate glasses

2.2.1 Network forming units

The composition of borophosphate glasses can be written in a generalized manner as $xR_{2/v}O$ $(1\text{-}x)[yB_2O_3$ $(1\text{-}y)P_2O_5]$, where $R_{2/v}O$ is a network modifying oxide with cation valence v, x is the molar fractional content of network modifying oxide, and y is the network former concentration of boron oxide. The SRO of borophosphate glasses can be seen as connections of the borate and phosphate NFUs shown in Figure 2.5.

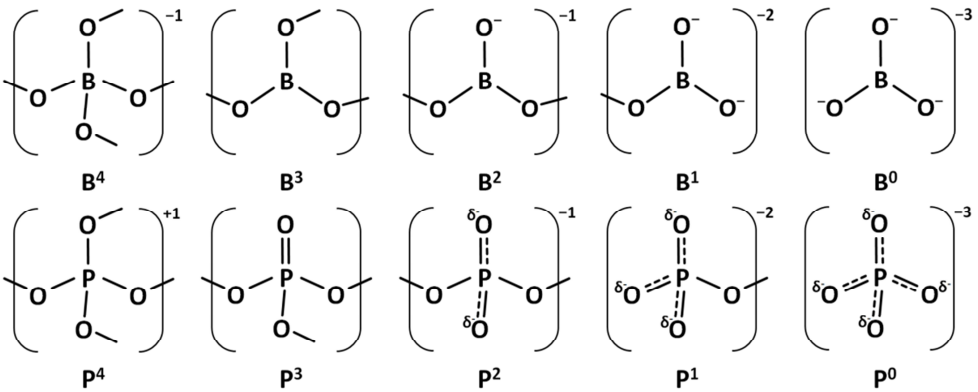

Figure 2.5: The network forming units (NFUs) that can occur in borophosphate glasses. B^4 and all the P NFUs are tetrahedra, while B^3, B^2, B^1 and B^0 are all planar triangles.

2.2.2 The maximum fraction of $[B^4] = y^*$

In borophosphate glasses, boron generally prefers to assume four-fold tetrahedral coordination (B^4). The usual scenario is that for a given x, B_2O_3 will initially occur fully as B^4, while above some critical value of $y = y^*$, the fraction of B^4 per network former remains approximately constant and equal to y^*, as seen in Figure 2.6. The critical value y^* and its

dependence on x will be derived based on a structural understanding of borophosphate glass compositions.

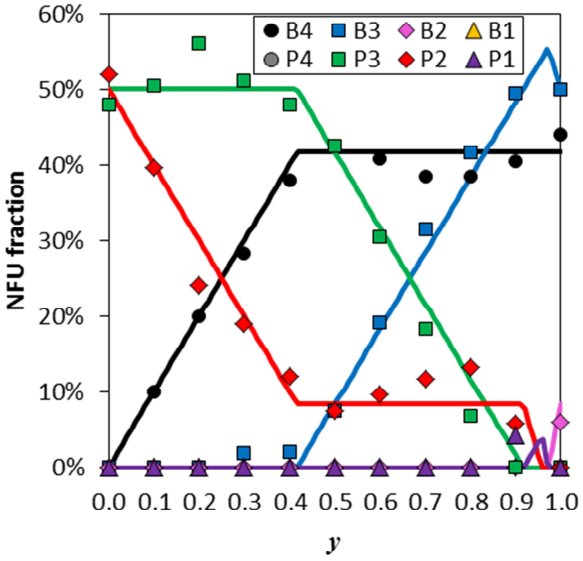

Figure 2.6: The fraction of the different network-forming units (NFU) as determined by ^{11}B and ^{31}P MAS-NMR of $1/3K_2O$ $2/3[yB_2O_3$ $(1\text{-}y)P_2O_5]$ glass compositions [52]. The solid lines indicate the structural model derived in this section with $f = 0$.

The limiting behavior of the B^4 incorporation in borophosphate glasses is analogous to the B^4–O–B^4 avoidance principle present in structural models of alkali and alkaline earth borate glasses [43]. In these binary borate glasses, modifying cations are preferentially charge stabilized by B^4, but only up to a maximum fraction of B^4 units of approximately 45 %. Further addition of modifying oxide will cause the formation of trigonal B^2 NFUs and a concurrent decrease of B^4 units. This occurs because negatively charged B^4 tetrahedra as direct neighbors are energetically unfavorable. When the B^4 fraction is so high that neighboring B^4 units become unavoidable, then the formation of B^4 units becomes unfavorable, and B^2 units are formed instead to balance the charge of the modifier. The B^2 units decrease the network connectivity, exacerbating the problem of B^4–O–B^4 avoidance, and so the B^4 concentration will decrease further.

In borophosphate glasses, the maximum fraction of B_2O_3 that can be incorporated as B^4 is denoted as y^* and depends on the modifying oxide content x. Schuch *et al*. derived an expression for y^* by considering how many B^4 can be incorporated into the borophosphate

network while avoiding unfavorable B^4–O–B^4 bonds [53]. The necessary condition for avoiding B^4–O–B^4 bond formation is that the number of bridging oxygen per B^4 tetrahedra must always be less than or equal to the number of bridging oxygen on the other structural groups in the network, denoted as DP:

$$(4-f)\times\left[\mathrm{B}^4\right] \le \mathrm{DP}(x,y), \tag{2.6}$$

$$\mathrm{DP}(x,y) = 4\times\left[\mathrm{P}^4\right] + 3\times\left(\left[\mathrm{B}^3\right]+\left[\mathrm{P}^3\right]\right) + 2\times\left(\left[\mathrm{B}^2\right]+\left[\mathrm{P}^2\right]\right) + 1\times\left(\left[\mathrm{B}^1\right]+\left[\mathrm{P}^1\right]\right). \tag{2.7}$$

f is the allowed number of B^4–O–B^4 bonds per B^4 unit. If $f = 0$, Eq. (2.6) is equivalent to the Beekenkamp model [54] or if $f = 1$, then pairs of B^4 tetrahedra are allowed as in the Gupta model [55] for alkali borate glasses.

An expression for y^* in $x\mathrm{R}_{2/v}\mathrm{O}$ $(1\text{-}x)[y\mathrm{B}_2\mathrm{O}_3$ $(1\text{-}y)\mathrm{P}_2\mathrm{O}_5]$ borophosphate glasses can be derived from a simple example. Glass compositions with a constant $x \le 0.5$ are considered, which contain only P^3, P^2 and B^4 for $y \le y^*$, like the compositions in Figure 2.6b. The fraction of P^3 and P^2 at $y = 0$ are given by Eq. (2.1) and (2.2). By inspecting Figure 2.6b, it is observed that for $y \le y^*$ the fraction of P^3 remains constant, and B^4 replaces P^2 in the network on a one-to-one basis. The fraction of B^4 must be equal to y, which is the total B_2O_3 content, and we can write:

$$\left[\mathrm{B}^4\right] = y \tag{2.8}$$

$$\left[\mathrm{P}^3\right] = \frac{1-2x}{1-x} \tag{2.9}$$

$$\left[\mathrm{P}^2\right] = \frac{x}{1-x} - y \tag{2.10}$$

Here $[P^2]$ is calculated by subtracting $[B^4]$ from Eq. (2.2). By setting $y = y^*$ and inserting Eqs. (2.8)-(2.10) into Eq. (2.6) and expression for y^* is obtained:

$$y^* = \frac{3-4x}{(1-x)\times(6-f)} = \frac{3-\dfrac{x}{1-x}}{6-f} \tag{2.11}$$

Eq. 2.11 relates y^* to the modifier content, x, and fraction of B^4–O–B^4 bonds per B^4 unit, f. Eq. (2.11) was derived in a simple example, yet the result is analytically correct for all

values of x. For $y > y^*$ then $[B^4] = y^*$ and excess B_2O_3 will be incorporated as neutral B^3 units, as seen in Figure 2.6. The validity of Eq. (2.11) for predicting y^* and $[B^4]$ as a function of x is tested for a series of xNa$_2$O (1-x)[1/2B$_2$O$_3$ 1/2P$_2$O$_5$] glasses [40] in Figure 2.7.

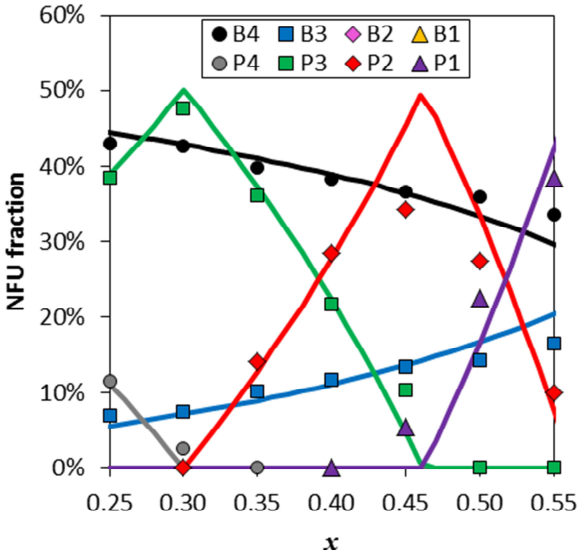

Figure 2.7: The fraction of the different network-forming units (NFU) as determined by ^{11}B and ^{31}P MAS-NMR of xNa$_2$O (1-x)[1/2B$_2$O$_3$ 1/2P$_2$O$_5$] glasses [40]. The solid lines indicate the structural model derived later in this section with $f = 0$.

The solid black line in Figure 2.7 represents the predicted $[B^4] = y^*$ by Eq. (2.11) with $f = 0$, and fits the experimental data well for to $x < 0.5$. The slight underestimation of $[B^4]$ for higher $x > 0.5$ could be caused by f increasing above 0.

The sequence in which the different negatively charged NFU occur with increasing x can be explained by the degree of charge delocalization in their NFUs. The degree of charge delocalization is the negative charge on the NFU divided by the number of oxygen bearing the charge [53]. By inspecting the structures and charges of the NFUs in Figure 2.5, the degree of charge delocalization decreases in the order $B^4 > P^2 > P^1 > P^0 > B^2 > B^1 > B^0$. This order is the same as the NFUs appearance with increasing x in Figure 2.6 and Figure 2.7.

The compositional dependence of fractions of the other NFUs in borophosphate glasses is derived by using the order of preferred charge compensation and the expression for y^* in Eq. (2.11) in conjunction with a chemically simple depolymerization model like that of Van Wazer [35], [49]. In order to simplify the mathematical expressions, the compositional space of $x\mathrm{R}_{2/\nu}\mathrm{O}\ (1-x)[y\mathrm{B}_2\mathrm{O}_3\ (1-y)\mathrm{P}_2\mathrm{O}_5]$ is divided into three different glass-forming regions, depending on which NFUs can occur in those regions.

2.2.3 Structural model for Region I: $x \leq 0.3$

Region I is characterized by B^4 being able to fully charge compensate the modifying oxide when $y \geq y^*$, where y^* was defined in Eq. (2.11). For $f > 0$, the region will extend to larger values of x. For example, if $f = 1$ as in the Gupta model [55], the limit of x will increase to 33%. In region I, the possible structural groups are B^4, P^4, B^3, P^3 and P^2. The P^4 unit is unique to the BPO_4 crystal structure [56] and borophosphate glasses in region I. P^4 is a tetrahedral phosphorous species with four bridging oxygen and can be thought of as the product of a reaction between the Lewis base double bonded oxygen (DBO) on a P^3 unit and a Lewis acid B^3. In our model P^4 is formed to charge stabilize B^4 when there is not enough modifying oxide to do so.

$$\left[\mathrm{B}^4\right] = \begin{cases} y, y \leq y^* \\ y^*, y^* < y \leq \dfrac{x}{1-x} + (1-y) \\ \dfrac{x}{1-x} + (1-y), \dfrac{x}{1-x} + (1-y) < y \end{cases} \tag{2.12}$$

$$\left[\mathrm{P}^4\right] = \begin{cases} \left[\mathrm{B}^4\right] - \dfrac{x}{1-x}, \dfrac{x}{1-x} \leq \left[\mathrm{B}^4\right] \\ 0, \left[\mathrm{B}^4\right] < \dfrac{x}{1-x} \end{cases} \tag{2.13}$$

$$\left[\mathrm{B}^3\right] = y - \left[\mathrm{B}^4\right] \tag{2.14}$$

$$\left[\mathrm{P}^3\right] = \begin{cases} (1-y) + \left(\dfrac{x}{1-x} - \left[\mathrm{B}^4\right]\right), \dfrac{x}{1-x} \leq \left[\mathrm{B}^4\right] \\ (1-y) - \left(\dfrac{x}{1-x} - \left[\mathrm{B}^4\right]\right), \left[\mathrm{B}^4\right] < \dfrac{x}{1-x} \end{cases} \tag{2.15}$$

$$\left[P^2\right]=\begin{cases}0, \dfrac{x}{1-x}\le\left[B^4\right]\\ \dfrac{x}{1-x}-\left[B^4\right], \left[B^4\right]<\dfrac{x}{1-x}\end{cases} \tag{2.16}$$

For $y \le y^*$, B_2O_3 is fully incorporated into the network as B^4, and for $y^* < y$, the fraction will plateau (equal to y^*) until there is not enough modifying oxide and P_2O_5 to balance the negative charge on B^4. Since B^4 is the preferentially formed negatively charged NFU its concentration prominently influences the behavior of the other network forming units, and $[B^4]$ is used as a variable in the equations. The fraction of P^4 is what is needed to balance the charge on B^4 when there is not enough modifier available. $[B^3]$ is determined by balancing the B_2O_3 content against $[B^4]$, and $[P^3]$ by balancing the P_2O_5 content against $[P^4]$ and $[P^2]$. $[P^2]$ is determined by charge-balancing the modifying oxide against $[B^4]$.

2.2.4 Structural model for Region II: $0.3 < x \le 0.5$

In region II, B^4 and B^2 alone are capable of charge compensating the modifying oxide when $y = 1$, but P^2, P^1 and P^0 will progressively form when $y^* < y \le 1$ as they are more stable than B^2 units. The value of f will not change the end-point of region II at $x = 0.5$. The possible structural groups in region II are B^4, B^3, P^3, B^2, P^2, P^1 and P^0.

$$\left[B^4\right]=\begin{cases}y, y\le y^*\\ y^*, y^*<y\end{cases} \tag{2.17}$$

$$\left[B^3\right]=\begin{cases}y-\left[B^4\right], \dfrac{x}{1-x}\le y^*+3\times(1-y)\\ y-\left[B^4\right]-\left(\dfrac{x}{1-x}-y^*-3\times(1-y)\right), y^*+3\times(1-y)<\dfrac{x}{1-x}\end{cases} \tag{2.18}$$

$$\left[P^3\right]=\begin{cases}(1-y)-\left(\dfrac{x}{1-x}-\left[B^4\right]\right), \dfrac{x}{1-x}\le y^*+(1-y)\\ 0, y^*+(1-y)<\dfrac{x}{1-x}\end{cases} \tag{2.19}$$

$$\left[B^2\right]=\begin{cases}0, \dfrac{x}{1-x}\le y^*+3\times(1-y)\\ \dfrac{x}{1-x}-y^*-3\times(1-y), y^*+3\times(1-y)<\dfrac{x}{1-x}\end{cases} \tag{2.20}$$

$$\left[P^2\right]=\begin{cases}\dfrac{x}{1-x}-\left[B^4\right], \dfrac{x}{1-x}\le y^*+(1-y)\\ 2\times(1-y)-\left(\dfrac{x}{1-x}-\left[B^4\right]\right), y^*+(1-y)<\dfrac{x}{1-x}\le y^*+2\times(1-y)\\ 0, y^*+2\times(1-y)<\dfrac{x}{1-x}\end{cases} \tag{2.21}$$

$$\left[P^1\right]=\begin{cases}0, \dfrac{x}{1-x}\le y^*+(1-y)\\ \left(\dfrac{x}{1-x}-\left[B^4\right]\right)-(1-y), y^*+(1-y)<\dfrac{x}{1-x}\le y^*+2\times(1-y)\\ 3\times(1-y)-\left(\dfrac{x}{1-x}-\left[B^4\right]\right), y^*+2\times(1-y)<\dfrac{x}{1-x}\le y^*+3\times(1-y)\\ 0, y^*+3\times(1-y)<\dfrac{x}{1-x}\end{cases} \tag{2.22}$$

$$\left[P^0\right]=\begin{cases}0, \dfrac{x}{1-x}\le y^*+2\times(1-y)\\ \left(\dfrac{x}{1-x}-B^4\right)-2\times(1-y), y^*+2\times(1-y)<\dfrac{x}{1-x}\le y^*+3\times(1-y)\\ (1-y), y^*+3\times(1-y)<\dfrac{x}{1-x}\end{cases} \tag{2.23}$$

As in region I, for $y \le y^*$, B_2O_3 is fully incorporated into the network as B^4, and for $y^* < y$, the B^4 fraction reaches a plateau with $[B^4]$ equal to y^*. $[B^3]$ is determined by balancing the B_2O_3 content against $[B^4]$ and $[B^2]$ which is formed only when B^4 and P_2O_5 can no longer charge compensate the modifying oxide. A modified version of Van Wazer's model is used for the phosphate network, which assumes that only two P species can occur at any given composition, and $[P^3]$ will go to zero before P^1 groups are formed. P^2. P^1 and P^0 are better charge compensators than B^2, and they progressively form as the P_2O_5 content decreases and their concentrations are determined by a charge balance.

2.2.5 Structural model for Region III: $0.5 < x \le 0.67$

Region III is very similar to Region II, the main difference being that B^1 units will occur. B^1 units will replace B^4 units initially, and then B^2 units when B^4 units are exhausted. There are some glass-forming compositions in Region III, but glass formation is not expected at higher x-values, and the structural model is not extended beyond Region III.

$$\left[B^4\right]=\begin{cases} y, y \le y^* \\ y^*, y^* < y, \dfrac{x}{1-x} \le y+3\times(1-y) \\ y^*-\left(\dfrac{x}{1-x}-3\times(1-y)-y\right), y+3\times(1-y)<\dfrac{x}{1-x}\le y+y^*+3\times(1-y) \\ 0, y+y^*+3\times(1-y)<\dfrac{x}{1-x} \end{cases} \quad (2.24)$$

$$\left[B^3\right]=\begin{cases} y-\left[B^4\right], \dfrac{x}{1-x} \le y^*+3\times(1-y) \\ y-\left[B^4\right]-\left(\dfrac{x}{1-x}-y^*-3\times(1-y)\right), y^*+3\times(1-y)<\dfrac{x}{1-x}\le y+3\times(1-y) \\ 0, y+3\times(1-y)<\dfrac{x}{1-x} \end{cases} \quad (2.25)$$

$$\left[B^2\right]=\begin{cases} 0, \dfrac{x}{1-x} \le y^*+3\times(1-y) \\ \dfrac{x}{1-x}-y^*-3\times(1-y), y^*+3\times(1-y)<\dfrac{x}{1-x}\le y+3\times(1-y) \\ 2y-\left[B^4\right]-\left(\dfrac{x}{1-x}-3\times(1-y)\right), y+3\times(1-y)<\dfrac{x}{1-x} \end{cases} \quad (2.26)$$

$$\left[B^1\right]=\begin{cases} 0, \dfrac{x}{1-x} \le y+3\times(1-y) \\ \dfrac{x}{1-x}-3\times(1-y)-y, y+3\times(1-y)<\dfrac{x}{1-x} \end{cases} \quad (2.27)$$

For $y \le y^*$, B_2O_3 is still fully incorporated into the network as B^4; and for $y^* < y$ the B^4 fraction reaches a plateau with $[B^4]$ equal to y^*. However, when B^1 starts to form, then B^4 units are converted to B^1. $[B^3]$ is determined by balancing the B_2O_3 content against $[B^4]$ and $[B^2]$ which is formed only when B^4 and P_2O_5 can no longer charge compensate the modifying oxide. The fractions of P^3, P^2, P^1 and P^0 are calculated as for region II.

2.2.6 Structure and topology of calcium borophosphate glasses

Changing the species of alkali oxide in alkali borophosphate glasses does not affect the NFU fractions much. For example in $1/3R_2O$ $2/3[yB_2O_3$ $(1\text{-}y)P_2O_5]$ glasses the largest

difference in [B^4] occurs at $y = 0.5$ where R = K gives [B^4] = 43% and R = Li has [B^4] = 39% [52]. Generally [B^4] decreases in the order K > Cs > Li, but the differences are slight [52].

In Paper V, a series of calcium borophosphates glasses were prepared and investigated in order to elucidate the effect of a typical alkaline earth modifier on the structure and properties of borophosphate glasses. The compositional join zCa(B_4O_7) (1-z)Ca(PO_3)$_2$ was chosen because both end-members are good glass-formers. Homogeneous and transparent glasses were prepared by the melt-quench technique in the compositional range $0 \leq z \leq 0.3$ and $z = 1$, but liquid-liquid phase separation prevented homogenous glass formation in the range $0.3 < z < 1$. The amorphous nature of these samples was confirmed by powder X-ray diffraction (XRD), and the glass compositions measured by induction coupled plasma atomic emission spectroscopy (ICP-AES). The measured compositions were within a maximum error of 2 % by mole of the constituent oxides. The NFU fractions were determined by ^{11}B and ^{31}P MAS-NMR and are shown in Figure 2.8.

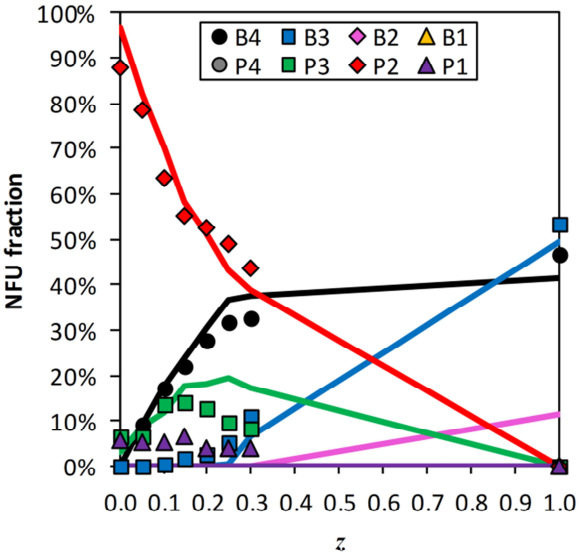

Figure 2.8: The fraction of the different network-forming units (NFU) as determined by ^{11}B and ^{31}P MAS-NMR of zCa(B_4O_7) (1-z)Ca(PO_3)$_2$ glasses (Paper V). The solid lines indicate the structural model derived in this section with $f = 0$.

Overall the structural model fits the measured NFU fractions reasonably well with some significant discrepancies noted. About 6 % of the P_2O_5 content exists as P^1 units, which is not reflected in the structural model. Disproportionation of P^2 units to P^3 and P^1 is known to

occur in calcium phosphates [57], but this cannot fully explain the high [P^1] content as the [P^3] is generally lower than expected. The [B^4] from z = 0.2 to z = 0.3 is lower than predicted with f = 0. This may be due to B^4−O−P^1 bridges not forming because of electrostatic repulsion [52]. The [B^4] at z = 1 is 5 % higher than the prediction by Eq. (2.17) with f = 0, and B^2 is not detected. This indicates that some B^4-O-B^4 bridges do occur in borate-rich compositions, and is backed up by the Raman spectrum in Figure 2.9.

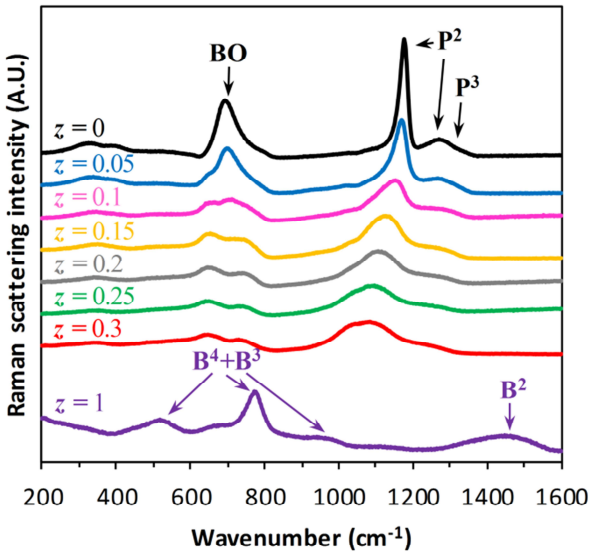

Figure 2.9: The Raman spectra of zCa$(PO_3)_2$ (1-z)CaB_4O_7 glasses are normalized by total scattering intensity. The arrows indicate the structural groups that are assigned to the major peaks in the end-member compositions. Peaks shift and broaden for 0 < z < 1 due to B-O-P bond formation. See text for details about the peak assignments and compositional trend.

The Raman spectrum for z = 1 contains five main features, and three of these can be assigned to the breathing motion of the pentaborate superstructural unit [43] at 521 cm^{-1}, 664 cm^{-1}, 773 cm^{-1} and some scattering expected at 890 cm^{-1} [58]. A signature of B^2 is found in the broad peak at approximately 1300 cm^{-1} to 1550 cm^{-1} assigned to symmetric stretching of BO_2^- [58]. The last low intensity feature at about 960 cm^{-1} is assigned to the breathing mode of the diborate superstructural unit, which also occurs in the crystalline form of $CaO•2B_2O_3$ [43], [58]. The diborate superstructural unit contains a B^4-O-B^4 bridge, and its presence explains why the z = 1 composition has f > 0.

The Raman scattering cross-section of the phosphate groups is much larger than that of the borate groups, and it is impossible to directly observe the borate bands in low-z glasses. However, the shifts of the peaks from the $z = 0$ compositions with increasing z are telling of the role of borate in the glassy network. The $z = 0$ composition has three major peaks, and similar to the sodium phosphates, these are assigned to the symmetrical stretching of P-O-P at 694 cm^{-1}, asymmetrical stretching of PO_2^- (P^2) at 1176 cm^{-1}, and symmetrical stretching also of PO_2^- at 1270 cm^{-1} [59]. Signatures of P^3 and P^1 are expected as a symmetrical stretching of PO_2 (P^3) at 1317cm^{-1} and symmetrical stretching of PO_2^{2-} (P^1) at 1022 cm^{-1} [59]. These features are not resolved, but are likely present in low concentration as found by ^{31}P MAS-NMR. With increasing z, an apparent shift of the three major peaks occurs. The most intense P^2 peak at 1176 cm^{-1} decreases in wavenumber and broadens greatly. This is interpreted as due to a progressive change in the next nearest neighbors of P^2 from P to B based NFUs [52]. There are also large changes in the P-O-P at 694 cm^{-1} with increasing z, which seems to split into a lower and a higher frequency peak. The symmetrical stretching of B-O-P is assigned to the peak centered at 653 cm^{-1} as this is an entirely new feature which grows with z. The peak at around 743 cm^{-1} is reminiscent of the shoulder of the P-O-P vibration for $z = 0$, which has previously been speculated to be caused by short phosphate units or ring structures [59]. The third peak at 1270 cm^{-1} was assigned to the symmetrical stretching of P^2 and P^3, and does not change significantly with z. This is in agreement with ^{31}P MAS-NMR showing the presence of P^2 and P^3 in roughly the same ratio for $0 \leq z \leq 0.3$.

The topology of the calcium borophosphate glasses is studied by O 1s X-ray photoelectron spectroscopy (XPS). The objective of this study is to verify the topological basis of the structural model, namely that the value of f fitted to the data is reasonable. For example, if B^4-O-B^4 bridges readily form in the glasses (*i.e.* f is high), then the observed [B^4] cannot be explained by Eq. (2.6), and the network topology does not determine [B^4].

The XPS measurements were performed on glass samples polished to a mirror-surface with 2000 grit SiC paper. In order to minimize surface contamination, the samples were polished immediately prior to XPS measurement, and stored in a desiccator under vacuum during transport. Some contamination by SiC was observed, but the O 1s spectra appeared to be unaffected by the preparation procedure. The binding energy (BE) was calibrated by the adventitious carbon C 1s peak at 284.8 eV [60]. The oxygen speciation was determined by least squares regression of up to four different contributions corresponding to NBO and three types of BO. The BE and line-width of each Gaussian peak was constrained in the fitting process. The oxygen fractions determined by XPS are given in Table I and shown in Figure 2.10. The results are in good agreement with those determined for $1/3K_2O$ $2/3[yB_2O_3$ $(1-y)P_2O_5]$ glasses by XPS and NMR [52]

Table I: The oxygen fractions of the zCa(B_4O_7) (1-z)Ca(PO_3)$_2$ as determined by the O 1s binding energy (BE) by XPS. The peaks were deconvoluted into a maximum of four different contributions corresponding to NBO and three types of BO. The fitting was constrained to only allow BE and FWHM (Δ) to vary to be 0.1 eV for the same peaks in different samples. The estimated error in the area fraction based on repeated measurements is 5 %.

Composition	O-type	BE (±0.1)/eV	Δ (±0.1)/eV	Area (±5)/%
z = 0.00	NBO	531.2	1.5	62
	P-O-P	532.9	1.7	38
z = 0.05	NBO	531.0	1.4	58
	P-O-B	532.1	1.8	6
	P-O-P	532.8	1.9	37
z = 0.10	NBO	531.1	1.5	56
	P-O-B	532.1	1.8	13
	P-O-P	532.7	1.9	31
z = 0.15	NBO	531.0	1.4	57
	P-O-B	532.1	1.8	16
	P-O-P	532.8	1.8	27
z = 0.20	NBO	531.1	1.4	51
	P-O-B	532.1	1.8	22
	P-O-P	532.8	1.9	27
z = 0.25	NBO	531.0	1.4	53
	P-O-B	532.2	1.8	22
	P-O-P	532.8	1.8	25
z = 0.30	NBO	531.1	1.3	45
	B-O-B	531.7	2.1	8
	P-O-B	532.2	1.8	21
	P-O-P	532.9	1.9	26
z = 1.00	B-O-B	531.8	2.0	100

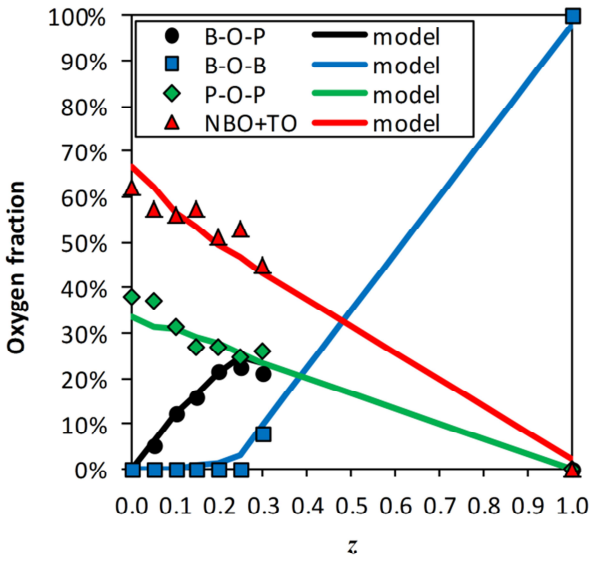

Figure 2.10: The measured oxygen speciation as determined by XPS. The details of the determination are given in the text and Table I. The XPS data agree with the topological model derived in this section within the estimated error of 5 %.

The fraction of BO and NBO can be predicted directly from the SRO measured by ^{11}B and ^{31}P MAS-NMR. However, by XPS it is also possible to determine the topology of the network by looking at the types and quantities of BO between the NFUs. In Figure 2.10 it is seen that B-O-B is not detected until $z = 0.3$, which has $y > y^*$ and contains significant amounts of B^3. This indicates that $B^4{-}O{-}B^4$ bridges do not occur below $z = 1$, and the fitted value of $f = 0$ in the topologically derived structural model is correct.

The BO speciation can be derived from the SRO by making some topological assumptions. If it is assumed that $B^4{-}O{-}P$ bonds are preferentially formed instead of $B^4{-}O{-}B^3$, and that $B^3{-}O{-}P$ bonds do not occur, then the modeled BO fraction in Figure 2.10 are obtained. This model fits the data well within the estimated error of the XPS measurements of 5 %.

2.3 Phosphosilicate glasses

2.3.1 Network forming units

The composition of phosphosilicate glasses can be written in a generalized manner as $xR_{2/v}O$ $(1\text{-}x)[ySiO_2$ $(1\text{-}y)P_2O_5]$, where $R_{2/v}O$ is a network modifying oxide with cation

valence *v*, *x* is the molar fractional content of network modifying oxide, and *y* is the network former concentration of silicon dioxide. The SRO of phosphosilicate glasses with $x \leq 0.5$ can be seen as connections of the silicate and phosphate NFUs shown in **Figure 2.11**.

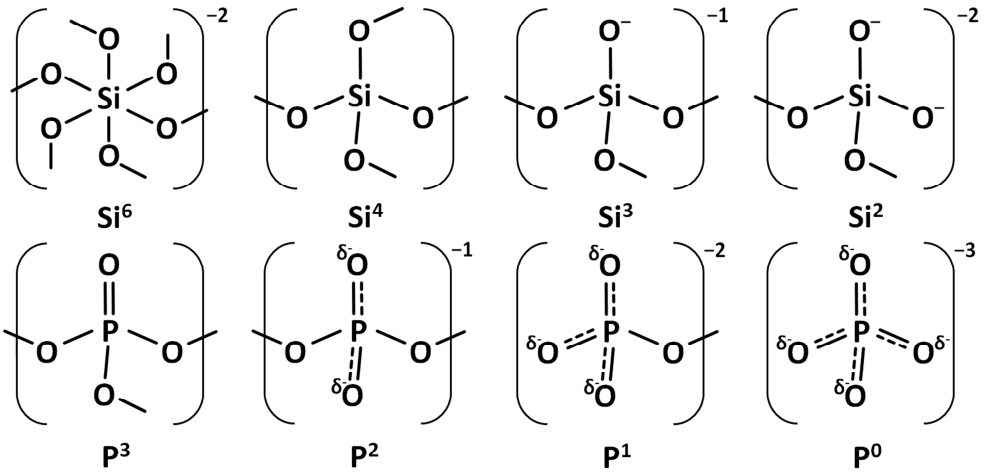

Figure 2.11: The network forming units (NFUs) that can occur in $xR_{2/v}O$ $(1\text{-}x)[ySiO_2$ $(1\text{-}y)P_2O_5]$ phosphosilicate glasses with $x \leq 0.5$. Si^6 is an octahedral species, while all other NFUs are tetrahedra.

The six-fold coordinated Si^6 NFU shown in Figure 2.11 occurs in phosphosilicate glasses with low values of *y*. The formation of Si^6 in phosphosilicate glasses is an interesting phenomenon because this usually occurs only in high-pressure crystals [61], [62]. Moreover, the generally accepted random network theory excludes the possibility of glass formation from network forming oxides with a coordination number above four [9], [63].

2.3.2 Structure and topology of sodium phosphosilicate glasses

In Paper VI, a series of sodium phosphosilicate glasses was prepared and investigated by ^{29}Si and ^{31}P MAS-NMR and Raman spectroscopy in order to understand the structure and topology of phosphosilicate glasses. The compositions of the phosphosilicate glasses were $0.3Na_2O$ $0.7[ySiO_2$ $(1\text{-}y)P_2O_5]$. The soda content was fixed and phosphorous pentoxide is substituted with silica because the study focused on the effect of the network former species on the structure and properties of the glasses. This effect is known as the mixed network former effect (MNFE).

The $0.3Na_2O$ $0.7[ySiO_2$ $(1\text{-}y)P_2O_5]$ glasses were prepared by melting high purity Na_2CO_3, SiO_2, and P_2O_5 powders in platinum crucibles. Some of these melts gave opaque

glasses when they were poured onto a stainless steel plate in air. However, clear glasses could be obtained by roller-quenching the melts for compositions containing up to 30 mole % of SiO_2 (y = 0.43). Two additional clear glasses were formed by mixing the y = 0.43 and y = 1 compositions, re-melting and roller-quenching, thereby yielding glasses with y = 0.54 and y = 0.89.

The amorphous nature of the clear samples was confirmed by X-ray diffraction (XRD), while the opaque silica-rich compositions were found to contain crystallized Na_3PO_4. The chemical compositions of the $0.3Na_2O$ $0.7[ySiO_2$ $(1\text{-}y)P_2O_5]$ glasses were determined by inductively coupled plasma atomic emission spectroscopy (ICP-AES). These analyzed compositions were found to be in good agreement with the batched ones. A notable exception was the phosphate-rich sample with y = 0, where the analyzed P_2O_5 content is lower than that batched, most likely due to the evaporation of P_2O_5 during melting.

The structure of the glasses were investigated by performing ^{29}Si and ^{31}P MAS-NMR spectroscopy on the $0.3Na_2O$ $0.7[ySiO_2$ $(1\text{-}y)P_2O_5]$ compositions with $y \leq 0.43$, and the spectra are shown in Figure 2.12.

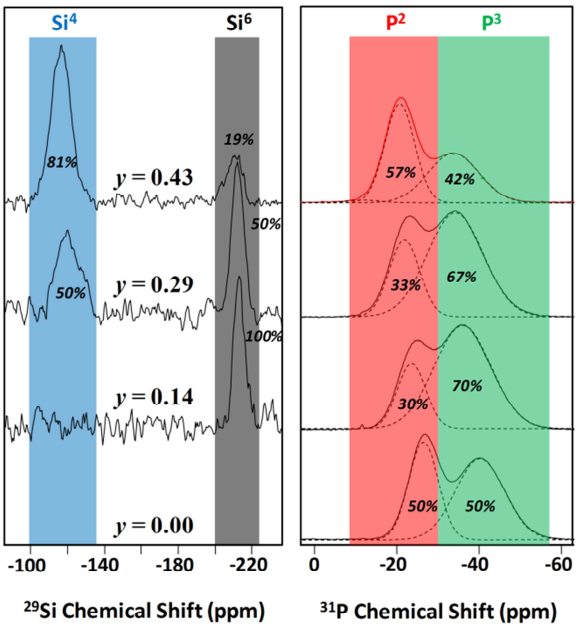

Figure 2.12: ^{29}Si and ^{31}P MAS-NMR spectra of the $0.3Na_2O$ $0.7[ySiO_2$ $(1\text{-}y)P_2O_5]$ glasses with $y \leq$ 0.43. The chemical shift ranges belonging to each NFU are highlighted, and the area ratios obtained

by deconvoluting the spectra are indicated. The ^{31}P MAS-NMR spectrum of a compositions with y = 0.57 was also determined, but is not shown here.

Tetrahedral Si^4 is found around −120 ppm in the ^{29}Si MAS-NMR spectra in Figure 2.12. In silicate glasses this peak is expected in the range of −70 ppm to −110 ppm [64], but it is more shielded in phosphosilicate glasses due to P NFU neighbors [65]. A distinct feature of Si^6 is found close to −215 ppm, which is very close to the chemical shift of Si^6 in crystalline SiP_2O_7 [64], [65]. The ^{31}P MAS-NMR has two-overlapping peaks at approximately −20 ppm and −40 ppm attributed to P^2 and P^3 NFUs respectively. These peaks were deconvoluted by least-squares regression of two Gaussian distributions. The central chemical shift of both the P^2 and P^3 peaks become more deshielded as y is increased. This deshielding can be caused by Si NFU neighbors [65], but also by an increase in the effective modifier concentration in the phosphate network [35]. The NFU fractions determined by NMR for the $0.3Na_2O$ $0.7[ySiO_2$ $(1\text{-}y)P_2O_5]$ glasses are plotted against y in Figure 2.13.

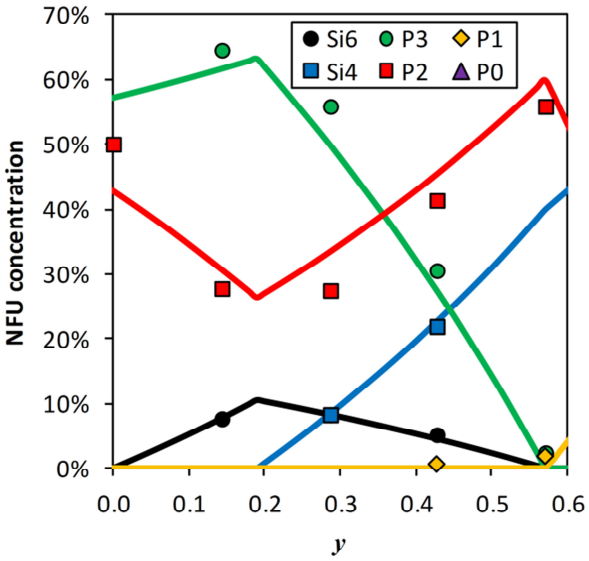

Figure 2.13: The network forming unit (NFU) fractions derived from the ^{29}Si and ^{31}P MAS-NMR spectra in Figure 2.12 and the compositions of the $0.3Na_2O$ $0.7[ySiO_2$ $(1\text{-}y)P_2O_5]$ glasses. The solid lines represent the structural model that is derived in this section.

In Figure 2.13, a maximum in $[P^3]$ and a minimum in $[P^2]$ is observed around y = 0.2, which clearly shows that the effective modifier concentration in the phosphate network is

decreasing. This minimum coincides with a maximum in [Si^6], and can be explained by Si^6 having two excess negative charges that are charge-balanced by the modifying cations, similar to B^4. This means that the formation of Si^6 converts P^2 to P^3 in order to satisfy charge- and oxygen-balance.

The topology of these glasses was investigated in order to understand how Si^6 and Si^4 are incorporated into phosphosilicate glasses. An attempt to measure the oxygen speciation by O 1s XPS was made, but the mixed network former glasses were too hygroscopic to even accurately measure the BO and NBO fractions, and deconvoluting the BO signal was thus out of the question. However, indirect evidence of the topology was found in the Raman spectra in Figure 2.14.

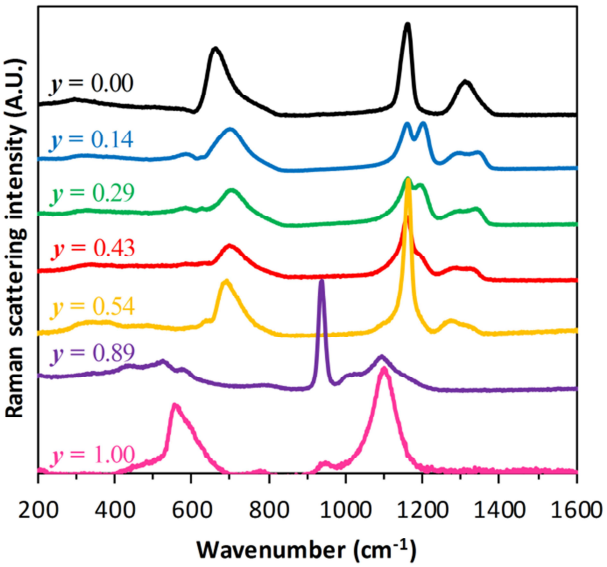

Figure 2.14: Raman spectra of $0.3Na_2O\ 0.7[ySiO_2\ (1\text{-}y)P_2O_5]$ glasses normalized by total scattering intensity. The Raman cross-section of P NFUs is much larger than for Si NFUs, and features of Si NFUs cannot be discerned in compositions with $0 \leq y \leq 0.54$. The band assignment is discussed in the text.

The Raman spectrum of the $y = 0$ composition contains three main peaks, and these are assigned to the symmetrical stretching of PO_2 (P^3) at 1310 cm^{-1}, symmetrical stretching of PO_2^- (P^2) at 1160 cm^{-1}, and symmetrical stretching of P−O−P at 667 cm^{-1} [48]. With increasing silica content, several changes occur in the Raman spectra and most importantly, a peak appears at 1200 cm^{-1}, which has previously been observed in Si^6-containing

phosphosilicate glasses [66]. This peak is assigned to the symmetrical PO_2 stretching of a P^3 NFU with a Si^6 NFU neighbor. This assignment is based on the correlation between peak intensity and [Si^6] and [P^3] in Figure 2.13 as determined from ^{29}Si and ^{31}P MAS-NMR spectroscopy.

The band originally centered at 1310 cm^{-1} is split into two at about 1340 cm^{-1} and 1290 cm^{-1}. A similar splitting of this band has been observed for modifier-free phosphosilicate glasses, and the splitting was attributed to the PO_2 (P^3) vibrational frequency changing with P^3 having an Si^4 NFU neighbor [67]. The Raman shift increases with a decreasing electron density in the P=O bond [67], and as Si is less electronegative than P, the low frequency component is expected to correspond to P^3 with Si NFU neighbors. However, the 1290 cm^{-1} peak intensity increases with *y*, while the 1340 cm^{-1} component decreases in intensity. A more thorough investigation is necessary to accurately assign these peaks.

The P−O−P band at 667 cm^{-1} found in the $y = 0$ composition is shifted to about 700 cm^{-1} upon silica addition. In sodium phosphate glasses, the frequency of this band increases with the Na_2O content, and a frequency of 700cm^{-1} is reached at the metaphosphate ($x = 0.5$) composition [48]. The blue-shift of this peak could be caused by the formation of P^3−O−Si bonds with low Raman intensity, which increases the P^2 contribution in the P−O−P bonding.

For the $y = 0.54$ composition, a sharp peak assigned to the symmetrical stretching of PO_2^- (P^2) dominates the spectrum, which agrees with the ^{31}P MAS-NMR measurements showing that the phosphorous speciation is dominated almost exclusively by P^2. The sharpness of the PO_2^- (P^2) peak could indicate that this composition is partially crystalline, although it is XRD amorphous. The same is the case for the $y = 0.89$ composition which is also XRD amorphous, but it has a dominant sharp peak at 940 cm^{-1} due to asymmetrical stretching of PO_2^{3-} (P^0), and possibly contains Na_3PO_4 crystals [68]. A small signature of P^1 units is found at 1000 cm^{-1}, which is the frequency of asymmetrical stretching of PO_2^{2-} (P^1) [68]. It is also possible to see low intensity features of the silicate network in this composition. The peak at 1100 cm^{-1} is caused by the symmetrical stretching of SiO_2^- (Si^3), and the shoulder at about 1150 cm^{-1} is due to SiO_2 (Si^4) [36], [68]. The bands in the range of 430 to 600 cm^{-1} are attributed to the symmetrical stretching of Si−O−Si with different numbers of bonding oxygen of the Si NFUs [36]. The Raman spectrum of the $y = 1$ composition almost exclusively shows Si^3 units and Si−O−Si bonding.

2.3.3 The formation mechanism of Si^6

In general, formation of Si^6 in phosphosilicate glasses can be understood by the concept of optical basicity [69]. Optical basicity is a measure of the effective negative charge on oxygen, and it is determined by the UV absorbance wavelength of probe ions such as Tl^+,

Pb^{2+} or Bi^{3+} [69]. There is a higher effective negative charge on the oxygen in SiO_2 than P_2O_5, because the optical basicity of SiO_2 is higher than that of P_2O_5 [66]. When a small amount of SiO_2 is added to P_2O_5, the positive charge on Si^{4+} must be balanced by oxygen with relatively low effective negative charge. Because more oxygen ions than the usual four are required to balance the positive charge on silicon, then silicon can assume a coordination number of six (Si^6) instead of the usual four (Si^4) in SiO_2. It has previously been attempted to quantitatively account for the concentration of Si^6 ($[Si^6]$) in alkali phosphosilicate glasses by optical basicity, but optical basicity alone cannot predict $[Si^6]$ [66].

A quantitative relation between $[Si^6]$ and $[P^3]$ has been observed for sodium phosphosilicate glasses [70]. It was found that $[Si^6]$ is approximately equal to one fourth of the expected $[P^3]$ in a variety of sodium phosphosilicate glasses. The same is the case for the $0.3Na_2O\ 0.7[ySiO_2\ (1\text{-}y)P_2O_5]$ glasses.

Miyabe et al. suggested a formation mechanism of Si^6 where a Si^4 NFU bound to four P NFUs can react with two P^2 NFUs to create a Si^6 with six P NFU neighbors [64]. The two P^2 NFUs are converted to P^3 in this reaction, and the modifying cations that were charge balancing P^2 will instead charge-balance the Si^6 NFU. Thus, Si^6 requires charge-balancing by the modifying ions much like four-fold coordinated boron (B^4) in borate and borophosphate glasses.

This formation mechanism agrees well with the decreasing $[P^2]$ and increasing $[P^3]$ with $[Si^6]$ obtained by NMR, and also the finding of a unique P^3 vibration by Raman spectroscopy in Si^6 containing glasses. Here, it is suggested that Si^6 is formed by the scheme in Figure 2.15.

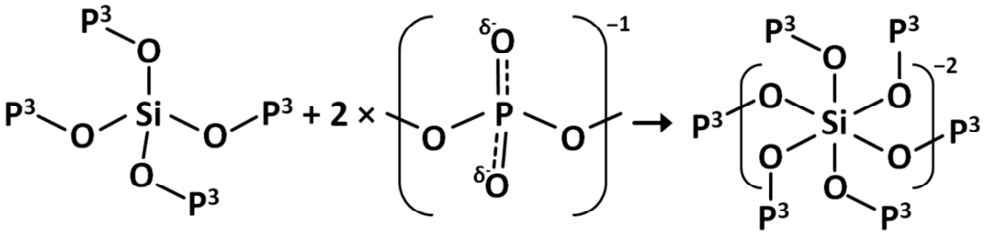

Figure 2.15: The proposed formation mechanism of the Si^6 NFU in phosphosilicate glasses: A Si^4 NFU having four P^3 NFU neighbors reacts with two P^2. The product is a Si^6 NFU with six P^3 NFU neighbors which is charge-balanced by the modifying cations.

Figure 2.15 shows a Si^4 NFU having four P^3 NFU neighbors reacting with two P^2. The product is a Si^6 NFU with six P^3 NFU neighbors and charge-balanced by modifying cations. The P^3 NFUs stabilize the formation of Si^6, possibly by charge-delocalization, and can therefore only have a single Si^6 NFU neighbor. This explains why $[Si^6]$ is approximately one-sixth of the actual $[P^3]$, or one-fourth of the expected $[P^3]$ if Si^6 was not charge compensated by the modifier.

The formation mechanism in Figure 2.15 inherently assumes that three factors limit the formation of Si^6: the modifying oxide, silica, and one-fourth $[P^3]$ before reaction. The NFU concentration of Si^6 ($[Si^6]$) in phosphosilicate glasses with the generalized composition $x R_{2/v}O\ (1-x)[ySiO_2\ (1-y)P_2O_5]$ can be quantified as:

$$\left[Si^6\right] = \min\left[\frac{x}{1-x}, \frac{y}{2-y}, \frac{2(1-y)-2\frac{x}{1-x}}{4(2-y)}\right] \tag{2.28}$$

Jiang et al. proposed an equation similar to Eq. (2.28) and showed that it could predict experimentally determined $[Si^6]$ very well for a range of phosphosilicate compositions [70]. However, they did not take into account that Si^6 requires charge-stabilization, and therefore did not limit $[Si^6]$ by the modifier content. Most of the investigated phosphosilicate compositions are not expected to have $[Si^6]$ limited by the modifier content. However, the compositions prepared by Jiang et al. were $x Na_2O\ (1-x)[0.2SiO_2\ 0.8P_2O_5]$ and $[Si^6]$ should be limited by the modifier content at low x [70]. In Figure 2.16, their ^{29}Si MAS-NMR results are compared to an X-ray absorption fine structure (XAFS) study of $x R_2O\ (1-x)[0.2SiO_2\ 0.8P_2O_5]$ glasses with R = Li, Na and K [71].

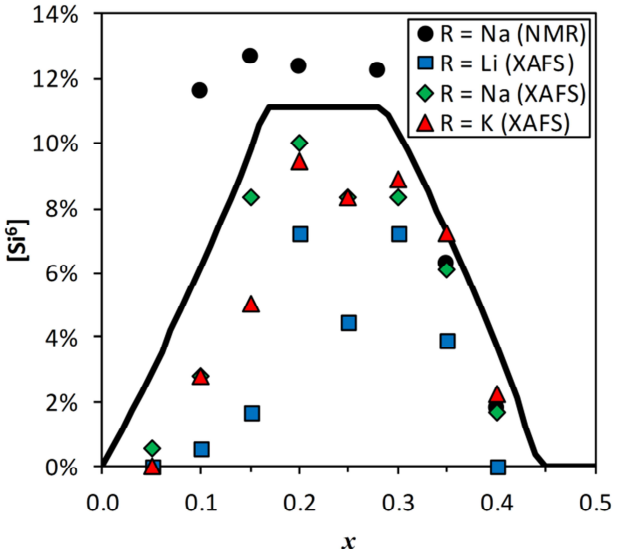

Figure 2.16: The NFU fraction of Si^6 ([Si^6]) in xR_2O $(1-x)[0.2SiO_2$ $0.8P_2O_5]$ glasses with R = Li, Na and K. The black circles is ^{29}Si MAS-NMR data [70], and the squares, diamonds and triangles are X-ray absorption fine structure data [71]. The solid line represents Eq. (2.28).

Eq. (2.28) is also plotted in Figure 2.16, where three different regimes exist regarding the modifier content dependence of [Si^6]. At low x, [Si^6] increases with x because it is limited by the modifier content, then it levels off because all Si are Si^6, and finally it decreases with [P^3]/6. Although the error in the XAFS data is considerable, it clearly follows a similar trend as Eq. (2.28). However, the ^{29}Si MAS-NMR data [70] for $x \leq 0.3$ is approximately constant and equal to the Si content. It is most likely that [Si^6] of the $x = 0.1$ glass, or the glass composition, is incorrect, and the data is best described by Eq. (2.28).

Nevertheless, the formation mechanism suggested in Figure 2.15 and Eq. (2.28) cannot account for the formation of Si^6 in modifier-free phosphosilicate glasses [61], [65], [72]. The formation of Si^6 in these modifier-free glasses has been linked to partial phase-separation of the two glass formers, and the phase separated regions containing Si^6 readily crystallize to SiP_2O_7 [65]. The charge-compensation for Si^6 in modifier-free glasses is most likely achieved by the formation of P^4 units, as was the case for borophosphate glasses with low modifier contents. This is the case in crystalline SiP_2O_7, which is comprised of P_2O_7 dimers sharing corners with three octahedral Si^6 NFUs [73]. These considerations indicate

that the formation of Si^6 in modifier-free glasses is related to phase separation or nucleation of crystalline SiP_2O_7, and Si^6 will not form to a significant degree in *homogeneous* glasses.

2.3.4 Structural model for phosphosilicate glasses with $x \leq 0.5$

The structural model of phosphosilicate glasses is derived in a similar manner as that of the borophosphate glasses. The preferred order of charge-compensation for phosphosilicate glasses is assumed to be: $Si^6 > P^2 > P^1 > P^0 > Si^3 > Si^2$. $[Si^6]$ is determined by Eq. (2.28), and the modifier content per NFU is used in a simple depolymerization model to calculate the NFU speciation. Most phosphosilicate glasses have $x \leq 0.5$, and for this reason, the structural model will only be derived for this subset of compositions. In order to simplify the equations three variables are defined. The first is the modifier content per NFU and is denoted [R]:

$$[\mathrm{R}] = \frac{2x}{(1-x)\times(2-y)} \tag{2.29}$$

The other two variables are the total fraction of Si NFUs ([Si]) and the total fraction of P NFUs ([P]):

$$[\mathrm{Si}] = \frac{y}{2-y} \tag{2.30}$$

$$[\mathrm{P}] = \frac{2(1-y)}{2-y} \tag{2.31}$$

With these variables defined, the analytical expressions for the NFU fractions can be expressed as:

$$\left[\mathrm{Si}^4\right] = \begin{cases} [\mathrm{Si}] - \left[\mathrm{Si}^6\right], [\mathrm{R}] \leq 3\times[\mathrm{P}] \\ [\mathrm{Si}] - ([\mathrm{R}] - 3\times[\mathrm{P}]), 3\times[\mathrm{P}] < [\mathrm{R}] \leq [\mathrm{Si}] + 3\times[\mathrm{P}] \end{cases} \tag{2.32}$$

$$\left[\mathrm{Si}^3\right] = \begin{cases} 0, [\mathrm{R}] \leq 3\times[\mathrm{P}] \\ [\mathrm{R}] - 3\times[\mathrm{P}], 3\times[\mathrm{P}] < [\mathrm{R}] \leq [\mathrm{Si}] + 3\times[\mathrm{P}] \\ 2\times[\mathrm{Si}] - ([\mathrm{R}] - 3\times[\mathrm{P}]), [\mathrm{Si}] + 3\times[\mathrm{P}] < [\mathrm{R}] \leq 2\times[\mathrm{Si}] + 3\times[\mathrm{P}] \end{cases} \tag{2.33}$$

$$\left[Si^{2}\right]=\begin{cases}0,3\times[P]<[R]\le[Si]+3\times[P]\\ [R]-([Si]+3\times[P]),[Si]+3\times[P]<[R]\le 2\times[Si]+3\times[P]\end{cases} \tag{2.34}$$

$$\left[P^{3}\right]=\begin{cases}[P]-[R]+2\times\left[Si^{6}\right],[R]\le[P]\\ 0,[P]<[R]\end{cases} \tag{2.35}$$

$$\left[P^{2}\right]=\begin{cases}[R]-2\times\left[Si^{6}\right],[R]\le[P]\\ 2\times[P]-[R],[P]<[R]\le 2\times[P]\\ 0,2\times[P]<[R]\end{cases} \tag{2.36}$$

$$\left[P^{1}\right]=\begin{cases}0,[R]\le[P]\\ [R]-[P],[P]<[R]\le 2\times[P]\\ 3\times[P]-[R],2\times[P]<[R]\le 3\times[P]\\ 0,3\times[P]<[R]\end{cases} \tag{2.37}$$

$$\left[P^{0}\right]=\begin{cases}0,[P]<[R]\le 2\times[P]\\ [R]-2\times[P],2\times[P]<[R]\le 3\times[P]\\ [P],3\times[P]<[R]\end{cases} \tag{2.38}$$

The structural model contained in Eqs. (2.28)-(2.38) is plotted together with the experimentally determined NFU fractions in Figure 2.13, and describes the data well.

2 Glass structure: Theory and models

3 Compositional dependence of dynamic properties

3.1 Definition and theories

3.1.1 Glass transition temperature

The glass transition temperature (T_g) is defined as a characteristic temperature in the glass transition range, over which a liquid transforms into a glassy solid, or vice versa. There are several definitions of T_g depending on the measured property. The viscous definition [74] is that the glass transition occurs when the average relaxation time of the liquid reaches ~100 s, corresponding to a viscosity close to:

$$\eta\left(T_g\right) \equiv 10^{12}\ \text{Pa s} \tag{3.1}$$

Most of the glasses discussed in this thesis have had T_g characterized by differential scanning calorimetry (DSC) or thermomechanical analysis (TMA). In these dynamic measurements, the glass transition is observed through the second-order thermodynamic derivative properties: constant pressure heat capacity or coefficient of thermal expansion, respectively. These definitions all correspond to the same temperature within the error of the measurement if using the appropriate experimental conditions [75].

In the framework of temperature dependent constraint theory, T_g is related to the average number of constraints per atom. The theoretical basis of this relation starts with the Adam-Gibbs theory of viscosity [76], [77]:

$$\log_{10}\eta\left(T,x\right) = \log_{10}\eta_{\infty} + \frac{B\left(x\right)}{TS_c\left(T,x\right)} \tag{3.2}$$

Here, $\eta(T,x)$ is the viscosity as a function of temperature (T) and composition (x), η_∞ is the high temperature limit of viscosity, $B(x)$ is related to the potential energy barrier to viscous flow and $S_c(T,x)$ is the configuration entropy of the melt. η_∞ is found to be almost independent of composition with a value close to 10^{-3} Pa s [4], [78], and $B(x)$ does not vary significantly within a class of materials when the mechanism of viscous flow is similar [79]. Both η_∞ and $B(x)$ are assumed to be constant. By applying Angell's definition of T_g by viscosity in Eq. (3.1) the following equality is obtained:

$$T_g\left(x\right)\times S_c\left[T_g\left(x\right),x\right] = T_g\left(x_{ref}\right)\times S_c\left[T_g\left(x_{ref}\right),x_{ref}\right] \tag{3.3}$$

Where x is the compositional variable and x_{ref} is a reference composition similar to x so that the assumption of constant $B(x)$ is not violated. It is possible to relate $T_g(x)$ to the number of constraints by using Naumis's result [80] of configurational entropy being largely due to the number floppy modes:

$$\frac{T_g(x)}{T_g(x_{ref})} = \frac{f\left[T_g(x_{ref}), x_{ref}\right]}{f\left[T_g(x), x\right]} = \frac{3 - N_c\left[T_g(x_{ref}), x_{ref}\right]}{3 - N_c\left[T_g(x), x\right]} \tag{3.4}$$

Where f represents the number of degrees of freedom (equal to $N_f - N_c$) and $N_c[T_g(x),x]$ is the number of rigid constraints at T_g per network forming atom.

According to classical constraint theory, $N_c[x]$ is determined by Eq. (1.4) and good glass formers have $N_c(x) \approx 3$. Stressed rigid compositions with $N_c(x) > 3$ can still form glasses if rapidly cooled. However, Eq. (3.4) strictly requires that $N_c[T_g(x),x] < 3$, meaning that all glasses are assumed to be floppy. The reason for this difference is that classical constraint theory does not consider the effect of temperature on the constraints and effectively enumerates the constraints existing at absolute zero. In temperature dependent constraint theory, each constraint has a type of activation energy and can become broken if the available thermal energy is sufficient.

When evaluating $N_c[T_g(x),x]$ in oxide glasses, NFUs are generally considered rigid, meaning that their linear and angular constraints are intact [32]. In contrast, the modifying cation polyhedra are considered floppy with their angular constraints broken and few or no intact linear constraints [32], [34], [81]. The bond-stretching constraints on oxygen are intact, but their bond-bending constraints are usually considered broken at T_g [81].

The oxygen angular constraint is considered broken at T_g because otherwise $N_c(T_g) \geq 3$ and Eq. (3.4) is violated for the three primary glass forming oxides: SiO_2, B_2O_3, and P_2O_5. For example, SiO_2 has $N_c = 3.67$ according to classical constraint theory and should be a poor glass former. On the other hand, if the BO bond-bending constraints are considered to be broken at T_g, then $N_c(T_g) = 3$, which agrees well with the good glass forming ability. This assumption is supported by experimental evidence showing that the oxygen bond angle distribution is very wide in SiO_2 glass [28], [41].

However, an increasing amount of experimental results seem to indicate that modified silicates have intact oxygen angular constraints [27], [28]. The broken oxygen angular constraints in SiO_2 may be a result of the very high $T_g \approx 1600$ K [15]. On the other hand, high-temperature Raman spectroscopy of B_2O_3 apparently supports the oxygen angular constraints becoming broken at $T_g \approx 533$ K [82]. This study finds that the boroxol rings

begin to break down above T_g. The breakdown of boroxol rings corresponds to a loss of oxygen angular rigidity because the oxygen atoms in the boroxol rings have a well-defined bond angle. At present, it is not clear if the oxygen angular constraints are intact, broken, or somewhere in between for low T_g glasses such as B_2O_3. The temperature dependent constraint modeling performed in this thesis will follow the approach of Mauro et al., who considers the oxygen angular constraint broken [32].

3.1.2 Fragility

Like the glass transition temperature, fragility can also be defined based on viscosity. The most common definition [74] is that fragility is the slope at T_g of a plot of the logarithm of viscosity plotted against T_g/T:

$$m \equiv \left. \frac{\partial \log_{10} \eta}{\partial \left(T_g / T \right)} \right|_{T=T_g} \tag{3.5}$$

The m in Eq. (3.5) is defined as the *liquid* fragility because it is found by measuring the temperature dependence of viscosity in a glass forming liquid. The Mauro-Yue-Ellison-Gupta-Allan (MYEGA) equation [4] can be used to find m from viscosity data:

$$\log_{10} \eta(T) = \log_{10} \eta_\infty + (12 - \log_{10} \eta_\infty) \times \frac{T_g}{T} \times \exp\left[\left(\frac{m}{12 - \log_{10} \eta_\infty} - 1 \right) \times \left(\frac{T_g}{T} - 1 \right) \right] \tag{3.6}$$

The MYEGA equation is derived by a temperature dependent constraint interpretation of the Adam-Gibbs relation in Eq. (3.2), and describes the temperature dependence of viscosity through three parameters: the infinite temperature viscosity ($\log_{10}\eta_\infty$), the glass transition temperature (T_g), and the liquid fragility (m). The 12 in the equation is actually $\log_{10}\eta(T_g)$, which is equal to 12 by the definition in Eq. (3.1). This means that the term (12 − $\log_{10}\eta_\infty$) has the physical meaning of the fragility of an ideally strong liquid. $\log_{10}\eta_\infty$ is found to be almost independent of composition with a value close to −3; therefore an ideally strong liquid has $m \approx 15$ [4], [78].

Fragility can also be thermodynamically defined by the temperature dependence of the configurational entropy, S_c, appearing in Eq. (3.2) [83]. However, it is not straight-forward to measure S_c of the liquid directly because S_c of the glass is obscured by the loss of ergodicity [7]. A quantity that can be reliably measured for real glass forming liquids and is related to S_c [84] is the constant pressure heat capacity jump at T_g:

$$\Delta C_p = C_{pl} - C_{pg} \tag{3.7}$$

Where C_{pl} is the extrapolated liquid heat capacity at T_g, and C_{pg} is the extrapolated glass heat capacity at T_g. Glasses have primarily vibrational degrees of freedom and therefore obey the Dulong-Petit law at T_g, giving $C_{pg} \approx 3R$. In contrast, the liquid state has both vibrational and configurational degrees of freedom [85]. It is tempting to take ΔC_p as the configurational heat capacity, but for the reason given earlier, this is not correct [7]. On the other hand, ΔC_p has been semi-empirically related to m in several theories [34], [86]. In this thesis, ΔC_p will be taken as a measure of thermodynamic fragility in order to support the liquid fragility measurements.

Several theories have tried to relate the fragility directly to the rigidity of the network and are mainly based on the observation of the intermediate phase in chalcogenide glasses having a very low fragility [20], [21]. Micoulaut theoretically derived from a harmonic oscillator model that an isostatic glass should have low fragility while floppy and stressed rigid glasses have higher fragilities [22]. He notes that the results do not seem to directly apply to silicate glasses, most likely because the modifier is weakly bonded in the network. Another approach used by Sidebottom is to relate fragility to the number of bridges per NFU in oxide glasses [87]–[89]. However, as discussed in Paper III, this approach does not give a universal description of fragility in oxide glasses and also cannot be compared to the results from chalcogenide glasses.

In the framework of temperature dependent constraint theory, m is not directly related to the number of network constraints, but to how fast their number changes with temperature. A simple expression is used to account for this behavior:

$$m(x) = m_0 \left(1 + \frac{\partial \ln f(T,x)}{\partial \ln T} \right) \Bigg|_{T=T_g(x)} \tag{3.8}$$

Here, $m_0 \approx$ 15-17 is the liquid fragility of a strong liquid such as SiO_2 [31]. A continuous function is needed in order to take the temperature derivative of $\ln f(T,x)$. The fraction of intact constraints at a given temperature is estimated:

$$q_i(T) = \left[1 - \exp\left(-\frac{\Delta F_i^*}{k_B T} \right) \right]^{\nu t_{obs}} \tag{3.9}$$

Where ΔF_i^* is the activation energy for breaking constraint i and vt_{obs} is the product of the vibrational attempt frequency and observation time [31]. The activation energy is related to a characteristic constraint onset temperature:

$$\Delta F_i^* = -k_B T_i \ln\left(1 - 2^{-1/vt_{obs}}\right) \tag{3.10}$$

Where T_i is the constraint onset temperature of constraint i, and is the temperature at which half the constraints are intact, and therefore marks the crossover from an intact to a broken constraint with increasing T [32].

3.2 Phosphate glasses

3.2.1 Phosphoric acids

The composition of phosphoric acids can be written as xH$_2$O (1-x)P$_2$O$_5$. H$_2$O depolymerizes the phosphate network like a modifying oxide, and the NFU speciation can be predicted by Van Vazer's model described in Section 2.1. One caveat is that hydrogen is covalently bonded to oxygen, and therefore the double-bonded terminal oxygen (TO) on P^3 is not converted to a NBO as the network is depolymerized. The structures of the NFUs in phosphoric acids are shown in Figure 3.1.

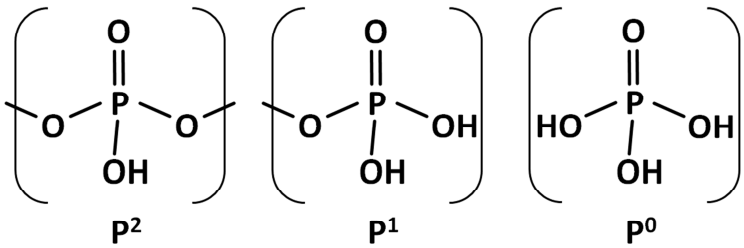

Figure 3.1: The structure of the NFUs in xH$_2$O (1-x)P$_2$O$_5$ glasses. Compositions with x > 0.75 are expected to consist of a mixture P^0 and H$_2$O molecules.

Phosphoric acids should be a simple case for the application of temperature dependent constraint theory because hydrogen is covalently bonded.

The constraints are evaluated by using Eq. (1.2) and (1.3). However, the case of one-fold coordinated atoms, such as H and TO, is special, and can either be treated by plucking these atoms from the network [90], [91], or counting half a linear constraint as by Eq. (1.2) [92]. Both options have been attempted, and it is found that plucking the TO from the network, and applying Eq. (1.2) to H gives the best description of the data.

3 Compositional dependence of dynamic properties

The linear constraints of the NFUs are all attributed to the oxygen, but the linear constraints between NBO and the modifier are all attributed to the modifier. Intact constraints at T_g are ranked in order of their strength:

- α: O−P−O angular constraints: There are three for P^3, P^2, P^1, and P^0. These NFUs are considered effective three-fold coordinated because the TO is not part of the network.
- β: P−O linear constraints: There are two at each BO and one at each NBO. None are counted at the double bonded terminal oxygen (TO), as it is not considered part of the network.
- γ: H−O linear constraints: There is one for each H.
- δ: P−O−P and P−O−H angular constraints: There is one for each BO and NBO.

The α, β, and γ constraints are all assumed intact at T_g. In contrast, the angular δ constraints on oxygen are considered broken at T_g, and so are any hydrogen bonds that may be intact below T_g [22]. By using the structural model in Section 2.1 and applying Eq. (1.4) the number of constraints per atom $N_c(x)$ is found:

$$\begin{aligned} N_c(x)\times N_{atoms}(x) = 3\times\left(\left[P^3\right]+\left[P^2\right]+\left[P^1\right]+\left[P^0\right]\right) \\ +2\times[BO]+1\times[NBO]+1\times[H] \end{aligned} \tag{3.11}$$

Here, $N_{atoms}(x)$ is the number of atoms per NFU and is necessary to convert from the 'per NFU' concentrations in the structural model to 'per atom' basis for the number of constraints. $N_{atoms}(x)$ is readily determined from the stoichiometry of $x$$H_2O$ (1-x)P_2O_5, while not counting the two TO in P_2O_5:

$$N_{atoms}(x) = \frac{3x+5\times(1-x)}{2\times(1-x)} \tag{3.12}$$

By rearranging Eq. (3.4) and using x_{ref} = 0.5 the scaling of T_g with x is obtained:

$$T_g(x) = \frac{3-N_c(0.5)}{3-N_c(x)}\times T_g(0.5) = \frac{3-\frac{7}{4}}{3-\frac{12-10x}{5-2x}}\times T_g(0.5) \tag{3.13}$$

Where $T_g(0.5)$ is the T_g of HPO_3 taken to be 263 K [93]. The predicted $T_g(x)$ for $x$$H_2O$ (1-x)P_2O_5 by Eq. (3.13) is compared to literature values of $T_g(x)$ in Figure 3.2.

3 Compositional dependence of dynamic properties

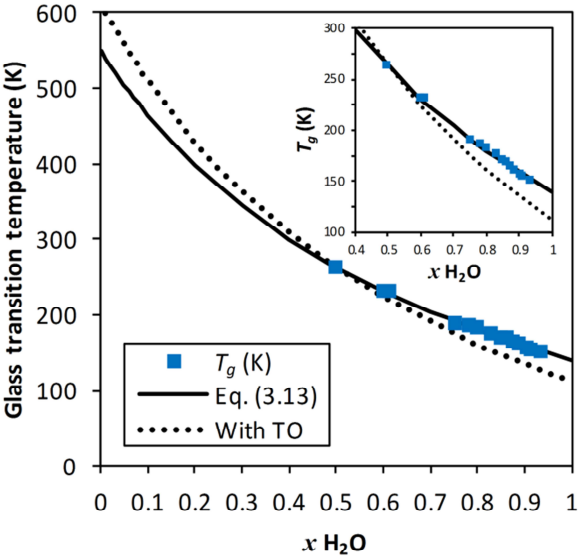

Figure 3.2: The $T_g(x)$ of the $x\mathrm{H_2O}$ $(1\text{-}x)\mathrm{P_2O_5}$ system for $x > 0.5$ was determined by DSC [94] and for $x = 0.5$ by dilatometer [93]. The solid line is the modeled $T_g(x)$ using Eq. (3.12) and the dotted line is the modeled $T_g(x)$ if the TO is taken as a network forming atom with one constraint for the P−TO bond and two additional β constraints for each P NFU. The inset shows the agreement between Eq. (3.12) and the experimental values in greater detail.

The agreement between model and experiment is excellent. Unfortunately, no data is available for $x < 0.5$, but Eq. (3.13) extrapolates to 548 K for $x = 0$. The T_g of P_2O_5 is reported to be between 590 K [95] and 665 K [96] by DSC, and as high as 692 K by photon correlation spectroscopy [97]. The difference between the reported T_g's and our extrapolated value could be attributed to a non-negligible difference between $B(0)$ and $B(0.5)$ which invalidates Eq. (3.3).

The dotted line in Figure 3.2 represents the predicted $T_g(x)$ by Eq. (3.4) if the TO are taken to be a network forming atom, which causes one α constraint per DBO and two additional β constraints per P NFU. This topological model results in a worse description of the $T_g(x)$ of polyphosphoric acids.

3.2.2 Alkali phosphates

The composition of alkali phosphate glasses can be written as $x\mathrm{R_2O}$ $(1\text{-}x)\mathrm{P_2O_5}$. The alkali oxide R_2O depolymerizes the phosphate network, and the NFU speciation can be

predicted by Van Vazer's model described in Section 2.1. The $T_g(x)$ of anhydrous lithium, sodium, and cesium phosphate glasses are shown in Figure 3.3.

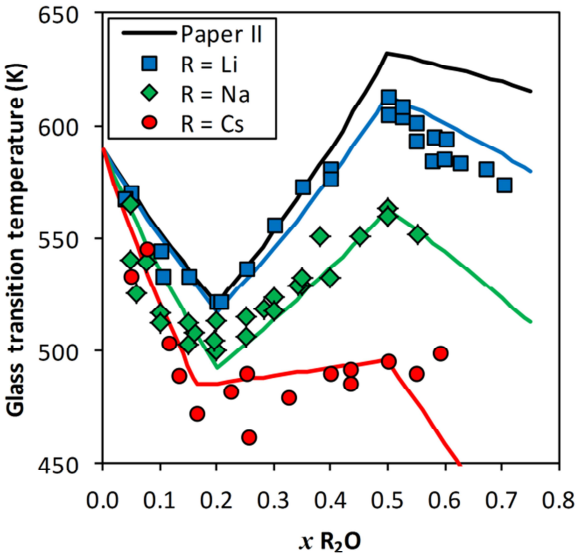

Figure 3.3: Compositional dependence of the glass transition temperature of $(x)R_2O$ $(1\text{-}x)P_2O_5$ glasses, where R_2O is an alkali oxide. The solid black curve shows the predicted glass transition temperature using the topological model developed in Paper II, with CN = 4 and $q_\gamma = 1$. The solid colored curves are the predicted $T_g(x)$ using the modified model from Eq. (3.16) and Table II. T_g data are literature values measured by DSC [98]–[100].

Unlike phosphoric acids, alkali phosphates do not exhibit a continuous decrease in $T_g(x)$ with increasing x. At low x the behavior is similar, but at $x \approx 0.2$, $T_g(x)$ begins to increase, peaking at the metaphosphate ($x = 0.5$) composition. The structure and speciation of the P NFU tetrahedra is similar for phosphoric acids and alkali phosphates, therefore the difference in magnitude and trend of $T_g(x)$ must be due to the SRO and topology of the alkali polyhedra.

In Paper II, a topological model of the alkali polyhedra in xR_2O $(1\text{-}x)P_2O_5$ was developed based on the work of Hoppe [51]. This topological model in combination with temperature dependent constraint theory explained the minimum in $T_g(x)$ by x_{crit} defined in Eq. (2.5). However, the magnitude of $T_g(x)$ was only replicated well for lithium phosphates. In Paper IV, the concept of 'constraint strength' was introduced to explain the differences in $T_g(x)$ depending on the alkali species.

3 Compositional dependence of dynamic properties

The topological model of the NFUs is similar to that for phosphoric acids, only that the structures of the NFUs are those previously shown in Figure 2.1. Below x_{crit}, the alkali polyhedra contain two NBO and are isolated in the network, but above x_{crit} a cross-linking unit starts to form. This cross-linking unit has a number of NBO equal to the preferred coordination number (CN) of the alkali. An example of these two SROs and topologies is shown for Li with CN = 4 in Figure 2.4. This cross-linking of the modifier for $x > x_{crit}$ is denoted as the 'modifying ion sub-network'.

The constraints are evaluated by using Eq. (1.2) and (1.3). The TO in the P^3 NFU is plucked from the network based on the result for phosphoric acids. The linear constraints of the NFUs are all attributed to the oxygen, but the linear constraints between NBO and the modifier are all attributed to the modifier. The constraints are ranked in order of their strength:

- α: O−P−O angular constraints: There are three for P^3, and five for P^2, P^1, and P^0. P^3 is considered effective three-fold coordinated because the TO is not part of the network.
- β: P−O linear constraints: There are two at each BO and one at each NBO. None are counted at the double bonded terminal oxygen (TO), as it is not considered part of the network.
- γ: R^+−NBO linear constraints: There are two for each R^+ added for $x < x_{crit}$, and CN constraints for each R^+ added for $x_{crit} < x$.
- δ: P−O−P angular constraints: There is one for each BO.

The α and β constraints are considered fully intact at T_g, while a fraction, q_γ, of the γ constraints are intact. The angular δ constraints on BO are considered broken, and so are angular constraints on NBO and R^+. By using the structural model in Section 2.1 and applying Eq. (1.4), the number of constraints per atom $N_c(x)$ is found:

$$\begin{aligned} N_c(x)\times N_{atoms}(x) = {} & 3\times[\mathrm{P^3}]+5\times\left([\mathrm{P^2}]+[\mathrm{P^1}]+[\mathrm{P^0}]\right) \\ & +2\times[\mathrm{BO}]+1\times[\mathrm{NBO}]+q_\gamma\times n_{c,\gamma}(x) \end{aligned} \tag{3.14}$$

Here, $N_{atoms}(x)$ is the number of atoms per NFU and is necessary to convert from the 'per NFU' concentrations in the structural model to 'per atom' basis for the number of constraints. $N_{atoms}(x)$ is readily determined from the stoichiometry of $x\mathrm{R_2O}$ $(1\text{-}x)\mathrm{P_2O_5}$, while not counting the TO in the P^3 NFU :

$$N_{atoms}(x)=\begin{cases}\dfrac{5}{2\times(1-x)}, x\le 0.5\\ \dfrac{3x+7\times(1-x)}{2\times(1-x)}, 0.5<x\end{cases} \tag{3.15}$$

By rearranging Eq. (3.4) and using x_{ref} = 0, then inserting Eqs. (3.14)-(3.15), the scaling of T_g with x is obtained:

$$T_g(x)=\frac{3-N_c(0)}{3-N_c(x)}\times T_g(0)=\frac{3-\frac{12}{5}}{3-\left(\frac{12-6x}{5}+q_\gamma\times n_{c,\gamma}(x)\right)}\times T_g(0), x\le 0.5 \tag{3.16}$$

Where x_{ref} = 0 is glassy P_2O_5 with $T_g(0)$ taken to be 590 K [95]. Eq. (3.17) is only defined up to x = 0.5 for the sake of simplicity, but can easily be extended beyond this region.

The term $q_\gamma \times n_{c,\gamma}(x)$ in Eq. (3.14) and (3.16) is the 'constraint strength' q_γ, taken as a fitting parameter, multiplied by the ideal the number of γ constraints per NFU:

$$n_{c,\gamma}(x)=\begin{cases}2\times[\mathrm{R}], x\le x_{crit}\\ \mathrm{CN}\times\left([\mathrm{R}]-[\mathrm{R}]\big|_{x=x_{crit}}\right)+2\times[\mathrm{R}]\big|_{x=x_{crit}}, x_{crit}<x\end{cases} \tag{3.17}$$

Values for CN is taken from literature studies of the coordination number of alkali cations in metaphosphate glasses, and used to calculate x_{crit} by Eq. (2.5). Then, q_γ is determined by fitting Eq. (3.16) to the T_g of the metaphosphate composition. The obtained values of these three parameters are found in Table II.

Table II. Alkali coordination number (CN), critical R_2O concentration for crosslinking of alkali coordination polyhedra (x_{crit}) and the fraction of intact γ constraints q_γ for lithium, sodium and cesium phosphate glasses. The literature references for CN are given in Paper IV. x_{crit} is calculated by Eq. (2.5) and q_γ by Eq. (3.16) from the T_g of the metaphosphate glass.

R	CN	x_{crit}	q_γ
Li	4	0.2[a]	0.97
Na	5	0.2	0.75
Cs	6	0.17	0.52

[a]This is calculated using CN = 5. It is assumed that Li^+ is 5-coordinated at around x_{crit}, but 4-coordinated in bridging sites above x_{crit}.

Using these parameters together with Eq. (3.16) and (3.17), the $T_g(x)$ can be modeled for the three types of alkali phosphate glasses, as seen in Figure 3.3. The agreement between data and model is quite good. The model proposed in Paper II does not take into account the constraint strength, and has $q_\gamma = 1$ and CN = 4, which is quite close to that observed for lithium phosphate glasses.

The simple model from Paper II has also been used to model the fragility of sodium phosphate glasses. The liquid fragilities of anhydrous sodium phosphate glasses were obtained from literature data of the heating rate dependence on the fictive temperature in DSC [96]. From these measurements, the apparent activation energy of the glass transition can be extracted [101]. This activation energy is equal to m if the temperature range is sufficiently narrow [102]. The liquid fragility (m) is calculated from the change in T_f as:

$$\log\left(\frac{q}{q_{ref}}\right) = m - m \cdot \frac{T_{f,ref}}{T_f}\bigg|_{T_f \approx T_{f,ref}} \tag{3.18}$$

q is the heating and previous cooling rate through the glass transition region, q_{ref} is the reference heating and cooling rate taken as 10 K/min and $T_{f,ref} = T_g$ is the fictive temperature corresponding to q_{ref}. The data is plotted in Figure 3.4, and has a similar trend as $T_g(x)$, initially decreasing to a minimum around $x = 0.2$ and then increasing.

3 Compositional dependence of dynamic properties

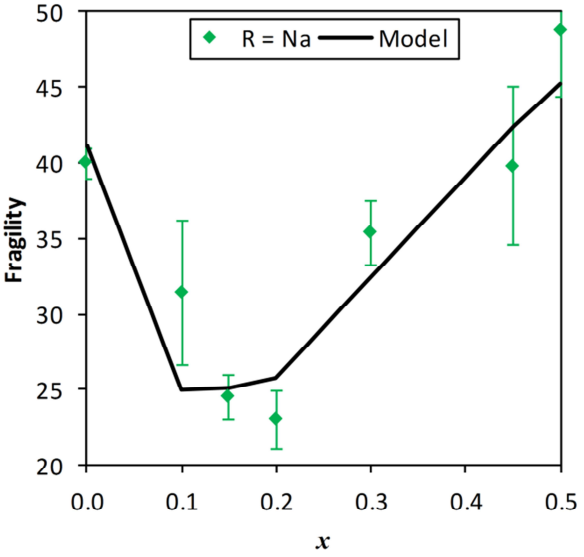

Figure 3.4: Compositional dependence of the liquid fragility of xNa$_2$O (1-x)P$_2$O$_5$ glass. The solid line shows the predicted fragility using the topological model developed in this paper. Experimental data points and error bars are obtained fitting Eq. (3.18) to the experimental data in [96].

The liquid fragility is calculated from a topological basis by Eqs. (3.8)-(3.10), where the constraint onset temperature and vt_{obs} are input parameters. The oxygen bond-bending constraint onset temperature T_δ is found to be 328 K for borate [32] and borosilicate [34] glass compositions, and we also fix it at this temperature. T_α, T_β, T_γ and vt_{obs} are determined by fitting to experimentally determined sodium phosphate liquid fragilities [96], with the restriction that $T_\alpha > T_\beta > T_\gamma > T_\delta = 328$ K. The constraint onset temperatures are found to be T_α = 1400 K, T_β = 850 K, T_γ = 590 K and vt_{obs} = 200. T_α and T_δ have relatively little influence on the liquid fragility, for example; lowering T_α by 200 K or raising T_δ by 100 K changes the liquid fragility of P$_2$O$_5$ by only 3%. vt_{obs} mainly affects the depth of the minimum in fragility and is fitted to be 200. In comparison vt_{obs} is 1000 for alkali borate compositions [32] and 60 for borosilicate compositions [34]. The modeled liquid fragility is plotted alongside experimental data in Figure 3.4 and has a similar trend with a broad minimum between x = 0.1 and x = 0.2. Another set of fragility data obtained by dynamic light scattering on sodium phosphates is fitted in Paper III.

3.2.3 Metaphosphates

The metaphosphate composition occurs at x = 0.5 in modified phosphate glasses with the general composition $x\mathrm{R}_{2/v}\mathrm{O}$ $(1\text{-}x)\mathrm{P}_2\mathrm{O}_5$. The metaphosphate composition can also be written as $\mathrm{R}(\mathrm{PO}_3)_v$, which illustrates that the glass consists of R^{v+} modifiers charge-balanced by P^2 NFUs. These P^2 NFUs occur as primarily as chains, but also in rings [35]. The T_g metaphosphate composition was used to determine the constraint strength (q_γ) of the R^+−NBO interaction in alkali phosphates. The metaphosphate is well suited for this purpose as the coordination sphere of R^{v+} ideally consists solely of NBO on P^2 NFUs. Also the metaphosphate is the composition with the best glass forming ability and lowest hygroscopicity in the $x\mathrm{R}_{2/v}\mathrm{O}$ $(1\text{-}x)\mathrm{P}_2\mathrm{O}_5$ system, and reliable data for physical properties such as T_g are usually available. In this section, literature data for the T_g of alkaline earth and rare earth metaphosphates are used to evaluate the effective number of modifier constraints, $q_\gamma \times n_{c,\gamma}$, and their dependence on the R^{v+} species.

A slightly difference version of Eq. (3.16) is used to determine $q_\gamma \times n_{c,\gamma}$ from T_g of the metaphosphates, because the number of atoms in the composition depends on v:

$$T_g\left(\mathrm{R}\left(\mathrm{PO}_3\right)_v\right) = \frac{3-\frac{12}{5}}{3-\left(\frac{9v}{1+4v}+q_\gamma \times n_{c,\gamma}\right)} \times T_g\left(\mathrm{P}_2\mathrm{O}_5\right), x = 0.5 \tag{3.19}$$

$q_\gamma \times n_{c,\gamma}$ is determined by fitting Eq. (3.19) to the literature T_g's in Paper IV, where the results, ionic radii and experimentally determined CNs of the modifying cations are reported. $q_\gamma \times n_{c,\gamma}$ per $\mathrm{R}^{v+}$is plotted against CN in Figure 3.5.

3 Compositional dependence of dynamic properties

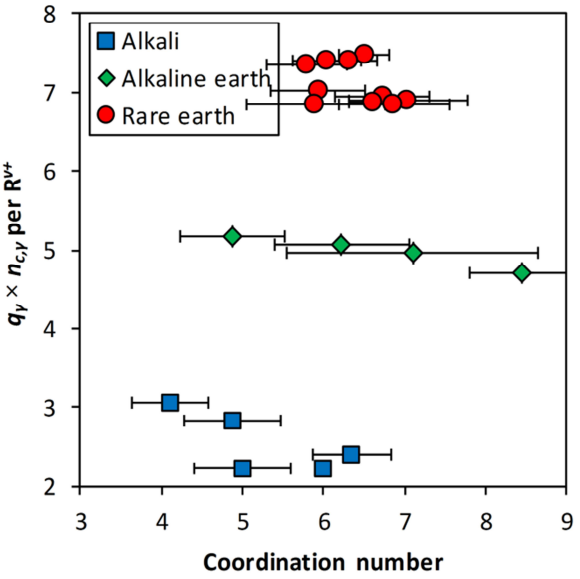

Figure 3.5: The effective number of constraints per modifying cation ($q_\gamma \times n_{c,\gamma}$ per R^{v+}) in alkali, alkaline earth and rare earth metaphosphate glasses plotted against the coordination number (CN) determined primarily by diffraction studies. The sources of the experimental data can be found in Paper IV.

Based on Eq. (1.2), a correlation between $q_\gamma \times n_{c,\gamma}$ per R^{v+} and CN is expected but is not observed. However, they both fall in the same range between 2 and 8, which is a hint that the γ constraints could be related to the SRO of the R^{v+} polyhedra. The lack of correlation to CN and strong influence of valence show that the nature of the R^{v+}−NBO interactions are of an ionic nature. $q_\gamma \times n_{c,\gamma}$ per R^{v+} is approximately twice the valence of the modifying cation, but the ionic radius having an effect as well.

The parameter that best describes the variation in $q_\gamma \times n_{c,\gamma}$ per R^{v+} is the charge-to distance ratio (σ) proposed by Eisenberg [93], which is a measure of the coulombic interaction between modifying cations and NBOs:

$$\sigma = \frac{v}{r_{R^{v+}} + r_{O^{2-}}} \tag{3.20}$$

Where r_R^{v+} is the ionic radius of the modifying cation and r_O^{2-} is the ionic radius of the NBO equal to 1.4 Å [103]. Fig. 4 shows an approximate linear relation between $q_\gamma \times n_{c,\gamma}$ per R^{v+} and σ for the metaphosphate compositions studied in Paper IV.

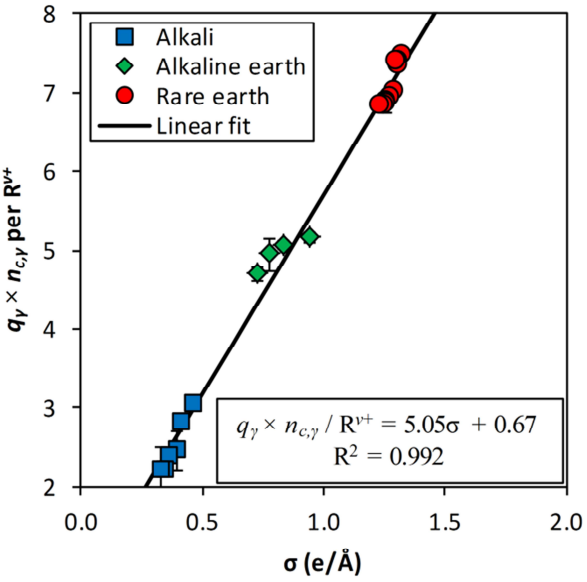

Figure 3.6: The effective number of constraints per modifying cation ($q_\gamma \times n_{c,\gamma}$ per R^{v+}) in alkali, alkaline earth and rare earth metaphosphate glasses against the charge-to-distance ratio (σ) defined in Eq. (3.20). The line is the best linear fit to data and R^2 is the coefficient of determination.

A similar correlation has been reported before, but using a different topological model and interpretation of 'constraint strength' [104]. These results are different because $q_\gamma \times n_{c,\gamma}$ per R^{v+} and observables like NBO/R^{v+} and CN fall in the same ranges, which substantiate that the γ constraints are related to the short range order around the modifying cations.

3.3 Borophosphate glasses

3.3.1 Alkali borophosphates

The composition of alkali borophosphate glasses can be written as $x$$R_2O$ (1-x)[$y$$B_2O_3$ (1-y)P_2O_5]. In borophosphate glasses, alkali oxide, R_2O, will cause the formation of B^4 NFUs as well as depolymerizes the glass network. The NFU speciation in borophosphate glasses can be predicted by the structural and topological model described in Section 2.2. The $T_g(x,y)$ of sodium borophosphates with y = 0, 0.5, and 1 are shown in Figure 3.7.

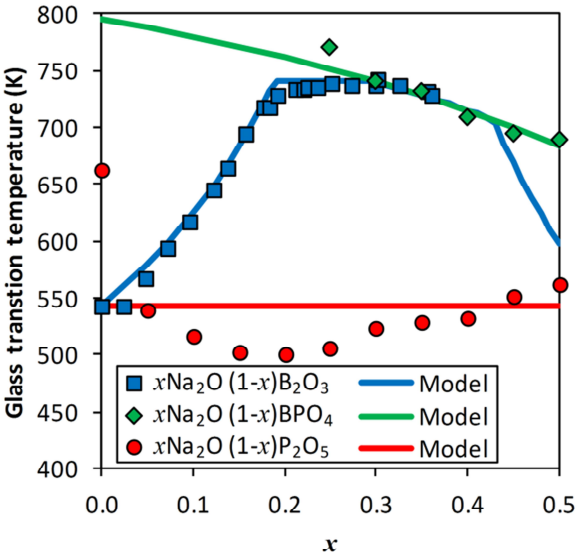

Figure 3.7: Experimental and modeled glass transition temperatures (T_g) by Eq. (3.23) is plotted as a function of x for three different series of $x\mathrm{Na_2O}$ (1-x)[$y\mathrm{B_2O_3}$ (1-y)$\mathrm{P_2O_5}$] glasses with y = 0 [96], 0.5 [40] and 1 [32].

The trend in $T_g(x,y)$ critically depends on the boron fraction, and to some extent follows the evolution of [B^4] that was described and characterized in Section 2.2. The plateau between about x = 0.2 to 0.4, however, does not fit the trend of [B^4]. It has recently been proposed that these compositions comprise an intermediate phase, but to achieve the isostatic criterion by Phillips' constraint counting, it is assumed that the network dimensionality changes with x [105]. This result seems very difficult to apply in practice, especially for mixed network former glasses. Another explanation for the plateau in $T_g(x,1)$ was proposed by Mauro, who argued that it is caused by the onset temperature of the O−B−O angular constraint being reached. This can also explain the high fragility ($m \approx 60$ to 85) of these compositions [32], whereas the intermediate phase is supposed to exhibit low fragility.

Temperature dependent constraint is used to describe the compositional dependence on T_g. The constraints are evaluated by using Eq. (1.2) and (1.3). The TO in the P^3 NFU is plucked from the network based on the result for phosphoric acids. The linear constraints of the NFUs are all attributed to the oxygen, but the linear constraints between NBO and the modifier are all attributed to the modifier. The number of constraints on modifiers is

evaluated assuming x_{crit} = 0 in Eq. (3.17) in order to simplify the mathematics. This simplification will only slightly affect the results for phosphate rich compositions. The constraints are ranked in order of their strength:

- α: B−O and P−O linear constraints. There are two at each BO and one at each NBO. None are counted at the double bonded terminal oxygen (TO) on P^3 as it is not considered part of the network.
- β: O−B−O and O−P−O angular constraints. There are three for B^3, B^2, B^1, B^0 and P^3. P^3 is considered effective three-fold coordinated because the TO is not part of the network. There are five angular constraints for B^4, P^4, P^2, P^1 and P^0.
- γ: R^+−NBO linear constraints. The number of constraints is equal to the oxygen coordination number (CN) of the R^+ charge balancing NBO. There are no constraints for R^+ charge balancing B^4.
- δ: B−O−B, B−O−P and P−O−P angular constraints. There is one for each BO.

For convenience, the B−O and P−O linear constraints are considered to be equivalent and denoted as the strongest (α) constraint. The second strongest (β) constraint is the O−B−O and O−P−O angular constraints. The O−B−O angular β constraint in binary sodium borate glasses was found to have an onset temperature T_β = 740 K and become partially broken to cause a plateau in $T_g(x,1)$ [32]. Here, the constraint will be considered intact, but the modeled $T_g(x)$ is limited by the onset temperature $T_{\beta,B}$. The R^+−NBO linear γ constraint in binary sodium phosphates was found to have an onset temperature T_γ = 590 K, and they are therefore only partially intact at T_g. The fraction of intact γ constraints is denoted q_γ and taken as a fitting parameter. The BO centered angular δ constraint is considered broken at T_g, as it is estimated to have an onset temperature T_δ = 328 K based on the Vogel temperature of B_2O_3 [32]. The angular constraints around the NBO and R^+ are not considered because their bonding is primarily ionic. Ionic bonding is by definition non-directional and therefore, these angular constraints are expected to be too weak to influence the physical properties.

By using the structural model in Section 2.2 and applying Eq. (1.4) the number of constraints per atom $N_c(x,y)$ is found:

$$\begin{aligned} N_c(x,y)\times N_{atoms}(x,y) = {} & 2\times[\mathrm{BO}]+1\times[\mathrm{NBO}] \\ & +3\times\left([\mathrm{P^3}]+[\mathrm{B^3}]+[\mathrm{B^2}]+[\mathrm{B^1}]+[\mathrm{B^0}]\right) \\ & +5\times\left([\mathrm{B^4}]+[\mathrm{P^2}]+[\mathrm{P^1}]+[\mathrm{P^0}]\right) \\ & +q_\gamma\times\mathrm{CN}\times[\mathrm{R}] \end{aligned} \tag{3.21}$$

Here, $N_{atoms}(x,y)$ is the number of atoms per NFU and is necessary to convert from the 'per NFU' concentrations in the structural model to 'per atom' basis for the number of constraints. $N_{atoms}(x,y)$ is readily determined from the NFU fractions of $x\mathrm{R_2O}$ $(1\text{-}x)[y\mathrm{B_2O_3}$ $(1\text{-}y)\mathrm{P_2O_5}]$, while not counting the TO in the P^3 NFU and the R^+ charge-stabilizing B^4:

$$\begin{aligned} N_{atoms}(x,y) = {} & 2.5\times\left(\left[\mathrm{B}^3\right]+\left[\mathrm{P}^3\right]\right)+3\times\left(\left[\mathrm{B}^4\right]+\left[\mathrm{P}^4\right]\right) \\ & +4\times\left[\mathrm{B}^2\right]+5.5\times\left[\mathrm{B}^1\right]+7\times\left[\mathrm{B}^0\right] \\ & +5\times\left[\mathrm{P}^2\right]+6.5\times\left[\mathrm{P}^1\right]+8\times\left[\mathrm{P}^0\right] \end{aligned} \tag{3.22}$$

Eq. (3.4) is modified to take into account the onset temperature $T_{\beta,\mathrm{B}}$ limiting the $T_g(x,y)$:

$$T_g(x,y) = \min\left[T_{\beta,\mathrm{B}}, T_{g,ref}\times\frac{3-N_{c,ref}\left(T_{g,ref},x_{ref},y_{ref}\right)}{3-N_c\left(T_g,x,y\right)}\right] \tag{3.23}$$

Based on the $T_g(x,y)$ data for alkali borophosphate glasses, it is proposed that $T_{\beta,\mathrm{B}}$ depends on the degree of polymerization (DP) of the NFU neighbors of B^4 as defined in Eq. (2.7). An empirical relation can describe the data well:

$$T_{\beta,\mathrm{B}}(x,y) = 55\times\mathrm{DP}(x,y)+(740-3\times55) \tag{3.24}$$

Eq. (3.24) entails that $T_{\beta,\mathrm{B}}$ is linearly proportional to DP and when DP = 3, then T_β = 740 K as found for binary sodium borate glasses [32]. The predictions of Eq. (3.23) are shown in Figure 3.7 for $x\mathrm{Na_2O}$ $(1\text{-}x)[y\mathrm{B_2O_3}$ $(1\text{-}y)\mathrm{P_2O_5}]$ glasses with varying x but constant y = 0, 0.5 and 1. B_2O_3 is used as the reference composition with $T_{g,ref}$ = 543 K and $N_{c,ref}(T_{g,ref})$ = 2.4 [32], and q_γ = 0.6 and CN = 5 for sodium. As expected, the model does not work very well for the sodium phosphate glasses due to the simplification in the treatment of the γ constraints, but the magnitude of T_g is reasonably accounted for. The agreement between model and data for the sodium borate and borophosphate glasses is very good.

In Figure 3.8, the effect of the alkali species is investigated for $x\mathrm{R_2O}$ $(1\text{-}x)[y\mathrm{B_2O_3}$ $(1\text{-}y)\mathrm{P_2O_5}]$ glasses with $x \approx 1/3$ and R = Li, Na, K, Cs [52], [106].

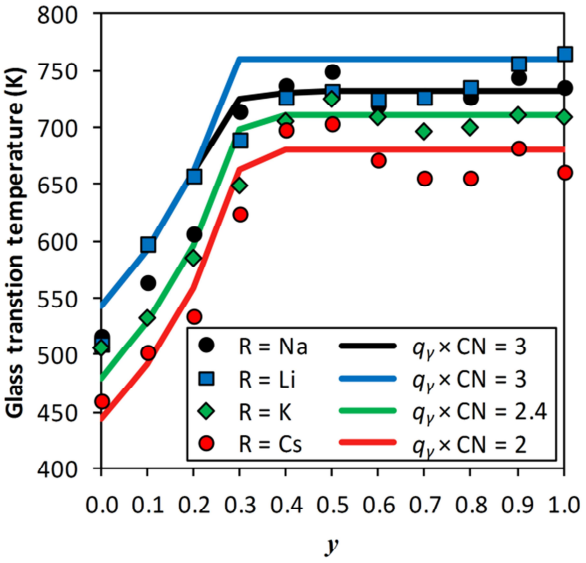

Figure 3.8: Experimental and modeled T_g is plotted as a function of y for three different series of $1/3R_2O$ $2/3[yB_2O_3$ $(1\text{-}y)P_2O_5]$ glasses with R = Li, K and Cs [52]. For R = Li then $q_\gamma = 0.75$, CN = 4 and $T_{\beta,B} = 760$ K, for R = K then $q_\gamma = 0.4$, CN = 6 and $T_{\beta,B} = 710$ K and for R = Cs then $q_\gamma = 0.33$, CN = 6 and $T_{\beta,B} = 680$ K. The R = Na series has a slightly different composition $0.35Na_2O$ $0.65[yB_2O_3$ $(1\text{-}y)P_2O_5]$ [106], and the model uses $q_\gamma = 0.6$, CN = 5 and $T_{\beta,B} = 740$ K.

The trend of $T_g(1/3,y)$ closely follows that of $[B^4]$ shown previously in Figure 2.6, but the magnitude depends on the alkali species. $T_g(1/3,y)$ decreases with the ionic radius of the alkali ion as was also found for the alkali phosphate glasses. By varying q_γ, the $T_g(1/3,y)$ dependence of alkali species for $y < y^*$ can be described. However, for $y > y^*$, it is necessary to use different $T_{\beta,B}$ to account for the behavior of $T_g(1/3,y)$, similarly to what has previously been postulated for soda lime borate glasses [81].

It does not make much sense that the overall similar behavior has two different explanations for $y < y^*$ and $y > y^*$. Also, there is no apparent reason why the B centered β constraint should break so rapidly on reaching the onset temperature, when the γ constraints and δ constraints exhibit a smooth and continuous behavior [28]. These reasons warrant a critical discussion on the use of $T_{\beta,B}$ to limit $T_g(x,y)$.

A structural model was developed in Section 2.2 and shown for the $1/3R_2O$ $2/3[yB_2O_3$ $(1\text{-}y)P_2O_5]$ glasses in Figure 2.6. For $y > y^*$, it can be seen that $[P^3]$ is substituted one-to-one for $[B^3]$. These two NFUs have the same number of constraints because the DBO is not

considered to be a part of the network. This entails that a plateau occurs for $y > y^*$, even without $T_{\beta,B}$ limiting $T_g(x,y)$. The only problem is that this plateau is significantly higher than what is observed, as shown in Figure 3.9.

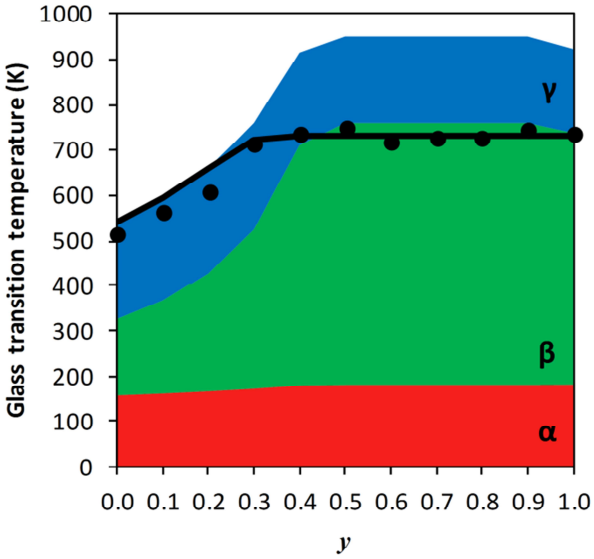

Figure 3.9: The contribution of each type of constraint, α, β, and γ, on the $T_g(1/3,y)$ predicted by Eq. (3.23) without limiting by $T_{\beta,B}$. The solid circles are experimental values for $0.35Na_2O\ 0.65[yB_2O_3\ (1-y)P_2O_5]$ glasses [106], and the black line is the prediction by Eq. (3.23) with limitation by $T_{\beta,B}$. The coincidence of the experimental $T_g(1/3,y)$ and edge of the β constraint contribution for $y > y^*$ is coincidental.

Figure 3.9 shows the contribution to $T_g(1/3,y)$ by each type of constraint. On inspection of this figure, one might think that the γ constraints are broken, and the β constraints intact, for $y > y^*$ because the edge of the β constraint range coincides well with $T_g(1/3,y)$. However, this is a complete coincidence, and does not happen for any other compositional series. What can be seen in Figure 3.9 is that the scaling of $T_g(x,y)$ with $N_c(x,y)$ apparently changes when $y \approx y^*$. This could be because the constraints are accounted for incorrectly, possibly by the softening of a constraint such as the B centered angular β constraint, or maybe by the rigidity being localized in the intermediate range order in borate-rich glasses. The reason is not known, but the apparent success of Eq. (3.24) to describe $T_g(x,y)$ for $y > y^*$ indicate that the topology of the network is still the crucial factor.

3.3.2 Calcium borophosphates

The T_g of the zCa(B_4O_7) (1-z)Ca(PO_3)$_2$ glasses was determined as the onset temperature of the glass transition by DSC at the standard heating/cooling rate of 10 K/min. The DSC scans are shown in Figure 3.10, where the inset shows the definition of T_g.

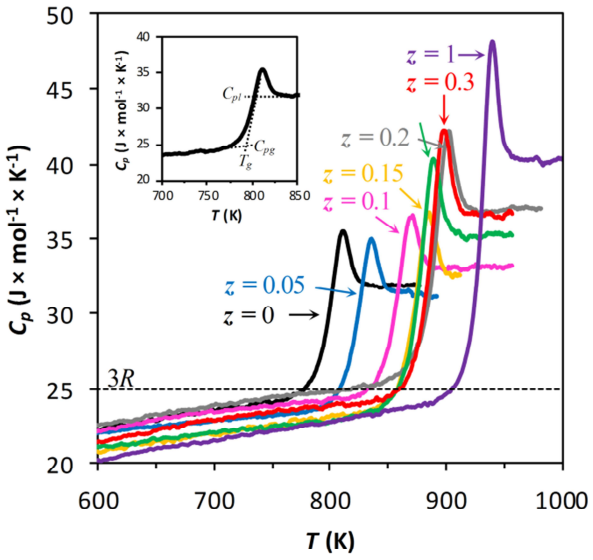

Figure 3.10: The DSC curves of zCa(PO_3)$_2$ (1-z)CaB_4O_7 glasses are measured at a heating rate of 10K/min after prior cooling from above T_g at the same cooling rate. T_g is defined as the onset temperature of the glass transition, as seen in the inset. ΔC_p is defined as C_{pl} - C_{pg} also shown in the inset. C_p and ΔC_p are given in joules per mol atoms per kelvin, which enables comparison between compositions as C_{pg} is approximately a constant equal to 3R.

The T_g determined by DSC for the zCa(B_4O_7) (1-z)Ca(PO_3)$_2$ glasses are plotted as a function of z in Figure 3.11.

3 Compositional dependence of dynamic properties

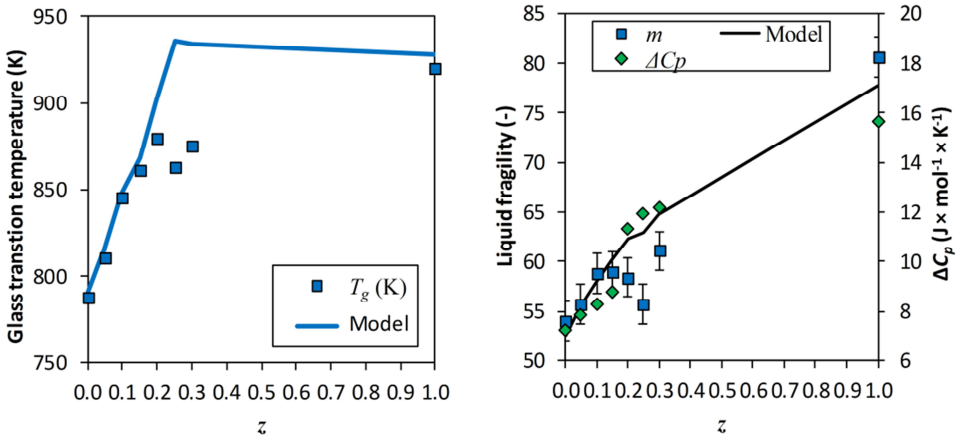

Figure 3.11: a) Experimental and modeled glass transition temperature (T_g) by Eq. (3.4) as a function of z for zCa(B_4O_7) (1-z)Ca(PO_3)$_2$ glasses. b) Experimental and modeled liquid fragility (m) by Eqs. (3.8)-(3.10). On the right hand side the thermodynamic fragility (ΔC_p) is plotted to scale with the m values. The onset temperatures used for the m model are T_α(B-O-P) = 1600 K, T_α(P-O) = T_β(P) = 1400 K, T_α(B-O) = 1100 K, T_β(B) = 1000 K, T_γ = 900 K and T_δ = 328 K with vt_{obs} = 100.

The structure and topology of the zCa(B_4O_7) (1-z)Ca(PO_3)$_2$ glasses are similar to that of the alkali borophosphate glasses, and only the γ constraints are treated differently in the constraint calculation:

$$\begin{aligned} N_c(z)\times N_{atoms}(z) = {} & 2\times[\mathrm{BO}]+1\times[\mathrm{NBO}] \\ & +3\times\left([\mathrm{P}^3]+[\mathrm{B}^3]+[\mathrm{B}^2]+[\mathrm{B}^1]+[\mathrm{B}^0]\right) \\ & +5\times\left([\mathrm{B}^4]+[\mathrm{P}^2]+[\mathrm{P}^1]+[\mathrm{P}^0]\right) \\ & +q_\gamma\times\left(\mathrm{CN}\times[\mathrm{Ca}]_{\mathrm{NBO}}+2\times[\mathrm{Ca}]_{\mathrm{B}^4}\right) \end{aligned} \tag{3.25}$$

Where q_γ = 5/6 and CN = 6 for calcium metaphosphate glass, as described in Paper V. The two constraints per Ca^{2+} at B^4 are linear constraints between two negatively charged B^4 units and the Ca^{2+} charge balancing them. $N_{atoms}(z)$ is slightly different than for alkali borophosphates, because of the larger valence of calcium oxide:

3 Compositional dependence of dynamic properties

$$\begin{aligned} N_{atoms}(z) = {} & 2.5\times\left(\left[B^3\right]+\left[P^3\right]\right)+3\times\left[P^4\right] \\ & +3.5\times\left(\left[B^4\right]+\left[B^2\right]\right)+4.5\times\left[B^1\right]+5.5\times\left[B^0\right] \\ & +4.5\times\left[P^2\right]+5.5\times\left[P^1\right]+6.5\times\left[P^0\right] \end{aligned} \tag{3.26}$$

Eq. (3.4) is used to predict $T_g(z)$, and not the modified Eq. (3.23) which limits T_g by the onset temperature of the B centered angular β constraint. This is because no evidence of a cross-over between $T_g(z)$ and T_β = 910 K [34] is found. However, this may be due to the glass forming range being limited to low z-values.

Since most of the glasses are rich in phosphate, the reference composition is taken as P_2O_5, and therefore $T_{g,ref}$ = 590 K [95] with $N_{c,ref}$ = 2.4 as found in Paper II. The modeled $T_g(z)$ is shown in Figure 3.11., and agrees well with the data, considering that [B^4] is overestimated by the structural for the z = 0.25 and z = 0.3 compositions.

The liquid and thermodynamic fragilities were also determined for these glasses. The viscosity in the glass transition range, $\eta = 10^{10}$ Pa s to $\eta = 10^{12}$ Pa s, was measured by ball penetration viscosity and m determined by linear fitting of $\log_{10}\eta$ vs T_g/T. ΔC_p was measured by DSC as the difference between the liquid heat capacity (C_{pl}) and the glass heat capacity at T_g (C_{pg}) as shown in the inset of Figure 3.10. The specific heat capacity C_p is given in units of joule per mol atoms per kelvin because this should give $C_{pg} = C_p(T_g) = 3R$ by the Dulong-Petit law, and thereby allow comparison of ΔC_p of between different glass compositions.

The experimental m and ΔC_p values are compared to modeled values by Eqs. (3.8)-(3.10) in Figure 3.11. In order for the model to achieve good agreement with the experimental fragility data, it is necessary to split up the α and β constraint depending on whether the constraint belongs to the P or B network. In the case of the α constraints, this was done by using the XPS measurements of oxygen speciation in Figure 2.10. The constraint onset temperatures are T_α(B-O-P) = 1600 K, T_α(P-O) = T_β(P) = 1400 K, T_α(B-O) = 1100 K, T_β(B) = 1000 K, T_γ = 900 K, T_δ = 328 K and vt_{obs} = 100. Several combinations of onset temperatures and vt_{obs} can give a similar compositional dependence of m. Therefore, the constraint onset temperatures and vt_{obs} cannot be precisely determined, but the fitted values agree well with those previously found for borate [32], [34], [81] and phosphate (Paper II) containing glasses. Also, with T_γ = 900 K gives $q_\gamma \approx 5/6$ around T_g by Eq. (3.9) as assumed previously for the $T_g(z)$ calculation.

3.4 Phosphosilicate glasses

3.4.1 Sodium phosphosilicates

The composition of alkali phosphosilicate glasses can be written generally as xR_2O (1-x)[$y SiO_2$ (1-y)P_2O_5], and the glasses investigated were sodium phosphosilicates with x = 0.3. In phosphosilicate glasses, the alkali oxide R_2O can cause the formation of Si^6 NFUs, as well as depolymerize the glass network. The NFU speciation in phosphosilicate glasses can be predicted by the structural and topological model described in Section 2.3.

The T_g's of the $0.3Na_2O$ 0.7[$y SiO_2$ (1-y)P_2O_5] glasses were determined by DSC with a heating/cooling rate of 10 K/min. The DSC scans are shown in Figure 3.12, and the determined T_g and ΔC_p values are plotted against y in Figure 3.13. The liquid fragility was inferred from the heating rate dependence of the onset of the glass transition in DSC, as described previously with Eq. (3.18).

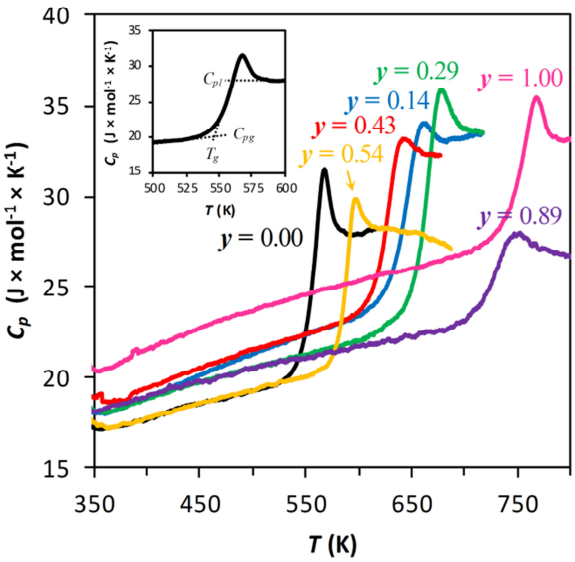

Figure 3.12: Differential scanning calorimetry scans for the $0.3Na_2O$ 0.7[$y SiO_2$ (1-y)P_2O_5] glass compositions. C_p is given per mole of atoms in the glass. The inset shows how T_g, C_{pg} and C_{pl} are determined. ΔC_p is defined as C_{pl} - C_{pg}.

3 Compositional dependence of dynamic properties

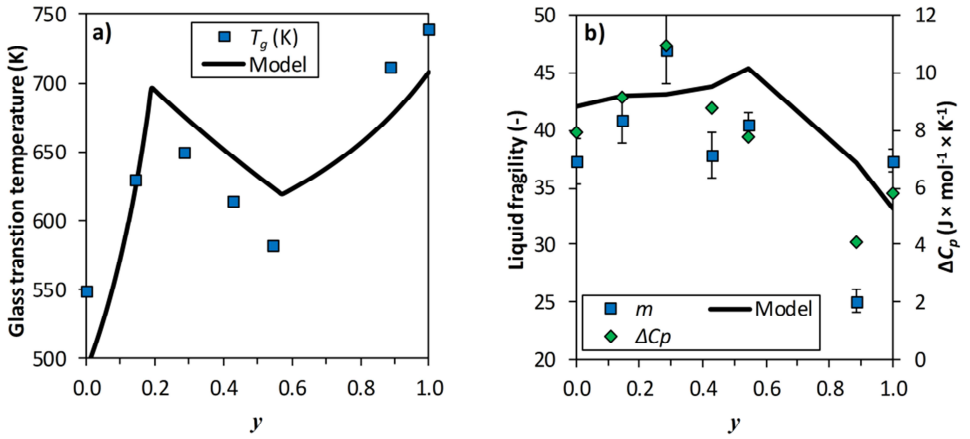

Figure 3.13: Compositional dependence a) of the glass transition temperature (T_g) and b) liquid fragility (m) and thermodynamic fragility (ΔC_p) for the $0.3Na_2O$ $0.7[ySiO_2$ $(1\text{-}y)P_2O_5]$ glass compositions. Liquid fragility was inferred from the heating rate dependence of the fictive temperature in a DSC experiment fitted to Eq. (3.18). The solid lines represent the modeled properties by Eq. (3.4) and Eq. (3.27) for T_g, and Eqs. (3.8)-(3.10) for m.

The trend in T_g generally increases with y, but with a sharp local maximum around y = 0.29, and a local minimum apparently around y = 0.54, which is at the edge of the glass-forming region. This trend in T_g closely matches the fraction of Si^6 from the structural model described in Section 2.3.

As done above, the compositional dependence of T_g is modeled with temperature dependent constraint theory. The following constraints are considered:

- α: Si−O and P−O linear constraints. There are two at each BO and one at each NBO. None are counted at the double bonded terminal oxygen (TO) on P^3 as it is not considered to be a part of the network. The topological model is:
- β: O−Si−O and O−P−O angular constraints. There are nine for Si^6, five for Si^4, Si^3, Si^2, Si^1, Si^0, P^2, P^1, and P^0, but only three for P^3. P^3 is considered to be effectively three-fold coordinated because the TO is not part of the network.
- γ: R^+−NBO linear constraints. The number of constraints is equal to the oxygen coordination number (CN) of R^+ charge balancing NBO. There are no constraints for R^+ charge balancing Si^6.
- δ: Si−O−Si, Si−O−P and P−O−P angular constraints. There is one for each BO. No angular constraints are counted for NBO.

3 Compositional dependence of dynamic properties

For the sake of convenience, the Si−O and P−O linear constraints are considered equivalent and denoted as the strongest (α) constraint. The second strongest (β) constraint is the O−Si−O and O−P−O angular constraints. The R^+−NBO linear γ constraint in sodium phosphate glasses is found to be only partially intact at T_g, and assumed the same here. The BO centered angular δ constraint is considered to be broken at T_g.

By using the structural model in Section 2.3 and applying Eq. (1.4) the number of constraints per atom $N_c(x,y)$ is found:

$$\begin{aligned} N_c(x,y)\times N_{atoms}(x,y) = {} & 2\times[\mathrm{BO}]+1\times[\mathrm{NBO}] \\ & +3\times[\mathrm{P^3}]+9\times[\mathrm{Si^6}] \\ & +5\times\left([\mathrm{Si^4}]+[\mathrm{Si^3}]+[\mathrm{Si^2}]+[\mathrm{P^2}]+[\mathrm{P^1}]+[\mathrm{P^0}]\right) \\ & +q_\gamma\times\mathrm{CN}\times[\mathrm{R}] \end{aligned} \tag{3.27}$$

Here, $N_{atoms}(x,y)$ is the number of atoms per NFU and is necessary to convert from the 'per NFU' concentrations in the structural model to 'per atom' basis for the number of constraints. $N_{atoms}(x,y)$ is readily determined from the NFU fractions of $x\mathrm{R_2O}$ $(1\text{-}x)[y\mathrm{SiO_2}$ $(1\text{-}y)\mathrm{P_2O_5}]$, while not counting the TO in the P^3 NFU and the R^+ charge-stabilizing Si^6:

$$\begin{aligned} N_{atoms}(x,y) = {} & 4\times[\mathrm{Si^6}]+3\times[\mathrm{Si^4}]+4.5\times[\mathrm{Si^3}]+6\times[\mathrm{Si^2}] \\ & +2.5\times[\mathrm{P^3}]+5\times[\mathrm{P^2}]+6.5\times[\mathrm{P^1}]+8\times[\mathrm{P^0}] \end{aligned} \tag{3.28}$$

Eq. (3.4) is used together with Eq. (3.27) and (3.28) to evaluate $T_g(x,y)$. The reference composition is P_2O_5, and therefore $T_{g,ref}$ = 590 K [95] with $N_{c,ref}$ = 2.4 as found in Paper II. Using CN = 5, the value of q_γ that best fit the data is 0.4 which yield an effective two constraints per Na^+. The modeled $T_g(0.3,y)$ is plotted in Figure 3.13. The overall trend and location of the local maximum and minimum is replicated well, but the magnitude deviates as much as 50 K. This is likely because the number of γ constraints per Na^+ depends on the composition. The two γ constraints per Na^+ fitted here is significantly less than the three γ constraints per Na^+ found for sodium borophosphate glasses, and there may well be further variation within the phosphosilicate glasses themselves.

The m values of the $0.3\mathrm{Na_2O}$ $0.7[y\mathrm{SiO_2}$ $(1\text{-}y)\mathrm{P_2O_5}]$ glasses are plotted as a function of y in Figure 3.13b. In this figure, the isobaric heat capacity jump at T_g (ΔC_p) is also plotted, and has a very similar trend as the m data. The y = 0.89 composition lower fragility than the compositional trend suggests. This could be caused by the P^0 units detected by Raman

spectroscopy not participating in the glassy network. The fragility peaks at the y = 0.29 composition, which also has the largest T_g and Si^6 content.

The fragility is modeled by applying Eqs. (3.8)-(3.10). Previous work on the topology of borosilicate glasses found that vt_{obs} = 60, and the oxygen bond stretching (α) constraint onset temperature T_α = 1600 K and $T_{\beta,Si}$ = 1425 K, and the same values are employed here [34]. $T_{\beta,P}$ = 850 K is taken from the previous analysis of sodium phosphate glasses in Paper II, and T_δ = 328 K is inferred from the Vogel temperature of B_2O_3 [32]. This leaves only the onset temperature of the modifying ion bond stretching γ constraint as a fitting parameter. By fitting to the experimental m values, the onset temperatures T_γ = 550 K is obtained, which agrees well with previous results on sodium phosphate in Paper II.

The modeled composition dependence of m is also plotted in Figure 3.13b. The maximum in the experimental liquid and thermodynamic fragilities occurring at y = 0.29 is not replicated by the model, possibly because α and β constraints in the Si^6 NFU are taken to have the same strength as in other Si NFUs. Otherwise the model reproduces the overall trend of m and ΔC_p with reasonable accuracy.

3 Compositional dependence of dynamic properties

4 Compositional dependence of mechanical properties

4.1 Definitions and theories

4.1.1 Indentation hardness

The ‘hardness’ of a material can be understood as the material resistance to surface damage. A common way to measure hardness is by indentation, where an indenter of known geometry is pressed into the sample at a fixed load, and the hardness is measured by the size of the indent that is created. A variety of indenter geometries exist, but in this thesis a diamond Vickers indenter is used. The Vickers indenter is a square-based pyramid with an angle θ = 136° between opposite pyramid faces. The Vickers indentation hardness is defined as:

$$H_V = \frac{2P\sin\theta}{d^2} = 1.8544\frac{P}{d^2} \tag{4.1}$$

Where P is the load and d is the diagonal of the indent. By this definition, the indentation hardness is the load on the projected area of the indent, or the force that can be sustained per initial surface area. Native silicate glasses generally have H_V in the range of 3 to 7 GPa.

Glass is often said to be an ideally elastic solid, and therefore it may be surprising that a permanent deformation takes place during indentation. The permanent deformation occurs as a result of gigapascal-range compressive and shear stresses, which do not occur in a tensile test. It has been established that there are three deformation mechanisms that can occur during indentation as illustrated in Figure 4.1 [107].

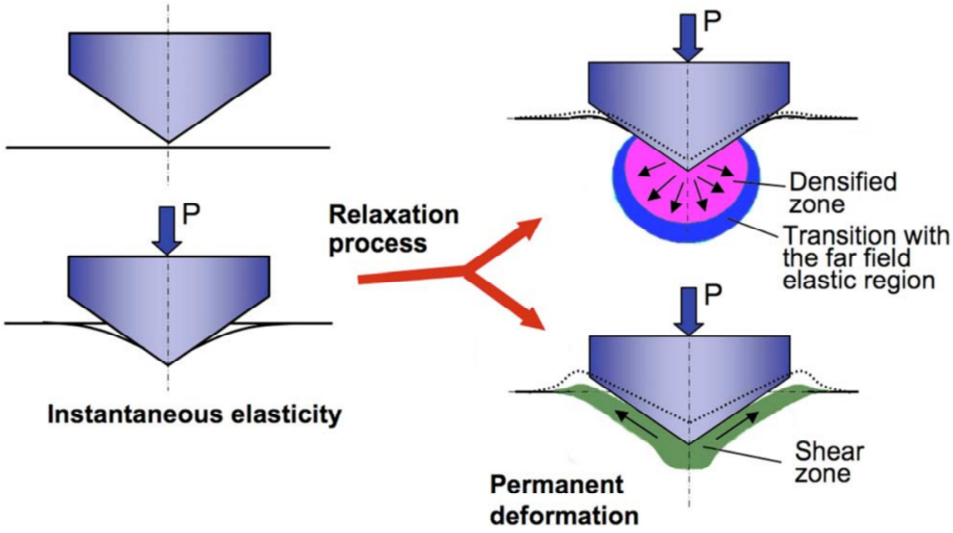

Figure 4.1: The three different deformation mechanisms that can occur during indentation: Elastic deformation, densification, and plastic deformation. Only the densification and plastic deformation are permanent. Adapted from [107].

The elastic deformation is difficult to observe because it is released upon unloading. The work of elastic and permanent deformation can be quantified by performing careful load-displacement indentation experiments. The elastic work is found to be around 70 % of the total work for silica glass [108]. This can explain why indentation hardness is strongly correlated with the elastic properties of materials [109].

Densification is a non-volume conservative collapse of the glass structure. The mechanism of densification during indentation seems to be the same as in hydrostatic compression experiments [110] based on their relatively low activation energies [111]–[113]. The densified glass can be relaxed to normal volume by annealing below T_g, such as 2 hours at $0.9 \times T_g$ [114]–[116].

Plastic flow in glasses is evidenced by the creation of pile-up regions on the indentation edge. These pile-up regions become more pronounced for sharp indenter geometries and soft glasses [117]. The mechanism of plastic deformation seems to be the same as viscous flow, just activated by the large shear stresses induced by indentation rather than temperature [117], [118].

Yamane & Mackenzie devised a semi-empirical model of indentation hardness by attributing a characteristic resistance to each of these deformation mechanisms, and taking the Vickers indentation hardness to be proportional to the geometric average [119]:

$$R_T = \left(R_E \times R_D \times R_P\right)^{1/3} = \left(K \times \sqrt{\alpha G K} \times \alpha G\right)^{1/3} = \sqrt{\alpha G K} \tag{4.2}$$

Where α is the average bond strength relative to silica glass, K is the bulk modulus, and G is the shear modulus. The average bond strength can be determined using Sun's table of bond strengths in oxide glasses [120]. The calculated Vickers hardness by the Yamane & Mackenzie model is compared to measured values for a variety of silicate glasses in Figure 4.2.

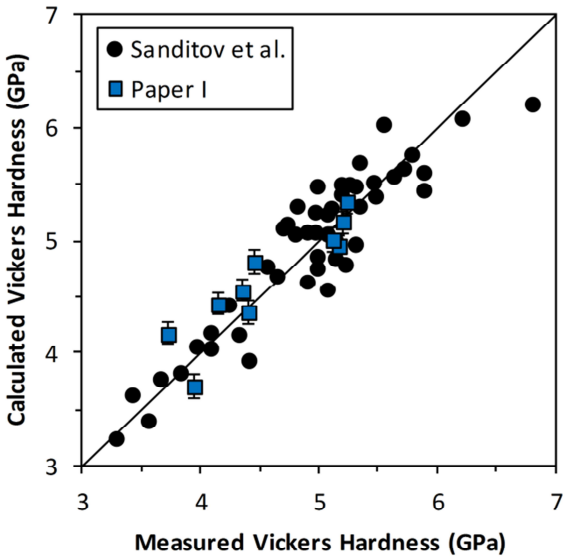

Figure 4.2: Comparison of the calculated Vickers hardness by the Yamane & Mackenzie model and the measured values for silicate glasses from Paper I and Sanditov et al. [121]. The proportionality constant is found by fitting the measured hardness values by Sanditov et al. to Eq. (4.2) and is equal to 0.18, very close to the proportionality constant equal to 0.19 found by fitting to silica glass [119].

As can be seen in Figure 4.2 the Yamane & Mackenzie model can describe the Vickers hardness of a variety of glass compositions within an error of about 10 %.

Smedskjaer et al. suggested that the indentation hardness can be determined in the framework of temperature dependent constraint theory [33]. They described the Vickers hardness as a linear function of the number of constraints at room temperature:

$$H_V(x) = \left(\frac{dH_V}{dN_c}\right) \times \left(N_c(x) - N_{c,crit}\right) \tag{4.3}$$

Where $N_c(x)$ is the number of constraints per network forming atom at room temperature for composition x, dH_V/dN_c is a constant and is found to be on the order of 7 to 10 GPa [33], [122]. This constant is expected to contain information about the bond strengths and molar volume of the glass [123]. In the Yamane & Mackenzie model the influence of these parameters is contained in the average bond strength, α, and the elastic constants [124]. $N_{c,crit}$ = 2.5 is the minimum number of constraints per atom necessary for the constraints to affect hardness, and is related to the dimensionality of the network [33].

This constraint approach has been used to accurately describe the compositional dependence of Vickers hardness for soda lime borate [33], borosilicate [34], and boroaluminosilicate glasses [122]. These glasses all have high degrees of polymerization, meaning that the constraints are mostly caused by the network formers. It remains to be seen if Eq. (4.3) can explain the hardness of glass compositions where the relatively weak constraints on the modifiers constitute a significant fraction of the total number of constraints.

4.1.2 Crack formation

During indentation, several types of cracks progressively occur as the load is increased which can in general be understood by the occurrence of an elastic/plastic contact [125], [126]. The type of cracks that form and the load they form at depend on factors such as atmosphere [127], surface condition [128], and temperature [129]. However, with careful measurements, a distinct dependence on glass composition can be measured [130]–[132]. Therefore, the load for crack initiation can be used as a measure of resistance to crack formation, or ‘crack resistance’.

One way of defining the crack resistance is the load corresponding to the formation of on average two radial cracks per Vickers indent [133], as shown in Figure 4.3.

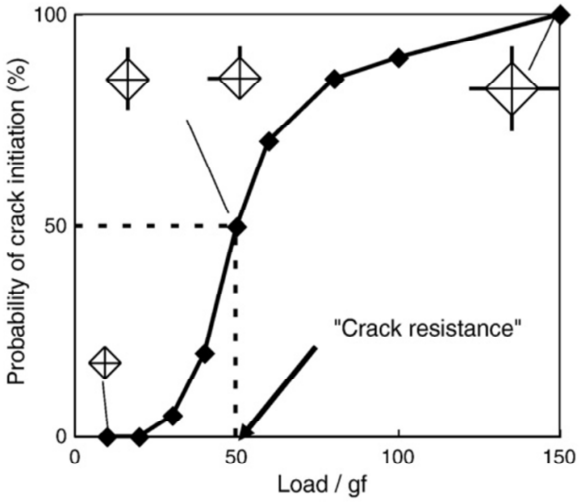

Figure 4.3: The probability of crack initiation as a function of applied load in gram force. The load for crack initiation, or 'crack resistance', corresponds to a probability of crack initiation of 50 %, as indicated by the dotted line [130].

The residual stress, which is the cause of crack formation in glasses [125], seems to be primarily due to the plastic deformation occurring during indentation, while the permanent deformation caused by densification has little or no influence [130], [132], [133].

4.2 Soda lime silicate glasses

4.2.1 Densification and plastic deformation

In Paper I, the compositional dependence of the densified and plastic deformation volumes was characterized for a variety of silicate glasses. The main object of this study was to substantiate the individual resistances to deformation proposed in the Yamane & Mackenzie model of indentation hardness [119].

The silicate glasses were prepared by the melt-quench technique. T_g was determined with a heating rate of 10 K/min using thermomechanical analysis and elastic moduli by ultrasonic measurement of the velocity of sound. The compositions and properties are given in Table III.

4 Compositional dependence of mechanical properties

Table III: The physical properties of the studied glasses: The glass transition temperature (T_g), average bond strength (α), bulk modulus (K), shear modulus (G) and Vickers hardness (H_V) measured at 245 mN and a dwell time of 15 s.

Composition	T_g (K)	α (-)	G (GPa)	K (GPa)	H_V (GPa)
$80SiO_2$ $15Na_2O$ 5CaO	814	0.678	28	39	5.2
$75SiO_2$ $15Na_2O$ 10CaO	841	0.663	29	43	5.2
$75SiO_2$ $15K_2O$ 10CaO	903	0.595	25	39	4.4
$75SiO_2$ $15Na_2O$ 10BaO	727	0.640	23	40	4.2
$75SiO_2$ $15K_2O$ 10BaO	841	0.576	21	34	4.0
$75SiO_2$ $25Na_2O$	763	0.594	24	37	3.7
$71.4SiO_2$ $23.8Na_2O$ 4.8CaO	786	0.585	26	41	4.4
$68.2SiO_2$ $22.7Na_2O$ 9.1CaO	806	0.577	28	45	4.5
$65.2SiO_2$ $21.7Na_2O$ 13CaO	818	0.570	29	48	5.1
$60SiO_2$ $20Na_2O$ 20CaO	831	0.556	31	53	5.2

The densification was quantified by the method used by Yoshida et al. [114]. Twenty crack-free indentations were made at 245 mN and 15 second dwell time, and then imaged by atomic force microscopy (AFM). The samples were annealed at $0.9T_g$ for two hours to relax the densified volume [113] and imaged again by AFM. Densified and plastic deformation volumes are calculated based on a volume balance with the initial indent volume:

$$V_d = \left(V_i^- - V_a^-\right) + \left(V_a^+ - V_i^+\right) \tag{4.4}$$

$$V_p = V_i^- - V_d \tag{4.5}$$

Where V_d is the densified volume and V_p is the plastic deformation volume. Subscript i represents the initial AFM measurement, and a is the AFM measurement after annealing. Superscript '–' indicates the volume beneath the surface level, and '+' above. The method is illustrated in Figure 4.4.

4 Compositional dependence of mechanical properties

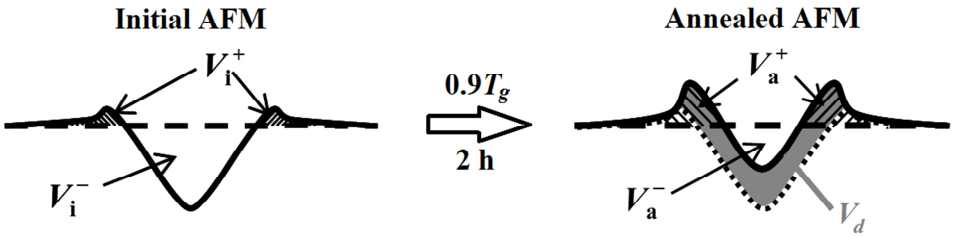

Figure 4.4: The method for determining the densified and plastic deformation volume. Subscript *i* represents the initial AFM measurement, and *a* the AFM measurement after annealing. Superscript – indicates the volume beneath the surface level, and + above. V_d and V_p are determined by the volume balances in Eqs. (4.4) and (4.5). Adapted from [115].

V_d and V_p determined from the AFM measurements before and after annealing are plotted in Figure 4.5.

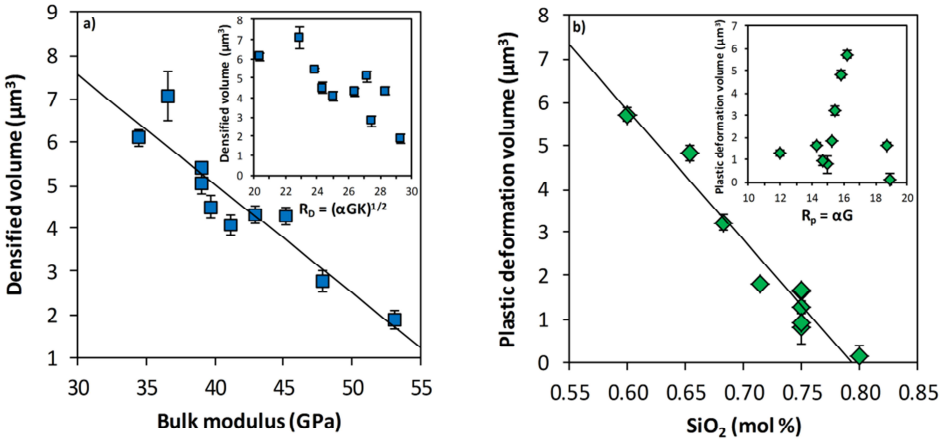

Figure 4.5: a) The best descriptor of the densified volume under a 245 mN indent is the bulk modulus (K). The inset shows the relation to the Yamane & Mackenzie resistance $R_D = (\alpha GK)^{1/2}$. b) For the plastic deformation volume the silica mole fraction (n_{SiO2}) is the best descriptor. The inset shows the relation to the Yamane & Mackenzie resistance $R_P = \alpha G$. The dashed lines are linear fits to the data.

In both the case of the densification and plastic deformation, the Yamane & Mackenzie resistances from Eq. (4.2) correlate rather poorly with the measured deformation volumes, as shown in the insets. The Yamane & Mackenzie model describes the Vickers hardness of the glasses well, as seen in Figure 4.2. However, since the specific resistances in the model do not have the physical meaning that is attributed to them, then the model as a whole must

be considered an empirical relation, which cannot explain the physical origin of indentation hardness.

A much better correlation is found between V_d and the bulk modulus K. K is the elastic resistance to hydrostatic compression, and approximately two-thirds of the mean pressure beneath the Vickers indenter is hydrostatic [134]. Densification is expected when the elastic compression reaches a certain yield value by increasing pressure. Such a yield compression has been observed for a variety of glasses under high pressure hydrostatic compression [110]. Since a higher bulk modulus is likely related to higher yield value, glasses with higher bulk modulus have lower densification volumes.

As shown in Figure 4.5b, the plastic deformation volume decreases linearly with the silica mole fraction. No effect of the modifying ion on the plastic deformation is seen, but this may be due to the low plastic deformation volumes and concurrent relatively high standard deviations of the $75SiO_2 \cdot 15X_2O \cdot 10MO$ (X = Na, K and M = Ca, Ba) glasses. Nonetheless, in the glasses investigated here, the silica content largely determines the compositional dependence of the plastic deformation volumes. It has been proposed that the mechanism of plastic deformation in glasses is slipping between modifier rich planes in the structure due to their relatively low bonding energy [135]. This could be a reason of the observed phenomenon. It is interesting to note that the deformation tends to zero around 80 mole % silica, which corresponds quite well to the concentration where modifier rich channels start forming according to the modified random network model [10], and has also been found to be isostatic in the case of sodium silicate [27].

It was attempted to use these correlations to create a new model in the spirit of Yamane & Mackenzie. Unfortunately, a better description of the Vickers hardness of glasses could not be found.

4.2.2 Relation between crack resistance and plastic deformation

Previous results indicate that the plastic deformation, and not the densification, occurring during indentation is the cause of residual stress that induces cracking in glass. If this is the case, then the compositions with low plastic deformation volumes are expected to have high crack resistances. In order to test this hypothesis the crack resistance of three of the low plastic deformation compositions was characterized. All samples were acclimatized for 24 hours to the testing conditions (25°C and 30% relative humidity) before the measurements. The crack resistance was determined as the load at which an average of two cracks initiated from the corners of the indent, as sketched in Figure 4.3. Twenty Vickers indentations were made at five to seven loads on each sample. The results are shown in Figure 4.6.

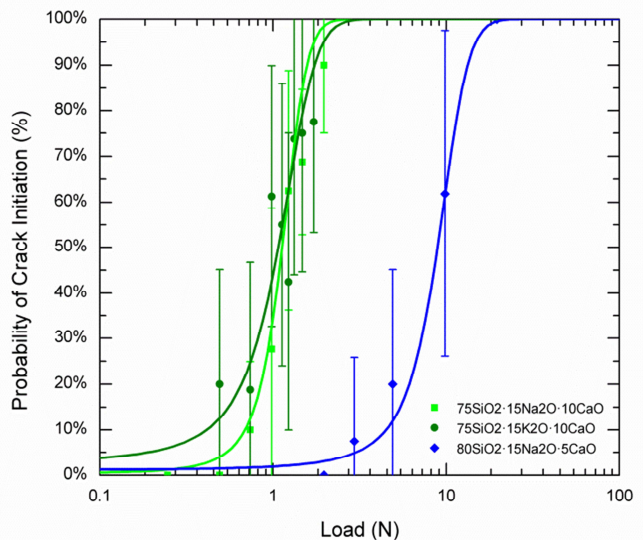

Figure 4.6: The probability of crack initiation vs. applied load for three glass compositions with low plastic deformation volumes at 245 mN. The crack resistance was determined by a sigmoidal fit to the data, and is defined as the load corresponding to a probability of crack initiation equal to 50 %.

The $80SiO_2$ composition has ~7 times larger crack resistance than the $75SiO_2$ compositions. The $75SiO_2$ compositions have about the same plastic deformation volumes at 245 mN as seen in Figure 4.5b, while the $80SiO_2$ composition has approximately zero plastic deformation at this load. The sample size in this study is very small due to the time consuming measurements, but the results support the previous studies that link the plastic deformation to the cracking behavior of glasses.

4.3 Calcium borophosphate glasses

The Vickers hardness of the $zCa(B_4O_7)$ $(1\text{-}z)Ca(PO_3)_2$ glasses was determined on mirror-polished samples as the average of 25 crack-free indentations performed at 490 mN with a 10 s dwell time. The Vickers hardness is plotted as a function of z together with T_g in Figure 4.7.

4 Compositional dependence of mechanical properties

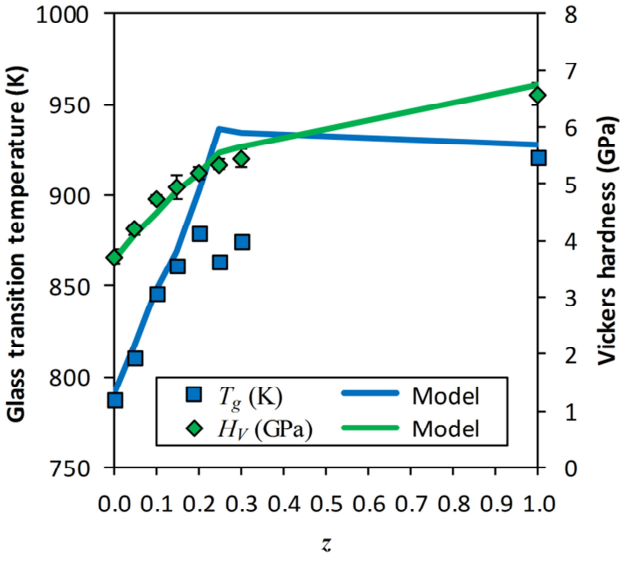

Figure 4.7: On the left hand axis are experimental and modeled glass transition temperature (T_g) by Eq. (3.4) and Eq. (3.25) is plotted as a function of z for zCa(B_4O_7) (1-z)Ca(PO_3)$_2$ glasses. On the right hand axis experimental and modeled Vickers hardness (H_V) by Eq. (4.3) and the room temperature constraints found in Eq. (3.26). dH_V/dN_c = 9.4 GPa is obtained by fitting, and $N_{c,crit}$ = 2.5 is assumed based on previous results [33], [34].

The general trend of H_V is similar to that of T_g, which indicates a similar origin of the two properties. Therefore, it was attempted to model H_V of the calcium borophosphate glasses by temperature dependent constraint theory and Eq. (4.3).

The same constraints as described in Section 3.3 are considered. The only difference is that more constraints are intact because indentation hardness is measured at room temperature. Specifically, the α, β, γ, and δ constraints are all considered fully intact, and the analytical expression for $N_c(z)$ becomes:

$$\begin{aligned} N_c(z)\times N_{atoms}(z) = {} & 3\times[\mathrm{BO}]+1\times[\mathrm{NBO}] \\ & +3\times\left(\left[\mathrm{P}^3\right]+\left[\mathrm{B}^3\right]+\left[\mathrm{B}^2\right]+\left[\mathrm{B}^1\right]+\left[\mathrm{B}^0\right]\right) \\ & +5\times\left(\left[\mathrm{B}^4\right]+\left[\mathrm{P}^2\right]+\left[\mathrm{P}^1\right]+\left[\mathrm{P}^0\right]\right) \\ & +\mathrm{CN}\times[\mathrm{Ca}]_{\mathrm{NBO}}+2\times[\mathrm{Ca}]_{\mathrm{B}^4} \end{aligned} \tag{4.6}$$

Where CN = 6, as found in Paper IV, and $N_{c,atoms}(z)$ is defined in Eq. (3.26). dH_V/dN_c = 9.4 GPa is obtained by fitting to the measured Vickers hardness, and $N_{c,crit}$ = 2.5 is assumed based on previous results [33], [34], [122]. The modeled $H_V(z)$ is plotted in Figure 4.7 and is in excellent agreement with data.

4.4 Sodium phosphosilicate glasses

The Vickers hardness of the $0.3Na_2O$ $0.7[ySiO_2$ $(1\text{-}y)P_2O_5]$ glasses was determined on mirror-polished samples as the average of 25 crack-free indentations performed at 490 mN with a 10 s dwell time. The Vickers hardness is plotted as a function of y together with T_g in Figure 4.8.

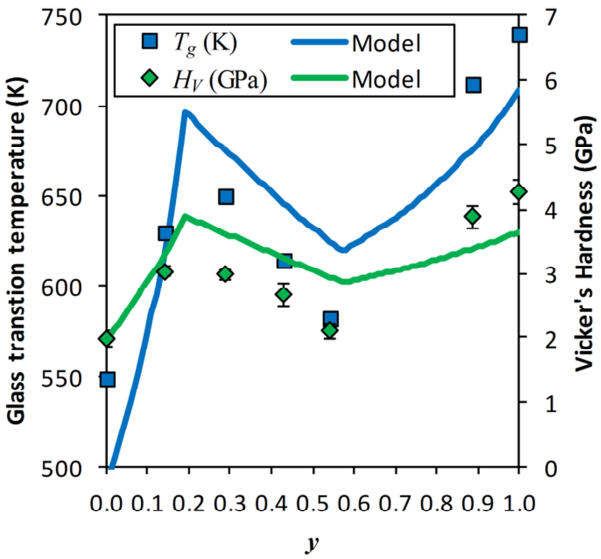

Figure 4.8: On the left hand axis are experimental and modeled glass transition temperature (T_g) by Eq. (3.4) and Eq. (3.7) is plotted as a function of y for $0.3Na_2O$ $0.7[ySiO_2$ $(1\text{-}y)P_2O_5]$ glasses. On the right hand axis are experimental and modeled Vickers hardness (H_V) by Eq. (4.3) and the room temperature constraints found in Eq. (4.7). dH_V/dN_c = 7.5 GPa is obtained by fitting, and $N_{c,crit}$ = 2.5 is assumed based on previous results [33], [34].

As for the calcium borophosphate glasses, the general trend of H_V is very similar to that of T_g. The H_V of the sodium phosphosilicate glasses is modeled by temperature dependent constraint theory and Eq. (4.3). The same constraints as described in Section 3.4 are considered. The only difference is that more constraints are intact because indentation hardness is measured at room temperature. Specifically, the α, β, δ constraints are all

considered fully intact. The number of γ constraints also increase, as the constraint strength at T_g, $q_\gamma = 0.4$, increases to $q_\gamma = 0.6$ at room temperature, corresponding to three constraints per Na^+. The analytical expression for $N_c(x,y)$ becomes:

$$\begin{aligned} N_c(x,y) \times N_{atoms}(x,y) = {} & 3\times[\mathrm{BO}] + 1\times[\mathrm{NBO}] \\ & + 3\times[\mathrm{P}^3] + 9\times[\mathrm{Si}^6] \\ & + 5\times\left([\mathrm{Si}^4] + [\mathrm{Si}^3] + [\mathrm{Si}^2] + [\mathrm{P}^2] + [\mathrm{P}^1] + [\mathrm{P}^0]\right) \\ & + q_\gamma \times \mathrm{CN} \times [\mathrm{R}] \end{aligned} \tag{4.7}$$

Where CN = 5 and N_{atoms} is defined in Eq. (3.28). The modeled composition dependence of H_V by Eq. (4.3) combined with Eq. (4.7) using $(dH_V/dN_c) = 7.5$ GPa and $N_{c,crit} = 2.5$ is plotted in Figure 4.8. The compositional trend is reasonably replicated, but with significant errors. The trend in the difference between model and experiment is very similar for both T_g and H_V, and is expected to have the same origin, but the magnitude is larger for H_V.

5 General discussion

Structural models of borophosphate and phosphosilicate glasses have been developed by invoking topological rules. For borophosphate glasses the rule is that B^4 network forming units (NFUs) cannot be direct neighbors, and for phosphosilicates the rule is that Si^6 bonds to 6 P^3 NFUs, which can only have one Si^6 NFU neighbor. The structural models are confirmed by nuclear magnetic resonance, Raman, and O 1s X-ray photoelectron spectroscopy. However, these topological models cannot describe finer details of the network former speciation, such as the fictive temperature dependence on the B^4 concentration [34], or disproportionation of P^2 in calcium phosphate glass [57]. In order to account for such effects, and develop a more accurate structural model, statistical mechanics can be employed [136]. However the simple topological models adequately describe the structure and topology of the mixed network former glasses for the present purpose.

The dynamic properties such as the glass transition temperature (T_g) and fragility have been related to the structure of the glass by temperature dependent constraint theory. The study of the compositional dependence of T_g of phosphoric acids clearly shows that depolymerizing the phosphate network decreases the number of constraints. It is also found that the one-fold coordinated double-bonded terminal oxygen (TO) are best treated by plucking them from the network, while the one-fold coordinated hydrogen are considered part of the network with one linear bond stretching constraint. The TO can also be treated in the same way, which gives a similar compositional dependence of T_g.

The trend in the compositional dependence of T_g in alkali phosphate glasses can be accounted for by the alkali ions forming cross-linking sites at concentrations above x_{crit}, which is related to the coordination number. This cross-linking of the modifier polyhedra is denoted as the modifying ion sub-network. Hoppe's structural model support the formation of a modifying ion sub-network based on based on numerous diffraction experiments of phosphate glasses [51]. The magnitude of T_g decreases with the size of the alkali ion in phosphate glasses. This effect can be quantified by a constraint strength parameter, which is a measure of the degree to which the modifier constraints are intact at T_g.

The number of intact modifier constraints at T_g for alkali, alkaline earth, and rare earth metaphosphate glasses is found to correlate with the charge-to-distance ratio, which is a measure of the coulombic force between the modifying ion and the non-bridging oxygen [93]. This result shows that the modifier constraints are of ionic nature, and provides a method for empirically finding their number. The maximum number of modifier constraints seems to be the coordination number of the modifier, and this maximum is achieved for small modifying ions with low coordination numbers. The universality of the results is

investigated by applying them to mixed network former borophosphate and phosphosilicate glasses.

For alkali borophosphate glasses the T_g appears to be limited by the onset temperature of the boron centered angular constraints, $T_{\beta,B}$, as previously found in alkali borates [32]. An empirical relation between this onset temperature and the degree of polymerization of the network is suggested, which is in excellent agreement with experimental results. Whether it is physically reasonable to assume that T_g is limited by such an onset temperature is critically discussed. The high fragility of the glasses with $T_g = T_{\beta,B}$ is in favor of the current explanation, but perhaps the intermediate range order in borate-rich glasses is the cause of the plateau in T_g. Interestingly, $T_{\beta,B}$ is not needed to explain the behavior of T_g in calcium borophosphate glasses, but the fragility data still suggest $T_g \approx T_{\beta,B}$.

The temperature dependent constraint model replicates the trend in T_g of the sodium phosphosilicate glasses well, with a local maximum at the peak of the Si^6 fraction, and a minimum Si^6 disappears. However, the model has significant positive and negative deviation from experiment. This deviation is thought to be caused by constraint strength of the modifier constraints changing from the phosphate-rich glasses to the silicate-rich. A recent molecular dynamics study of soda lime silicate glasses show that the number of modifier constraints changes with the composition in silicate glasses [30].

The temperature dependent nature of the constraints is verified by modeling the indentation hardness of calcium borophosphate and sodium phosphosilicate glasses. The compositional trend of Vickers hardness, H_V, mimics that of T_g for both systems, which indicates that a constraint interpretation of indentation hardness is reasonable. H_V could be modeled for both systems by taking the bridging oxygen angular constraint to be intact and increasing the modifier constraint strength. For calcium borophosphate glasses the modifier constraint strength is found to be unity, as expected, however for sodium phosphosilicate glasses the modifier constraint strength is only 0.6 at room temperature. More work is necessary to determine if the temperature interval where the sodium modifier constraints go from intact to broken is very wide, or if there is another explanation for this unexpected result.

The origin of hardness is investigated in more detail by characterizing the densification and plastic deformation occurring during indentation for a series of soda lime silicate glasses. Specifically, the assumptions of specific resistances to densification and plastic deformation in the semi-empirical Yamane & Mackenzie model is tested [119]. The proposed resistances are found not to describe the measured deformation volumes well. Instead it is proposed that the resistance to densification is the bulk modulus, and the

resistance to plastic deformation is the silica content. However, it was not possible to use these findings to create an improved model for indentation hardness. In fact, the now confirmed empirical Yamane & Mackenzie model can describe the Vickers hardness of the glasses quite well. Perhaps the Yamane & Mackenzie model has a still unknown physical interpretation that explains its predictive power.

The relation between crack resistance and plastic deformation is investigated for the silicate glasses exhibiting low plastic deformation. The glass with the lowest degree of plastic deformation has ~7 times higher crack resistance than two glasses which exhibit higher and similar plastic deformation volumes. These results indicate that a low bulk modulus and high silica fraction should give a highly crack resistant silicate glass.

5 General discussion

6 Conclusion and perspectives

The relation between structure and properties has been investigated for phosphate-based glasses by use of temperature dependent constraint theory. This investigation has yielded insight into what determines properties such as the glass transition temperature, fragility, and indentation hardness, and how to deal with one-fold coordinated atoms and network modifiers in the framework of temperature dependent constraint theory.

The network modifiers are found to strongly influence the properties of phosphate-based glasses, both by their depolymerizing effect, but also by their ionic bonding to non-bridging oxygen. The compositional dependence of the glass transition temperature of alkali phosphate glasses was explained by the concept of a 'modifying ion sub-network', which is a cross-linking of modifier polyhedra occurring at a certain critical concentration of modifier.

Although the modifier constraints are of an ionic nature, the number of modifier constraints at the glass transition temperature is still equal to their coordination numbers in the limit of high charge-to-distance modifiers. Larger alkali ions have higher coordination numbers, but give a lower glass transition temperature in phosphate-based glasses. This is because they have weaker coulombic interaction with the non-bridging oxygen, as seen by their lower charge-to-distance ratio. The concept of 'constraint strength' was introduced to quantify this effect.

Structural models have been developed for mixed network former borophosphate and phosphosilicate glasses based on the measured structure and topology. These structural models can predict the short-range order and topology of the mixed network former glasses with reasonable accuracy by assuming some simple topological rules.

The structural models for borophosphate and phosphosilicate glasses were used in conjunction with temperature dependent constraint theory to prove the universality of the results obtained for binary phosphate glasses. For borophosphate glasses the modifying ion sub-network and constraint strength does very well in describing the compositional dependence of glass transition temperature, fragility, and indentation hardness. In the case of phosphosilicate glasses the compositional trends of these properties are replicated well, but with some errors in magnitude.

The relation between hardness and permanent deformation mechanisms has also been investigated for the commercially important soda lime silicate system, as well as analogous potassium and barium silicates. The densification was found to decrease approximately linearly with the bulk modulus, and the plastic deformation with silica content. However,

no apparent correlation was found between these deformation mechanism and indentation hardness. Another mechanical property, the crack resistance, was found to be related to the plastic deformation. The glass with the lowest degree of plastic deformation has ~7 times higher crack resistance than the glasses with the second lowest degree of plastic deformation.

The results obtained in this thesis have important implications for understanding glass formation and the glass transitions, and for characterizing composition-structure-property relations in oxide glasses. Simple topological models have been derived that predict the general structural trends in mixed network former borophosphate and phosphosilicate glasses. Also, several difficulties in applying temperature dependent constraint theory to oxide glasses have been addressed, such as the effect on one-fold coordinated atoms, and the how to treat the network modifiers. The picture that emerges is that the network formers are straightforward to deal with, but the network modifiers are more difficult. In this thesis it is suggested to treat the modifier constraints semi-empirically through a constraint strength parameter. The advantage of this approach is that the calculations are fairly simple and can be performed with pen and paper or a spreadsheet. The disadvantage is that this approach may ignore important aspects of the structure-property relation.

The study of the composition dependence of the deformation mechanisms in silicate glasses revealed that the Yamane & Mackenzie model for indentation hardness is empirical. Moreover, the relations between the deformation volumes and glass properties could not be used to develop a better model for indentation hardness. It must be concluded that our understanding of indentation hardness as a material property is still incomplete. The compositional dependence of indentation hardness in borophosphate and phosphosilicate glasses was described well by a linear scaling with the number of network constraints. This result indicates that a microscopic description of indentation hardness could be within reach. This is in contrast to the macroscopic description employed by Yamane & Mackenzie, who use macroscopic properties such as the average bond strength and the elastic constants to theoretically describe hardness.

7 Bibliography

[1] M. D. Lund, “Tensile strength of glass fibers,” Aalborg University, 2010.

[2] L. Wondraczek, J. C. Mauro, J. Eckert, U. Kühn, J. Horbach, J. Deubener, and T. Rouxel, “Towards Ultrastrong Glasses,” *Adv. Mater.*, vol. 23, pp. 4578–4586, Sep. 2011.

[3] J. E. Shelby, *Introduction To Glass Science and Technology*, 2nd ed. Cambridge: The Royal Society of Chemistry, 2005.

[4] J. C. Mauro, Y.-Z. Yue, A. J. Ellison, P. K. Gupta, and D. C. Allan, “Viscosity of glass-forming liquids.,” *Proc. Natl. Acad. Sci. U. S. A.*, vol. 106, no. 47, pp. 19780–4, Nov. 2009.

[5] P. W. Anderson, “Through the glass lightly,” *Science (80-.).*, vol. 267, p. 1615, 1995.

[6] J. C. Mauro, P. K. Gupta, and R. J. Loucks, “Continuously broken ergodicity.,” *J. Chem. Phys.*, vol. 126, no. 18, p. 184511, May 2007.

[7] J. C. Mauro, R. J. Loucks, and S. Sen, “Heat capacity, enthalpy fluctuations, and configurational entropy in broken ergodic systems.,” *J. Chem. Phys.*, vol. 133, no. 16, p. 164503, Oct. 2010.

[8] J. C. Phillips, “The Physics of glass,” *Phys. Today*, vol. 35, no. 2, pp. 27–33, 1982.

[9] W. H. Zachariasen, “The atomic arrangement in glass,” *J. Am. Chem. Soc.*, vol. 54, no. 10, pp. 3841–3851, Oct. 1932.

[10] G. N. Greaves and S. Sen, “Inorganic glasses, glass-forming liquids and amorphizing solids,” *Adv. Phys.*, vol. 56, no. 1, pp. 1–166, Jan. 2007.

[11] A. I. Priven, “General method for calculating the properties of oxide glasses and glass forming melts from their composition and temperature,” *Glas. Technol.*, vol. 45, no. 6, pp. 244–54, 2004.

[12] G. N. Greaves, W. Smith, E. Giulotto, and E. Pantos, “Local structure, microstructure and glass properties,” *J. Non. Cryst. Solids*, vol. 222, pp. 13–24, 1997.

[13] J. C. Maxwell, “On the calculation of the equilibrium and stiffness of frames,” *Philos. Mag.*, vol. 27, p. 294, 1864.

[14] J. C. Phillips, “Topology of covalent non-crystalline solids I: Short-range order in chalcogenide alloys,” *J. Non. Cryst. Solids*, vol. 34, pp. 153–181, 1979.

[15] M. Bauchy, M. Micoulaut, M. Celino, S. Le Roux, M. Boero, and C. Massobrio, “Angular rigidity in tetrahedral network glasses with changing composition,” *Phys. Rev. B*, vol. 84, no. 5, p. 054201, Aug. 2011.

7 Bibliography

[16] P. Boolchand, D. G. Georgiev, and B. Goodman, “Discovery of the intermediate phase in chalcogenide glasses,” *J. Optoelectron. Adv. Mater.*, vol. 3, no. 3, pp. 703–720, 2001.

[17] P. Boolchand, D. G. Georgiev, and M. Micoulaut, “Nature of glass transition in chalcogenides,” *J. Optoelectron. Adv. Mater.*, vol. 4, no. 4, pp. 823–836, 2002.

[18] M. Micoulaut, “Rigidity and intermediate phases in glasses driven by speciation,” *Phys. Rev. B*, vol. 74, no. 18, pp. 2–6, Nov. 2006.

[19] M. Micoulaut, “Simple clues and rules for self-organized rigidity in glasses,” *J. Optoelectron. Adv. Mater.*, vol. 9, no. 10, pp. 3235–3240, 2007.

[20] M. Tatsumisago, B. L. Halfpap, J. L. Green, S. M. Lindsay, and C. A. Angell, “Fragility of Ge-As-Se glass-forming liquids in relation to rigidity percolation, and the Kauzmann paradox,” *Phys. Rev. Lett.*, vol. 64, no. 13, pp. 1549–1552, 1990.

[21] K. Gunasekera, S. Bhosle, P. Boolchand, and M. Micoulaut, “Superstrong nature of covalently bonded glass-forming liquids at select compositions.,” *J. Chem. Phys.*, vol. 139, no. 16, p. 164511, Oct. 2013.

[22] M. Micoulaut, “Linking rigidity transitions with enthalpic changes at the glass transition and fragility: insight from a simple oscillator model.,” *J. Phys. Condens. Matter*, vol. 22, no. 28, p. 285101, Jul. 2010.

[23] G. Yang, B. Bureau, T. Rouxel, Y. Gueguen, O. Gulbiten, C. Roiland, E. Soignard, J. Yarger, J. Troles, J.-C. Sangleboeuf, and P. Lucas, “Correlation between structure and physical properties of chalcogenide glasses in the As(x)Se(1−x) system,” *Phys. Rev. B*, vol. 82, no. 19, pp. 1–8, Nov. 2010.

[24] G. Yang, Y. Gueguen, J.-C. Sangleboeuf, T. Rouxel, C. Boussard-Plédel, J. Troles, P. Lucas, and B. Bureau, “Physical properties of the Ge(x)Se(1−x) glasses in the $0<x<0.42$ range in correlation with their structure,” *J. Non. Cryst. Solids*, vol. 377, pp. 54–59, Oct. 2013.

[25] T. Wang, O. Gulbiten, R. Wang, Z. Yang, A. Smith, B. Luther-Davies, and P. Lucas, “Relative contribution of stoichiometry and mean coordination to the fragility of Ge-As-Se glass forming liquids.,” *J. Phys. Chem. B*, vol. 118, no. 5, pp. 1436–1442, Feb. 2014.

[26] Y. Vaills, T. Qu, M. Micoulaut, F. Chaimbault, and P. Boolchand, “Direct evidence of rigidity loss and self-organization in silicate glasses,” *J. Phys. Condens. Matter*, vol. 17, no. 32, pp. 4889–4896, Aug. 2005.

[27] M. Micoulaut, “Constrained interactions, rigitidy, adaptive networks, and their role for the description of silicates,” *Am. Mineral.*, vol. 93, no. 11–12, pp. 1732 – 1748, Nov. 2008.

7 Bibliography

[28] M. Bauchy and M. Micoulaut, “Atomic scale foundation of temperature-dependent bonding constraints in network glasses and liquids,” *J. Non. Cryst. Solids*, vol. 357, no. 14, pp. 2530–2537, Jul. 2011.

[29] J. C. Phillips and R. Kerner, “Structure and function of window glass and Pyrex.,” *J. Chem. Phys.*, vol. 128, no. 17, p. 174506, May 2008.

[30] O. Laurent, B. Mantisi, and M. Micoulaut, “Structure and topology of soda-lime silicate glasses: implications for window glass.,” *J. Phys. Chem. B*, vol. 118, no. 44, pp. 12750–62, Nov. 2014.

[31] P. K. Gupta and J. C. Mauro, “Composition dependence of glass transition temperature and fragility. I. A topological model incorporating temperature-dependent constraints.,” *J. Chem. Phys.*, vol. 130, no. 9, p. 094503, Mar. 2009.

[32] J. C. Mauro, P. K. Gupta, and R. J. Loucks, “Composition dependence of glass transition temperature and fragility. II. A topological model of alkali borate liquids.,” *J. Chem. Phys.*, vol. 130, no. 23, p. 234503, Jun. 2009.

[33] M. M. Smedskjaer, J. C. Mauro, and Y.-Z. Yue, “Prediction of Glass Hardness Using Temperature-Dependent Constraint Theory,” *Phys. Rev. Lett.*, vol. 105, p. 115503, 2010.

[34] M. M. Smedskjaer, J. C. Mauro, R. E. Youngman, C. L. Hogue, M. Potuzak, and Y.-Z. Yue, “Topological principles of borosilicate glass chemistry.,” *J. Phys. Chem. B*, vol. 115, no. 44, pp. 12930–12946, Nov. 2011.

[35] R. K. Brow, “Review: the structure of simple phosphate glasses,” *J. Non. Cryst. Solids*, vol. 263–264, pp. 1–28, Mar. 2000.

[36] P. McMillan, “Structural studies of silicate glasses and melts-applications and limitations of Raman spectroscopy,” *Am. Mineral.*, vol. 69, pp. 622–644, 1984.

[37] Q. Zheng, M. M. Smedskjaer, R. E. Youngman, M. Potuzak, J. C. Mauro, and Y. Yue, “Influence of aluminum speciation on the stability of aluminosilicate glasses against crystallization,” *Appl. Phys. Lett.*, vol. 101, no. 4, p. 041906, 2012.

[38] M. G. Mortuza, J. a. Chudek, G. Hunter, and M. R. Ahsan, “First evidence for the coexistence of four-, five- and six-coordinated silicon in glasses prepared at ambient pressure,” *Chem. Commun.*, no. 20, pp. 2055–2056, 2000.

[39] P. K. Gupta and A. R. Cooper, “Topologically Disordered Networks of Rigid Polytopes,” *J. Non. Cryst. Solids*, vol. 123, pp. 14–23, 1990.

[40] M. T. Rinke and H. Eckert, “The mixed network former effect in glasses: solid state NMR and XPS structural studies of the glass system (Na2O)(x)(BPO4)(1-x).,” *Phys. Chem. Chem. Phys.*, vol. 13, no. 14, pp. 6552–65, Apr. 2011.

[41] K. J. Rao, *Structural Chemistry of Glasses*. Oxford: Elsevier, 2002.

7 Bibliography

[42] R. Kerner and J. C. Phillips, “Quantitative principles of silicate glass chemistry,” *Solid State Commun.*, vol. 117, pp. 47–51, 2000.

[43] A. C. A. C. Wright, “Borate Structures: Crystalline and Vitreous,” *Phys. Chem. Glas. Eur. J. Glas. Sci. Technol. B*, vol. 51, no. 1, pp. 1–39, 2008.

[44] U. Hoppe, D. Stache, and D. Beyer, “The Oxygen Coordination of Metal Ions in Phosphate and Silicate Glasses Studied by a Combination of X-ray and Neutron Diffraction,” *Phys. Scr.*, vol. 57, pp. 122–126, 1995.

[45] T. M. Alam, S. Conzone, R. K. Brow, and T. J. Boyle, “6Li, 7Li nuclear magnetic resonance investigation of lithium coordination in binary phosphate glasses,” *J. Non. Cryst. Solids*, vol. 258, pp. 140–154, 1999.

[46] G. N. Greaves, “EXAFS and the structure of glass,” *J. Non. Cryst. Solids*, vol. 71, pp. 203–217, 1985.

[47] K. Suzuya, D. L. Price, C.-K. Loong, and S. W. Martin, “Structure of vitreous P2O5 and alkali phosphate glasses,” *J. Non. Cryst. Solids*, vol. 232–234, pp. 650–657, Jul. 1998.

[48] J. J. Hudgens, R. K. Brow, D. R. Tallant, and S. W. Martin, “Raman spectroscopy study of the structure of lithium and sodium ultraphosphate glasses,” *J. Non. Cryst. Solids*, vol. 223, pp. 21–31, 1998.

[49] J. R. Van Wazer, *Phosphorous and its Compounds*. New York: Interscience, 1958.

[50] R. K. Brow, D. R. Tallant, J. J. Hudgens, S. W. Martin, and A. D. Irwin, “The short-range structure of sodium ultraphosphate glasses,” *J. Non. Cryst. Solids*, vol. 177, pp. 221–228, Nov. 1994.

[51] U. Hoppe, “A structural model for phosphate glasses,” *J. Non. Cryst. Solids*, vol. 195, no. 1–2, pp. 138–147, Feb. 1996.

[52] D. Larink, H. Eckert, M. Reichert, and S. W. Martin, “Mixed Network Former Effect in Ion-Conducting Alkali Borophosphate Glasses: Structure/Property Correlations in the System [M2O]1/3[(B2O3)x(P2O5)1−x]2/3 (M = Li, K, Cs),” *J. Phys. Chem. C*, vol. 116, pp. 26162–26176, 2012.

[53] M. Schuch, C. Trott, and P. Maass, “Network forming units in alkali borate and borophosphate glasses and the mixed glass former effect,” *RSC Adv.*, vol. 1, no. 7, pp. 1370–1382, 2011.

[54] P. Beekenkamp, “Physics of Non-Crystalline Solids,” in *Physics of Non-Crystalline Solids*, J. A. Prins, Ed. Amsterdam: North-Holland, 1965, p. 512.

[55] P. K. Gupta, “The Random-Pair Model of Four-Coordinatied Borons in Alkali-Borate Glasses,” in *International Congress on Glass*, 1986, pp. 1–10.

[56] M. Schmidt, B. Ewald, Y. Prots, R. Cardoso-Gil, M. Armbrüster, I. Loa, L. Zhang, Y.-X. Huang, U. Schwarz, and R. Kniep, “Growth and Characterization of BPO4

Single Crystals," *Zeitschrift für Anorg. und Allg. Chemie*, vol. 630, no. 5, pp. 655–662, May 2004.

[57] J. P. Fletcher, R. J. Kirkpatrick, D. Howell, and S. H. Risbud, "31P Magic-angle spinning nuclear magnetic resonance spectroscopy of calcium phosphate glasses," *J. Chem. Soc. Faraday Trans.*, vol. 89, no. 17, pp. 3297–3299, 1993.

[58] D. Maniu, T. Iliescu, I. Ardelean, S. Cinta-Pinzaru, N. Tarcea, and W. Kiefer, "Raman study on B2O3–CaO glasses," *J. Mol. Struct.*, vol. 651–653, pp. 485–488, Jun. 2003.

[59] J. E. Pemberton, L. Latifzadeh, J. P. Fletcher, and S. H. Risbud, "Raman Spectroscopy of Calcium Phosphate Glasses with Varying CaO Modifier Concentrations," *Chem. Mater.*, vol. 3, pp. 195–200, 1991.

[60] T. L. Barr and S. Seal, "Nature of the use of adventitious carbon as a binding energy standard," *J. Vac. Sci. Technol. A Vacuum, Surfaces, Film.*, vol. 13, no. 3, p. 1239, May 1995.

[61] T. L. Weeding, B. H. W. S. de Jong, W. S. Veeman, and B. G. Aitken, "Silicon coordination changes from 4-fold to 6-fold on devitrification of silicon phosphate glass," *Nature*, vol. 318, pp. 352–353, 1985.

[62] J. A. Duffy and D. E. Macphee, "The Coordination Number of Silicon in Silicon - Oxygen Compounds : The Special Case of 6-Fold Coordination in Thaumasite," *J. Phys. Chem. B*, vol. 111, pp. 8740–8745, 2007.

[63] J. D. Mackenzie, "Applications of Zachariasen's Rules to Different Types of Non-Crystalline Solids," *J. Non. Cryst. Solids*, vol. 96, pp. 441–448, 1987.

[64] D. Miyabe, M. Takahashi, Y. Tokuda, T. Yoko, and T. Uchino, "Structure and formation mechanism of six-fold coordinated silicon in phosphosilicate glasses," *Phys. Rev. B*, vol. 71, no. 17, p. 172202, May 2005.

[65] R. E. Youngman, C. L. Hogue, and B. G. Aitken, "Crystallization of Silicon Pyrophosphate from Silicophosphate Glasses as Monitored by Multi-Nuclear NMR," *MRS Proc.*, vol. 984, pp. 0984–MM12–03, 2006.

[66] H. Yamashita, H. Yoshino, K. Nagata, I. Yamaguchi, M. Ookawa, and T. Maekawa, "NMR and Raman Studies of Na2O-P2O5-SiO2 Glasses," *J. Ceram. Soc. Japan*, vol. 106, no. 6, pp. 539–544, 1998.

[67] V. G. Plotnichenko, V. O. Sokolov, V. V. Koltashev, and E. M. Dianov, "On the structure of phosphosilicate glasses," *J. Non. Cryst. Solids*, vol. 306, no. 3, pp. 209–226, Sep. 2002.

[68] B. Mysen, "Phosphorus speciation changes across the glass transition in highly polymerized alkali silicate glasses and melts," *Am. Mineral.*, vol. 81, pp. 1531–1534, 1996.

7 Bibliography

[69] J. a. Duffy, “Optical Basicity: A Practical Acid-Base Theory for Oxides and Oxyanions,” *J. Chem. Educ.*, vol. 73, no. 12, p. 1138, Dec. 1996.

[70] Q. Jiang, H. Zeng, X. Li, J. Ren, G. Chen, and F. Liu, “Tailoring sodium silicophosphate glasses containing SiO6-octahedra through structural rules and topological principles.,” *J. Chem. Phys.*, vol. 141, no. 12, p. 124506, Sep. 2014.

[71] J. Ide, K. Ozutsumi, H. Kageyama, K. Handa, and N. Umesaki, “XAFS study of six-coordinated silicon in R2O–SiO2–P2O5 (R=Li, Na, K) glasses,” *J. Non. Cryst. Solids*, vol. 353, no. 18–21, pp. 1966–1969, Jun. 2007.

[72] T. Sekiya, N. Mochida, A. Ohtsuka, and K. Uchida, “6-Coordinated Si4+ in SiO2-PO5/2 Glasses,” *J. Ceram. Soc. JAPAN*, vol. 96, no. 5, pp. 571–573, 1988.

[73] K. Leinenweber, L. a. Stearns, J. M. Nite, P. Németh, and T. L. Groy, “Structure of a new form of silicon phosphate (SiP2O7) synthesized at high pressures and temperatures,” *J. Solid State Chem.*, vol. 190, pp. 221–225, Jun. 2012.

[74] C. A. Angell, “Formation of glasses from liquids and biopolymers,” *Science (80-.).*, vol. 267, pp. 1924–1935, Mar. 1995.

[75] Y.-Z. Yue, “The iso-structural viscosity, configurational entropy and fragility of oxide liquids,” *J. Non. Cryst. Solids*, vol. 355, no. 10–12, pp. 737–744, May 2009.

[76] G. Adam and J. H. Gibbs, “On the Temperature Dependence of Cooperative Relaxation Properties in Glass-Forming Liquids,” *J. Chem. Phys.*, vol. 43, no. 1, pp. 139–146, 1965.

[77] Y. Bottinga and P. Richet, “Silicate melt structural relaxation: rheology, kinetics, and Adam-Gibbs theory,” *Chem. Geol.*, vol. 128, pp. 129–141, Jun. 1996.

[78] Q. Zheng, J. C. Mauro, A. J. Ellison, M. Potuzak, and Y.-Z. Yue, “Universality of the high-temperature viscosity limit of silicate liquids,” *Phys. Rev. B*, vol. 83, no. 21, p. 212202, Jun. 2011.

[79] M. J. Toplis, “Energy barriers to viscous flow and the prediction of glass transition temperatures of molten silicates,” *Am. Mineral.*, vol. 83, pp. 480–490, 1998.

[80] G. G. Naumis, “Energy landscape and rigidity,” *Phys. Rev. E*, vol. 71, no. 2, p. 026114, Feb. 2005.

[81] M. M. Smedskjaer, J. C. Mauro, S. Sen, and Y.-Z. Yue, “Quantitative Design of Glassy Materials Using Temperature-Dependent Constraint Theory,” *Chem. Mater.*, vol. 2, no. 7, pp. 445–452, Sep. 2010.

[82] A. K. Hassan, L. M. Torell, L. Börjesson, and H. Doweidar, “Structural changes of B2O3 through the liquid-glass transition range: A Raman-scattering study,” *Phys. Rev. B*, vol. 45, no. 22, pp. 12797–12805, 1992.

[83] L. M. Martinez and C. A. Angell, “A thermodynamic connection to the fragility of glass-forming liquids.,” *Nature*, vol. 410, no. 6829, pp. 663–7, Apr. 2001.

7 Bibliography

[84] R. J. Speedy, “Relations between a Liquid and Its Glasses,” *J. Phys. Chem. B*, vol. 103, no. 20, pp. 4060–4065, May 1999.

[85] M. Potuzak, J. C. Mauro, T. J. Kiczenski, A. J. Ellison, and D. C. Allan, “Communication: Resolving the vibrational and configurational contributions to thermal expansion in isobaric glass-forming systems.,” *J. Chem. Phys.*, vol. 133, no. 9, p. 091102, Sep. 2010.

[86] L.-M. Wang, C. A. Angell, and R. Richert, “Fragility and thermodynamics in nonpolymeric glass-forming liquids.,” *J. Chem. Phys.*, vol. 125, no. 7, p. 074505, Aug. 2006.

[87] R. Fabian and D. Sidebottom, “Dynamic light scattering in network-forming sodium ultraphosphate liquids near the glass transition,” *Phys. Rev. B*, vol. 80, no. 6, p. 064201, Aug. 2009.

[88] D. L. Sidebottom and S. E. Schnell, “Role of intermediate-range order in predicting the fragility of network-forming liquids near the rigidity transition,” *Phys. Rev. B*, vol. 87, no. 5, p. 054202, Feb. 2013.

[89] D. L. Sidebottom, T. D. Tran, and S. E. Schnell, “Building up a weaker network: The effect of intermediate range glass structure on liquid fragility,” *J. Non. Cryst. Solids*, vol. 402, pp. 16–20, Oct. 2014.

[90] M. F. Thorpe, “Continuous deformations in random networks,” *J. Non. Cryst. Solids*, vol. 57, pp. 355–370, 1983.

[91] G. H. Döhler, R. Dandoloff, and H. Bilz, “A Topological-Dynamical Model of Amorphycity,” *J. Non. Cryst. Solids*, vol. 42, pp. 87–96, 1980.

[92] P. Boolchand and M. F. Thorpe, “Glass-forming tendency, percolation of rigidity, and onefold-coordinated atoms in covalent networks,” *Phys. Rev. B*, vol. 50, no. 14, pp. 10366–10368, 1994.

[93] A. Eisenberg, H. Farb, and L. G. Cool, “Glass transition in ionic polymers,” *J. Polym. Sci. Part A-2*, vol. 4, pp. 855–868, 1966.

[94] H. R. Corti, F. J. Nores-Pondal, and C. A. Angell, “Heat capacity and glass transition in P2O5-H2O solutions: support for Mishima’s conjecture on solvent water at low temperature.,” *Phys. Chem. Chem. Phys.*, vol. 13, no. 44, pp. 19741–8, Nov. 2011.

[95] S. W. Martin and C. A. Angell, “On the Glass Transition and Viscosity of P2O5,” *J. Phys. Chem.*, vol. 90, pp. 6736–6740, 1986.

[96] J. J. Hudgens, “The structure and properties of anhydrous, alkali ultra-phosphate glasses,” Iowa State University, 1994.

7 Bibliography

[97] D. Sidebottom and J. Changstrom, “Viscoelastic relaxation in molten phosphorus pentoxide using photon correlation spectroscopy,” *Phys. Rev. B*, vol. 77, no. 2, p. 020201, Jan. 2008.

[98] J. J. Hudgens and S. W. Martin, “Glass transition and infrared spectra of low-alkali, anhydrous lithium phosphate glasses,” *J. Am. Ceram. Soc.*, vol. 76, no. 7, pp. 1691–1696, 1993.

[99] M. Doreau, A. Abou El Anouar, and G. Robert, “Domaine vitreux, structure et conductivite electrique des verres du systeme LiCl-Li2O-P2O5,” *Mat. Res. Bull.*, vol. 15, pp. 285–294, 1980.

[100] C. A. Click, R. K. Brow, and T. M. Alam, “Properties and structure of cesium phosphate glasses,” *J. Non. Cryst. Solids*, vol. 311, no. 3, pp. 294–303, Dec. 2002.

[101] C. T. Moynihan, A. J. Easteal, M. A. DeBolt, and J. Tucker, “Dependence of the Fictive Temperature of Glass on Cooling Rate,” *J. Am. Ceram. Soc.*, vol. 59, no. 1–2, pp. 12–16, 1976.

[102] S. Striepe and J. Deubener, “Viscosity and kinetic fragility of alkaline earth zinc phosphate glasses,” *J. Non. Cryst. Solids*, pp. 3–8, Apr. 2012.

[103] R. D. Shannon, “Revised Effective Ionic Radii and Systematic Studies of Interatomic Distances in Halides and Chalcogenides,” *Acta Crystallogr. Sect. A*, vol. 32, pp. 751–767, 1976.

[104] B. P. Rodrigues and L. Wondraczek, “Cationic constraint effects in metaphosphate glasses,” *J. Chem. Phys.*, vol. 140, p. 214501, 2014.

[105] K. Vignarooban, P. Boolchand, M. Micoulaut, M. Malki, and W. J. Bresser, “Rigidity transitions in glasses driven by changes in network dimensionality and structural groupings,” *A Lett. J. Explor. Front. Phys.*, vol. 108, p. 56001, 2014.

[106] R. Christensen, J. Byer, T. Kaufmann, and S. W. Martin, “Structure – property relationships in the mixed glass former system Na2O–B2O3–P2O5,” *Phys. Chem. Glas. Eur. J. Glas. Sci. Technol. B*, vol. 50, no. 4, pp. 237–242, 2009.

[107] T. Rouxel, H. Ji, J. P. Guin, F. Augereau, and B. Rufflé, “Indentation deformation mechanism in glass: Densification versus shear flow,” *J. Appl. Phys.*, vol. 107, no. 9, p. 094903, 2010.

[108] K. Suzuki, Y. Benino, T. Fujiwara, and T. Komatsu, “Densification Energy during Nanoindentation of Silica Glass,” *J. Am. Ceram. Soc.*, vol. 85, p. 3102, 2002.

[109] F. Gao, “Hardness estimation of complex oxide materials,” *Phys. Rev. B*, vol. 69, no. 9, pp. 1–6, Mar. 2004.

[110] T. Rouxel, H. Ji, T. Hammouda, and a. Moréac, “Poisson’s Ratio and the Densification of Glass under High Pressure,” *Phys. Rev. Lett.*, vol. 100, no. 22, pp. 1–4, Jun. 2008.

7 Bibliography

[111] J. D. Mackenzie, “High-Pressure Effects on Oxide Glasses: I, Densification in Rigid State,” *J. Am. Ceram. Soc.*, vol. 46, no. 10, pp. 461–470, 1963.

[112] J. D. Mackenzie, “High-pressure effects on oxide glass: II. Subsequent heat treatment.,” *J. Am. Ceram. Soc.*, vol. 46, p. 470, 1963.

[113] S. Yoshida, S. Isono, J. Matsuoka, and N. Soga, “Shrinkage Behaviour of Knoop Indentations in Silica and Soda-Lime-Silica Glasses,” *J. Am. Ceram. Soc.*, vol. 84, no. 9, p. 2141, 2001.

[114] S. Yoshida, J. Sanglebœuf, and T. Rouxel, “Quantitative evaluation of indentation-induced densification in glass,” *J. Mater. Res.*, vol. 20, no. 12, p. 3404, 2005.

[115] S. Yoshida, Y. Hayashi, A. Konno, T. Sugawara, Y. Miura, and J. Matsuoka, “Indentation induced densification of sodium borate glasses,” *Phys. Chem. Glas. Eur. J. Glas. Sci. Technolology B*, vol. 50, no. 1, pp. 63–70, 2009.

[116] H. Sawasato, S. Yoshida, T. Sugawara, Y. Miura, and J. Matsuoka, “Relaxation behaviors of Vickers indentations in soda-lime glass,” *J. Ceram. Soc. Japan*, vol. 116, no. 1356, pp. 864–868, 2008.

[117] K. W. Peter, “Densification and flow phenomena of glass in indentation experiments,” *J. Non. Cryst. Solids*, vol. 5, no. 2, pp. 103–115, Nov. 1970.

[118] E. Le Bourhis and T. Rouxel, “Indentation response of glass with temperature,” *J. Non. Cryst. Solids*, vol. 316, pp. 153–159, 2003.

[119] M. Yamane and J. D. Mackenzie, “Vicker’s Hardness of Glass,” *J. Non. Cryst. Solids*, vol. 15, pp. 153–164, 1974.

[120] K. H. Sun and M. L. Huggins, “Energy Additivity in Oxygen-Containing Crystals and Glasses II,” *J. Phys. Colloid Chem.*, vol. 51, no. 2, pp. 438–443, 1947.

[121] D. S. Sanditov, F. J. Baltá Calleja, and V. P. Privalko, “Review: the microhardness of non-crystalline materials,” *J. Mater. Sci.*, vol. 7, pp. 4507 – 4516, 2002.

[122] M. M. Smedskjaer, “Topological Model for Boroaluminosilicate Glass Hardness,” *Front. Mater.*, vol. 1, no. October, pp. 1–6, Oct. 2014.

[123] M. M. Smedskjaer, M. Jensen, and Y.-Z. Yue, “Theoretical Calculation and Measurement of the Hardness of Diopside,” *J. Am. Ceram. Soc.*, vol. 91, no. 2, pp. 514–518, Feb. 2008.

[124] A. Makishima and J. D. Mackenzie, “Calculation of bulk modulus, shear modulus and poisson’s ratio of glass,” *J. Non. Cryst. Solids*, vol. 17, pp. 147–157, 1975.

[125] B. R. Lawn, A. G. Evans, and D. B. Marshall, “Elastic/Plastic Indentation Damage in Ceramics: the Median/Radial Crack System,” *J. Ceram. Soc.*, vol. 63, pp. 574–581, 1980.

7 Bibliography

[126] S. S. Chiang, “The response of solids to elastic/plastic indentation. I. Stresses and residual stresses,” *J. Appl. Phys.*, vol. 53, no. 1, p. 298, 1982.

[127] T. M. Gross, M. Tomozawa, and A. Koike, “A glass with high crack initiation load: Role of fictive temperature-independent mechanical properties,” *J. Non. Cryst. Solids*, vol. 355, no. 9, pp. 563–568, Apr. 2009.

[128] Varner, W. JR;, S. CJ;, and R, “Evaluating effects of processing and surface finishing on crack-initiation behavior using recording microindentation,” *Finish. Adv. Ceram. Glas.*, vol. 102, pp. 321–329, 1999.

[129] N. M. Keulen and N. Dissel, “Temperature Dependence of Indentation Cracking in Soda Lime Silicate Glass,” *Glas. Technol.*, vol. 34, no. 5, pp. 200–205, 1993.

[130] Y. Kato, H. Yamazaki, Y. Kubo, and S. Yoshida, “Effect of B2O3 content on crack initiation under Vickers indentation test,” *J. Ceram. Soc. Japan*, vol. 118, no. 9, pp. 792–798, 2010.

[131] Y. Kato, H. Yamazaki, S. Itakura, S. Yoshida, and J. Matsuoka, “Load dependence of densification in glass during Vickers indentation test,” *J. Ceram. Soc. Japan*, vol. 119, no. 2, pp. 110–115, 2011.

[132] P. Sellappan, T. Rouxel, F. Celarie, E. Becker, P. Houizot, and R. Conradt, “Composition dependence of indentation deformation and indentation cracking in glass,” *Acta Mater.*, vol. 61, no. 16, pp. 5949–5965, Sep. 2013.

[133] Y. Kato, H. Yamazaki, S. Yoshida, and J. Matsuoka, “Effect of densification on crack initiation under Vickers indentation test,” *J. Non. Cryst. Solids*, vol. 356, no. 35–36, pp. 1768–1773, Aug. 2010.

[134] G. F. Vander Voort, *Metallography, Principles and Practice*, 4th ed. ASM International, 2007, p. 336.

[135] K. Peter, “Densification and flow phenomena of glass in indentation experiments,” *J. Non. Cryst. Solids*, vol. 5, no. 2, pp. 103–115, Nov. 1970.

[136] J. C. Mauro, “Statistics of modifier distributions in mixed network glasses.,” *J. Chem. Phys.*, vol. 138, p. 12A522, Mar. 2013.

Paper I

LETTER TO THE EDITOR

Journal of Non-Crystalline Solids 364 (2013) 40–43

Contents lists available at SciVerse ScienceDirect

Journal of Non-Crystalline Solids

journal homepage: www.elsevier.com/ locate/ jnoncrysol

Letter to the Editor

Densification and plastic deformation under microindentation in silicate glasses and the relation to hardness and crack resistance

C. Hermansen [a], J. Matsuoka [b], S. Yoshida [b], H. Yamazaki [c], Y. Kato [c], Y.Z. Yue [a,*]

[a] Section of Chemistry, Aalborg University, Sohngaardsholmsvej 57, DK-9000 Aalborg, Denmark
[b] The University of Shiga Prefecture, Hikone, Shiga 522-8533, Japan
[c] Nippon Electric Glass Co., Ltd., Otsu, Shiga 520-8639, Japan

ARTICLE INFO

Article history:
Received 4 September 2012
Received in revised form 26 December 2012
Available online xxxx

Keywords:
Soda lime silicate;
Plastic deformation;
Densification;
Hardness;
Crack resistance

ABSTRACT

To quantify and study the densification and plastic deformation under Vicker's indentation we prepared a series of simple soda-lime-silicate glasses with different modifying ion contents and four glasses with constant silica content but potassium and/or barium substituted for sodium and/or calcium. The densification and plastic deformation in these glasses were determined using atomic force microscopy (AFM) by measuring each sample twice, i.e., once immediately following indentation, and once after annealing to relax the densified volume. The results show that the densified volume of the glasses decreases approximately linearly with the bulk modulus, and the plastic deformation volume with silica mole fraction. These results have important implications in the prediction of hardness and crack resistance (i.e. load for crack initiation) from composition.

1. Introduction

With the advent of flat panel display glasses for TV, monitors, and touchscreen devices, surface mechanical properties, such as scratch and fracture resistance emerge as important material properties [1]. These properties are usually evaluated using the method of microindentation of glasses by relating hardness to scratch resistance, and relating the crack resistance (or load for crack initiation) to fracture resistance [2]. Despite the profusion of microindentation measurements the deformation processes occurring under indentation are not well understood, and this inhibits a deep understanding of the properties measured through microindentation. The three deformation processes are an elastic deflection of the surface fully recovered upon unloading, a volume-conservative plastic flow induced by the gigapascal-range shear stresses, and a non-volume conservative densification of the structure in a hemispherical region under the indent [3]. A physical understanding of these deformation processes is crucial for establishing accurate predictive models of indentation related properties. For example, the deformation mechanisms are used in a semi-empirical model to calculate indentation hardness from composition [4]. The model predicts hardness quite well using only qualitative data for the compositional variation of the deformation mechanisms. More recently, a promising approach for predicting the glass hardness from chemical compositions has been established, which is based on the temperature dependent constraint theory [5]. The hardness values of a soda-lime-borate glass series can be predicted by using this approach and are in good agreement with the measured ones. However, temperature dependent constraint theory does not take into account the different deformation processes occurring during indentation, and this is exactly what the authors give as the key reason for discrepancies between the calculated and measured hardness values when extending the method to borosilicate glass compositions [6]. A relation between the fracture of glass and the relative contributions of densification and plastic deformation has been suggested by Kato and his co-workers [7–9]. They found that crack initiation is governed by residual stress induced by plastic deformation. As the plastic deformation increases with applied load the residual stress will reach a critical value at some point, and cracks will initiate. Although the plastic deformation universally increases with applied load (and the relative amount of densification decreases), there are significant differences in the degree of plastic deformation exhibited by the investigated glass compositions; thus leading to cracking occurring at different loads.

Therefore, we believe that quantitative knowledge of the compositional dependence of the different deformation mechanisms will be useful for the prediction of indentation related properties, such as hardness and crack resistance. In the present work we determine the contribution by volume of plastic deformation and densification in a series of soda-lime-silicate model glasses, and also investigate the effect of substituting Na_2O for K_2O and/or CaO for BaO on both the hardness and the deformation volumes at constant silica content. The relative amount of densification is known to decrease with load, even so, the effect of composition is clearly discernible [9]. The deformation volumes will be determined at a single load in order to focus

* Corresponding author. Tel.: +45 99408522; fax: +45 96350558.
E-mail address: yy@bio.aau.dk (Y.Z. Yue).

0022-3093/$ – see front matter © 2013 Elsevier B.V. All rights reserved.
http://dx.doi.org/10.1016/j.jnoncrysol.2012.12.047

Table 1
Nominal compositions of the silica-sodium oxide–calcium oxide (SNC) series with changing silica content and modifier substituted compositions with constant silica content but changing modifying ions used in this work. The glass names are used throughout the text and figures.

Glass name	Oxide (mol%)					T_g[a] (K)
	SiO_2	Na_2O	CaO	K_2O	BaO	
80SNC	80.0	15.0	5.0	–	–	814
75SNC	75.0	25.0	–	–	–	763
71SNC	71.4	23.8	4.8	–	–	786
68SNC	68.2	22.7	9.1	–	–	806
65SNC	65.2	21.7	13.0	–	–	818
60SNC	60.0	20.0	20.0	–	–	831
75S15K10B	75.0	–	–	15.0	10.0	841
75S15N10B	75.0	15.0	–	–	10.0	727
75S15K10C	75.0	–	10.0	15.0	–	903
75S15N10C	75.0	15.0	10.0	–	–	841

[a] Measured by dilatometer. Error is estimated to be ±3 K [22].

on the effect of glass composition. We attempt to relate the hardness and the measured deformation volumes to the elastic moduli, as these represent resistances to different deformation modes in the elastic regime, and are thought to be related to the resistances to permanent deformation as well. We also measure the crack resistances of the compositions exhibiting the lowest plastic deformation volumes.

2. Experimental

The glasses were prepared from analytical reagent-grade raw materials: SiO_2, Na_2CO_3, $CaCO_3$, K_2CO_3 and $BaCO_3$ powders. The glass compositions are given in Table 1. The raw materials were mixed and melted at 1575 °C for 2 h in a platinum crucible. After this the melt was cast, crushed, and re-melted for 1 h, then quenched on a brass plate and immediately annealed at the glass transition temperature (T_g) for 2 h, and cooled at 1 K/min. T_g was determined with a heating rate of 10 K/min using a dilatometer (TMA/SS6000, Seiko Instruments Inc.), density by the Archimedes method in toluene, and elastic moduli by ultrasonic measurement of the velocity of sound (DPR300, JSR). Coplanar samples polished to a mirror finish were prepared and used for Vicker's microindentation (MVK-H2, Akashi). Twenty crack-free indentations were made at 245 mN (the highest load giving crack-free indents for all compositions) and 15 s dwell time, and then imaged by atomic force microscopy (AFM, SPA400, Seiko Instruments Inc.). The samples were annealed at $0.9T_g$ for 2 h to relax the densified volume [10] and imaged again by AFM. Densified and plastic deformation volumes were calculated as specified in [11]. Before initiating crack resistance measurements all samples were acclimatised for 24 h to the testing conditions (25 °C and 30% relative humidity). The crack resistance was determined as the load at which an average of two cracks initiated from the corners of the indent. Twenty Vicker's indentations (MXT50, Matsuzawa) were made at five to seven loads on each sample.

3. Results

The variations of Vicker's hardness, plastic deformation volume and densified volume with composition are shown in Fig. 1a and b. The Vicker's hardness varies widely across the investigated compositions, ranging from 3.7 GPa to 5.2 GPa with no apparent compositional trend. The densified volume generally increases with silica content, but with large scatter. The plastic deformation volume however is well described by the silica content. It is attempted to relate the Vicker's hardness and deformation volumes to the elastic constants of the glass compositions. It is found that the Vicker's hardness correlates well to the Young's modulus (Table 2), and the variation in densified volume is described well by the bulk moduli (Fig. 2a), yet the change in plastic deformation volume shows no compelling relation to an elastic constant, but is described best by the silica contents (Fig. 2b). The volume recovery ratio, defined as the ratio of recovered densified to the total deformation volume (equal to the volume of the indent [11]) is plotted against composition in Fig. 3a. The volume recovery ratio increases strongly and approximately linearly with silica content, ranging from about 20% at 60 mol% silica to about 100% at 80 mol% silica. The volume recovery ratio has previously been linked to the Poisson's ratio [11–13], and this relationship is plotted in Fig. 3b. Fig. 4 shows the data and procedure for determining the crack resistances of three compositions exhibiting low plastic deformation volumes. The crack resistances were determined to be 7.0 N±2 N for 80SNC, 1.1 N±0.2 N for 75S15K10C and 1.0 N±0.1 N for 75S15N10C.

4. Discussion

Of the four elastic constants listed in Table 2 it is Young's modulus that best correlates with the Vicker's hardness. Such an empirical relation is well known, but has significant scatter [14,15]. The correlation could be an indication that the elastic deformation largely determines the indentation hardness, which fits well with the finding from nanoindentation studies that the work of elastic deformation is commonly larger than that of permanent deformation [16]. A strong correlation between the densified volume and the bulk modulus was discovered (Fig. 3a). Since the bulk modulus is the elastic resistance to hydrostatic compression, and approximately two-thirds of the mean pressure beneath the indenter is hydrostatic [17], densification occurs when the elastic compression reaches a certain yield value by increasing pressure. Such a yield compression has been observed for a variety of glasses under high pressure

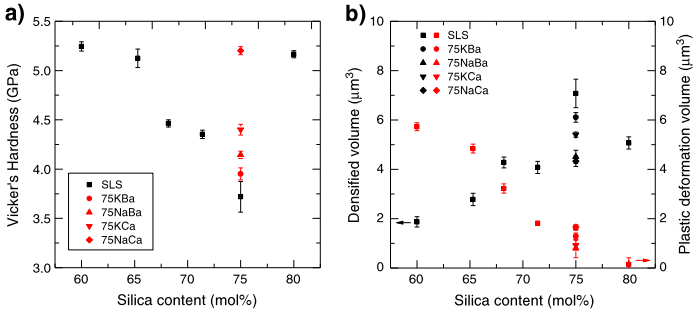

Fig. 1. a) The compositional variation of Vicker's hardness, and b) densified and plastic deformation volume. Arrows: The axis on which the densified volume and plastic deformation volume should be read.

Table 2
The physical and mechanical properties of the studied glasses: density (δ), Poisson's ratio (ν), Young's modulus (E), bulk modulus (K), shear modulus (G) and Vicker's hardness measured at 245 mN and a dwell time of 15 s (H_v).

Glass	δ (g/cm^3)	ν (−)	E (GPa)	K (GPa)	G (GPa)	H_V (GPa)
80SNC	2.412	0.21	67.6	39	27.9	5.2
75SNC	2.435	0.23	59.2	37	24.1	3.7
71SNC	2.480	0.24	65.2	41	26.4	4.4
68SNC	2.524	0.25	68.8	45	27.6	4.5
65SNC	2.572	0.25	72.3	48	29.0	5.1
60SNC	2.637	0.26	77.9	53	31.0	5.2
75S15K10B	2.445	0.25	52.0	34	20.8	4.0
75S15N10B	2.461	0.26	58.5	40	23.3	4.2
75S15K10C	2.468	0.23	62.7	39	25.4	4.4
75S15N10C	2.484	0.22	71.4	43	29.2	5.2
Max. error	±0.001	±0.01	±0.6	±1.4	±0.3	±0.1

hydrostatic compression [18]. Since a higher bulk modulus is probably related to higher yield value, glasses with higher bulk modulus have lower densification volumes at a given load.

As shown in Fig. 2b, the plastic deformation volume decreases linearly with the silica mole fraction. Given this relation, it is interesting to note that amorphous silica is generally believed not to deform plastically on indentation [19], and the volume recovery ratio has previously been determined to be 92%±4% at a load of 100 mN [11]. The effect of the modifying ion on the plastic deformation is rather small, with the plastic deformation volumes for the 75 mol% SiO_2 glasses ranging from 0.8 μm^3 to 1.7 μm^3, with a maximum standard deviation of 0.6 μm^3. The influence of the type of modifying oxides tested here (Na_2O, K_2O, CaO and BaO) is small relative to the influence of the silica content on the plastic deformation volume. The effect could be caused by silica constituting the major component in the compositions, and thus masking the influence of the type of modifying oxides. However, it has been proposed that the mechanism of plastic deformation in glasses is slipping between modifier rich planes in the structure due to their relatively low bonding energy [19]. Another interpretation of the observed phenomenon is that the type of modifier does not affect the plastic deformation volume much, because they per definition have the weakest bonds in a silicate glass, and the exact strength of these weak bonds is less important than their concentration. It is interesting to note that the plastic deformation tends to zero around 80 mol% silica, which corresponds quite well to the concentration where modifier rich channels start forming according to the modified random network model [20]. The volume recovery ratio is an important parameter in that it does not change as drastically with load as the deformation volumes. The volume recovery ratio is found to increase approximately linearly with the silica mole fraction, although the 75S15N10C composition deviates from the trend (Fig. 3a). This fits well with the plastic deformation volume decreasing with the silica content. The relation to silica mole fraction is more compelling than the one previously suggested to Poisson's ratio [11–13], as shown in Fig. 3b. Poisson's ratio is an elastic constant that can be interpreted as a measure of the relative susceptibility to shear deformation versus hydrostatic compression; a material with low Poisson's ratio is easily compressed, but difficult to

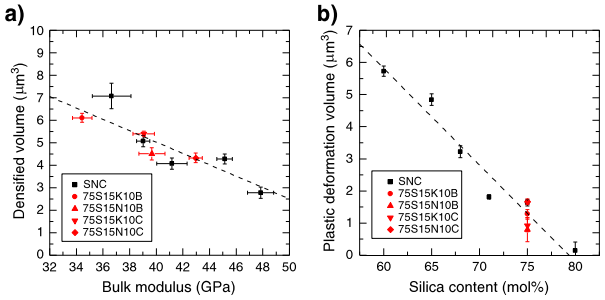

Fig. 2. a) The best fit to the densified volume under a 245 mN indent as measured by AFM was found to be the bulk modulus (K). b) For the plastic deformation volume the silica mole fraction gave the best fit. The dashed lines are the best linear fits to the data.

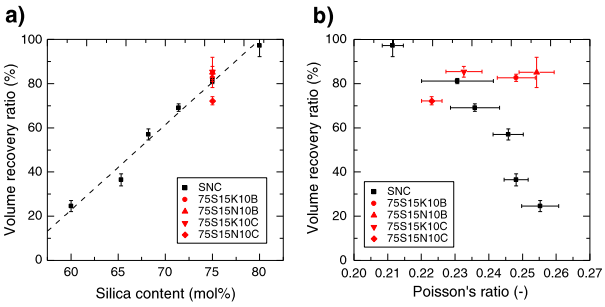

Fig. 3. a) The volume recovery ratio (ratio of densified volume to total deformation volume) as a function of the silica content. The dashed line is the best linear fit to data. b) The volume recovery ratio as a function of Poisson's ratio.

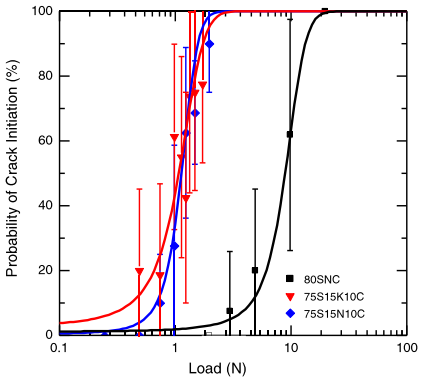

Fig. 4. The probability of crack initiation at different applied loads. The probability is determined as the average number of radial cracks per corner out of 20 indents at a given load. The crack resistance is the load where the probability of crack initiation is equal to 50% (i.e. on average two corners out of four will contain cracks). The crack resistances are determined from a sigmoidal fit to the data.

shear, while $\nu = 0.5$ describes a perfectly incompressible material [18]. That the relation between the volume recovery ratio and Poisson's ratio is not very convincing is in agreement with the plastic deformation volume apparently not being strongly correlated with the shear modulus. This is surprising, and may be caused by the inherent nanometer-scale heterogeneity of glass, namely the modifier channels previously mentioned [20].

The 80SNC composition is known to have low brittleness [2], which normally indicates high crack resistance, but the crack resistance has not previously been determined. We show that the 80SNC glass composition has approximately zero plastic deformation at 245 mN, and that the crack resistance is about seven times larger than that of the 75S15K10C and 75S15N10C compositions (see Fig. 4). The latter compositions have higher plastic deformation volumes at 245 mN. This suggests that the silica content of a glass has a large impact on both crack resistance and plastic deformation volume. Although the load dependence of the plastic deformation has not been taken into account, this supports the work reported in [7–9], where it is believed that the plastic deformation induces residual stress that causes cracking. Other highly crack-resistant glasses also have silica contents around 80 mol%, such as $80SiO_2 \cdot 10Al_2O_3 \cdot 10CaO$ with crack resistance of ~10 N in a nitrogen glove bag [1], and Asahi less-brittle glass of composition $79SiO_2 \cdot 2Al_2O_3 \cdot 13Na_2O \cdot 1K_2O \cdot 4MgO \cdot 1CaO$ that does not crack at loads up to around ~35 N in a nitrogen glove box [2]. Our results suggest that these high crack resistances are obtained largely because of the low plastic deformation volumes, or conversely large volume recovery ratios of high silica glass. However other factors are known to play a role, like the load dependence of the plastic deformation, but also the susceptibility to water in the atmosphere. For example, amorphous silica has a crack resistance around ~2.5 N in a nitrogen glove bag [1], yet can achieve crack-free indentations up to ~10 N under identical conditions by etching away the hydrated surface layer [21].

5. Conclusions

A quantitative correlation of densified volume, plastic deformation volume, and the volume recovery ratio to elastic constants and composition has been reported. As hardness must ultimately be governed by the resistances to the individual deformation processes occurring during indentation, this discovery could lead to an improved predictive hardness model. Our results are also relevant for describing the compositional dependence of the crack resistance. We show that the crack resistance of an 80 mol% SiO_2 composition is ~7 N, compared to around ~1 N of the 75 mol% SiO_2 compositions. We believe that this large difference is caused by the 80 mol% SiO_2 composition exhibiting small plastic deformation.

References

[1] T.M. Gross, M. Tomozawa, A. Koike, J. Non-Cryst. Solids 355 (2009) 563.
[2] J. Sehgal, S. Ito, J. Am. Ceram. Soc. 81 (1998) 2485.
[3] T. Rouxel, H. Ji, J.P. Guin, F. Augereau, B. Ruffle, J. Appl. Phys. 107 (2010) 094903.
[4] M. Yamane, J.D. Mackenzie, J. Non-Cryst. Solids 15 (1974) 153.
[5] M.M. Smedskjaer, Phys. Rev. Lett. 105 (2010) 115503.
[6] M.M. Smedskjaer, D.J. Mauro, R.E. Youngman, C.L. Hogue, M. Potuzak, Y.Z. Yue, J. Phys. Chem. B 115 (2011) 12930.
[7] Y. Kato, H. Yamazaki, Y. Kubo, S. Yoshida, J. Ceram. Soc. Jpn. 118 (2010) 792.
[8] Y. Kato, H. Yamazaki, S. Yoshida, J. Matsuoka, J. Non-Cryst. Solids 356 (2010) 1768.
[9] Y. Kato, H. Yamazaki, S. Itakura, S. Yoshida, J. Matsuoka, J. Ceram. Soc. Jpn. 119 (2011) 110.
[10] S. Yoshida, S. Isono, J. Matsuoka, N. Soga, J. Am. Ceram. Soc. 84 (2001) 2141.
[11] S. Yoshida, J. Sanglebœuf, T. Rouxel, J. Mater. Res. 20 (2005) 3404.
[12] S. Yoshida, Y. Hayashi, A. Konno, T. Sugawara, Y. Miura, J. Matsuoka, Phys. Chem. Glasses B 50 (2009) 63–70.
[13] H. Ji, V. Keryvin, T. Rouxel, T. Hammouda, Scripta Mater. 55 (2006) 1159.
[14] F. Gao, Phys. Rev. B 69 (2004) 1.
[15] R.J. Hand, D.R. Tadjiev, J. Non-Cryst. Solids 356 (2010) 2417.
[16] A. Chorfa, M.A. Madjoubi, M. Hamidouche, N. Bouras, J. Rubio, F. Rubio, Ceram. Silik. 54 (2010) 225.
[17] G.F. Vander Voort, Metallography, Principles and Practice, 4th ed. ASM International, 2007.
[18] T. Rouxel, H. Ji, T. Hammouda, A. Moréac, Phys. Rev. Lett. 100 (2008) 1.
[19] K.W. Peter, J. Non-Cryst. Solids 5 (1970) 103.
[20] G.N. Greaves, S. Sen, Adv. Phys. 56 (2007) 1.
[21] T.M. Gross, M. Tomozawa, J. Non-Cryst. Solids 354 (2008) 5567.
[22] Q. Zheng, M. Potuzak, D.J. Mauro, M.M. Smedskjaer, R.E. Youngman, Y.Z. Yue, J. Non-Cryst. Solids 358 (2012) 993.

Paper II

THE JOURNAL OF CHEMICAL PHYSICS **140**, 154501 (2014)

A model for phosphate glass topology considering the modifying ion sub-network

Christian Hermansen,[1] John C. Mauro,[2] and Yuanzheng Yue[1,3,a)]
[1]*Section of Chemistry, Aalborg University, 9000 Aalborg, Denmark*
[2]*Science and Technology Division, Corning Incorporated, Corning, New York 14831, USA*
[3]*State Key Laboratory of Silicate Materials for Architecture, Wuhan University of Technology, Wuhan 430070, China*

(Received 27 January 2014; accepted 27 March 2014; published online 16 April 2014)

In the present paper we establish a temperature dependent constraint model of alkali phosphate glasses considering the structural and topological role of the modifying ion sub-network constituted by alkali ions and their non-bonding oxygen coordination spheres. The model is consistent with available structural data by NMR and molecular dynamics simulations and with dynamic data such glass transition temperature (T_g) and liquid fragility (m). Alkali phosphate glasses are exemplary systems for developing constraint model since the modifying cation network plays an important role besides the primary phosphate network. The proposed topological model predicts the changing trend of the T_g and m with increasing alkali oxide content for alkali phosphate glasses, including an anomalous minimum at around 20 mol.% alkali oxide content. We find that the minimum in T_g and m is caused by increased connectivity of the modifying ion sub-network, as the alkali ions must share non-bonding oxygen to satisfy their coordination requirements at higher alkali oxide contents. We argue that the systematically decreasing the T_g values of alkali phosphate glasses from Li_2O to Na_2O to Cs_2O could be caused by a weakening of the modifying ion sub-network and can be accounted for by lower constraint onset temperatures. © *2014 AIP Publishing LLC*. [http://dx.doi.org/10.1063/1.4870764]

I. INTRODUCTION

Phosphorus pentoxide (P_2O_5) is one of the prototypical glass forming oxides[1] and has important applications for solid state lasers,[2] biocompatible bone replacement materials,[3–7] solid-state ionic devices,[8,9] and glass-to-metal seals, due to their low glass transition temperatures (T_g) and high coefficient of thermal expansion.[10] Phosphate glasses are also very interesting from a scientific point of view, as many of the binary phosphates exhibit anomalous compositional dependence of properties such as T_g, density, and index of refraction.[11,12] These anomalies do not seem to be related to any changes in the phosphate network, but depend strongly on the type of network modifier alloyed with P_2O_5.[13] As such, phosphate glasses seem to be an ideal candidate as a modified random network glass as proposed by Greaves,[14] and much can be learned from investigating their structures and properties. Despite this, phosphate glasses have not been studied as extensively as silicates and borates because the preparation and characterization of glasses containing over 50% by mole P_2O_5 is difficult due to their volatile and highly hygroscopic nature.[13]

Recently there have been efforts to apply temperature dependent constraint theory to predict the anomalous glass transition temperature of alkali phosphates.[15,16] We suggest an alternative model for two reasons: First, when we attempted to model the properties of alkali borophosphate glasses using the topological models for alkali phosphates[15] and alkali borates,[17] we realized that the constraints on vitreous P_2O_5 and B_2O_3 must be similar for a topological model to work, as they have similar glass transition temperatures of 543 K[18] and between 590 K and 663 K[11,19,20] respectively. Second, we clarify why different alkali oxides give significantly different T_g values in phosphate glasses.[16]

We have collected the most accurate data of T_g of anhydrous alkali phosphates available in the literature, which clearly show anomalous minima and maxima. Then we have constructed a topological model in accordance with available structural data for alkali phosphate glasses and used temperature dependent constraint theory to calculate T_g as a function of composition. The model accurately predicts T_g for lithium phosphate glasses, including the anomalies which are caused by changes in the alkali coordination environment. The topological model developed in this work is compatible with that for alkali borates[17] and provides new insights into the peculiar properties of alkali phosphate glasses and the application of temperature constraint theory to glasses that can be described as modified random networks.

II. THEORY

Topological constraint theory as applied to glasses was introduced in a series of seminal papers by Phillips and Thorpe,[21–29] and extended by Gupta and Mauro[17,30] to give a temperature dependent form that can quantitatively predict important glass properties such as T_g, liquid fragility and indentation hardness.[17,30–32] The theory has been successfully applied to chalcogenide,[30] borate,[17,31] silicate,[32] and most recently phosphate glasses.[15] Topological constraint theory has also been applied to simulated glass forming liquid under high

a)Electronic mail: yy@bio.aau.dk

pressure and found to predict property variations as a function of pressure.[33,34]

The first step in applying temperature dependent constraint theory is to obtain quantitative structural data of the short range order in the glass, i.e., the concentration of each network forming unit. With this information the intact constraints at the temperature range of interest must be identified, e.g., T_g is determined from the rigid constraints at this temperature, but indentation hardness from the constraints at room temperature.[31] The constraints are normally counted by nearest neighbor interactions only,[21] i.e., linear constraints from covalent or mixed-covalent bonds and angular constraints from bond angles. The number of linear and angular constraints around a network forming atom can be calculated by

$$n_{c,linear} = \frac{1}{2} C^n \Big|_{C^n \geq 2}, \tag{1}$$

$$n_{c,angular} = (2C^n - 3)\big|_{C^n \geq 2}, \tag{2}$$

where n_c are the number of constraints around an atom and C^n is the coordination number of that atom to other network forming atoms.[25] There is controversy as to whether single coordinated atoms should be considered a part of the network or not.[25,35,36] We believe that the single coordinated double bonded oxygen should not be considered part of the network, as they are effectively dead-ends, which is why we denote them as terminal oxygen. Both the linear and angular constraints are generally intact at or below T_g for network forming atoms in oxide glasses, but the angular constraints around oxygen are broken for vitreous SiO_2[37,38] and assumed the same for alkali borate[17] and alkali phosphate glasses.[15]

We use the Adam-Gibbs theory of the glass transition[39,40] and Naumis's result[41] of configurational entropy being largely due to the number floppy modes to calculate T_g:

$$\frac{T_g(x)}{T_g(x_{ref})} = \frac{f[T_g(x_{ref}), x_{ref}]}{f[T_g(x), x]} = \frac{3 - N_c[T_g(x_{ref}), x_{ref}]}{3 - N_c[T_g(x), x]}. \tag{3}$$

x is the compositional variable, x_{ref} is the reference composition, f is the number of degrees of freedom, and N_c is the number of rigid constraints at T_g per network forming atom. Equation (3) requires that $0 < f[T_g,x] < 3$.

The liquid fragility is related to the change in degrees of freedom per atom at T_g, and can be computed by

$$m(x) = m_0 \left(1 + \frac{\partial \ln f(T,x)}{\partial \ln T}\right)\Big|_{T=T_g(x)}. \tag{4}$$

m_0 is the liquid fragility of an ideally strong liquid and taken to be 17.[30] In order to take the temperature derivative of $\ln f(T,x)$ a continuous function is needed. We estimate the fraction of constraints that are rigid at a given temperature as

$$q_i(T) = \left[1 - \exp\left(-\frac{\Delta F_i^*}{k_B T}\right)\right]^{\nu t_{obs}}. \tag{5}$$

ΔF_i^* is the activation energy for breaking constraint i and νt_{obs} is the product of the vibrational attempt frequency and observation time.[30] The activation energy is related to a characteristic constraint onset temperature as

$$\Delta F_i^* = -k_B T_i \ln(1 - 2^{-1/\nu t_{obs}}), \tag{6}$$

where T_i is the constraint onset temperature of constraint i and can be considered to be the temperature at which the constraint goes from intact to broken.[17]

III. STRUCTURE

Pure phosphorous pentoxide glass is composed exclusively of phosphate tetrahedra containing three bridging oxygen (BO) and one double bonded terminal oxygen (TO). The tetrahedral unit in P_2O_5 is denoted as a Q^3 unit, where the superscript indicates the number of BO attached to the phosphorous atom. Addition of alkali oxides causes BO to be converted to non-bridging oxygen (NBO), which do not bridge to other phosphate tetrahedra, but instead coordinate to the alkali ions. The TO on a Q^3 unit will also become a NBO due to the electron delocalization as a Q^3 becomes a Q^2 unit, and a Q^2 unit therefore carries two BOs and two NBOs.[13] The depolymerization of the network occurs stepwise from Q^3 to Q^2, Q^2 to Q^1, and Q^1 to Q^0, as predicted by Van Wazer.[13] These units are bonded together in a random manner.[42–44] There are never detectable amounts of more than two different structural units in an alkali phosphate glass. The four possible structural units are shown in Fig. 1, and the relative amounts of Q^n species, BO, NBO, and R^+ in $(x)R_2O \cdot (1-x)P_2O_5$ are given by Eqs. (7)–(13) and shown in Fig. 2. The equations are derived by considering first the change in the number of the respective network forming atom due to substitution of x R_2O and then the change in speciation due to depolymerization. The denominator represents the total sum of atoms at a given composition (given as the black sum line in Fig. 2):

$$Q^3(x) = \begin{cases} \dfrac{2-4x}{5}, 0 \leq x < \dfrac{1}{2} \\ 0, \dfrac{1}{2} \leq x \leq \dfrac{3}{4} \end{cases}, \tag{7}$$

$$Q^2(x) = \begin{cases} \dfrac{2x}{5}, 0 \leq x < \dfrac{1}{2} \\ \dfrac{4-6x}{7-4x}, \dfrac{1}{2} \leq x < \dfrac{2}{3} \\ 0, \dfrac{2}{3} \leq x \leq \dfrac{3}{4} \end{cases}, \tag{8}$$

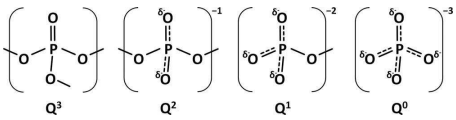

FIG. 1. The four possible tetrahedral units that can occur in alkali phosphate glasses.

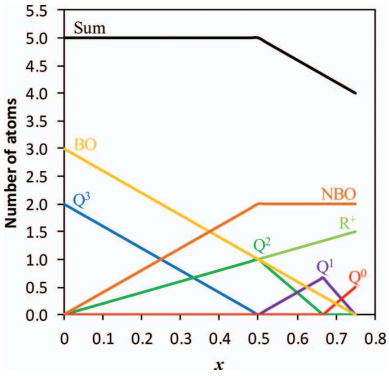

FIG. 2. The amounts of each type of atom participating in network formation in $xR_2O\,(1-x)P_2O_5$ glass, where R_2O is an alkali oxide. Double-bonded terminal oxygen (TO) is not considered a network forming atom, and therefore not shown, but follow the Q^3 line. The figure is based on Eqs. (7)–(13) which describe a stepwise depolymerization of the phosphate network from Q^3 to Q^2, Q^2 to Q^1, and Q^1 to Q^0. For example, the metaphosphate composition is RPO_3, with one Q^2, one BO, two NBO, and one R^+.

$$Q^1(x) = \begin{cases} 0, 0 \le x < \frac{1}{2} \\ \frac{4x-2}{7-4x}, \frac{1}{2} \le x < \frac{2}{3} \\ \frac{6-8x}{7-4x}, \frac{2}{3} \le x \le \frac{3}{4} \end{cases}, \tag{9}$$

$$Q^0(x) = \begin{cases} 0, 0 \le x < \frac{2}{3} \\ \frac{6x-4}{7-4x}, \frac{2}{3} \le x \le \frac{3}{4} \end{cases}, \tag{10}$$

$$BO(x) = \begin{cases} \frac{3-4x}{5}, 0 \le x < \frac{2}{3} \\ \frac{3-4x}{7-4x}, \frac{2}{3} \le x \le \frac{3}{4} \end{cases}, \tag{11}$$

$$NBO(x) = \begin{cases} \frac{4x}{5}, 0 \le x < \frac{1}{2} \\ \frac{2}{7-4x}, \frac{1}{2} \le x \le \frac{3}{4} \end{cases}, \tag{12}$$

$$R^+(x) = \begin{cases} \frac{2x}{5}, 0 \le x < \frac{1}{2} \\ \frac{2x}{7-4x}, \frac{1}{2} \le x \le \frac{3}{4} \end{cases}. \tag{13}$$

Although the short and medium range structure of the phosphate network is well characterized, significantly less is known about the structures surrounding the modifying ions in phosphate glass. Hoppe[45] proposed that there exists a critical concentration of modifying oxide, below which the modifying ions will be isolated in the phosphate network, and above which modifying ion coordination polyhedra must share vertices or edges. Hoppe used this argument to explain a density minimum in some alkaline earth phosphate glasses.[45–47] A similar density minimum is seen for lithium and sodium phosphates at $x = 0.2$.[48] For alkali phosphates the critical alkali oxide concentration can be found as

$$x_{crit} = \frac{1}{C^n}. \tag{14}$$

x_{crit} is the critical concentration of alkali oxide for the density minimum and C^n is the oxygen coordination number adopted by the alkali ion in phosphate glass at the critical concentration. If the model by Hoppe[45] is applicable to alkali phosphate glasses, then the density minimum for lithium and sodium phosphate glasses at $x_{crit} = 0.2$ can be explained by the alkali ions having an oxygen coordination number of 5 at this composition. Below the critical concentration the alkali ions are thought to be coordinated to and charge compensated by two NBOs on the same Q^2 unit.[48] The rest of the alkali coordination polyhedron is suggested to be made up of TOs from the Q^3 units. Molecular orbital calculations[49] and NMR experiments[50–52] are consistent with this view. Addition of alkali oxide beyond the critical concentration causes the alkali to coordinate to NBOs on different phosphorous tetrahedra, and at the same time NBOs become shared between alkali ions.[48] In other words the structure changes from edge-sharing to corner-sharing between the alkali polyhedra and phosphate tetrahedra. The alkali polyhedra are isolated from each other at or below the critical concentration, but must share vertices and/or edges to satisfy their coordination requirements as the alkali oxide content is increased. The end result is an interconnected network of phosphate tetrahedra and alkali polyhedra. NMR experiments,[51–53] molecular dynamics simulation,[54] and the chain-form crystal structures of $LiPO_3$ and $NaPO_3$[55,56] are all consistent with this structural model.

In the polyphosphate region ($x > 0.5$) it is expected that the added alkali ions have difficulty satisfying their coordination requirements with NBOs. This occurs as only one BO is converted to a NBO per added alkali ion, and the alkali ions have preferred coordination numbers of four or higher. Assuming an alkali coordination number of four and each NBO being shared between two alkalis, then no more than 50 mol % R_2O can be incorporated in the network. The coordination number of the alkali ions must be lower than four, the NBOs are shared between more than two alkali ions each, or BOs participate in the coordination of alkali ions. The MD simulation of $LiPO_3$ glass by Vogel[57] finds that there is a mixture of lithium sites. The sites showing the highest lithium residence times have four oxygen nearest neighbors (presumably NBOs); however, about two-thirds of sites have lower coordination numbers and smaller residence times. Also, some NBOs are in sites not associated with a lithium ion. These results indicate that on average less than four NBOs will be associated with a lithium ion at the metaphosphate (50 mol.% R_2O) composition. Prabakar *et al.*[51] conclude from cross-polarization NMR that the structure around the NBOs on Q^2 species is similar in sodium metaphosphate and polyphosphate glasses. A mixture of NBOs coordinated to two and

three alkalis are found in the crystal structures of $Li_4P_2O_7$ and $Na_4P_2O_7$, which exclusively contain Q^1 phosphorous as pyrophosphate groups.[58,59] This indicates that at very high concentrations of alkali oxide (close to $x = 0.67$) some NBOs may coordinate to more than two alkali ions.

IV. TOPOLOGY

Given the structural description of alkali phosphate glasses in Sec. III we envision two characteristic structures around the alkali ions which occur at different concentrations of alkali oxide – these structures are shown in Fig. 3. Initial addition of alkali oxide to P_2O_5 causes isolated alkali coordination polyhedra in the phosphate network, where a single alkali is coordinated by the two NBOs on a single Q^2 unit, and TO of several Q^3 units, as seen in structure A. This structure is exclusive up to x_{crit}. Further alkali oxide addition causes a lack of TOs to satisfy the coordination requirements of the alkali ion, and structure B will occur, which has clusters of edge sharing alkali tetrahedra. Our topological model will be constructed based on the known structure of the phosphate network and these proposed characteristic structures around the alkali ions. As glass is a non-equilibrium solid there will necessarily exist a spectrum of structures with different potential energies, as also evidenced in a molecular dynamics simulation of $LiPO_3$ glass.[57] Moreover it is known that different alkali ions occupy dissimilar sites in phosphate glasses, but by the current techniques it has not been possible to specify the differences in short range order.[53,60,61] Therefore, the suggested characteristic structures cannot fully describe the glassy network but may still serve as a basis for a topological model, as they agree well with the structural data presented in Sec. III.

In our topological model we consider constraints arising from the phosphate network backbone, as well as constraints related to the characteristic structures surrounding the alkali ions in the glass. In order of their strength the constraints are

- α: O–P–O angular constraints. There are three angular constraints on each Q^3 phosphorous and five at each Q^2, Q^1, and Q^0 phosphorous.
- β: P–O linear constraints. There are two of these at each BO and one at each NBO. None are counted at the TOs as they are not thought to be a part of the glassy network.
- γ: R^+–O linear constraints. These constraints are between the alkali ion and the NBOs. There are two constraints for structure A, and four constraints for structure B.
- δ: P–O–P angular constraints. There is one at each BO.
- ε: P–O–R^+ angular constraints. There is one constraints for each NBO in structure A and two constraints for each NBO in structure B.
- ζ: O–R^+–O angular constraints. There is one constraint for structure A and five constraints for structure B.

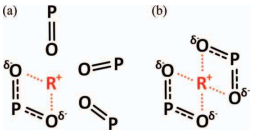

FIG. 3. The characteristics structures around the alkali ion (R^+) occurring in each compositional regime of $(x)R_2O\ (1-x)P_2O_5$ glass. (a) Up to $x_{crit} = 0.2$ R_2O is incorporated into the phosphate glass as structure A. (b) Above x_{crit} alkali ions form corner or edge-sharing tetrahedra with their NBO nearest neighbors.

We believe that the O–P–O angular constraint is stronger than the P–O linear constraint as $NaPO_3$ is found to show rapid bond interchange at a relatively low temperature of 875 K.[62] The analytical expressions for the number of constraints per atom associated with each type of constraint are given below:

$$n_{c,\alpha}(x) = 3 \times \mathrm{Q}^3(x) + 5 \times [\mathrm{Q}^2(x) + \mathrm{Q}^1(x) + \mathrm{Q}^0(x)], \tag{15}$$

$$n_{c,\beta}(x) = 2 \times \mathrm{BO}(x) + 1 \times \mathrm{NBO}(x), \tag{16}$$

$$n_{c,\gamma}(x) = \begin{cases} 2 \times \mathrm{R}^+(x); 0 \le x \le x_{crit} \\ 4 \times \mathrm{R}^+(x - x_{crit}) + n_{c,\gamma}(x_{crit}); x_{crit} < x \end{cases}, \tag{17}$$

$$n_{c,\delta}(x) = 1 \times \mathrm{BO}(x), \tag{18}$$

$$n_{c,\varepsilon}(x) = \begin{cases} 1 \times \mathrm{NBO}(x); 0 \le x \le x_{crit} \\ 2 \times \mathrm{NBO}(x - x_{crit}) + n_{c,\varepsilon}(x_{crit}); x_{crit} < x \end{cases}, \tag{19}$$

$$n_{c,\zeta}(x) = \begin{cases} 1 \times \mathrm{R}^+(x); 0 \le x \le x_{crit} \\ 5 \times \mathrm{R}^+(x - x_{crit}) + n_{c,\zeta}(x_{crit}); x_{crit} < x \end{cases}. \tag{20}$$

It is worth noting that we do not consider the TOs to contribute to the connectivity of the network, and therefore there are no constraints associated with the TOs.[25] The relative strength of these constraints are in the order given, with the α constraint being intact up to the highest temperatures, and the ζ constraints being the weakest. The available degrees of freedom as functions of composition and temperature can be seen in Fig. 4.

V. GLASS TRANSITION TEMPERATURE

T_g can be modeled by Eq. (3) if the number of intact constraints at this temperature is known. We assume the α, β, and γ constraints to be intact at T_g, but not the δ, ε, and ζ constraints. The α and β constraints account for rigid corner-sharing phosphate tetrahedra as the basic building block of phosphate glasses. The γ constraints are associated with interactions between alkali ions and NBOs in the glass and have qualitatively been linked to the anomalous minimum in T_g and density of alkali and some alkaline earth phosphate glasses,[45,46,52] why we consider them intact at T_g. As for the oxygen bond-bending (δ) constraints, these have been found to be broken at T_g for alkali borates,[17] alkali tellurates,[38] and vitreous SiO_2.[63] Moreover, if they were intact, then vitreous

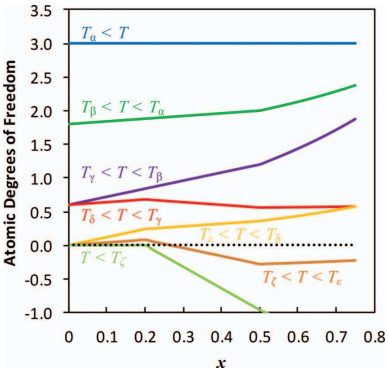

FIG. 4. Temperature and compositional dependence of the average atomic degrees of freedom per network forming atom in $(x)R_2O\ (1-x)P_2O_5$ glass, where R_2O is an alkali oxide. In order of decreasing strength the constraints are: α O−P−O angular constraints, β P–O linear constraints, γ R^+–O linear constraints, δ P–O–P angular constraints, ε P–O–R^+ angular constraints, and ζ O–R^+–O angular constraints.

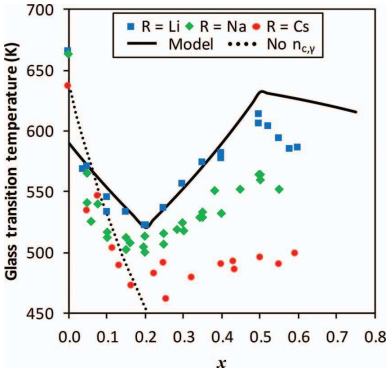

FIG. 5. Compositional dependence of the glass transition temperature of $(x)R_2O\ (1-x)P_2O_5$ glass, where R_2O is an alkali oxide. The solid line shows the predicted glass transition temperature using the topological model developed in this paper. The dotted line represents the predicted T_g with no modifier related γ constraints and $T_g(0) = 637$ K. Experimental data points are given in Refs. 11, 64, and 65.

P_2O_5 would be ideally constrained ($f = 3 - n_c = 0$) as seen in Fig. 4, and violate the condition that $0 < f[T_g,x] < 3$ implicit in Eq. (3). The ε and ζ bond-bending constraints are considered weaker than the δ constraint as the R^+-O bond has significant ionic character.

The compositional dependence of the number of rigid constraints at the glass transition temperature can be calculated by summing Eqs. (15)–(17) and substituting with Eqs. (7)–(13):

$$N_c(x) = \sum_i n_{c,i} = \begin{cases} \dfrac{12-2x}{5}, 0 \le x < \dfrac{1}{5} \\ \dfrac{11.2-2x}{5}, \dfrac{1}{5} \le x < \dfrac{1}{2} \\ \dfrac{17.2-10x}{7-4x}, \dfrac{1}{2} \le x < \dfrac{3}{4} \end{cases}. \quad (21)$$

By using Eq. (3) we obtain the following scaling of T_g with composition:

$$T_g(x) = \begin{cases} \dfrac{3}{3-2x} \times T_g(0), 0 \le x < \dfrac{1}{5} \\ \dfrac{3}{3.8-2x} \times T_g(0), \dfrac{1}{5} \le x < \dfrac{1}{2} \\ \dfrac{21-12x}{19-10x} \times T_g(0), \dfrac{1}{2} \le x < \dfrac{3}{4} \end{cases}. \quad (22)$$

The modeled $T_g(x)$ is compared to three sets of literature data[11,20,64,65] in Fig. 5. These three sets of data are thought to be the most accurate in the literature, as the glasses have been prepared in sealed silica ampules under vacuum. The glass transition temperatures have been measured by differential scanning calorimetry or differential thermal analysis at heating rates of 10 K/min or 20 K/min.

All three series of alkali phosphate glasses have a minimum in glass transition temperature in the vicinity of $x = 0.2$, which is consistent with formation of an alkali sub-network in the glass. A maximum in T_g is found at the metaphosphate ($x = 0.5$) composition. The maximum and minimum are less pronounced both in depth and sharpness for the sodium and cesium phosphate compositions. Our topological model uses the T_g of pure P_2O_5 glass of 590 K given by Martin and Angell.[19] The model correctly predicts the composition of the minimum T_g at $x = 0.2$, which is caused by alkali polyhedra beginning to share NBOs and therefore edges and gives additional constraints against the straight depolymerization of the phosphate network. A maximum is predicted at the metaphosphate composition, which is due to the conversion of Q^3 to Q^2 increasing the number of angular constraints in the tetrahedron by 2, while the number of angular constraints do not change from Q^2 to Q^1 or Q^1 to Q^0.

VI. LIQUID FRAGILITY

The liquid fragilities of anhydrous sodium phosphate glasses were determined by analyzing the variation of fictive temperature (T_f) as a function of heating rate by DSC in previously published findings.[20] The liquid fragility (m) is calculated from the change in T_f as in Eq. (23).

$$\log\left(\frac{q}{q_{ref}}\right) = m - m \times \frac{T_{f,ref}}{T_f}. \quad (23)$$

q is heating and previous cooling rate through the glass transition region, q_{ref} is the reference heating and cooling rate taken as 10 K/min and $T_{f,ref}$ is the fictive temperature corresponding to q_{ref}. The data are plotted in Fig. 6 and have a similar trend as $T_g(x)$, initially decreasing to a minimum around $x = 0.2$ and then increasing.

The liquid fragility is calculated from a topological basis by Eqs. (4)–(6), where the constraint onset temperature and vt_{obs} are input parameters. The oxygen bond-bending constraint onset temperature T_δ is found to be 328 K for borate[17]

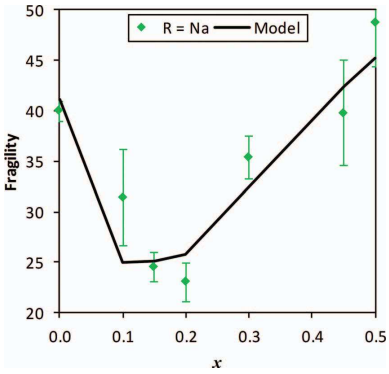

FIG. 6. Compositional dependence of the liquid fragility of $(x)Na_2O\,(1-x)P_2O_5$ glass. The solid line shows the predicted fragility using the topological model developed in this paper. Experimental data points and error bars are obtained fitting Eq. (23) to the experimental data in Ref. 20.

and borosilicate[32] glass compositions, and we also fix it at this temperature. T_α, T_β, T_γ, and vt_{obs} are determined by fitting to experimentally determined sodium phosphate liquid fragilities,[20] with the restriction that $T_\alpha > T_\beta > T_\gamma > T_\delta = 328$ K $> T_\varepsilon > T_\zeta$. The constraint onset temperatures are found to be $T_\alpha = 1400$ K, $T_\beta = 850$ K, $T_\gamma = 590$ K, and $vt_{obs} = 200$. T_α and T_δ have relatively little influence on the liquid fragility, for example; raising or lowering T_α by 200 K or T_δ by 100 K changes the liquid fragility of P_2O_5 by 3% at most. T_ε and T_ζ have essentially no effect on fragility given the requirement that they are lower than the P–O–P angular constraint onset temperature $T_\delta = 328$ K. vt_{obs} mainly affects the depth of the minimum in fragility and is fitted to be 200. In comparison vt_{obs} is 1000 for alkali borate compositions[17] and 60 for borosilicate compositions.[32] The modeled liquid fragility is plotted alongside experimental data in Fig. 6 and has a similar trend with a broad minimum between $x = 0.1$ and $x = 0.2$.

VII. DISCUSSION

The modeled and experimental $T_g(x)$ agree well for lithium phosphate compositions up to the metaphosphate composition, beyond which the model overestimates T_g. This indicates that as the NBO:R^+ ratio decreases above $x = 0.5$ then R^+ coordinates to less than four NBOs as suggested by structure B in Fig. 3. The topological model works well for lithium phosphate compositions, but less so for sodium phosphate and cesium phosphate compositions, which have lower $T_g(x)$ and broader minima. This could be due to higher water contents of the sodium and cesium phosphate compositions, as they have been prepared from P_4O_{10} and $(NaPO_3)_x$ or glassy $CsPO_3$ which are prone to retain water, while the lithium phosphates have been prepared from P_4O_{10} and Li_2O.

The average coordination number of the R^+ ion in alkali phosphate glasses increases from lithium at about four,[13,57,66–69] to sodium at five,[13,50,70,71] and cesium at six.[11] Due to this increase in coordination number, it could be expected that there should be more constraints on R^+ in sodium and cesium phosphate compositions, and $T_g(x)$ generally would be higher than for lithium compositions. The lowering of $T_g(x)$ when substituting a larger alkali ion in $(x)R_2O\cdot(1-x)P_2O_5$ glass has been linked to their lower charge-to-size ratio;[62,72] however, we propose an alternative explanation within the topological constraint theory framework. The dotted line in Fig. 5 represents the predicted $T_g(x)$ using the P_2O_5 reference $T_g(0) = 637$ K[11] and assuming the modifier-related γ constraints to be broken at T_g. Without the γ constraints $T_g(x)$ has an exponential-like decrease caused by the depolymerizing effect of R_2O on the phosphate network. These assumptions work well for predicting the initial decrease of $T_g(x)$, especially so for the cesium phosphates where $T_g(x)$ levels off around 480 K, but also sodium phosphates where $T_g(x)$ levels off around 510 K and then later increases. This is evidence that the assumption of intact γ constraints at T_g may not be valid throughout the compositional regime, and indeed the constraint onset temperature found by applying Eqs. (4)–(6) to fragility data of sodium phosphates is 590 K, not too far from the 510 K where the two models diverge. We believe that the lower $T_g(x)$ of sodium and cesium phosphate compositions could be caused by lower constraint onset temperatures of the γ constraints with larger alkali ions, which is associated with a weaker and more ionic character of the R^+–NBO bond.[72]

The modeled liquid fragilities of sodium phosphate glass forming liquids agree well with the available experimental data considering the experimental error. The broad minimum of liquid fragility spanning from $x = 0.1$ to $x = 0.2$ in the model is largely caused by the minimum in T_g in this compositional interval. As T_g becomes increasingly lower than the R^+–O linear constraint onset temperature $T_\gamma = 590$ K the change in degrees of freedom with temperature at T_g is less drastic, and the liquid fragility is lower. A minimum in liquid fragility has previously been linked to the intermediate phase in chalcogenide glasses.[73–75] The intermediate phase is defined as a range of glass forming compositions that have $f[T = 0,x] = 0$. If we also count constraints at 0 K then we find that compositions from $x = 0$ to $x = 0.2$ are isostatic ($f[T = 0,x] = 0$) and compositions with $x > 0.2$ are stressed-rigid ($f[T = 0,x] < 0$). Therefore our model predicts that at $x = 0.2$ there is a transition from an isostatic network to a stressed rigid network, and an intermediate phase is expected around this composition. This result agrees with the finding of an intermediate phase in $AgPO_3$–AgI glasses where the $AgPO_3$ composition is stressed rigid, but softens with the addition of AgI.[76] It is interesting to point out that there are two ways of counting the constraints for a given glass composition: the classical approach at absolute zero where are bond stretching and bond bending constraints are considered intact,[21–29] and the temperature dependent approach where some constraints are considered intrinsically broken by virtue of their low strength vs. thermal energy in the system.[17,30] Both of these approaches give insights into the underlying physics of the glass network. For example, the minimum in liquid fragility in Ge–Se chalcogenide glasses has both been linked to the intermediate phase by the classical approach[74]

and modeled along with $T_g(x)$ by the temperature-dependent approach.[30]

VIII. CONCLUSION

A topological model for alkali phosphate glasses was constructed based on structural data and the idea of a modifying ion sub-network. The model accurately predicts the glass transition temperatures of lithium phosphate glasses and reproduces the trend for sodium and cesium phosphate glasses. The minimum in $T_g(x)$ that occurs around $x_{crit} = 0.2$ in alkali phosphate glasses is explained by the increased connectivity of alkali ion sub-network as alkali ions must share non-bridging oxygen to satisfy their coordination requirements as x increases above x_{crit}. The lower glass transition temperatures of sodium and cesium phosphate glasses than that predicted by the model is explained by lower onset temperatures of their γ constraints related to the modifying ion sub-network. The model successfully predicts the liquid fragility of sodium ultraphosphate compositions, including the minimum seen around $x_{crit} = 0.2$. This minimum is reproduced in the model mainly due to the interplay between the minimum in $T_g(x)$ and the constraint onset temperature of the γ constraint T_γ. This is likely to correspond to an "intermediate phase" that is formed around $x_{crit} = 0.2$, which is compatible with our model using classical constraint counting at 0 K. However, whether there is an "intermediate phase" in general is still under debate.[77,78] Our model for the topology of phosphate glasses is compatible with previously derived topological models for borate and silicate glassy networks and can be used for mixed network former glasses.

Temperature dependent constraint theory is a powerful tool for predicting glass transition temperatures if the short range order is well defined and known. Our results show both the strengths and difficulties in applying temperature dependent constraint theory to modified random networks, such as alkali phosphate glasses, where relatively weak interactions are important.

ACKNOWLEDGMENTS

We gratefully acknowledge valuable discussions with Jonas Kjeldsen and also the work of Anna I. Fu in initially applying constraint theory to phosphate glasses.

[1] W. H. Zachariasen, J. Am. Chem. Soc. **54**, 3841 (1932).
[2] W. F. Krupke, W. D. Shinn, T. A. Kirchoff, C. B. Finch, and L. A. Boatner, Appl. Phys. Lett. **51**, 2186 (1987).
[3] T. Kasuga, Acta Biomater. **1**, 55 (2005).
[4] A. Garcia, M. Cicuéndez, I. Izquierdo-Barba, D. Arcos, and M. Vallet-Regí, Chem. Mater. **21**, 5474 (2009).
[5] L. Varila, S. Fagerlund, T. Lehtonen, J. Tuominen, and L. Hupa, J. Eur. Ceram. Soc. **32**, 2757 (2012).
[6] M. A. Karakassides, A. Saranti, and I. Koutselas, J. Non-Cryst. Solids **347**, 69 (2004).
[7] A. Saranti, I. Koutselas, and M. A. Karakassides, J. Non-Cryst. Solids **352**, 390 (2006).
[8] R. C. Agrawal and R. K. Gupta, J. Mater. Sci. **34**, 1131 (1999).
[9] P. S. Anantha and K. Hariharan, Mater. Chem. Phys. **89**, 428 (2005).
[10] R. K. Brow and D. R. Tallant, J. Non-Cryst. Solids **222**, 396 (1997).
[11] C. A. Click, R. K. Brow, and T. M. Alam, J. Non-Cryst. Solids **311**, 294 (2002).
[12] V. E. Kordes, W. Vogel, and R. Feterowsky, Z. Elektrochem. **57**, 282 (1953).
[13] R. K. Brow, J. Non-Cryst. Solids **263–264**, 1 (2000).
[14] G. N. Greaves and S. Sen, Adv. Phys. **56**, 1 (2007).
[15] A. I. Fu and J. C. Mauro, J. Non-Cryst. Solids **361**, 57 (2013).
[16] B. P. Rodrigues and L. Wondraczek, J. Chem. Phys. **138**, 244507 (2013).
[17] J. C. Mauro, P. K. Gupta, and R. J. Loucks, J. Chem. Phys. **130**, 234503 (2009).
[18] S. V. Nemilov, Neorg. Mater. **2**, 349 (1966).
[19] S. W. Martin and C. A. Angell, J. Phys. Chem. **90**, 6736 (1986).
[20] J. J. Hudgens, *The Structure and Properties of Anhydrous, Alkali Ultra-Phosphate Glasses* (Iowa State University, 1994).
[21] J. C. Phillips, J. Non-Cryst. Solids **34**, 153 (1979).
[22] J. C. Phillips, J. Non-Cryst. Solids **43**, 37 (1981).
[23] J. C. Phillips, J. Non-Cryst. Solids **44**, 17 (1981).
[24] M. F. Thorpe, J. Non-Cryst. Solids **57**, 355 (1983).
[25] J. C. Phillips and M. F. Thorpe, Solid State Commun. **53**, 699 (1985).
[26] H. He and M. F. Thorpe, Phys. Rev. Lett. **54**, 2107 (1985).
[27] M. F. Thorpe, J. Non-Cryst. Solids **76**, 109 (1985).
[28] M. F. Thorpe and Y. Cai, Phys. Rev. B **40**, 10535 (1989).
[29] M. F. Thorpe, M. V. Chubynsky, D. J. Jacobs, and J. C. Phillips, Glass Phys. Chem. **27**, 160 (2001).
[30] P. K. Gupta and J. C. Mauro, J. Chem. Phys. **130**, 094503 (2009).
[31] M. M. Smedskjaer, J. C. Mauro, and Y.-Z. Yue, Phys. Rev. Lett. **105**, 115503 (2010).
[32] M. M. Smedskjaer, J. C. Mauro, R. E. Youngman, C. L. Hogue, M. Potuzak, and Y.-Z. Yue, J. Phys. Chem. B **115**, 12930 (2011).
[33] M. Micoulaut and M. Bauchy, Phys. Status Solidi B **250**, 976 (2013).
[34] M. Micoulaut and M. Bauchy, Phys. Rev. Lett. **110**, 095501 (2013).
[35] P. Boolchand and M. F. Thorpe, Phys. Rev. B **50**, 10366 (1994).
[36] Y. Wang, J. Wells, D. G. Georgiev, P. Boolchand, K. Jackson, and M. Micoulaut, Phys. Rev. Lett. **87**, 185503 (2001).
[37] M. Bauchy, M. Micoulaut, M. Celino, S. Le Roux, M. Boero, and C. Massobrio, Phys. Rev. B **84**, 054201 (2011).
[38] M. Zhang and P. Boolchand, Science **266**, 1355 (1994).
[39] G. Adam and J. H. Gibbs, J. Chem. Phys. **43**, 139 (1965).
[40] Y. Bottinga and P. Richet, Chem. Geol. **128**, 129 (1996).
[41] G. G. Naumis, Phys. Rev. E **71**, 026114 (2005).
[42] T. M. Alam and R. K. Brow, J. Non-Cryst. Solids **223**, 1 (1998).
[43] C. Jäger, M. Feike, R. Born, and H. W. Spiess, J. Non-Cryst. Solids **180**, 91 (1994).
[44] M. Feike, C. Jäger, and H. W. Spiess, J. Non-Cryst. Solids **223**, 200 (1998).
[45] U. Hoppe, J. Non-Cryst. Solids **195**, 138 (1996).
[46] U. Hoppe, G. Walter, R. Kranold, D. Stachel, and A. Barz, J. Non-Cryst. Solids **192–193**, 28 (1995).
[47] G. Walter, U. Hoppe, T. Baade, R. Kranold, and D. Stachel, J. Non-Cryst. Solids **217**, 299 (1997).
[48] R. K. Brow, C. A. Click, and T. M. Alam, J. Non-Cryst. Solids **274**, 9 (2000).
[49] T. Uchino and Y. Ogata, J. Non-Cryst. Solids **181**, 175 (1995).
[50] W. Strojek and H. Eckert, Phys. Chem. Chem. Phys. **8**, 2276 (2006).
[51] S. Prabakar, R. M. Wenslow, and K. T. Mueller, J. Non-Cryst. Solids **263–264**, 82 (2000).
[52] L. Van Wüllen, H. Eckert, and G. Schwering, Chem. Mater. **12**, 1840 (2000).
[53] J. Tsuchida, J. Schneider, A. Orlandi de Oliveira, M. T. Rinke, and H. Eckert, Phys. Chem. Chem. Phys. **12**, 2879 (2010).
[54] T. M. Alam, J.-J. Liang, and R. T. Cygan, Phys. Chem. Chem. Phys. **2**, 4427 (2000).
[55] E. V. Murashova and N. N. Chudinova, Crystallogr. Rep. **46**, 942 (2001).
[56] A. McAdam, K. H. Jost, and B. Beagley, Acta Cryst. **B24**, 1621 (1968).
[57] M. Vogel, Phys. Rev. B **70**, 094302 (2004).
[58] A. Daidouh, M. L. Veiga, C. Pico, and M. Martinez-Ripoll, Acta Cryst. **C53**, 167 (1997).
[59] K. Y. Leung and C. Calvo, Can. J. Chem. **50**, 2519 (1972).
[60] S. Prabakar and K. T. Mueller, J. Non-Cryst. Solids **349**, 80 (2004).
[61] R. M. Wenslow and K. T. Mueller, J. Non-Cryst. Solids **231**, 78 (1998).
[62] A. Eisenberg, H. Farb, and L. G. Cool, J. Polym. Sci. Part A-2 **4**, 855 (1966).
[63] M. Bauchy and M. Micoulaut, J. Non-Cryst. Solids **357**, 2530 (2011).
[64] J. J. Hudgens and S. W. Martin, J. Am. Ceram. Soc. **76**, 1691 (1993).
[65] M. Doreau, A. Abou El Anouar, and G. Robert, Mater. Res. Bull. **15**, 285 (1980).

[66]K. Muruganandam, M. Seshasayee, and S. Patnaik, Solid State Ionics **89**, 313 (1996).
[67]T. M. Alam, S. Conzone, R. K. Brow, and T. J. Boyle, J. Non-Cryst. Solids **258**, 140 (1999).
[68]T. Uchino and T. Yoko, J. Non-Cryst. Solids **263–264**, 180 (2000).
[69]L. Swenson, A. Matic, A. Brodin, L. Börjesson, and W. S. Howells, Phys. Rev. B **58**, 11331 (1998).
[70]U. Hoppe, J. Non-Cryst. Solids **183**, 85 (1995).
[71]U. Hoppe, G. Herms, W. Gerike, and J. Sakowski, J. Phys. Condes. Matter **8**, 8077 (1996).
[72]L. Muñoz-Senovilla and F. Muñoz, J. Non-Cryst. Solids **385**, 9 (2014).
[73]P. Boolchand, D. G. Georgiev, and B. Goodman, J. Optoelectron. Adv. Mater. **3**, 703 (2001).
[74]K. Gunasekera, S. Bhosle, P. Boolchand, and M. Micoulaut, J. Chem. Phys. **139**, 164511 (2013).
[75]M. Micoulaut, J. Phys.: Condens. Matter **22**, 285101 (2010).
[76]D. I. Novita, P. Boolchand, M. Malki, and M. Micoulaut, J. Phys.: Condens. Matter **21**, 205106 (2009).
[77]G. Yang, B. Bureau, T. Rouxel, Y. Gueguen, O. Gulbiten, C. Roiland, E. Soignard, J. L. Yarger, J. Troles, J.-C. Sangleboeuf, and P. Lucas, Phys. Rev. B **82**, 195206 (2010).
[78]T. Wang, O. Gulbiten, R. Wang, Z. Yang, A. Smith, B. Luther-Davies, and P. Lucas, J. Phys. Chem. B **118**, 1436 (2014).

Paper III

Response to comment on "A model for phosphate glass topology considering the modifying ion sub-network" [J. Chem. Phys. 140, 154501 (2014)]

Christian Hermansen[1], John C. Mauro[2], Yuanzheng Yue[1,1)]
[1]*Section of Chemistry, Aalborg University, Fredrik Bajers Vej 7H, Aalborg 9220, Denmark*
[2]*Science and Technology Division, Corning Incorporated, Corning, New York 14831, USA*

In our recent paper [J. Chem. Phys. 140, 154501 (2014)], we applied temperature-dependent constraint theory to model the glass transition temperature (T_g) and liquid fragility index (m) of alkali phosphate glasses. Sidebottom commented on this paper concerning the m values obtained by differential scanning calorimetry (DSC).[1] We have considered Sidebottom's comments carefully and conclude that the m values of phosphate liquids obtained by DSC are mostly reliable, except for the $NaPO_3$ and possibly P_2O_5 compositions. Based on his dynamic light scattering (DLS) measurements, Sidebottom has found that P_2O_5 is a strong liquid with $m \approx 20$. However, based on the heat capacity jump at T_g and the stretching exponent of the relaxation function, P_2O_5 should be classified as an intermediate fragile liquid with $m \approx 40$. We also argue that m cannot be universally related to the average connectivity of the network and point out several inconsistencies with this view.

Anhydrous binary alkali phosphate glasses, written as xR_2O $(1\text{-}x)P_2O_5$, have an anomalous minimum in their compositional variation of the glass transition temperature (T_g) around $x = 0.2$. In our recent paper[2] the minimum in $T_g(x)$ was modeled using temperature-dependent constraint theory and found to be caused by crosslinking of the modifying ion sub-network. Temperature-dependent constraint theory can also predict the liquid fragility

[1)]Electronic mail: yy@bio.aau.dk

(*m*). We compared the predicted *m* values of sodium phosphates to experimental data from the differential scanning calorimetry (DSC) data of Hudgens[3]. These experimental results were obtained using the well-known method of Moynihan.[4,5]

In his comment, Sidebottom argues that the liquid fragility data derived from the DSC measurements by Hudgens[3] are incorrect.[1] Instead he relies on the *m* data obtained through dynamic light scatting (DLS) measurements.[6,7] Sidebottom believes that the DLS data are accurate, and he also discusses his interpretation regarding the theoretical origin of liquid fragility.[1] We respond to each of the points raised by Sidebottom in detail below.

A. Is DLS more suitable for liquid fragility measurements on sodium phosphates than DSC?

Sidebottom[1] argues that DLS is more suitable technique for determination of *m* compared to DSC because it is an *in situ* measurement with lower risk of contamination by water and because it spans a greater range of reduced temperatures, viz., from $T_g/T = 0.6$ to 0.9.[6,7]

There is little evidence of significant water contamination in Hudgens' DSC measurements.[3] The water content for the sodium phosphate glasses is estimated to be < 1 mole% H_2O based on elemental analysis of hydrogen content and intensity of the P-OH stretching vibration in infrared spectroscopy.[3] The DSC measurements were performed *ex situ*, but in hermetically sealed aluminium pans. Moreover, as Sidebottom points out in his comment, the DSC T_g of P_2O_5 at 653 K is close to the T_g estimated by DLS, i.e., 670 K.[6]

The range of T_g/T values explored by DSC is indeed quite narrow, with heating rates from 5 to 40 K/min typical values are $T_g/T = 0.97$ to 1.01. However, DSC has the advantage of directly measuring *m* in the temperature region around T_g, i.e., corresponding directly to the definition of *m* by Angell.[8] With DSC, an extrapolation of the heating rate-T_g/T relation to T_g is not required for determination of *m*. In contrast, the DLS approach[6] requires an extrapolation from high temperatures, which can lead to underestimation of *m*. The *m* derived from DSC has been found to agree with that from viscosity data for numerous glass systems.[5]

It should be noted that the DLS[6,7] and DSC data[3] actually agree quite well in the range of x = 0.1 to 0.4, so the main differences occur for the P_2O_5 and $NaPO_3$ compositions. The m values calculated from Hudgens' DSC data[3] are 40 ± 1 for P_2O_5 and 49 ± 4 for $NaPO_3$, but in Sidebottom's DLS data[6] m is 20 ± 2 for P_2O_5 and 80 ± 4 for $NaPO_3$.

The liquid fragility of $NaPO_3$ was recently measured directly by the temperature dependence of viscosity, and found to be m = 71.8 by fitting to the MYEGA equation.[9,10] The poor agreement between the DSC m of $NaPO_3$ and the viscosity m is most likely caused by only three heating rates having been used for this composition, versus five heating rates for the other compositions, leading to an unreliable m value for this composition. It is necessary to determine the liquid fragility of anhydrous P_2O_5 by viscosity measurements in order to conclusively settle the discrepancy between the m measured by DSC and DLS. However circumstantial evidence indicates that P_2O_5 is of intermediate fragility with $m \approx 40$, as we will discuss next.

B. Is P_2O_5 a strong liquid in terms of thermodynamic fragility?

There is a well-known relationship between thermodynamic and kinetic liquid fragility.[10,11] In general, the heat capacity jump from glass to liquid state, $\Delta C_p(T_g)$, can be regarded as a measure of thermodynamic fragility. Sidebottom[1] argues that P_2O_5 is strong since its $\Delta C_p(T_g)$ (= 6.29 cal/(mol K)) according to Hudgens' measurement is small.[3] However, a typical strong liquid like SiO_2 has a $\Delta C_p(T_g)$ value of 0.64 cal/(mol K),[11] which is 10 times lower than that of P_2O_5. We note that the $\Delta C_p(T_g)$ value of P_2O_5 is actually very close to that of $Na_2O{\bullet}2SiO_2$,[3] which has an intermediate m value of 45.[12,13]

Also, the stretching exponent (β) of P_2O_5 at T_g measured by Sidebottom[6] is estimated to be $\beta(T_g) \approx 0.5$ at T_g, which implies multiple activation barriers to viscous flow, i.e., non-Arrhenius dynamics characteristic of a more fragile liquid.[12,14] In contrast, $\beta(T_g)$ of for the prototypical strong liquids SiO_2 and GeO_2 are reported to be $\beta(T_g) \approx 0.7$ and $\beta(T_g) \approx 1.0$, respectively.[12]

C. Should the modifier-related γ constraints be flexible at T_g?

Sidebottom believes that the constraint onset temperature (T_γ = 590 K[2]) of modifier-related γ constraints is too high relative to the $T_g(x)$ of $x$$Na_2O$

$(1\text{-}x)P_2O_5$. Our recent work[15] concurs with this assessment, and for sodium phosphates the γ constraints are only partially intact at T_g. However some γ constraints could explain the high T_g of sodium phosphate glasses. For instance, T_g of $NaPO_3$ is 567 K,[3] whereas that of HPO_3 is 263 K due to lack of crosslinking of the modifying oxide.[16]

In Fig. 1 we fit the liquid fragility data by Sidebottom's DLS data[7] using Eq. (4) in our original paper[1] and our refined model for sodium phosphates[15] and find a value of T_γ = 575 K. By definition, half of the constraints are intact at $T = T_\gamma$, and so a T_γ slightly above T_g agrees well with our value of the constraint strength $q_\gamma = 0.75$ for sodium phosphate glasses.[15]

Molecular dynamics (MD) simulations on $Na_2O{\bullet}2SiO_2$ by Bauchy and Micoulaut[17] confirm that Eq. (5) in our original paper[2] is a good description of the fraction of intact constraints, but find that the constraint onset temperature for the $Na^+{-}O$ stretching constraint (equivalent to the γ constraint) in silicate glasses is only 360 K. However, the temperatures derived from MD simulations often cannot be directly applied to real systems, and phosphate liquids have not been investigated by their method. Also, physically the rigid-to-flexible transition is not a discontinuous transition, i.e., there is a range of temperatures over which the rigidity transition occurs.

D. Is fragility governed by the average connectivity of the liquid?

Instead of considering the liquid fragility to be related to the first derivative of the degrees of atomic freedom over temperature, as derived in temperature-dependent constraint theory, Sidebottom[1] argues that it is directly related to the topology of the network through the average connectivity of the network (ϕ), defined as the number of connections per network forming unit. Universally m should decrease steeply with increasing ϕ for $\phi < 2.4$, and for $\phi > 2.4$ m should level off or decrease slightly.[18–20] The obvious challenge for Sidebottom's idea is to explain why some glass formers instead shows an increase of m with ϕ. Alkali borates and alkali germanates are two systems that have increasing m with ϕ, and Sidebottom explained their deviating trends by their intermediate range order affecting the results.[19,20] However, this explanation would give incorrect trends for the scaling of glass transition temperature with composition.

We agree that in many glass-forming systems, m – with the notable exceptions of borates and germanates – tends to decrease with ϕ, but disagree that this is universally true. Sidebottom originally proposed this hypothesis because the measured m vs. ϕ curve in phosphates agrees well with a reported minimum in m at the average coordination number $\langle r \rangle = 2.4$ for chalcogenide glasses.[19,21,22] However ϕ and $\langle r \rangle$ are not the same, since ϕ does not take into account the coordination number of oxygen and $\langle r \rangle$ is defined as the average coordination number across all atoms in the glass. For example, for P_2O_5 $\phi = 3$ but $\langle r \rangle = 2.29$. Moreover, the reported minimum in m at $\langle r \rangle = 2.4$ for chalcogenides is an issue currently under debate.[23,24]

Apart from borates and germanates there are also other common glass formers that do not agree well with Sidebottom's view, e.g., SiO_2 with $\phi = 4$ and $m = 20$,[12] $CaO{\bullet}Al_2O_3$ with $\phi \approx 4$ and $m = 119$[25,26] and $Na_2O{\bullet}2SiO_2$ with $\phi = 3$ and $m = 45$.[12,13] The dependence of m on ϕ also cannot explain why m varies with varying the type of modifying oxides[9,27] or with mixing of two alkali oxides.[28,29] In contrast, the equation for fragility in temperature-dependent constraint theory is derived directly from Angell's definition of fragility,[8] which gives a physically meaningful and quantitatively predictive connection between fragility and the *change* in the number of rigid constraints with temperature at the glass transition.

FIGURES

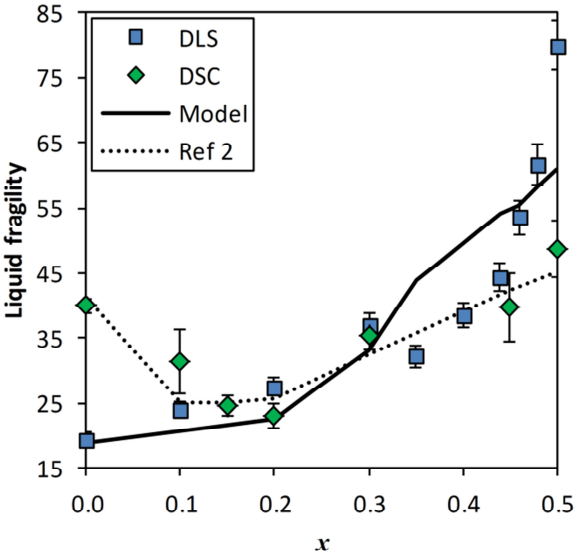

FIG 1. The liquid fragility (m) measured by DLS[6,7] and DSC[3] as a function of x in $x\mathrm{Na_2O}$ $(1\text{-}x)\mathrm{P_2O_5}$. The model is fitted to the DLS data using Eq. (4) in Ref. 2, and using a slightly revised topological model.[15] The constraint onset temperatures are T_α = 1400 K, T_β = 1100 K, T_γ = 575 K and T_δ = 328 K. vt_{obs} = 2000 and m_0 = 17. The lower m of this model compared to the previous[2] is due to a higher T_β = 1100 K compared to 850 K. The higher m at x = 0.5 is related to the higher number of γ constraints in our revised model[15] and a higher vt_{obs} = 2000 compared to vt_{obs} = 250 in Ref. 2.

REFERENCES

[1] D.L. Sidebottom, J. Chem. Phys. **In press**, (2014).
[2] C. Hermansen, J.C. Mauro, and Y.-Z. Yue, J. Chem. Phys. **140**, 154501 (2014).
[3] J.J. Hudgens, The Structure and Properties of Anhydrous, Alkali Ultra-Phosphate Glasses, Iowa State University, 1994.
[4] C.T. Moynihan, A.J. Easteal, M.A. DeBolt, and J. Tucker, J. Am. Ceram. Soc. **59**, 12 (1976).

[5] L.-M. Wang, V. Velikov, and C. a. Angell, J. Chem. Phys. **117**, 10184 (2002).
[6] D. Sidebottom and J. Changstrom, Phys. Rev. B **77**, 020201 (2008).
[7] R. Fabian and D. Sidebottom, Phys. Rev. B **80**, 064201 (2009).
[8] C.A. Angell, Science (80-.). **267**, 1924 (1995).
[9] L. Muñoz-Senovilla and F. Muñoz, J. Non. Cryst. Solids **385**, 9 (2014).
[10] J.C. Mauro, Y.-Z. Yue, A.J. Ellison, P.K. Gupta, and D.C. Allan, Proc. Natl. Acad. Sci. U. S. A. **106**, 19780 (2009).
[11] P. Richet, Y. Bottinga, L. Denielou, J.P. Petitet, and C. Tequi, Geochim. Cosmochim. Acta **46**, 2639 (1982).
[12] R. Böhmer, K.L. Ngai, C. a. Angell, D.J. Plazek, and R. Böhmer, J. Chem. Phys. **99**, 4201 (1993).
[13] M.D. Ediger, P. Harrowell, and L. Yu, J. Chem. Phys. **128**, 034709 (2008).
[14] L.-M. Wang, C.A. Angell, and R. Richert, J. Chem. Phys. **125**, 074505 (2006).
[15] C. Hermansen, B. Rodrigues, L. Wondraczek, and Y.-Z. Yue, J. Chem. Phys. **Under revi**, (2014).
[16] A. Eisenberg, H. Farb, and L.G. Cool, J. Polym. Sci. Part A-2 **4**, 855 (1966).
[17] M. Bauchy and M. Micoulaut, J. Non. Cryst. Solids **357**, 2530 (2011).
[18] T.D. Tran and D.L. Sidebottom, J. Am. Ceram. Soc. **96**, 2147 (2013).
[19] D.L. Sidebottom and S.E. Schnell, Phys. Rev. B **87**, 054202 (2013).
[20] D.L. Sidebottom, T.D. Tran, and S.E. Schnell, J. Non. Cryst. Solids **402**, 16 (2014).
[21] K. Gunasekera, S. Bhosle, P. Boolchand, and M. Micoulaut, J. Chem. Phys. **139**, 164511 (2013).
[22] M. Tatsumisago, B.L. Halfpap, J.L. Green, S.M. Lindsay, and C.A. Angell, Phys. Rev. Lett. **64**, 1549 (1990).
[23] H.Y. Zhao, Y.P. Koh, M. Pyda, S. Sen, and S.L. Simon, J. Non. Cryst. Solids **368**, 63 (2013).
[24] T. Wang, O. Gulbiten, R. Wang, Z. Yang, A. Smith, B. Luther-Davies, and P. Lucas, J. Phys. Chem. B **118**, 1436 (2014).
[25] J.W.E. Drewitt, S. Jahn, V. Cristiglio, A. Bytchkov, M. Leydier, S. Brassamin, H.E. Fischer, and L. Hennet, J. Phys. Condens. Matter **24**, 099501 (2012).

[26] M. Bouhadja, N. Jakse, and A. Pasturel, Mol. Simul. **40**, 251 (2013).
[27] M.M. Smedskjaer, J.C. Mauro, and Y.-Z. Yue, J. Chem. Phys. **131**, 244514 (2009).
[28] J.R. Changstrom and D.L. Sidebottom, J. Phys. Condens. Matter **20**, 285103 (2008).
[29] K. Putz and P.F. Green, J. Non. Cryst. Solids **337**, 254 (2004).

Paper IV

An extended topological model for binary phosphate glasses

Christian Hermansen,[1] Bruno P. Rodrigues,[2] Lothar Wondraczek,[2] and Yuanzheng Yue[1,3,a)]
[1]*Section of Chemistry, Aalborg University, 9000 Aalborg, Denmark*
[2]*Otto Schott Institute of Materials Research, University of Jena, 07743 Jena, Germany*
[3]*State Key Laboratory of Silicate Materials for Architecture, Wuhan University of Technology, Wuhan 430070, China*

(Received 19 September 2014; accepted 1 December 2014; published online XX XX XXXX)

We present a topological model for binary phosphate glasses that builds on the previously introduced concepts of the modifying ion sub-network and the strength of modifier constraints. The validity of the model is confirmed by the correct prediction of $T_g(x)$ for covalent polyphosphoric acids where the model reduces to classical constraint counting. The constraints on the modifying cations are linear constraints to first neighbor non-bridging oxygens, and all angular constraints are broken as expected for ionic bonding. For small modifying cations, such as Li^+, the linear constraints are almost fully intact, but for larger ions, a significant fraction is broken. By accounting for the fraction of intact modifying ion related constraints, q_γ, the $T_g(x)$ of alkali phosphate glasses is predicted. By examining alkali, alkaline earth, and rare earth metaphosphate glasses, we find that the effective number of intact constraints per modifying cation is linearly related to the charge-to-distance ratio of the modifying cation to oxygen. © *2014 AIP Publishing LLC.* [http://dx.doi.org/10.1063/1.4904287]

I. INTRODUCTION

Temperature-dependent constraint theory is a powerful tool for prediction of glass properties such as glass transition temperature (T_g), liquid fragility, heat capacity jump at T_g and indentation hardness. The theory has been applied for property prediction of chalcogenide,[1] borate,[2,3] borosilicate,[4] and most recently phosphate glasses.[5] Phosphate glasses are special since their properties are strongly affected by the modifying oxides, and constraint theory is usually concerned only with the network formers. Recently, there has been much attention on how to apply constraint theory to phosphate glasses and how to account for the effect of the modifying oxide.[5–9]

In the first application of temperature-dependent constraint theory to alkali phosphate glasses by Fu and Mauro, the constraint count on the network-forming phosphate species was done on the basis of hypothetic P_2O_5 groups.[6] This led to an offset in the number of constraints but did not affect prediction of the compositional trends in the original paper and, most importantly, their relation to experimental data.[6] This ambiguity was later resolved by Hermansen *et al.*[5] by proposing a model where P_2O_5 is topologically equivalent to B_2O_3, and by considering a modifying ion sub-network, the T_g and liquid fragility of lithium and sodium phosphate glasses was modeled. In this work, we generalize our model for lithium phosphate glasses[5] to work for other types of modifying oxide. Our results are consistent with those for the constraints on the modifying cations being caused by short-range interaction between the modifying cation and negatively charged non-bridging oxygen (NBO).

a)Electronic mail: yy@bio.aau.dk

II. THEORY

Topological constraint theory as applied to glasses was introduced in a series of seminal papers by Phillips and Thorpe,[10–18] and extended by Naumis,[19] Gupta and Mauro[1,2] to give a temperature dependent form that can quantitatively predict important glass properties such as T_g, liquid fragility and indentation hardness.[1–4]

The first step in applying temperature dependent constraint theory is to obtain quantitative structural data of the short range order in the glass, i.e., the concentration of each network forming unit. With this information, the intact constraints at the temperature range of interest must be identified, e.g., T_g is determined from the rigid constraints in the glass transition range, but indentation hardness from the constraints at room temperature.[3] The constraints are normally counted by nearest neighbor interactions only,[10] i.e., linear constraints from covalent or mixed-covalent bonds and angular constraints from bond angles. The number of linear and angular constraints around a network forming atom can be calculated by[16]

$$n_{c,linear} = \frac{1}{2}\mathrm{CN}\Big|_{\mathrm{CN}\geq 2}, \quad (1)$$

$$n_{c,angular} = (2\mathrm{CN}-3)|_{\mathrm{CN}\geq 2}, \quad (2)$$

where n_c are the number of constraints around an atom and CN is the coordination number of that atom to other network forming atoms. The case of one-fold coordinated atoms is special, and can either be treated by plucking these atoms from the network,[13,20] or counting half a linear constraint as by Eq. (1).[21] Both the linear and angular constraints are generally intact at or below T_g for network forming atoms in oxide glasses, but the angular constraints around oxygen are broken for vitreous

SiO_2[22,23] and assumed the same for alkali borate[2] and alkali phosphate glasses.[5,6]

The first step in relating the network constraints to the glass transition temperature is the Adam-Gibbs theory of the glass transition[24,25]

$$\log_{10}\eta(T,x) = \log_{10}\eta_\infty + \frac{B(x)}{TS_c(T,x)}, \tag{3}$$

where η is the viscosity as a function of temperature (T) and composition (x), η_∞ is the infinite temperature viscosity, $B(x)$ is related the potential energy barrier to viscous flow, and $S_c(T,x)$ is the configuration entropy of the melt. η_∞ is regarded as a constant around 10^{-3} Pa s,[26,27] and $B(x)$ does not vary significantly within a class of materials when the mechanism of viscous flow is similar.[28] We assume η_∞ and $B(x)$ to be constant and use Angell's definition of T_g occurring at a viscosity of 10^{12} Pa s.[29] With these assumptions, Eq. (3) entails the equality

$$T_g(x)\times S_c(T_g,x) = T_g(x_{ref})\times S_c(T_g,x_{ref}), \tag{4}$$

where x is the compositional variable and x_{ref} is a composition similar to x so that the assumption of constant $B(x)$ is not violated. Using Naumis's result of configurational entropy being largely due to the number floppy modes,[19] it is possible to relate T_g to the number of constraints

$$\frac{T_g(x)}{T_g(x_{ref})} = \frac{f(T_g(x_{ref}),x_{ref})}{f(T_g(x),x)} = \frac{3-N_c(T_g(x_{ref}),x_{ref})}{3-N_c(T_g(x),x)}, \tag{5}$$

where f is the number of degrees of freedom and N_c is the number of intact constraints per network forming atom at T_g. Equation (5) requires that $0 < f(T_g,x) < 3$.

We will now apply the topological constraint model to binary phosphate glass compositions containing various kinds of network modifying oxides.

III. POLYPHOSPHORIC ACIDS

Phosphoric acids nominally consists of a binary mixture of H_2O and P_2O_5, and their composition can be specified by the compositional variable x, as in $x H_2O\ (1-x)P_2O_5$. Up to $x = 0.75$ (orthophosphoric acid), H_2O dissolves in P_2O_5 as hydroxyl groups, which has hydrogen strictly covalently bonded to oxygen. Due to the covalent nature of the H–O and P–O bonding in this binary system, we can apply Eqs. (1) and (2) to find the number of network constraints from the structure of the glasses and calculate T_g with Eq. (5).

The short-range structure of two characteristic compositions, metaphosphoric acid ($x = 0.5$) and orthophosphoric acid ($x = 0.75$) are given in Fig. 1. The Q^n terminology is used to distinguish different phosphate tetrahedral units, where n denotes the number of bridging oxygen (BO) that bonds to other phosphate tetrahedra. There are two other types of oxygen, the double-bonded terminal oxygen (DBO) and NBO forming the O–H bond.

The structural evolution of $x H_2O\ (1-x)P_2O_5$ with x is described by the model of Van Wazer,[30] where the network is progressively depolymerized from Q^3 units ($x = 0$) to Q^2 units ($x = 0.5$) to Q^1 units ($x = 0.67$) and finally Q^0 units ($x = 0.75$) with a maximum of two Q^n coexisting at any given x. For

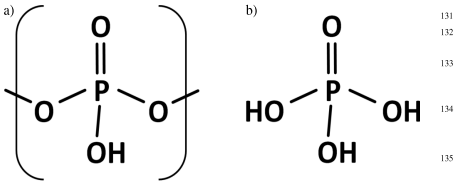

FIG. 1. (a) The structure of metaphosphoric acid (HPO_3; $x = 0.5$) ideally consist of chains and rings of Q^2 phosphate moieties. (b) The structure of orthophosphoric acid (H_3PO_4; $x = 0.75$) ideally consists of fully depolymerized Q^0 phosphate moieties and can be considered a molecular glass. For $x H_2O\ (1-x)P_2O_5$ compositions with $x > 0.75$, the structure consists of Q^0 units mixed with water molecules.

$x > 0.75$, the structure consists of Q^0 units and molecular water. A mathematical description of the structure is presented in our previous work.[5]

In our topological model, the DBO is not considered to be a part of the network because it is only one-fold coordinated, and phosphorous is effectively three-fold coordinated and topologically equivalent to B_2O_3.[5] Hydrogen is also one-fold coordinated but is considered part of the network, in line with recent molecular dynamics result of the topology of calcium-silicate-hydrate phase in cement.[31] Thus, for $x H_2O(1-x)P_2O_5$, the relevant constraints are

$$n_{c,\alpha}(x) = 3\times\left[Q^3(x)+Q^2(x)+Q^1(x)+Q^0(x)\right], \tag{6}$$

$$n_{c,\beta}(x) = 2\times \mathrm{BO}(x) + 1\times \mathrm{NBO}(x), \tag{7}$$

$$n_{c,\gamma}(x) = 1\times \mathrm{H}(x), \tag{8}$$

$$n_{c,\delta}(x) = 1\times[\mathrm{BO}(x)+\mathrm{NBO}(x)]. \tag{9}$$

Since every Q^n species has a DBO, which does not contribute to the network constraints, they are all effectively three-fold coordinated, and have 3 bond-bending (α) constraints. The bond stretching constraints in the phosphate network (β) are most easily counted at the oxygen, where each BO bonds to two P and each NBO bonds to 1 P. The H–O bond is the γ constraint. The α, β, and γ constraints are assumed to be intact at T_g, while the oxygen centered bond bending constraint (δ) is considered broken. By rearranging Eq. (5) and using $x_{ref} = 0.5$, we obtain the scaling of T_g with x

$$T_g(x) = \frac{3-N_c(0.5)}{3-N_c(x)}\times T_g(0.5) = \frac{3-\frac{7}{4}}{3-\frac{12-10x}{5-2x}}\times T_g(0.5), \tag{10}$$

where $T_g(0.5)$ is the T_g of HPO_3 taken to be 263 K.[32] The T_g of HPO_3 was used as the reference in the calculations because it is much closer to the compositional range we are modeling, meaning that the base assumptions of Eqs. (4) and (5) are not violated. The predicted $T_g(x)$ for $x H_2O\ (1-x)P_2O_5$ by Eq. (10) is shown along with experimental data in Fig. 2. The agreement between model and experiment is excellent. Unfortunately, no data is available for $x < 0.5$, but Eq. (8) extrapolates to 548 K for $x = 0$, which is very close to the T_g of the topologically equivalent glassy B_2O_3. The T_g of P_2O_5 has been measured to be between 590 K[33] and 665 K[34] by differential scanning

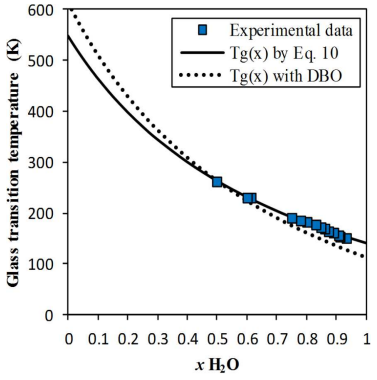

FIG. 2. $T_g(x)$ of the $x\mathrm{H_2O}$ $(1-x)\mathrm{P_2O_5}$ system as predicted by Eq. (10) and experimental data. Data for $x > 0.5$ were determined by DSC[93] and for $x = 0.5$ by dilatometer.[32] The largest discrepancy between the experimentally determined and the modeled T_g values is 4 K. The dotted line is for a topological model taking the DBO as a network forming atom with one constraint for the P–DBO bond and two additional α constraints for each Q^n.

calorimetry (DSC), and as high as 692 K by photon correlation spectroscopy.[35] The difference between the reported T_g's and our extrapolated value could be attributed to a non-negligible difference between $B(0)$ and $B(0.5)$ which invalidates Eq. (4) but could also be due to not accounting for the DBO.

The dotted line in Fig. 2 represents the predicted $T_g(x)$ by Eq. (5) if the DBO are taken to be a network forming atom, which causes two additional α constraints per Q^n and one β constraint per DBO. This topological model results in a worse description of the $T_g(x)$ of polyphosphoric acids. However, the extrapolated $T_g(0) = 614$ K is in the range experimentally determined for P_2O_5, indicating that taking into account the DBO might work better for the $x < 0.5$ compositional range. However, we previously found that the $T_g(x)$ of lithium ultraphosphate glasses can be described well without considering the DBO,[5] and this model will be extended to other alkalis in Sec. IV.

IV. ALKALI PHOSPHATES

The composition of alkali phosphates can be written as $x\mathrm{R}_{2/v}\mathrm{O}$ $(1-x)\mathrm{P_2O_5}$, where R^{v+} is the alkali ion and v is the valence equal to 1. Alloying R_2O into P_2O_5 causes the formation of negatively charged NBO to which the R^+ ions are ionically bound. The number of constraints on the R^+ cannot be quantified by Eqs. (1) and (2) because the ionic bonding is non-directional (i.e., $n_{c,angular} = 0$), and the R^+ is not strongly bound to all of its nearest neighbor NBO (i.e., $n_{c,linear} \leq {}^1/_2\mathrm{CN}$), as confirmed by molecular dynamics simulation on sodium disilicate glass.[36] For the sodium disilicate glass, the radial distribution of NBO around Na^+ was found to have smoothly increasing standard deviation with neighbor number up to CN = 5.[36] This radial standard deviation increases substantially with temperature.[36] The authors concluded that only one Na^+–NBO radial standard deviation was low enough to consider as an intact constraint at 300 K.[36] In our previous work, we developed a topological model for alkali phosphate glasses that takes into account constraints from the R^+ coordinating to NBOs.[5] This model works well for lithium phosphates where Li^+ has a coordination number around four[37–44] and Eq. (1) approximately holds, but R^+ with larger coordination numbers show increasing deviation from the model.[5] This reason, the concept of constraint strength was introduced which assigns a strength factor to each modifier ion.[8] Both model extensions–the modifier sub-network and the constraint strength–were recently applied in the prediction of T_g of binary alkali ultraphosphates.[9] Here, we also use the concept of constraint strength to generalize our topological model of alkali phosphate glasses even for alkali ions with large coordination numbers.

The structure of the phosphate network in alkali phosphate glasses is very similar to that of the phosphoric acids, where the structure is depolymerized by the addition of R_2O. A major difference is that the alkali donates its valence electron to NBO, causing the NBO to carry a negative charge. The negative charge is delocalized across both the NBO and DBO, and the two are indistinguishable in Q^2, Q^1, and Q^0 units.[45]

Alkali phosphate glasses exhibit an anomalous minimum in density and T_g.[34] A similar minimum for alkaline earth phosphate glasses led Hoppe[46–49] to propose that the minimum is caused by the structure around the modifying ions. At low x, there are enough NBO and DBO per modifying ion (R^{v+}, where v is the valence) to satisfy their preferred coordination number, and R^{v+} occurs in isolated coordination polyhedra in the phosphate matrix. At higher x, there are less DBO, and the R^{v+} polyhedra crosslink and share NBO, increasing the density and constraints in the network. The crossover is expected to occur at the $R_{2/v}O$ concentration x_{crit}, where all R^{v+} can satisfy their preferred CN without sharing NBO

$$x_{crit} = \frac{v}{CN}. \tag{11}$$

x_{crit} by Eq. (11) has been found to coincide with minima or plateaus in density and T_g, as well as the onset of R^{v+}–O–R^{v+} correlations and decreasing R^{v+} CN by diffraction experiments.[47,50]

The topological model for alkali phosphates glasses is

$$n_{c,\alpha}(x) = 3\times\mathrm{Q}^3(x) + 5\times\left[\mathrm{Q}^2(x) + \mathrm{Q}^1(x) + \mathrm{Q}^0(x)\right], \tag{12}$$

$$n_{c,\beta}(x) = 2\times\mathrm{BO}(x) + 1\times\mathrm{NBO}(x), \tag{13}$$

$$n_{c,\gamma}(x) = \begin{cases} 2\times\mathrm{R}^+(x); 0 \leq x \leq x_{crit} \\ \mathrm{CN}\times\mathrm{R}^+(x - x_{crit}) + 2\times\mathrm{R}^+(x_{crit}); x_{crit} < x \end{cases}, \tag{14}$$

$$n_{c,\delta}(x) = 1\times\mathrm{BO}(x). \tag{15}$$

As for the polyphosphoric acids in Sec. III, the α represents the P centered bond bending constraints, β is P–O bond stretching constraint, γ is the modifier related constraints, and δ is the O centered bond bending constraints. As R_2O is added to P_2O_5, the DBO on the Q^3 unit is turned into a NBO on Q^2, Q^1, or Q^0 units. Because the NBO participates in the glassy network, but the DBO does not, the number of P centered bond bending constraints (α) increases from 3 for Q^3 to 5 for Q^2,

Q^1, and Q^0. The γ constraints in Eq. (14) are linear constraints between R^+ and nearest neighbor NBO. When $x < x_{crit}$, the R^+ is coordinated with two NBO on P^2 units, with each NBO supplying half a negative charge to balance the positive R^+. The rest of the coordination shell is made up of DBO, and there are only two bond stretching γ constraints between R^+ and NBO. For $x_{crit} < x$, then R^+ must share NBO to satisfy their oxygen CN, and there are CN bond stretching γ constraints per R^+ added beyond x_{crit}. CN and x_{crit} for each alkali ion are given in Table I. We assume that the α and β constraints are fully intact at T_g, but consider the modifier related γ constraints to be partially broken, as also found in molecular dynamics simulation of sodium disilicate glass.[36] The fraction of intact γ constraints is denoted q_γ and can be thought of as a constraint strength. q_γ is usually taken to be temperature dependent,[1,2] but in this work, only the variation with the R^+ species is considered. The total number of intact constraints per atom at T_g is

$$N_c(x) = n_{c,\alpha}(x) + n_{c,\beta}(x) + q_\gamma \times n_{c,\gamma}(x). \quad (16)$$

By merging Eq. (16) with Eq. (5) and taking the reference composition to be P_2O_5 ($x_{ref} = 0$) and $T_g(0) = 590$ K,[33] an expression for $T_g(x)$ is obtained

$$T_g(x) = \frac{3 - N_c(0)}{3 - N_c(x)} \times T_g(0) = \frac{3 - \frac{12}{5}}{3 - \left(\frac{12}{5 + \frac{2x}{v} - 2x} - \frac{6x}{5 + \frac{2x}{v} - 2x} + q_\gamma \times n_{c,\gamma}\right)} \times T_g(0), 0 \le x \le \frac{1}{2}. \quad (17)$$

Here, $(5 + 2x/v - 2x)$ is the number of atoms in the composition $xR_{2/v}O\,(1-x)P_2O_5$ without counting the DBO. For the alkali phosphates $v = 1$ and there are simply 5 network forming atoms for $0 \le x \le 1/2$. $n_{c,\gamma}$ is determined from composition and modifying ion CN as by Eq. (14). We determine the fraction of intact γ constraints, q_γ, by fitting Eq. (17) to the experimentally determined metaphosphate ($x = 0.5$) T_g and CN. Equation (17) is only valid until the metaphosphate composition because it is based on Q^3 to Q^2 conversion, but it can easily be extended beyond $x = 0.5$ by accounting for the fraction of network forming units in this compositional range as previously shown.[5] The calculated q_γ for three alkali species are listed in Table I, and can be seen to decrease with increasing size and CN of the alkali ion.

TABLE I. Alkali CN, critical R_2O concentration for crosslinking of alkali coordination polyhedra (x_{crit}), and the fraction of intact γ constraints q_γ for lithium, sodium, and cesium phosphate glasses. CN is given in Fig. 1, x_{crit} calculated by Eq. (11), and q_γ by Eq. (17) from the T_g of the metaphosphate glass.

R^+	CN	x_{crit}	q_γ
Li^+	4[37–44]	0.2[a]	0.97
Na^+	5[44,46,52–54]	0.2	0.75
Cs^+	6[55]	0.17	0.52

[a]This is calculated using CN = 5. We assume that Li^+ is 5 coordinated at around x_{crit}, but 4 is coordinated in bridging sites above x_{crit}.

The effective number of intact constraints is the product $q_\gamma \times n_{c,\gamma}$ and is given for the metaphosphate compositions in Table II. For $NaPO_3$, then $q_\gamma \times n_{c,\gamma} = 2.8$, which is significantly higher than the single constraint per Na^+ found by molecular dynamics simulation of sodium disilicate glas.[36] One reason why the phosphate system has more γ constraints is likely that the NBO has a net negative charge of one half, which necessitates close interaction between Na^+ and two NBO, in contrast to the NBO having a net full negative charge in silicates. Since q_γ is a parameter that takes into account, the ionicity of the R^+–NBO bonding then by applying Eq. (17) with the parameters given in Table I, the $T_g(x)$ of the different alkali phosphate glasses can be predicted much better than our previously published model.[5] The predicted $T_g(x)$ are show in Fig. 3 along with the previous model using CN = 4 and $q_\gamma = 1$.

The advantage of our approach over the recent paper[9] that initially used a constraint strength to account for the compositional variation of T_g in alkali phosphate glasses is that we do not need to postulate a negative number of constraints in the isolated modifying ion sites occurring below x_{crit}, and a single value of q_γ is used for both isolated and crosslinking sites.

V. METAPHOSPHATES

The metaphosphate composition can be written as $R(PO_3)_v$, and corresponds to $x = 0.5$ for $v = 1$ and 2, and $x = 0.25$ for $v = 3$ in the general composition $xR_{2/v}O\,(1-x)P_2O_5$. This section will focus on how the γ constraints depend on v in iso-structural metaphosphate glasses, and we therefore prefer writing the composition as $R(PO_3)_v$ because this emphasizes that the glass consists of R^{v+} charge balanced by Q^2 tetrahedra. These Q^2 units contain two BO and two NBO and occur as chains or rings. In Sec. IV, the T_g of the metaphosphate composition was used to determine the constraint strength (q_γ) of the R^+–NBO interaction. The metaphosphate is well suited for this purpose as the coordination sphere of R^{v+} ideally consists solely of NBO on Q^2 units. Also, the metaphosphate is the composition with the best glass forming ability and lowest hygroscopicity in the $xR_{2/v}O\,(1-x)P_2O_5$ system, and reliable data for physical properties such as T_g are usually available. In this section, we use literature data for the T_g of alkaline earth and rare earth metaphosphates to evaluate $q_\gamma \times n_{c,\gamma}$ (i.e., the effective number of modifier constraints) in order to explain their dependence on the R^{v+} species.

$q_\gamma \times n_{c,\gamma}$ is determined by fitting Eq. (17) to the literature T_g's in Table II, where the results, ionic radii, and experimentally determined CNs of the modifying cations are also reported. There is no strong correlation between CN and $q_\gamma \times n_{c,\gamma}$ per R^{v+}, as found previously,[8] but they fall in the same range between 2 and 8 indicating that the γ constraints are related to the R^{v+}–NBO bonds. The lack of correlation to CN and strong influence of valence are evidence that the nature of the R^{v+}–NBO interactions is of an ionic nature. $q_\gamma \times n_{c,\gamma}$ per R^{v+} is approximately twice the valence of the modifying cation (equal to the number of NBOs per R^{v+}), but with a distinct dependence of ionic radius. We find that the variation

TABLE II. Literature data for glass transition temperature (T_g), R–O CN and ionic radius, effective number of constraints at T_g per modifying cation ($q_\gamma \times n_{c,\gamma}$) by Eq. (17). T_g has been determined by DSC, differential thermal analysis, and TMA, and CN by XRD, negative differential conductivity, and MD on compositions that as far as possible are anhydrous metaphosphates of correct stoichiometry without significant Al_2O_3 or SiO_2 impurities. Ionic radii are effective Shannon radii in 6-fold coordination,[51] and charge-to-distance ratios (σ) are calculated from Eq. (18) with the Shannon radii and $r_{O^{2-}} = 1.4$ Å.[51]

$R(PO_3)_v$	T_g (K)	CN	$q_\gamma \times n_{c,\gamma}$	Ionic radius (pm)	σ (e/Å)
$LiPO_3$	604[42,45,56–63]	4.1[37–44]	3.1	76	0.46
$NaPO_3$	560[45,56–59,64]	4.9[44,46,52–54]	2.8	102	0.41
$AgPO_3$	502[59,65]	3.6[66,67]	2.5	115	0.39
KPO_3	494[59,68,69]	6.4[46]	2.4	138	0.36
$RbPO_3$	468[59]	5.0[38]	2.2	152	0.34
$CsPO_3$	470[55,59]	6.0[55]	2.2	167	0.33
$Mg(PO_3)_2$	830[69,70]	4.9[44,46,54,71–73]	5.2	72	0.94
$Ca(PO_3)_2$	809[70,74,75]	6.2[44,46,54,76]	5.1	100	0.83
$Sr(PO_3)_2$	787[77,78]	7.1[46]	5.0	118	0.78
$Ba(PO_3)_2$	741[69,74,79,80]	8.5[46,54]	4.7	135	0.73
$Yb(PO_3)_3$	1018[81]	6.5[82]	7.5	87	1.32
$Er(PO_3)_3$	1000[81]	6.3[82–86]	7.4	89	1.31
$Ho(PO_3)_3$	990[81]	5.8[83,84]	7.4	90	1.30
$Dy(PO_3)_3$	998[87]	6.0[82–85]	7.4	91	1.30
$Tb(PO_3)_3$	923[88]	5.9[83,84,89]	7.0	92	1.29
$Sm(PO_3)_3$	908[88]	6.7[82–85]	6.9	96	1.27
$Nd(PO_3)_3$	903[81,87]	7.0[82–86]	6.9	98	1.26
$Pr(PO_3)_3$	898[81,87]	6.6[82,83]	6.9	99	1.26
$Ce(PO_3)_3$	893[81]	5.9[83,84]	6.8	101	1.24
$La(PO_3)_3$	892[90,91]	6.9[46,50,82,83,85,92]	6.8	103	1.23

in $q_\gamma \times n_{c,\gamma}$ per R^{v+} for different modifying ions is related to the charge-to-distance ratio (σ) proposed by Eisenberg,[32] which is a measure of the coulombic interaction between modifying cations and NBOs and defined as

$$\sigma = \frac{v}{r_{R^{v+}} + r_{O^{2-}}}, \tag{18}$$

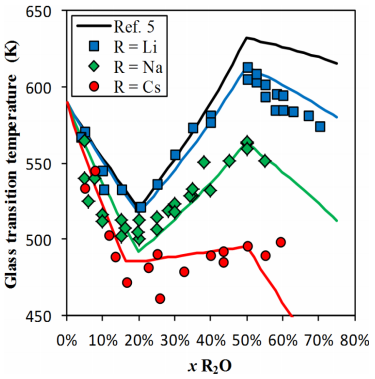

FIG. 3. Compositional dependence of the glass transition temperature of $(x)R_2O\,(1-x)P_2O_5$ glass, where R_2O is an alkali oxide. The solid black curve shows the predicted glass transition temperature using the topological model developed previously, having CN = 4 and $q_\gamma = 1$.[5] The solid colored curves are the predicted T_g using the modified model from Eq. (17) and Table I. Experimental data points are measured by DSC.[55,63,94]

where $r_{R^{v+}}$ is the ionic radius of the modifying cation and $r_{O^{2-}}$ is the ionic radius of the NBO equal to 1.4 Å.[51] Fig. 4 shows an approximate linear relation between $q_\gamma \times n_{c,\gamma}$ per R^{v+} and σ for the metaphosphate compositions in Table II. A similar correlation was reported before, but using a different topological model and interpretation of "constraint strength."[8] Our result different because $q_\gamma \times n_{c,\gamma}$ per R^{v+} and observables like NBO/R^{v+} and CN fall in the same ranges, which hints that the γ constraints are related to the short range order around the modifying cations.

By using the semi-empirical relation between $q_\gamma \times n_{c,\gamma}$ and σ given in Fig. 4 and calculating x_{crit} by Eq. (11), it is possible to evaluate the compositional dependence properties as was done for the $T_g(x)$ of alkali phosphates in Sec. IV. The preferred CN is needed to evaluate x_{crit} by Eq. (11), which can be obtained directly by diffraction experiments of compositions close to x_{crit}, inferred from relevant crystal structures, but also evaluated by the presence of a minimum or plateau in the compositional variation of properties such as density, molar volume, or T_g. It is necessary to perform systematic studies of the indentation hardness and T_g in anhydrous alkaline earth and rare earth phosphate glasses in order to test the predictions of the topological model of binary phosphate glasses presented in this work.

VI. CONCLUSION

The topological model for binary phosphate glasses developed in this paper can predict the compositional variation of T_g of polyphosphoric acids using classical constraint counting.

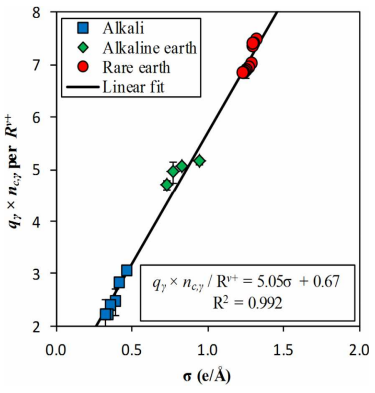

FIG. 4. The effective number of constraints per modifying cation ($q_\gamma \times n_{c,\gamma}$ per R^{v+}) in alkali, alkaline earth, and rare earth metaphosphate glasses against the charge-to-distance ratio (σ) defined in Eq. (18). The line is the best linear fit to data and R^2 is the correlation coefficient reflecting the fitting quality.

Previously a model for lithium phosphate glasses was developed[5] using classical constraint counting in the phosphate network, but only considering linear Li^+–NBO interactions on the Li^+ ions. Two different Li^+-sites were considered based on experimental data of density and T_g minimum and Li–O coordination number, one site being isolated with 2 Li^+–NBO constraints and another being crosslinking with 4 Li^+–NBO constraints creating a modifying ion sub-network.[5]

This work builds on previous efforts[5,8] to generalize the approach for other modifying oxides using the concept of constraint strength. A factor q_γ is introduced which indicates the fraction of intact modifying ion related constraints. q_γ is found to decrease with ionic size and coordination number of the alkali ion introduced into the phosphate glass.

The value of q_γ depends on temperature according to temperature dependent constraint theory, and is expected to be unity at low temperatures. By measuring a low temperature property which is related to the number of constraints in the system, such as indentation hardness, it is possible to substantiate our interpretation of q_γ as constraint strength.

When applying the model to alkali, alkaline earth, and rare earth metaphosphate glasses, it is found that the number of constraints per modifying ion is approximately twice the valence (equal to the number of NBO per modifying ion) and does not exceed the maximum expected coordination number of 8. An empirical relation between the effective number of constraints per modifying ion and the charge-to-distance ratio were confirmed.[8] This relation can be used to determine the compositional variation of properties such as T_g of phosphate glasses containing these modifying oxides.

[1]P. K. Gupta and J. C. Mauro, J. Chem. Phys. **130**, 094503 (2009).
[2]J. C. Mauro, P. K. Gupta, and R. J. Loucks, J. Chem. Phys. **130**, 234503 (2009).
[3]M. M. Smedskjaer, J. C. Mauro, and Y.-Z. Yue, Phys. Rev. Lett. **105**, 115503 (2010).
[4]M. M. Smedskjaer, J. C. Mauro, R. E. Youngman, C. L. Hogue, M. Potuzak, and Y.-Z. Yue, J. Phys. Chem. B **115**, 12930 (2011).
[5]C. Hermansen, J. C. Mauro, and Y.-Z. Yue, J. Chem. Phys. **140**, 154501 (2014).
[6]A. I. Fu and J. C. Mauro, J. Non-Cryst. Solids **361**, 57 (2013).
[7]B. P. Rodrigues and L. Wondraczek, J. Chem. Phys. **138**, 244507 (2013).
[8]B. P. Rodrigues and L. Wondraczek, J. Chem. Phys. **140**, 214501 (2014).
[9]B. P. Rodrigues, J. C. Mauro, Y. Yue, and L. Wondraczek, J. Non-Cryst. Solids **405**, 12 (2014).
[10]J. C. Phillips, J. Non-Cryst. Solids **34**, 153 (1979).
[11]J. C. Phillips, J. Non-Cryst. Solids **43**, 37 (1981).
[12]J. C. Phillips, J. Non-Cryst. Solids **44**, 17 (1981).
[13]M. F. Thorpe, J. Non-Cryst. Solids **57**, 355 (1983).
[14]J. C. Phillips and M. F. Thorpe, Solid State Commun. **53**, 699 (1985).
[15]H. He and M. F. Thorpe, Phys. Rev. Lett. **54**, 2107 (1985).
[16]M. F. Thorpe, J. Non-Cryst. Solids **76**, 109 (1985).
[17]M. F. Thorpe and Y. Cai, Phys. Rev. B **40**, 10535 (1989).
[18]M. F. Thorpe, M. V. Chubynsky, D. J. Jacobs, and J. C. Phillips, Glass Phys. Chem. **27**, 160 (2001).
[19]G. G. Naumis, Phys. Rev. E **71**, 026114 (2005).
[20]G. H. Döhler, R. Dandoloff, and H. Bilz, J. Non-Cryst. Solids **42**, 87 (1980).
[21]P. Boolchand and M. F. Thorpe, Phys. Rev. B **50**, 10366 (1994).
[22]M. Bauchy, M. Micoulaut, M. Celino, S. Le Roux, M. Boero, and C. Massobrio, Phys. Rev. B **84**, 054201 (2011).
[23]M. Zhang and P. Boolchand, Science **266**, 1355 (1994).
[24]G. Adam and J. H. Gibbs, J. Chem. Phys. **43**, 139 (1965).
[25]Y. Bottinga and P. Richet, Chem. Geol. **128**, 129 (1996).
[26]J. C. Mauro, Y.-Z. Yue, A. J. Ellison, P. K. Gupta, and D. C. Allan, Proc. Natl. Acad. Sci. U. S. A. **106**, 19780 (2009).
[27]Q. Zheng, J. C. Mauro, A. J. Ellison, M. Potuzak, and Y.-Z. Yue, Phys. Rev. B **83**, 212202 (2011).
[28]M. J. Toplis, Am. Mineral **83**, 480 (1998).
[29]C. A. Angell, Science **267**, 1924 (1995).
[30]R. K. Brow, J. Non-Cryst. Solids **263-264**, 1 (2000).
[31]M. Bauchy, M. J. A. Qomi, C. Bichara, F.-J. Ulm, and R.J.-M. Pellenq, J. Phys. Chem. C **118**, 12485 (2014).
[32]A. Eisenberg, H. Farb, and L. G. Cool, J. Polym. Sci., Part A-2 **4**, 855 (1966).
[33]S. W. Martin and C. A. Angell, J. Phys. Chem. **90**, 6736 (1986).
[34]J. J. Hudgens, "The structure and properties of anhydrous," *Alkali Ultra-Phosphate Glasses* (Iowa State University, 1994).
[35]D. Sidebottom and J. Changstrom, Phys. Rev. B **77**, 020201 (2008).
[36]M. Bauchy and M. Micoulaut, J. Non-Cryst. Solids **357**, 2530 (2011).
[37]T. M. Alam, S. Conzone, R. K. Brow, and T. J. Boyle, J. Non-Cryst. Solids **258**, 140 (1999).
[38]L. Swenson, A. Matic, A. Brodin, L. Börjesson, and W. S. Howells, Phys. Rev. B **58**, 11331 (1998).
[39]T. M. Alam, J.-J. Liang, and R. T. Cygan, Phys. Chem. Chem. Phys. **2**, 4427 (2000).
[40]A. Karthikeyan, P. Vinatier, A. Levasseur, and K. J. Rao, J. Phys. Chem. B **103**, 6185 (1999).
[41]K. Muruganandam, M. Seshasayee, and S. Patnaik, Solid State Ionics **89**, 313 (1996).
[42]L. van wüllen, H. Eckert, and G. Schwering, Chem. Mater. **12**, 1840 (2000).
[43]M. Vogel, Phys. Rev. B **70**, 094302 (2004).
[44]Y. Waseda, E. Matsubara, K. Sugiyama, I. K. Suh, T. Kawazoe, O. Kasu, M. Ashizuka, and E. Ishida, Sci. Rep. Res. Inst., Tohoku Univ., Ser. A **35**, 19 (1990).
[45]J. J. Hudgens, R. K. Brow, D. R. Tallant, and S. W. Martin, J. Non-Cryst. Solids **223**, 21 (1998).
[46]U. Hoppe, G. Walter, R. Kranold, and D. Stachel, J. Non-Cryst. Solids **263-264**, 29 (2000).
[47]U. Hoppe, J. Non-Cryst. Solids **195**, 138 (1996).
[48]U. Hoppe, G. Walter, R. Kranold, D. Stachel, and A. Barz, J. Non-Cryst. Solids **192-193**, 28 (1995).
[49]G. Walter, U. Hoppe, T. Baade, R. Kranold, and D. Stachel, J. Non-Cryst. Solids **217**, 299 (1997).
[50]U. Hoppe, E. Metwalli, R. K. Brow, and J. Neuefeind, J. Non-Cryst. Solids **297**, 263 (2002).
[51]R. D. Shannon, Acta Crystallogr., Sect. A **32**, 751 (1976).
[52]U. Hoppe, L. Delevoye, L. Montagne, M. V. Zimmermann, and A. C. Hannon, Phys. Chem. Chem. Phys. **15**, 8520 (2013).
[53]A. Speghini, E. Sourial, T. Peres, G. Pinna, M. Bettinelli, and J. A. Capobianco, Phys. Chem. Chem. Phys. **1**, 173 (1999).
[54]U. Hoppe, D. Stache, and D. Beyer, Phys. Scr. **57**, 122 (1995).

[55]C. A. Click, R. K. Brow, and T. M. Alam, J. Non-Cryst. Solids **311**, 294 (2002).
[56]D. L. Sidebottom, P. F. Green, and R. K. Brow, J. Mol. Struct. **479**, 219 (1999).
[57]P. F. Green, E. F. Brown, and R. K. Brow, J. Non-Cryst. Solids **255**, 87 (1999).
[58]R. Chen, R. Yang, B. Durand, A. Pradel, and M. Ribes, Solid State Ionics **53-56**, 1194 (1992).
[59]J. Tsuchida, J. Schneider, R. R. Deshpande, and H. Eckert, J. Phys. Chem. C **116**, 24449 (2012).
[60]J. R. Changstrom and D. L. Sidebottom, J. Phys.: Condens. Matter **20**, 285103 (2008).
[61]P. Mošner, K. Vosejpková, and L. Koudelka, J. Therm. Anal. Calorim. **95**, 53 (2009).
[62]B. K. Money and K. Hariharan, Appl. Phys. A **88**, 647 (2007).
[63]J. J. Hudgens and S. W. Martin, J. Am. Ceram. Soc. **76**, 1691 (1993).
[64]J. Schneider, S. L. Oliveira, L. A. O. Nunes, and H. Panepucci, J. Am. Ceram. Soc. **86**, 317 (2003).
[65]D. I. Novita, P. Boolchand, M. Malki, and M. Micoulaut, J. Phys.: Condens. Matter **21**, 205106 (2009).
[66]A. Musinu, G. Piccaluga, and G. Pinna, J. Chem. Phys. **89**, 1074 (1988).
[67]A. Musinu, G. Paschina, G. Piccaluga, and G. Pinna, J. Non-Cryst. Solids **177**, 97 (1994).
[68]J. Tsuchida, J. Schneider, M. T. Rinke, and H. Eckert, J. Phys. Chem. C **115**, 21927 (2011).
[69]E. Metwalli and R. K. Brow, J. Non-Cryst. Solids **289**, 113 (2001).
[70]P. Prokupková, P. Mošner, L. Koudelka, and M. Vlček, J. Mater. Sci. **33**, 743 (1998).
[71]K. Suzuya, D. L. Price, C.-K. Loong, and S. Kohara, J. Phys. Chem. Solids **60**, 1457 (1999).
[72]U. Hoppe, R. Kranold, A. Barz, D. Stachel, J. Neuefeind, and D. Keen, J. Non-Cryst. Solids **293-295**, 158 (2001).
[73]E. Sourial, T. Peres, J. A. Capobianco, A. Speghini, and M. Bettinelli, Phys. Chem. Chem. Phys. **1**, 2013 (1999).
[74]E. T. Y. Lee and E. R. M. Taylor, Opt. Mater. **28**, 200 (2006).
[75]J. Schneider, S. L. Oliveira, L. A. O. Nunes, F. Bonk, and H. Panepucci, Inorg. Chem. **44**, 423 (2005).
[76]U. Hoppe, J. Non-Cryst. Solids **183**, 85 (1995).
[77]I. Konidakis, C. E. Varsamis, E. I. Kamitsos, D. Möncke, and D. Ehrt, J. Phys. Chem. C **114**, 9125 (2010).
[78]S. M. Hsu, J. J. Wu, S. W. Yung, T. S. Chin, T. Zhang, Y. M. Lee, C. M. Chu, and J. Y. Ding, J. Non-Cryst. Solids **358**, 14 (2012).
[79]J. E. Shelby, J. Non-Cryst. Solids **263-264**, 271 (2000).
[80]J. S. Hassan and M. Hafid, Mater. Res. Bull. **39**, 1123 (2004).
[81]V. A. Levenberg and S. G. Lunter, Fiz. Khim. Stekla **5**, 740 (1979).
[82]U. Hoppe, R. K. Brow, D. Ilieva, P. Jóvári, and A. C. Hannon, J. Non-Cryst. Solids **351**, 3179 (2005).
[83]R. Anderson, T. Brennan, J. M. Cole, G. Mountjoy, D. M. Pickup, R. J. Newport, and G. A. Saunders, J. Mater. Res. **14**, 4706 (1999).
[84]J. M. Cole, E. R. H. van eck, G. Mountjoy, R. Anderson, T. Brennan, G. Bushnell-Wye, R. J. Newport, and G. A. Saunders, J. Phys.: Condens. Matter **13**, 4105 (2001).
[85]J. M. Cole, R. J. Newport, D. T. Bowron, R. F. Pettifer, G. Mountjoy, T. Brennan, and G. A. Saunders, J. Phys.: Condens. Matter **13**, 6659 (2001).
[86]M. Karabulut, G. Marasinghe, E. Metwalli, A. Wittenauer, R. Brow, C. Booth, and D. Shuh, Phys. Rev. B **65**, 104206 (2002).
[87]D. Ilieva, D. Kovacheva, J. M. Cole, and I. Gutzow, Phosphorous Res. Bull. **13**, 137 (2002).
[88]T. Komiyama, Bull. Gov. Ind. Res. Inst., Osaka **25**, 84 (1974).
[89]E. B. Clark, R. N. Mead, and G. Mountjoy, J. Phys.: Condens. Matter **18**, 6815 (2006).
[90]G. Harley, K.-D. Kreuer, J. Maier, and L. C. De Jonghe, J. Non-Cryst. Solids **355**, 932 (2009).
[91]M. Karabulut, E. Metwalli, and R. Brow, J. Non-Cryst. Solids **283**, 211 (2001).
[92]U. Hoppe, R. Kranold, D. Stachel, A. Barz, and A. C. Hannon, J. Non-Cryst. Solids **232-234**, 44 (1998).
[93]H. R. Corti, F. J. Nores-Pondal, and C. A. Angell, Phys. Chem. Chem. Phys. **13**, 19741 (2011).
[94]M. Doreau, A.A.El. Anouar, and G. Robert, Mater. Res. Bull. **15**, 285 (1980).

Paper V

Paper V

Structural and topological aspects of borophosphate glasses and their relation to physical properties

Christian Hermansen,[1] Randall E. Youngman,[2] John Wang[3], and Yuanzheng Yue[1,4,a)]

[1]*Section of Chemistry, Aalborg University, Sohngaardsholmvej 57, Aalborg 9000, Denmark*

[2]*Science and Technology Division, Corning Incorporated, Corning, New York 14831, USA*

[3]*Department of Materials Science and Engineering, National University of Singapore, Engineering Drive 1, Singapore 117574, Singapore*

[4]*State Key Laboratory of Silicate Materials for Architecture, Wuhan University of Technology, Wuhan 430070, China*

[a)]*Electronic mail: yy@bio.aau.dk*

We establish a temperature dependent constraint model of alkali borophosphate and calcium borophosphate glasses that describes both the effect of the network formers and network modifiers on physical properties. We show that the glass transition temperature (T_g), Vickers hardness (H_V), liquid fragility (m) and thermodynamic fragility (ΔC_p) of these glasses are related to the network topology, which is determined by structure of the glass. Therefore, we also demonstrate that the temperature dependent constraint theory can quantitatively explain the mixed network former effect (MNFE) in borophosphate glasses. The origin of the effect of the type of network modifying oxide on T_g, H_V, m and ΔC_p of calcium borophosphate glasses is revealed in terms of the modifying ion sub-network. The same topological principles quantitatively explain the significant differences in physical properties between the alkali and the calcium borophosphate glasses. This work has implications for quantifying structure-property relations in complex glass forming systems containing several types of network forming and modifying oxides.

Paper V

I. INTRODUCTION

Borophosphate glass compositions are a prototypical example of the mixed network former effect (MNFE) showing highly non-linear evolution of properties with composition. Some of the affected properties are ionic conductivity, glass transition temperature and water solubility, which are generally all higher in the mixed glasses than the pure borate or phosphate compositions, thus making borophosphate glasses of interest for application in batteries, glass-to-metal seals and bone replacement materials.

Nuclear magnetic resonance (NMR) and Raman spectroscopy investigations have shown a strong preference of boron to assume four-fold coordination (B^4), to the extent that phosphorous will charge compensate if there is no modifier available, as in the crystal structure of BPO_4 which is isomorphous with α-cristobalite.[1] The MNFE in borophosphate glasses is believed to be due to a non-linear variation of the structural units with composition, which is caused by the high affinity of boron and phosphorous oxide.[2] Although numerous studies of the structure of borophosphate glasses have been reported, a quantitative structure-property relation has not been fully established and understood.

Temperature dependent constraint theory has emerged as a powerful tool to predict properties such as glass transition temperature[3], fragility[3] and indentation hardness[4] from glass structure. Temperature dependent constraint theory is an extension of the classical constraint theory of Phillips and Thorpe,[5–13] and has been applied to alkali borates[14] and phosphates[15,16], as well as borosilicates[17] which also exhibit a MNFE. The structure-property relation of sodium borophosphate glasses have been modeled with temperature dependent constraint theory by Jiang et al.[18] They achieved some promising results, yet their model is not predictive since the experimental T_g of the entire $x$$Na_2O$ (1-x)P_2O_5 and $x$$Na_2O$ (1-x)[0.4B_2O_3 0.6P_2O_5] pseudobinary systems are used to scale their modeled T_g. In other words, the work by Jiang et al.[18] cannot be used to predict the properties of borophosphate glasses *ab initio*.

In this work we first derive a simple structural model of borophosphate glasses in good agreement with available structural data by assuming the maximum incorporation of B^4 tetrahedra while avoiding energetically unfavorable B^4–O–B^4 bonds.[19] The B^4 avoidance principle is a common feature of structural models of borate glasses, for example the Beekenkamp model,[20] to which our structural model reduces in the borate rich limit. The structural model is used to apply temperature dependent constraint theory to investigate the structural origin of the MNFE in borophosphate glasses.

Based on the structural model we construct a predictive topological model of borophosphate glass properties, in which only the properties of a single reference composition such as B_2O_3 or P_2O_5 are utilized. The topological model agrees well

with experimental data of physical properties for borophosphate glasses as well as binary borate and phosphate glasses, for which it is equivalent to or an approximation of previously reported topological models.[4,14,16,21,22] The MNFE is quantitatively linked to the properties of borophosphate glasses, and so is the recently proposed modifying ion sub-network.[16,22] The constraints of the modifying ion sub-network constraints are derived for Li-, Na-, K-, Cs- and Ca borophosphate glass compositions.

II. THEORY

When applying temperature dependent constraint theory it is necessary to have experimental structural data of the short range order in the glass, i.e., the concentration of each network forming unit. With this information in hand the intact constraints in the temperature range of interest must be identified, e.g., indentation hardness is determined from the constraints at room temperature,[4] but T_g from the rigid constraints in the glass transition range. The constraints are normally counted by considering nearest neighbor interactions only,[5] i.e., linear constraints from covalent or mixed-covalent bonds and angular constraints from bond angles. The number of linear and angular constraints around a network forming atom can be calculated by:[11]

$$n_{c,linear} = \frac{1}{2}\mathrm{CN}\Big|_{\mathrm{CN}\geq 2}, \tag{1}$$

$$n_{c,angular} = \left(2\mathrm{CN}-3\right)\Big|_{\mathrm{CN}\geq 2}. \tag{2}$$

where n_c are the number of constraints around an atom and CN is the coordination number of that atom to other network forming atoms. The case of one-fold coordinated atoms is special, and can either be treated by plucking these atoms from the network,[8,23] or counting half a linear constraint as by Eq. (1).[24] The indentation hardness can be related to the intact constraints at room temperature, which for network forming cations and oxygen are calculated by Eqs. (1) and (2), but for network modifying cations the constraints may be different.[4] The indentation hardness in soda lime borate glasses has been found to be linearly dependent on the number of constraints as described by[4]

$$H_V\left(x\right) = \left(\frac{dH_V}{dN_c}\right)\times\left(N_c\left(x\right) - N_{c,crit}\right), \tag{3}$$

where $N_c(x)$ is the number of constraints per network forming atom at room temperature for composition x, dH_V/dN_c is a constant and is found to be on the order of 10 GPa,[4] and $N_{c,crit}$ is the minimum number of constraints per atom necessary for the constraints to affect hardness and has been found to be approximately 2.5.[4]

Both the linear and angular constraints are generally intact for network forming atoms in oxide glasses in the glass transition temperature range, but the angular constraints around oxygen are broken for vitreous SiO_2[25,26] and the same is

assumed for alkali borate[14] and alkali phosphate glasses.[15,16] After determining the intact constraints at T_g, the next step in relating T_g to the network constraints is the Adam-Gibbs theory of the glass transition[27,28]

$$\log_{10}\eta(T,x)=\log_{10}\eta_{\infty}+\frac{B(x)}{TS_c(T,x)}, \tag{4}$$

where η is the viscosity, η_∞ is the high temperature limit of viscosity, $B(x)$ is related to the potential energy barrier to viscous flow and $S_c(T,x)$ is the configuration entropy of the melt. η_∞ is found to be a universal constant independent of composition around 10^{-3} Pa s,[29,30] and $B(x)$ does not vary significantly within a class of materials when the mechanism of viscous flow is similar.[31] We assume η_∞ and $B(x)$ to be constant and consider T_g to correspond to the viscosity of 10^{12} Pa s.[32] With these assumptions Eq. (4) entails the equality

$$T_g(x)\times S_c\left(T_g,x\right)=T_g\left(x_{ref}\right)\times S_c\left(T_g,x_{ref}\right), \tag{5}$$

where x is the compositional variable and x_{ref} is a composition similar to x so that the assumption of constant $B(x)$ is not violated. It is possible to relate T_g to the number of constraints by using Naumis's result of configurational entropy being largely due to the number of floppy modes[33]

$$\frac{T_g(x)}{T_g\left(x_{ref}\right)}=\frac{f\left[T_g\left(x_{ref}\right),x_{ref}\right]}{f\left[T_g(x),x\right]}=\frac{3-N_c\left[T_g\left(x_{ref}\right),x_{ref}\right]}{3-N_c\left[T_g(x),x\right]}, \tag{6}$$

where f is the number of degrees of freedom and N_c is the number of rigid constraints at T_g per network forming atom. Eq. (5) requires that $0<f[T_g,x]<3$.

The liquid fragility is related to the change in degrees of freedom per atom at T_g, and can be computed by

$$m(x)=m_0\left(1+\frac{\partial\ln f(T,x)}{\partial\ln T}\right)\Bigg|_{T=T_g(x)}, \tag{7}$$

where m_0 is the liquid fragility of an ideally strong liquid and taken to be 17.[3] In order to take the temperature derivative of $\ln f(T,x)$ a continuous function is needed. We estimate the fraction of constraints that are rigid at a given temperature with

$$q_i(T)=\left[1-\exp\left(-\frac{\Delta F_i^*}{k_BT}\right)\right]^{vt_{obs}}, \tag{8}$$

where ΔF_i^* is the activation energy for breaking constraint i and vt_{obs} is the product of the vibrational attempt frequency and observation time [3]. The activation energy is related to a characteristic constraint onset temperature as

$$\Delta F_i^*=-k_BT_i\ln\left(1-2^{-1/vt_{obs}}\right), \tag{9}$$

where T_i is the constraint onset temperature of constraint i, and is the temperature at which half the constraints are intact, and therefore marks the crossover from an intact to a broken constraint with increasing T.[14]

Before the temperature dependent constraint theory can be applied to borophosphate glasses the short range order structure must be known, which is the focus of the following section.

III. STRUCTURE

The composition of borophosphate glasses can be written in a generalized manner as $xR_{2/v}O$ $(1\text{-}x)[yB_2O_3$ $(1\text{-}y)P_2O_5]$ with $R_{2/v}O$ being a network modifying oxide with cation valence v, x denoting the molar fractional content of network modifying oxide, and y denoting the network former concentration of boron oxide. The short range structure of borophosphate glasses can be seen as connections of the borate and phosphate network forming units shown in Fig. 1. In borophosphate glasses at low y, boron generally prefers to assume four-fold coordination (B^4). The usual scenario is that for a given x, B_2O_3 will for low y occur fully as B^4, while above some critical value of $y = y^*$, the fraction of B^4 per network former remains approximately constant, as seen in Fig. 2b. The critical value y^* and its dependence on x will be derived based on a structural understanding of borophosphate glass compositions.

The limiting behavior of the B^4 incorporation in borophosphate glasses is analogous to the B^4–O–B^4 avoidance principle present in structural models of alkali and alkaline earth borate glasses.[19] In these binary borate glasses the modifying cations are preferentially charge stabilized by B^4, but only up to a maximum fraction of B^4 units of approximately 45%.[19] Further addition of modifying oxide will cause the formation of trigonal non-bridging oxygen (NBO) bearing B^2 units and a decreasing fraction of B^4 units.[19] The results are explained by it being energetically unfavorable for the negatively charged B^4 tetrahedra to be direct neighbors of each other. When the B^4 fraction is so high that neighboring B^4 units become unavoidable, then the formation of B^4 units becomes unfavorable, and B^2 units are formed instead to balance the charge of the modifying oxide. The B^2 units decrease the network connectivity, exacerbating the problem of B^4–O–B^4 avoidance, and so the B^4 concentration will decrease further.

In borophosphate glasses the maximum fraction of B_2O_3 that can be incorporated as B^4 is denoted as y^* and depends on the modifying oxide content x. Schuch et al[34] derived an expression for y^* by considering how many B^4 can be incorporated into the borophosphate network while avoiding unfavorable B^4–O–B^4 bonds. The necessary condition for avoiding B^4–O–B^4 bond formation is that the number of bridging oxygen per B^4 tetrahedra must always be less than or equal to the number of bridging oxygen on the other structural groups in the network (denoted DP) and is expressed by

$$(4-f)\times\left[\mathrm{B}^4\right] \le \mathrm{DP}(x,y), \tag{10a}$$

$$\mathrm{DP}(x,y) = 4\times\left[\mathrm{P}^4\right] + 3\times\left(\left[\mathrm{B}^3\right]+\left[\mathrm{P}^3\right]\right) + 2\times\left(\left[\mathrm{B}^2\right]+\left[\mathrm{P}^2\right]\right) + 1\times\left(\left[\mathrm{B}^1\right]+\left[\mathrm{P}^1\right]\right). \tag{10b}$$

Here f is the allowed number of B^4–O–B^4 bonds per B^4 unit. If $f = 0$; Eq. (10) is equivalent to the Beekenkamp model[20] or if $f = 1$, then pairs of B^4 tetrahedra are allowed as in the Gupta model[35] for alkali borate glasses. The modification of the borophosphate network is a stepwise process that occurs in the order $B^4 > P^2 > P^1 > P^0 > B^2 > B^1 > B^0$ and this order can be explained by a decrease in the degree of delocalization of the negative charge. Using this order of charge compensation of the modifying oxide together with Eq. (10) and the mole and charge balances given in the following equations

$$\mathrm{B}^4(x,y) + \mathrm{B}^3(x,y) + \mathrm{B}^2(x,y) + \mathrm{B}^1(x,y) + \mathrm{B}^0(x,y) = 2\times(1-x)\times y, \tag{11a}$$

$$\mathrm{P}^4(x,y) + \mathrm{P}^3(x,y) + \mathrm{P}^2(x,y) + \mathrm{P}^1(x,y) + \mathrm{P}^0(x,y) = 2\times(1-x)\times(1-y), \tag{11b}$$

$$1\times\left[\mathrm{B}^4(x,y) - \mathrm{P}^4(x,y)\right] + 1\times\left[\mathrm{B}^2(x,y) + \mathrm{P}^2(x,y)\right] + 2\times\left[\mathrm{B}^1(x,y) + \mathrm{P}^1(x,y)\right] + 3\times\left[\mathrm{B}^0(x,y) + \mathrm{P}^0(x,y)\right] = 2x, \tag{11c}$$

we can predict the compositional dependence of each network forming unit (NFU). Thus, the fraction of B^4 per NFU ($[B^4]$) should be

$$\left[\mathrm{B}^4\right] = \frac{\mathrm{B}^4(x,y)}{2\times(1-x)} = \begin{cases} y,\ y \le y^* \\ y^*,\ y^* < y \le \dfrac{x}{1-x} + (1-y) \\ \dfrac{x}{1-x} + (1-y),\ \dfrac{x}{1-x} + (1-y) < y \end{cases}. \tag{12}$$

The fractions of other NFUs in borophosphate glass are derived in a similar manner as shown in the Appendix. When $y = y^*$ then the left and right hand side of Eq. (10a) will be equal, and by using the structural model derived from Eq. (8) then y^* is found to vary with x as

$$y^* = \frac{3 - \dfrac{x}{1-x}}{6-f}. \tag{13}$$

y^* denotes the maximum y fraction of B_2O_3 that can be incorporated exclusively as B^4 and demarcates two very different regimes in the y dimension: For $y \le y^*$ all B_2O_3 occurs as B^4 units, while for $y \ge y^*$ the fraction of B^4 per network former is approximately constant and equal to y^*, until the formation of B^1 units becomes necessary.

The structural model with $f = 0$ is plotted with experimental NFU fraction obtained by MAS-NMR for xNa$_2$O (1-x)[1/2B$_2$O$_3$ 1/2P$_2$O$_5$][36] in Fig. 2a and for 1/3K$_2$O 2/3[yB$_2$O$_3$ (1-y)P$_2$O$_5$][2] in Fig. 2b. [B^4] in Fig. 2a is an excellent test of Eq. (13) because for this series $y \geq y^*$. The agreement between experiment and model is generally excellent, but we observe some minor inconsistencies. In Fig. 2a the experimental [B^4] is higher than the modeled for $x > 0.45$, which indicates that $f > 0$ in Eq. (10) for these x values. In Fig. 3a [B^4] exhibits a small local minimum for $y \geq y^*$, while our model predicts a constant [B^4] = y^*.

IV. TOPOLOGY OF ALKALI BOROPHOSPHATES

The topology of alkali borophosphate glasses is derived from the structural model from Section III and Eqs. (1) and (2).

- α: B−O and P−O linear constraints. There are two at each BO and one at each NBO. None are counted at the double bonded terminal oxygen (TO) on P^3 as it is not considered part of the network.
- β: O−B−O and O−P−O angular constraints. There are three for B^3, B^2, B^1, B^0 and P^3. P^3 is considered effective three-fold coordinated because the TO is not part of the network. There are five angular constraints for B^4, P^4, P^2, P^1 and P^0.
- γ: R$^+$−NBO linear constraints. The number of constraints is equal to the oxygen coordination number (CN) of the R$^+$ charge balancing NBO. There are no constraints for R$^+$ charge balancing B^4.
- δ: B−O−B, B−O−P and B−O−B angular constraints. There is one for each BO.

The analytical expressions for the constraints in borophosphate glasses xR$_2$O (1-x)[yB$_2$O$_3$ (1-y)P$_2$O$_5$] are given as

$$n_{c,\alpha}(x,y) = 2\times \mathrm{BO}(x,y) + 1\times \mathrm{NBO}(x,y), \tag{14a}$$

$$\begin{aligned} n_{c,\beta}(x,y) = {} & 3\times\left[\mathrm{B}^3(x,y) + \mathrm{P}^3(x,y) + \mathrm{B}^2(x,y) + \mathrm{B}^1(x,y) + \mathrm{B}^0(x,y)\right] \\ & +5\times\left[\mathrm{B}^4(x,y) + \mathrm{P}^4(x,y) + \mathrm{P}^2(x,y) + \mathrm{P}^1(x,y) + \mathrm{P}^0(x,y)\right], \end{aligned} \tag{14b}$$

$$n_{c,\gamma}(x,y) = \mathrm{CN}\times \mathrm{R}^+_{\mathrm{NBO}}(x,y), \tag{14c}$$

$$n_{c,\delta}(x,y) = 1\times \mathrm{BO}(x,y). \tag{14d}$$

For convenience we consider the B−O and P−O linear constraints to be equivalent and denote it as the strongest (α) constraint. The second strongest (β) constraint is the O−B−O and O−P−O angular constraints. The O−B−O angular β constraint in binary sodium borate glasses was found to have an onset temperature T_β = 740 K and becomes partially broken to cause a plateau in $T_g(x)$.[14] The R$^+$−NBO linear γ constraint in binary sodium phosphates was found to have an onset temperature T_γ = 590 K and are therefore only partially intact at T_g. The BO centered angular δ constraint is estimated to have an onset temperature T_δ = 328 K based on the Vogel temperature of B$_2$O$_3$.[14] The angular constraints around the NBO and R$^+$

are left out in Eq. 14 because their bonding is primarily ionic. Ionic bonding is by definition non-directional and therefore these angular constraints are expected to be too weak to influence the physical properties.

The constraint onset temperatures are ordered such that

$$T_\delta < T_\gamma \approx T_g(x,y) \le T_\beta < T_\alpha . \tag{15}$$

This means that at $T_g(x,y)$ the α constraint is always intact, the β constraint is generally intact but limits the T_g of the most rigid compositions, the γ constraint is partially broken due to the constraint strength q_γ, and the δ constraint is always fully broken. At room temperature, where indentation hardness is determined, all constraints are fully intact.

The average number of constraint per atom then becomes

$$\begin{aligned} N_c(x,y,T_g) = {} & 2\times \mathrm{BO}(x,y) + 1\times \mathrm{NBO}(x,y) \\ & +3\times\left[\mathrm{B}^3(x,y)+\mathrm{P}^3(x,y)+\mathrm{B}^2(x,y)+\mathrm{B}^1(x,y)+\mathrm{B}^0(x,y)\right] \\ & +5\times\left[\mathrm{B}^4(x,y)+\mathrm{P}^4(x,y)+\mathrm{P}^2(x,y)+\mathrm{P}^1(x,y)+\mathrm{P}^0(x,y)\right] \\ & +q_\gamma \times \mathrm{CN}\times \mathrm{R}^+_{\mathrm{NBO}}(x,y) \end{aligned} . \tag{16}$$

The number of γ constraints was treated in detail in our previous work on binary alkali phosphate glasses.[16,22] Here we utilize a simplified approach given in Eq. (14c) with $q_\gamma = 0.6$ and CN = 5[37–41] for sodium. This gives the effective number of γ constraints at T_g per sodium ion equal to 3, which is equivalent to previous work on soda-lime-borate glasses.[21] The simplified approach eases calculation and approximately holds in the binary alkali phosphate system.

The T_g is modeled with Eq. (6) by inputting the constraints enumerated in Eq. (16). However this can cause the calculated T_g to exceed T_β, which invalidates the assumption of Eq. (16) that all β constraints are intact. Physically T_g will not increase above T_β, because the β constraints will become increasingly broken near T_β when $N_c(x,y,T_g)$ by Eq. (16) is increasing, and as a consequence the real $N_c(x,y,T_g)$ will stay constant. This effect causes $T_g \le T_\beta$ and in order to reflect this Eq. (6) is modified to

$$T_g(x,y) = \min\left[T_\beta(x,y), T_{g,ref}\times\frac{3-N_{c,ref}\left(T_{g,ref}\right)}{3-N_c\left(T_g,x,y\right)}\right]. \tag{17}$$

The reference composition used here is B_2O_3 with $T_{g,ref}$ = 543 K and $N_{c,ref}(T_{g,ref})$ = 2.4.[14] T_β has previously been found to depend on the type of modifier, being T_β = 760 K for lithium borates, T_β = 740 K for sodium borates and T_β = 910 K for calcium borates.[14,17] Based on the experimental $T_g(x,y)$ data[36] for alkali borophosphate glasses we propose that T_β also depends on the degree of polymerization (DP) of the next nearest NFU neighbors of B^4 as defined in Eq. (7a) and we attempt to quantify the relationship between T_β and DP as

$$T_\beta(x,y) = 55\times \mathrm{DP}(x,y) + (740 - 3\times 55). \quad (18)$$

Eq. (18) entails that T_β is linearly proportional to DP and when DP = 3 then T_β = 740 K as found for binary sodium borate glasses[14] In the model by Jiang et al[18] for 0.4 < y they use y = 0.4 as the reference composition, which serves a similar role as the varying T_β in Eq. (18) which is to limit the modeled $T_g(x,y)$ when $y^* < y$. y = 0.4 seems to be an approximation of y^* as $0.33 \le y^* \le 0.44$ for $0.25 \le x \le 0.5$ which spans the majority of the glass forming compositions. In this scheme the plateau in $T_g(x,y)$ for $y^* < y$ occurs because the main structural change with increasing y is substitution of P^3 for B^3 units, which are topologically equivalent. However using x,y^* as the reference composition is unjustified and works poorly for $y < y^*$. Using x,y^* as the reference composition also cannot explain the plateau in $T_g(x)$ of binary alkali borates. Our suggestion of a composition dependent T_β in Eq. (18) is a minor modification of the accepted theory of the plateau in T_g and agrees well with the available data for T_g and m.

The $T_g(x,y)$ modeled by Eq. (17) is plotted versus experimental data in Fig. 3. In Fig. 3a x is the compositional variable and y is a constant equal to 0, 0.5 or 1. The model works well for sodium borate and borophosphate glasses, but not so well for the sodium phosphates. We have previously modeled the T_g of alkali phosphate glasses by accounting for the modifying-ion sub-network and constraint strength,[16,22] but in this work the modifier-related γ constraints are treated in a simplified manner to ease calculation. In Fig. 3b y is the compositional variable and x = 1/3 but the alkali species is different. The trend mimics that of the alkali phosphates where T_g decreases for larger alkalis.[16] The data have been modeled with Eq. (16) and (17) by fitting the constraint strength (q_γ) and using experimentally confirmed CN in metaphosphate glasses[22], and T_β has been taken to vary with alkali species as found previously.[14] The local maxima at y = 0.5 and minima at y = 0.7 are thought to be related to the same tendency in [B^4] in Fig. 2b, and if the minimum can be accounted for in the structural model it is expected to also show in the T_g model.

V. TOPOLOGY OF CALCIUM BOROPHOSPHATES

Using the calcium borophosphate composition we explore the effect of an alkaline earth modifying oxide on the structure and properties. Using the derived structural information we predict physical properties T_g, H_V, m and ΔC_p by means of temperature-dependent constraint theory. The compositional join $z\mathrm{Ca(B_4O_7)}$ $(1\text{-}z)\mathrm{Ca(PO_3)_2}$ was chosen because both end-members are good glass-formers. Homogeneous and transparent glasses were prepared by the melt-quench technique in the compositional range $0 \le z \le 0.3$ and z = 1, but liquid-liquid phase separation prevented homogenous glass formation in the range $0.3 < z < 1$. The glass composition was confirmed by inductively coupled plasma atomic emission spectroscopy (ICP-AES) to be within a maximum error of 2% by mole of the constituent oxides, and the measured compositions will be used for all calculations.

Paper V

The NFU fractions were determined by ^{11}B and ^{31}P MAS-NMR and oxygen speciation by XPS, both of which agree well with the structural model derived in Section III, as seen in Fig. 4. About 6 % of the P_2O_5 content exists as P^1 units, which is not reflected in the structural model. Disproportionation of P^2 units to P^3 and P^1 is known to occur in calcium phosphates,[42] but this cannot fully explain the high [P^1] content as the [P^3] is generally lower than expected. The [B^4] at $z = 1$ is higher than predicted by Eq. (13) with $f = 0$ and instead we use $f = 0.5$ for this composition.

In order to compliment the MAS-NMR and XPS data the calcium borophosphate glasses were also investigated by Raman spectroscopy, as seen in Fig. 5. The Raman scattering cross section of the phosphate groups is much larger than that of the borate groups. For this reason the overall spectral intensity decreases with z, and no peaks directly related to the borate groups can be distinguished in the mixed glasses. Starting with $z = 0$ there are three major peaks, and these are assigned to the symmetrical stretching of P-O-P at 694 cm^{-1}, asymmetrical stretching of PO_2^- (P^2) at 1176 cm^{-1}, and symmetrical stretching also of PO_2^- at 1270 cm^{-1}.[43] Signatures of P^3 and P^1 are expected as a symmetrical stretching of PO_2 (P^3) at 1317 cm^{-1} and symmetrical stretching of PO_2^{2-} (P^1) at 1022 cm^{-1}.[43] These features are not resolved, but likely present in low concentration as found by MAS-NMR. With increasing z an apparent shift of the three major peaks occurs. The most intense P^2 peak at 1176 cm^{-1} decreases in wavenumber and broadens greatly. This is interpreted as due to a progressive change in the next nearest neighbors of P^2 from P to B based NFUs.[2] There are also large changes in the P-O-P at 694 cm^{-1} with increasing z, which seems to split into a lower and a higher frequency peak. We assign the symmetrical stretching of B-O-P to the peak centered at 653 cm^{-1}, as this is an entirely new feature which grows with z. The peak at around 743 cm^{-1} is reminiscent of the shoulder of the P-O-P vibration for $z = 0$, which has previously been speculated to be caused by short phosphate units or ring structures.[43] The third peak at 1270 cm^{-1} was assigned to the symmetrical stretching of P^2 and P^3, and does not change significantly with z. This is in agreement with MAS-NMR showing the presence of P^2 and P^3 in roughly the same ratio for $0 \leq z \leq 0.3$. For $z = 1$ there are five main features, and three of these can be assigned to the breathing motion of the pentaborate superstructural unit[44] at 521 cm^{-1}, 664 cm^{-1}, 773cm^{-1} and some scattering expected at 890 cm^{-1}.[45] A signature of B^2 is found in the broad peak at approximately 1300 cm^{-1} to 1550 cm^{-1} assigned to symmetric stretching of BO_2^-.[45] The last low intensity feature at about 960 cm^{-1} is assigned to the breathing mode of the diborate superstructural unit, which also occurs in the crystalline form of $CaO{\bullet}2B_2O_3$.[44,45] The diborate superstructural unit contains a B^4-O-B^4 bridge, and its presence explains why the $z = 1$ composition has $f > 0$.

With the structure of the calcium borophosphate glasses being established, we can now develop a topological model. The topology of calcium borophosphate glasses is similar to that of the alkali borophosphate glasses, and only the γ constraints in Eq. (14c) are treated differently as

$$n_{c,\gamma}(x,y) = \mathrm{CN}\times \mathrm{Ca}^{2+}_{\mathrm{NBO}}(x,y) + 2\times \mathrm{Ca}^{2+}_{\mathrm{B}^4}(x,y), \tag{19}$$

where CN = 6.[22] The two constraints per Ca^{2+} at B^4 are linear constraints between two negatively charged B^4 units and the Ca^{2+} charge balancing them. The order of the constraint onset temperatures are the same as in Eq. (15), and the average number of constraints per atom at T_g is

$$\begin{aligned} N_c(z,T_g) = {} & 2\times \mathrm{BO}(z) + 1\times \mathrm{NBO}(z) \\ & +3\times\left[\mathrm{B}^3(z) + \mathrm{P}^3(z) + \mathrm{B}^2(z) + \mathrm{B}^1(z) + \mathrm{B}^0(z)\right] \\ & +5\times\left[\mathrm{B}^4(z) + \mathrm{P}^4(z) + \mathrm{P}^2(z) + \mathrm{P}^1(z) + \mathrm{P}^0(z)\right] \\ & +q_\gamma\times\left[\mathrm{CN}\times \mathrm{Ca}^{2+}_{\mathrm{NBO}}(z) + 2\times \mathrm{Ca}^{2+}_{\mathrm{B}^4}(z)\right] \end{aligned}. \tag{20}$$

$T_g(z)$ is modeled with Eq. (6) and (20) using CN = 6 and q_γ = 5/6 as found for binary phosphate glasses,[22] and because P_2O_5 is the major network former in the melted glasses we take $T_{g,ref}$ = 590 K for P_2O_5[46] with $N_{c,ref}$ = 2.4.[16,22] The modeled $T_g(z)$ is compared with experimental T_g measured by DSC at the standard rate of 10 K/min[47] (equal to the prior cooling rate.) The DSC scans are found in Fig. 6, and the inset shows how to find T_g as the onset temperature of the glass transition. The experimental T_g are compared to the modeled values in Fig. 7a. For binary calcium borates it is thought that T_β = 910 K,[14,17] however in our data there is no evidence of a crossover between $T_g(z)$, and therefore the β constraints are taken to be fully intact. The overestimation of $T_g(z)$ for z = 0.25 and z = 0.3 is caused by the structural model also overestimating the [B^4] content for these compositions, as seen in Fig. 4a.

In Fig. 7a the measured Vickers hardness numbers (H_V) are also compared with the values modeled by Eq. (3) using the room temperature constraints where the α, β, γ and δ constraints are all fully intact,

$$\begin{aligned} N_c(z,T=298\mathrm{K}) = {} & 2\times \mathrm{BO}(z) + 1\times \mathrm{NBO}(z) \\ & +3\times\left[\mathrm{B}^3(z) + \mathrm{P}^3(z) + \mathrm{B}^2(z) + \mathrm{B}^1(z) + \mathrm{B}^0(z)\right] \\ & +5\times\left[\mathrm{B}^4(z) + \mathrm{P}^4(z) + \mathrm{P}^2(z) + \mathrm{P}^1(z) + \mathrm{P}^0(z)\right] \\ & +\mathrm{CN}\times \mathrm{Ca}^{2+}_{\mathrm{NBO}}(z) + 2\times \mathrm{Ca}^{2+}_{\mathrm{B}^4}(z) \\ & +1\times \mathrm{BO}(z) \end{aligned}. \tag{21}$$

The Vickers hardness data in Fig. 7a is fitted using dH_V/dN_c = 9.4 GPa at a load of 0.49 N and $N_{c,crit}$ = 2.5, and the model is in excellent agreement with both our calcium borophosphate data presented here and with results from soda-lime-borate glasses.[4] As for the $T_g(z)$ model $H_V(z)$ is overestimated for z = 0.25 and z = 0.3 because of the structural model overestimating the [B^4] content.

The liquid fragility (m) is the slope of $\log_{10}\eta$ plotted against T_g/T at T_g/T = 1. The viscosity was measured in the range of $\eta = 10^{10}$ Pa s to $\eta = 10^{12}$ Pa s by ball penetration viscosity and m determined by linear fitting of $\log_{10}\eta$ vs T_g/T. The heat

capacity jump at T_g (ΔC_p) was also determined as a measure of thermodynamic fragility.[48–50] ΔC_p was measured by DSC as the difference between the liquid heat capacity (C_{pl}) and the glass heat capacity at T_g (C_{pg}) as shown in the inset of Fig. 6. The specific heat capacity C_p is given in units of joule per mol atoms per kelvin, because this should give $C_{pg} = C_p(T_g) = 3R$ by the Dulong-Petit law, and thereby allow comparison of ΔC_p between different glass compositions.

The experimental m and ΔC_p values are compared to modeled values by Eqs. (7)-(9) in Fig. 7b. In order for the model to achieve good agreement with the experimental fragility data it is necessary to split up the α and β constraint depending on whether the constraint belongs to the phosphorous or boron network. In the case of the α constraints this was done by using the XPS measurements of oxygen speciation in Fig. 4b. The constraint onset temperatures are T_α(B-O-P) = 1600 K, T_α(P-O) = T_β(P) = 1400 K, T_α(B-O) = 1100 K, T_β(B) = 1000 K, T_γ = 900 K, T_δ = 328 K and vt_{obs} = 100. Several combinations of onset temperatures and vt_{obs} can give a similar compositional dependence of m. Therefore the constraint onset temperatures and vt_{obs} cannot be precisely determined, but the fitted values agree well with those previously found for borate[14,17,21] and phosphate[16] containing glasses. Also, with T_γ = 900 K gives $q_\gamma \approx 5/6$ around T_g by Eq. (8) as assumed previously for the $T_g(z)$ calculation.

VI. CONCLUSION

The properties of borophosphate glasses such as T_g, H_V, m and ΔC_p were quantitatively linked to their structure by using temperature dependent constraint theory, thereby explaining the mixed network former effect (MNFE) in these glasses. To do so, we applied a structural model capable of accounting for the major structural features of borophosphate glasses, and hence developed a predictive topological model. The physical properties modeled using only a single reference composition such as B_2O_3 or P_2O_5 are consistent with the experimentally determined values. The topological model can account not only for the effect of the network former, but also of the network modifier on the physical properties, as evidenced by slight differences between borophosphate glasses with different alkali oxide species. However major changes in the modeled properties occur when calcium oxide is incorporated. The topological model naturally accounts for these differences by the number and strength of the modifying cation to non-bridging oxygen constraints.

ACKNOWLEDGEMENTS

We gratefully acknowledge Jonas Kjeldsen, Morten M. Smedskjaer and John C. Mauro for valuable discussions.

APPENDIX

Glass formation in ternary borophosphate glasses with composition $x\mathrm{R}_{2/v}\mathrm{O}$ (1-x)[$y\mathrm{B}_2\mathrm{O}_3$ (1-y)$\mathrm{P}_2\mathrm{O}_5$] has been achieved between $0.15 \le x \le 0.55$ by the melt-quenching technique.[2,34,36,51–65] In the following we derive analytical expressions for the amount of B and P network forming units (NFU) in borophosphate glasses spanning $0 \le x \le 0.67$, which is well beyond the conventional glass forming region. The structural description is simplified by separating the compositional diagram into three regions, in which different structural units exist.

A. REGION I: $x \le 30\%$

Region I is characterized by B^4 being able to fully charge compensate the modifying oxide when $y \ge y^*$, where y^* was defined in Eq. (13). For $f > 0$ the region will extend to larger values of x, for example if $f = 1$ as in the Gupta model[35] the limit of x will increase to 33%. In region I the possible structural groups are B^4, P^4, B^3, P^3 and P^2. The P^4 unit is unique to the BPO_4 crystal structure[1] and borophosphate glasses in region I. P^4 is a tetrahedral phosphorous species with four bridging oxygen and can be thought of as the product of a reaction between the Lewis base double bonded oxygen (DBO) on a P^3 unit and a Lewis acid B^3. In our model P^4 is formed to charge stabilize B^4 when there is not enough modifying oxide to do so.

$$\left[\mathrm{B}^4\right] = \begin{cases} y, y \le y^* \\ y^*, y^* < y \le \dfrac{x}{1-x} + (1-y) \\ \dfrac{x}{1-x} + (1-y), \dfrac{x}{1-x} + (1-y) < y \end{cases} \tag{22a}$$

$$\left[\mathrm{P}^4\right] = \begin{cases} \left[\mathrm{B}^4\right] - \dfrac{x}{1-x}, \dfrac{x}{1-x} \le \left[\mathrm{B}^4\right] \\ 0, \left[\mathrm{B}^4\right] < \dfrac{x}{1-x} \end{cases} \tag{22b}$$

$$\left[\mathrm{B}^3\right] = y - \left[\mathrm{B}^4\right] \tag{22c}$$

$$\left[\mathrm{P}^3\right] = \begin{cases} (1-y) + \left(\dfrac{x}{1-x} - \left[\mathrm{B}^4\right]\right), \dfrac{x}{1-x} \le \left[\mathrm{B}^4\right] \\ (1-y) - \left(\dfrac{x}{1-x} - \left[\mathrm{B}^4\right]\right), \left[\mathrm{B}^4\right] < \dfrac{x}{1-x} \end{cases} \tag{22d}$$

$$\left[\mathrm{P}^2\right] = \begin{cases} 0, \dfrac{x}{1-x} \le \left[\mathrm{B}^4\right] \\ \dfrac{x}{1-x} - \left[\mathrm{B}^4\right], \left[\mathrm{B}^4\right] < \dfrac{x}{1-x} \end{cases} \tag{22e}$$

For $y \le y^*$ B_2O_3 is fully incorporated into the network as B^4, and for $y^* < y$ the fraction will plateau (equal to y^*) until there is not enough modifying oxide and P_2O_5 to charge balance B^4. Since B^4 is the preferentially formed charge-balancing species its concentration prominently influences the behavior of the other network forming units, and we have kept $[B^4]$ as a variable in Eq. 22. The fraction of P^4 is what is needed to charge balance B^4 when there is not enough modifier available. $[B^3]$ is determined by balancing the B_2O_3 content against $[B^4]$, and $[P^3]$ by balancing the P_2O_5 content against $[P^4]$ and $[P^2]$. $[P^2]$ is determined by charge-balancing the modifying oxide against $[B^4]$.

B. REGION II: 30% < *x* ≤ 50%

In region II B^4 and B^2 alone are capable of charge compensating the modifying oxide when $y = 1$, but P^2, P^1 and P^0 will progressively form when $y^* < y \le 1$ as they are more stable than B^2 units. The value of f will not change the end-point of region II at $x = 50\%$. The possible structural groups in region II are B^4, B^3, P^3, B^2, P^2, P^1 and P^0.

$$\left[B^4\right] = \begin{cases} y, y \le y^* \\ y^*, y^* < y \end{cases} \tag{23a}$$

$$\left[B^3\right] = \begin{cases} y - \left[B^4\right], \frac{x}{1-x} \le y^* + 3\times(1-y) \\ y - \left[B^4\right] - \left(\frac{x}{1-x} - y^* - 3\times(1-y)\right), y^* + 3\times(1-y) < \frac{x}{1-x} \end{cases} \tag{23b}$$

$$\left[P^3\right] = \begin{cases} (1-y) - \left(\frac{x}{1-x} - \left[B^4\right]\right), \frac{x}{1-x} \le y^* + (1-y) \\ 0, y^* + (1-y) < \frac{x}{1-x} \end{cases} \tag{23c}$$

$$\left[B^2\right] = \begin{cases} 0, \frac{x}{1-x} \le y^* + 3\times(1-y) \\ \frac{x}{1-x} - y^* - 3\times(1-y), y^* + 3\times(1-y) < \frac{x}{1-x} \end{cases} \tag{23d}$$

$$\left[P^2\right] = \begin{cases} \frac{x}{1-x} - \left[B^4\right], \frac{x}{1-x} \le y^* + (1-y) \\ 2\times(1-y) - \left(\frac{x}{1-x} - \left[B^4\right]\right), y^* + (1-y) < \frac{x}{1-x} \le y^* + 2\times(1-y) \\ 0, y^* + 2\times(1-y) < \frac{x}{1-x} \end{cases} \tag{23e}$$

$$\left[P^1\right]=\begin{cases} 0, \dfrac{x}{1-x} \le y^* + (1-y) \\ \left(\dfrac{x}{1-x} - \left[B^4\right]\right) - (1-y), y^* + (1-y) < \dfrac{x}{1-x} \le y^* + 2\times(1-y) \\ 3\times(1-y) - \left(\dfrac{x}{1-x} - \left[B^4\right]\right), y^* + 2\times(1-y) < \dfrac{x}{1-x} \le y^* + 3\times(1-y) \\ 0, y^* + 3\times(1-y) < \dfrac{x}{1-x} \end{cases} \tag{23f}$$

$$\left[P^0\right]=\begin{cases} 0, \dfrac{x}{1-x} \le y^* + 2\times(1-y) \\ \left(\dfrac{x}{1-x} - B^4\right) - 2\times(1-y), y^* + 2\times(1-y) < \dfrac{x}{1-x} \le y^* + 3\times(1-y) \\ (1-y), y^* + 3\times(1-y) < \dfrac{x}{1-x} \end{cases} \tag{23g}$$

As in region I for $y \le y^*$ B_2O_3 is fully incorporated into the network as B^4, and for $y^* < y$ the B^4 fraction reaches a plateau with $[B^4]$ equal to y^*. $[B^3]$ is determined by balancing the B_2O_3 content against $[B^4]$ and $[B^2]$ which is formed only when B^4 and P_2O_5 can no longer charge compensate the modifying oxide. We use Van Wazer's binary model for the phosphate network which assumes that only two P species can occur at any given composition, and $[P^3]$ will go to zero before P^1 groups are formed. P^2. P^1 and P^0 are better charge compensators than B^2, and they progressively form as the P_2O_5 content decreases and their concentrations are determined by a charge balance.

C. REGION III: 50% < *x* ≤ 67%

$$\left[B^4\right]=\begin{cases} y, y \le y^* \\ y^*, y^* < y, \dfrac{x}{1-x} \le y + 3\times(1-y) \\ y^* - \left(\dfrac{x}{1-x} - 3\times(1-y) - y\right), y + 3\times(1-y) < \dfrac{x}{1-x} \le y + y^* + 3\times(1-y) \\ 0, y + y^* + 3\times(1-y) < \dfrac{x}{1-x} \end{cases} \tag{24a}$$

$$\left[B^3\right]=\begin{cases} y - \left[B^4\right], \dfrac{x}{1-x} \le y^* + 3\times(1-y) \\ y - \left[B^4\right] - \left(\dfrac{x}{1-x} - y^* - 3\times(1-y)\right), y^* + 3\times(1-y) < \dfrac{x}{1-x} \le y + 3\times(1-y) \\ 0, y + 3\times(1-y) < \dfrac{x}{1-x} \end{cases} \tag{24b}$$

$$\left[\mathrm{B^2}\right]=\begin{cases}0,\dfrac{x}{1-x}\le y^*+3\times(1-y)\\ \dfrac{x}{1-x}-y^*-3\times(1-y),\ y^*+3\times(1-y)<\dfrac{x}{1-x}\le y+3\times(1-y)\\ 2y-\left[\mathrm{B^4}\right]-\left(\dfrac{x}{1-x}-3\times(1-y)\right),\ y+3\times(1-y)<\dfrac{x}{1-x}\end{cases} \tag{24c}$$

$$\left[\mathrm{B^1}\right]=\begin{cases}0,\dfrac{x}{1-x}\le y+3\times(1-y)\\ \dfrac{x}{1-x}-3\times(1-y)-y,\ y+3\times(1-y)<\dfrac{x}{1-x}\end{cases} \tag{24d}$$

For $y \le y^*$ B_2O_3 is still fully incorporated into the network as B^4, and for $y^* < y$ the B^4 fraction reaches a plateau with $[B^4]$ equal to y^*. However, when B^1 starts to occur then B^4 units are converted to B^1. $[B^3]$ is determined by balancing the B_2O_3 content against $[B^4]$ and $[B^2]$ which is formed only when B^4 and P_2O_5 can no longer charge compensate the modifying oxide. The fractions of P^2, P^1 and P^0 are calculated as in Eq. 23 for region II.

D. OXYGEN SPECIATION

The structural model for the boron oxide and phosphorous oxide network formers given in this section can be readily used to calculate the amount of bridging oxygen (BO), non-bridging oxygen (NBO) and double-bonded terminal oxygen (DBO) in a given composition. It is also possible to predict the nearest neighbors of the BO, as Eq. 8 entails that the phosphorous oxide tetrahedra are bonded to B^4 units, but not to B^3 units. If we assume that B^4–O–P bonds are preferentially formed, and that B^3–O–P bonding does not occur, then we predict the oxygen fractions to depend on composition as

$$\left[\mathrm{B^4\text{-}O\text{-}P}\right]=\begin{cases}\dfrac{(4-f)\times\left[\mathrm{B^4}\right]}{\left(x+(1-x)\times\left(3y+5(1-y)\right)\right)\Big/\left(2\times(1-x)\right)},\ y\le y^*\\ \dfrac{4\times\left[\mathrm{P^4}\right]+3\times\left[\mathrm{P^3}\right]+2\times\left[\mathrm{P^2}\right]+1\times\left[\mathrm{P^1}\right]}{\left(x+(1-x)\times\left(3y+5(1-y)\right)\right)\Big/\left(2\times(1-x)\right)},\ y^*<y\end{cases} \tag{25a}$$

$$\left[\mathrm{B\text{-}O\text{-}B}\right]=\begin{cases}\dfrac{\frac{1}{2}\times\left(3\times\left[\mathrm{B^3}\right]+2\times\left[\mathrm{B^2}\right]+1\times\left[\mathrm{B^1}\right]\right)}{\left(x+(1-x)\times\left(3y+5(1-y)\right)\right)\Big/\left(2\times(1-x)\right)},\ y\le y^*\\ \dfrac{\frac{1}{2}\times\left(4\times\left[\mathrm{B^4}\right]+3\times\left[\mathrm{B^3}\right]+2\times\left[\mathrm{B^2}\right]+1\times\left[\mathrm{B^1}\right]\right)}{\left(x+(1-x)\times\left(3y+5(1-y)\right)\right)\Big/\left(2\times(1-x)\right)}-\dfrac{1}{2}\times\left[\mathrm{B^4\text{-}O\text{-}P}\right],\ y^*<y\end{cases} \tag{25b}$$

$$\left[\mathrm{P\text{-}O\text{-}P}\right]=\begin{cases}\dfrac{\frac{1}{2}\times\left(4\times\left[\mathrm{P^4}\right]+3\times\left[\mathrm{P^3}\right]+2\times\left[\mathrm{P^2}\right]+1\times\left[\mathrm{P^1}\right]\right)}{\left(x+(1-x)\times\left(3y+5(1-y)\right)\right)\Big/\left(2\times(1-x)\right)}-\dfrac{1}{2}\times\left[\mathrm{B^4\text{-}O\text{-}P}\right],\ y\le y^*\\ 0,\ y^*<y\end{cases} \tag{25c}$$

$$[\mathrm{NBO}] = \frac{1\times\left[\mathrm{B}^{2}\right] + 2\times\left(\left[\mathrm{B}^{1}\right] + \left[\mathrm{P}^{2}\right]\right) + 3\times\left(\left[\mathrm{B}^{0}\right] + \left[\mathrm{P}^{1}\right]\right) + 4\times\left[\mathrm{P}^{0}\right]}{\left(x + (1-x)\times\left(3y + 5(1-y)\right)\right) \Big/ \left(2\times(1-x)\right)} \tag{25d}$$

$$[\mathrm{DBO}] = \frac{1\times\left[\mathrm{P}^{3}\right]}{\left(x + (1-x)\times\left(3y + 5(1-y)\right)\right) \Big/ \left(2\times(1-x)\right)} \tag{25e}$$

Here $x + (1\text{-}x)\times(3y+5(1\text{-}y))$ is the total number of oxygen atoms in the composition $x\mathrm{R_2O}$ $(1\text{-}x)[y\mathrm{B_2O_3}$ $(1\text{-}y)\mathrm{P_2O_5}]$ and $2\times(1\text{-}x)$ is a factor that corrects for the B and P species concentration being relative to the $\mathrm{B_2O_3} + \mathrm{P_2O_5}$ content. This model of the oxygen speciation was found by Larink et al.[2] to agree well with oxygen fractions measured by XPS for potassium borophosphate glass compositions with $x = 1/3$. We also applied this model to describe the oxygen fractions by XPS of a series of calcium borophosphate glasses in Fig. 4b.

FIGURES AND TABLES

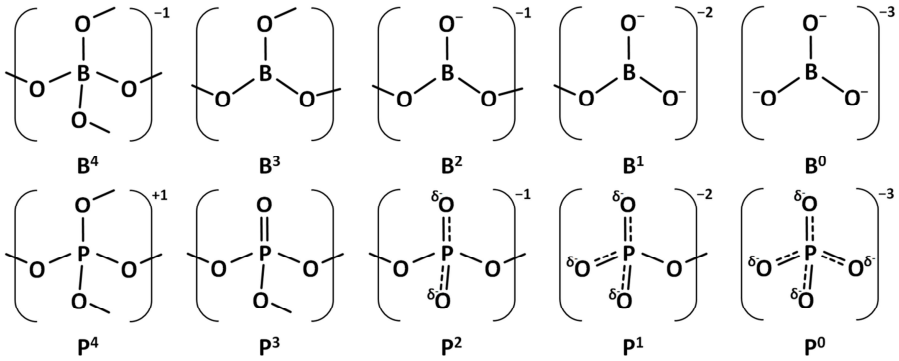

FIG. 1. The network forming units (NFUs) that can occur in borophosphate glasses. The net charge of the NFU is given outside the parenthesis. The NFUs are named based on the central atom and the number of bridging oxygen branching out from the NFU.

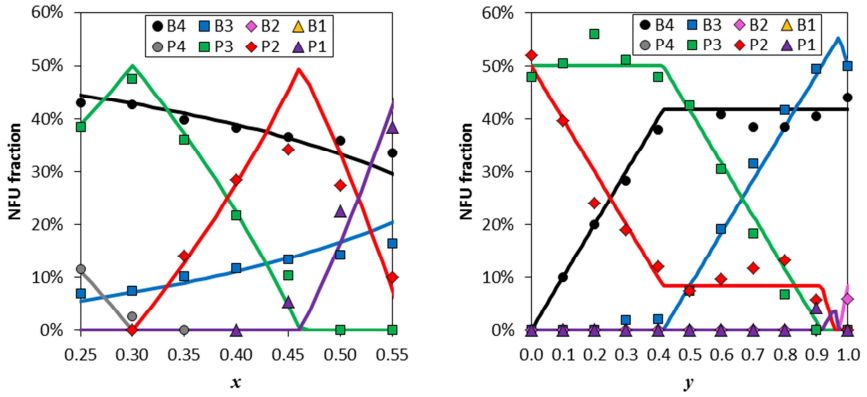

FIG. 2. The fraction of the different network-forming units (NFU) as determined by ^{11}B and ^{31}P MAS-NMR of a) xNa$_2$O (1-x)[1/2B$_2$O$_3$ 1/2P$_2$O$_5$][36] and b) 1/3K$_2$O 2/3[yB$_2$O$_3$ (1-y)P$_2$O$_5$][2] glass compositions. The solid lines indicate predicted fractions from the structural model derived in Section III.

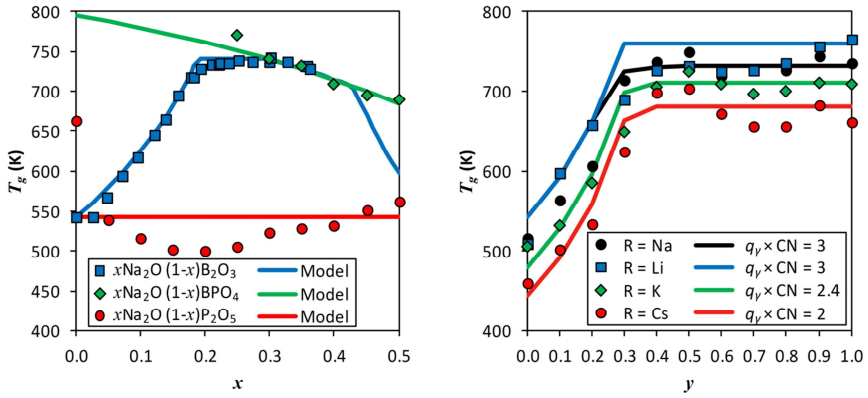

FIG. 3. a) Experimental and modeled glass transition temperatures (T_g) by Eqs. (16) and (17) is plotted as a function of x for three different series of xNa$_2$O (1-x)[yB$_2$O$_3$ (1-y)P$_2$O$_5$] glasses with y = 0[16,66], 0.5[36] and 1.[14,67] b) Experimental and modeled T_g is plotted as a function of y for three different series of 1/3R$_2$O 2/3[yB$_2$O$_3$ (1-y)P$_2$O$_5$] glasses with R =Li, K and Cs.[2] R = Li then q_y = 0.75, CN = 4[22] and T_β = 760 K,[14] for R = K then q_y = 0.4, CN = 6[22] and T_β = 710 K and for R = Cs then q_y = 0.33, CN = 6[22] and T_β = 680 K. The R = Na series has a slightly different composition 0.35Na$_2$O 0.65[yB$_2$O$_3$ (1-y)P$_2$O$_5$] and the model uses q_y = 0.6, CN = 5[37–41] and T_β = 740 K.[14]

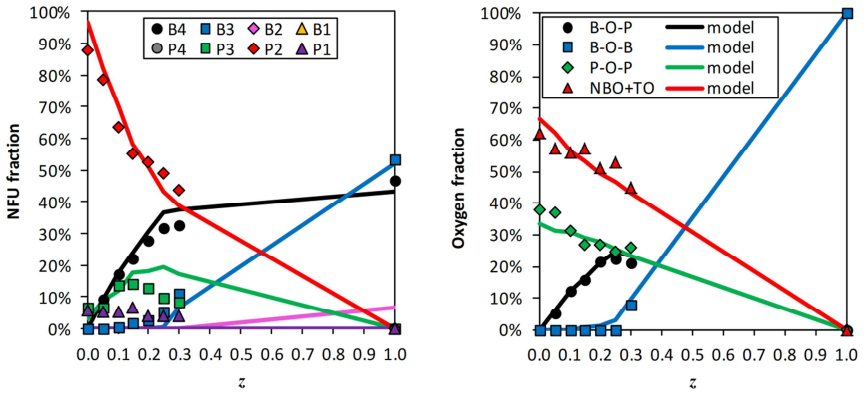

FIG. 4. a) Network forming unit (NFU) fractions of zCa(B$_4$O$_7$) (1-z)Ca(PO$_3$)$_2$ glasses by the structural model from Section III with f = 0.5 compared to measured fractions by ^{11}B and ^{31}P MAS-NMR. b) A structural model for oxygen speciation assuming maximum connectivity between B^4 and the phosphorous network but no connection between B^3 and phosphorous. Data points are determined by XPS.

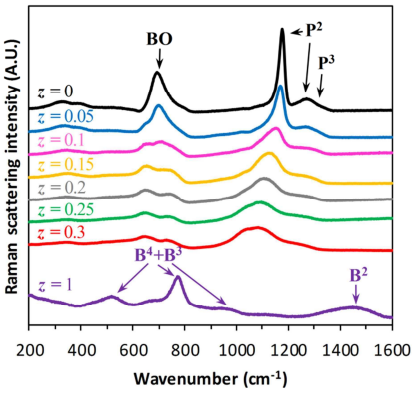

FIG. 5. The Raman spectra of zCa(PO$_3$)$_2$ (1-z)CaB$_4$O$_7$ glasses are normalized by total scattering intensity. The arrows indicate the structural groups that are assigned to the major peaks in the end-member compositions. Peaks shift and broaden for $0 < z < 1$ due to B-O-P bond formation. See text for details about the peak assignments and compositional trend.

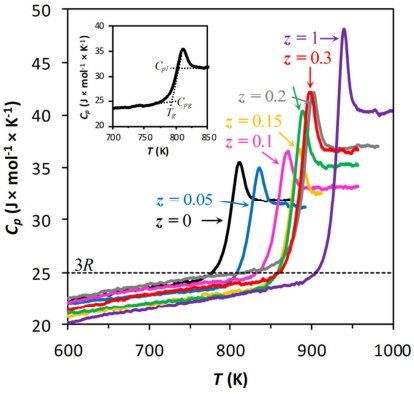

FIG. 6. The DSC curves of zCa(PO$_3$)$_2$ (1-z)CaB$_4$O$_7$ glasses are measured at a heating rate of 10K/min after prior cooling from above T_g at the same cooling rate. T_g is defined as the onset temperature of the glass transition, as seen in the inset. ΔC_p is defined as C_{pl} - C_{pg} also shown in the inset. C_p and ΔC_p are given in joules per mol atoms per kelvin, which enables comparison between compositions as C_{pg} is approximately a constant equal to 3R.

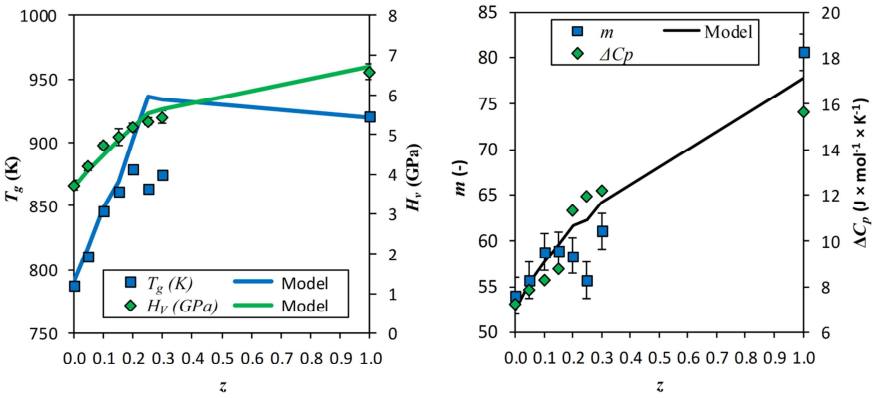

FIG. 7. a) On the left hand axis are experimental and modeled glass transition temperature (T_g) by Eq. (6) and Eq. (20) is plotted as a function of z for zCa(B_4O_7) (1-z)Ca(PO_3)$_2$ glasses. On the right hand axis experimental and modeled Vickers hardness (H_V) by Eq. (3) and the room temperature constraints found in Eq. (21). b) Experimental and modeled liquid fragility (m) by Eq. (7) and (21). On the right hand side the thermodynamic fragility (ΔC_p) is plotted to scale with the m values. The onset temperatures used for the m model are T_α(B-O-P) = 1600 K, T_α(P-O) = T_β(P) = 1400 K, T_α(B-O) = 1100 K, T_β(B) = 1000 K, T_γ = 900 K and T_δ = 328 K with vt_{obs} = 100.

REFERENCES

[1] M. Schmidt, B. Ewald, Y. Prots, R. Cardoso-Gil, M. Armbrüster, I. Loa, L. Zhang, Y.-X. Huang, U. Schwarz, and R. Kniep, Zeitschrift Für Anorg. Und Allg. Chemie **630**, 655 (2004).

[2] D. Larink, H. Eckert, M. Reichert, and S.W. Martin, J. Phys. Chem. C **116**, 26162 (2012).

[3] P.K. Gupta and J.C. Mauro, J. Chem. Phys. **130**, 094503 (2009).

[4] M.M. Smedskjaer, J.C. Mauro, and Y.-Z. Yue, Phys. Rev. Lett. **105**, 115503 (2010).

[5] J.C. Phillips, J. Non. Cryst. Solids **34**, 153 (1979).

[6] J.C. Phillips, J. Non. Cryst. Solids **43**, 37 (1981).

[7] J.C. Phillips, J. Non. Cryst. Solids **44**, 17 (1981).

[8] M.F. Thorpe, J. Non. Cryst. Solids **57**, 355 (1983).

[9] J.C. Phillips and M.F. Thorpe, Solid State Commun. **53**, 699 (1985).

[10] H. He and M.F. Thorpe, Phys. Rev. Lett. **54**, 2107 (1985).

[11] M.F. Thorpe, J. Non. Cryst. Solids **76**, 109 (1985).

[12] M.F. Thorpe and Y. Cai, Phys. Rev. B **40**, 10535 (1989).

[13] M.F. Thorpe, M. V Chubynsky, D.J. Jacobs, and J.C. Phillips, Glas. Phys. Chem. **27**, 160 (2001).

[14] J.C. Mauro, P.K. Gupta, and R.J. Loucks, J. Chem. Phys. **130**, 234503 (2009).

[15] A.I. Fu and J.C. Mauro, J. Non. Cryst. Solids **361**, 57 (2013).

[16] C. Hermansen, J.C. Mauro, and Y.-Z. Yue, J. Chem. Phys. **140**, 154501 (2014).

[17] M.M. Smedskjaer, J.C. Mauro, R.E. Youngman, C.L. Hogue, M. Potuzak, and Y.-Z. Yue, J. Phys. Chem. B **115**, 12930 (2011).

[18] Q. Jiang, H. Zeng, Z. Liu, J. Ren, G. Chen, Z. Wang, L. Sun, and D. Zhao, J. Chem. Phys. **139**, 124502 (2013).

[19] A.C.A.C. Wright, Phys. Chem. Glas. Eur. J. Glas. Sci. Technolology B **51**, 1 (2010).

[20] P. Beekenkamp, in *Phys. Non-Crystalline Solids*, edited by J.A. Prins (North-Holland, Amsterdam, 1965), p. 512.

[21] M.M. Smedskjaer, J.C. Mauro, S. Sen, and Y.-Z. Yue, Chem. Mater. **2**, 445 (2010).

[22] C. Hermansen, B. Rodrigues, L. Wondraczek, and Y.-Z. Yue, J. Chem. Phys. **Under revi**, (2014).

[23] G.H. Döhler, R. Dandoloff, and H. Bilz, J. Non. Cryst. Solids **42**, 87 (1980).

[24] P. Boolchand and M.F. Thorpe, Phys. Rev. B **50**, 10366 (1994).

Paper V

[25] M. Bauchy, M. Micoulaut, M. Celino, S. Le Roux, M. Boero, and C. Massobrio, Phys. Rev. B **84**, 054201 (2011).

[26] M. Zhang and P. Boolchand, Science **266**, 1355 (1994).

[27] G. Adam and J.H. Gibbs, J. Chem. Phys. **43**, 139 (1965).

[28] Y. Bottinga and P. Richet, Chem. Geol. **128**, 129 (1996).

[29] J.C. Mauro, Y.-Z. Yue, A.J. Ellison, P.K. Gupta, and D.C. Allan, Proc. Natl. Acad. Sci. U. S. A. **106**, 19780 (2009).

[30] Q. Zheng, J.C. Mauro, A.J. Ellison, M. Potuzak, and Y.-Z. Yue, Phys. Rev. B **83**, 212202 (2011).

[31] M.J. Toplis, Am. Mineral. **83**, 480 (1998).

[32] C.A. Angell, Science (80-.). **267**, 1924 (1995).

[33] G.G. Naumis, Phys. Rev. E **71**, 026114 (2005).

[34] M. Schuch, C. Trott, and P. Maass, RSC Adv. **1**, 1370 (2011).

[35] P.K. Gupta, in *Int. Congr. Glas.* (Unpublished, New Delhi, India, 1986), pp. 1–10.

[36] M.T. Rinke and H. Eckert, Phys. Chem. Chem. Phys. **13**, 6552 (2011).

[37] Y. Waseda, E. Matsubara, K. Sugiyama, I.K. Suh, T. Kawazoe, O. Kasu, M. Ashizuka, and E. Ishida, Sci. Reports Res. Institutes, Tohoku Univ. Ser. A Physics, Chem. Metall. **35**, 19 (1990).

[38] U. Hoppe, L. Delevoye, L. Montagne, M. v. Zimmermann, and A.C. Hannon, Phys. Chem. Chem. Phys. **15**, 8520 (2013).

[39] A. Speghini, E. Sourial, T. Peres, G. Pinna, M. Bettinelli, and J.A. Capobianco, Phys. Chem. Chem. Phys. **1**, 173 (1999).

[40] U. Hoppe, D. Stache, and D. Beyer, Phys. Scr. **57**, 122 (1995).

[41] U. Hoppe, G. Walter, R. Kranold, and D. Stachel, J. Non. Cryst. Solids **263&264**, 29 (2000).

[42] J.P. Fletcher, R.J. Kirkpatrick, D. Howell, and S.H. Risbud, J. Chem. Soc. Faraday Trans. **89**, 3297 (1993).

[43] J.E. Pemberton, L. Latifzadeh, J.P. Fletcher, and S.H. Risbud, Chem. Mater. **3**, 195 (1991).

[44] A.C. Wright, Phys. Chem. Glas. Eur. J. Glas. Sci. Technol. B **51**, 1 (2010).

[45] D. Maniu, T. Iliescu, I. Ardelean, S. Cinta-Pinzaru, N. Tarcea, and W. Kiefer, J. Mol. Struct. **651-653**, 485 (2003).

[46] S.W. Martin and C.A. Angell, J. Phys. Chem. **90**, 6736 (1986).

[47] Y.-Z. Yue, J. Non. Cryst. Solids **355**, 737 (2009).

[48] Q. Zheng, M. Potuzak, J.C. Mauro, M.M. Smedskjaer, R.E. Youngman, and Y.-Z. Yue, J. Non. Cryst. Solids **358**, 993 (2012).

Paper V

[49] L.-M. Wang, V. Velikov, and C. a. Angell, J. Chem. Phys. **117**, 10184 (2002).

[50] L.M. Martinez and C.A. Angell, Nature **410**, 663 (2001).

[51] M. Storek, R. Böhmer, S.W. Martin, D. Larink, H. Eckert, and R. Böhmer, J. Chem. Phys. **137**, 124507 (2012).

[52] P.S. Anantha and K. Hariharan, Mater. Chem. Phys. **89**, 428 (2005).

[53] J.J. Videau, J.F. Ducel, K.S. Suh, and J. Senegas, **188**, 157 (1992).

[54] R. Christensen, J. Byer, T. Kaufmann, and S.W. Martin, Phys. Chem. Glas. Eur. J. Glas. Sci. Technol. B **50**, 237 (2009).

[55] D. Zielniok, C. Cramer, and H. Eckert, Chem. Mater. **19**, 3162 (2007).

[56] J.F. Ducel and J.J. Videau, Mater. Lett. **13**, 271 (1992).

[57] N.-J. Kim, S.-H. Im, D.-H. Kim, D.-K. Yoon, and B.-K. Ryu, Electron. Mater. Lett. **6**, 103 (2010).

[58] Y. Jin, X. Chen, and X. Huang, J. Non. Cryst. Solids **112**, 147 (1989).

[59] S. Elbers, W. Strojek, L. Koudelka, and H. Eckert, Solid State Nucl. Magn. Reson. **27**, 65 (2005).

[60] G. Sedmale, J. Vaivads, U. Sedmalis, V.O. Kabanov, and O.V. Yanush, J. Non. Cryst. Solids **129**, 284 (1991).

[61] F. Muñoz, L. Montagne, L. Pascual, and A. Durán, J. Non. Cryst. Solids **355**, 2571 (2009).

[62] F. Tian and L. Pan, J. Non. Cryst. Solids **112**, 142 (1989).

[63] T.D. Tho, R. Prasada Rao, and S. Adams, Eur. Phys. J. E. Soft Matter **35**, 8 (2012).

[64] D. Qiu, P. Guerry, I. Ahmed, D.M. Pickup, D. Carta, J.C. Knowles, M.E. Smith, and R.J. Newport, Mater. Chem. Phys. **111**, 455 (2008).

[65] V.K. Michaelis, P. Kachhadia, and S. Kroeker, Phys. Chem. Glas. Eur. J. Glas. Sci. Technol. B **54**, 20 (2013).

[66] J.J. Hudgens, The Structure and Properties of Anhydrous, Alkali Ultra-Phosphate Glasses, Iowa State University, 1994.

[67] S. V. Nemilov, Neorg. Mater. **2**, 349 (1966).

Paper VI

Paper VI

Structure-Topology-Property Correlations of Sodium Phosphosilicate Glasses

Christian Hermansen,[1] Xiaoju Guo,[2] Randall E. Youngman,[2] John C. Mauro,[2] Morten M. Smedskjaer[1] and Yuan-zheng Yue[1,3,a)]

[1]*Section of Chemistry, Aalborg University, Fredrik Bajers Vej 7H, Aalborg 9220, Denmark*

[2]*Science and Technology Division, Corning Incorporated, Corning, New York 14831, USA*

[3]*State Key Laboratory of Silicate Materials for Architecture, Wuhan University of Technology, Wuhan 430070, China*

[a)]*Electronic mail: yy@bio.aau.dk*

Mixed network former phosphosilicate glasses are known for their complex atomic structure depending on the details of their composition, but they have found important technological applications, e.g., as bioactive glasses for regeneration of bone and tissue in the human body. In this work, we investigate the relation between structure and properties in sodium phosphosilicate glasses from pure phosphate to pure silicate end members. The network structure is characterized by ^{29}Si and ^{31}P magic-angle spinning (MAS) nuclear magnetic resonance (NMR) and Raman spectroscopy, which show the formation of six-fold coordinated silicon species in phosphorous-rich glasses. Based on these structural data, we propose a formation mechanism of the six-fold coordinated silicon that is used to develop a quantitative structural model, which predicts the speciation of the network forming units in phosphosilicate glasses as a function of chemical composition. This structural picture is then used to derive a temperature-dependent constraint model of phosphosilicate glasses that enables prediction of glass transition temperature, indentation hardness, and liquid fragility. The topological constraint model successfully accounts for the structural origin of the mixed network former effect in phosphosilicate glasses.

Paper VI

I. INTRODUCTION

Phosphosilicate glasses consist of a mixture of two prototypical network forming oxides (P_2O_5 and SiO_2), and their composition can be generalized as $x$$Na_2O$ (1-x)[$y$$SiO_2$ (1-y)P_2O_5] where Na_2O is a representative modifying oxide. Phosphosilicate glasses exhibit highly non-linear variation in their physical and chemical properties when one network former is substituted for the other at constant network modifier content. This effect is a general occurrence in mixed network former glasses, and is dubbed the mixed network former effect (MNFE).[1–6]

Application of phosphosilicate glasses are mainly focused on silica-rich (high y) compositions. For example, P_2O_5 can be added as a nucleating agent in the production of silicate and aluminosilicate based glass ceramics.[7,8] The original Bioglass® which is used for regeneration of bone and tissue in the human body is a soda lime phosphosilicate glass with y = 0.95.[9] Both of these applications rely on the ability of P_2O_5 to preferentially react with the modifying oxide and form pyrophosphate (P^1) or orthophosphate (P^0) units.[10] These P^1 and P^0 units tend to phase separate or crystallize from the glass due to their low connectivity.[11–13]

Phosphosilicate glass compositions rich in phosphorous (low y) form homogeneous glasses,[8,14–19] but their physical properties have not been studied well, probably due to the poor chemical durability of phosphate-based glasses.[20] However, these compositions are interesting from a structural point of view, as they can contain six-fold coordinated silicon (Si^6).[8,16,19,21–23] The formation of Si^6 in phosphosilicate glasses is interesting because Si^6 usually only occurs in high-pressure crystals.[22,24] Moreover, the accepted random network theory of glass structure by Zachariasen[25] rejects glass formation for network forming oxides with a coordination number above four.

Phosphosilicate glasses exhibit a large MNFE due to the different behaviors of the constituent network forming oxides.[26,27] At low y, the Si^6 species strongly increase the degree of network connectivity of the glass, whereas at high y, P_2O_5 preferentially reacts with the modifying oxides and decreases the degree of network connectivity of the phosphate network, while increasing that of the silicate network. Especially the low-y compositions containing Si^6 could have useful physical properties due to the rigid network structure,[26] and it is thus important to characterize and understand the MNFE in phosphosilicate glasses both from a technological and scientific point of view.

In this work, we characterize the structure and physical properties, such as glass transition temperature (T_g), Vickers indentation hardness (H_V), liquid fragility index (m), and jump in isobaric heat capacity at the glass transition (ΔC_p) of a series of sodium phosphosilicate glasses with composition 0.3Na_2O 0.7[$y$$SiO_2$ (1-y)P_2O_5]. We propose a structural model of Si^6 formation, where a Si^4 unit reacts with 2 P^2 units to create one Si^6 and 2 P^3 units. This scheme can quantitatively account for the observation that the Si^6 content is approximately one quarter of the P^3 content. This structural model is used in conjunction with Gupta-Mauro[28,29] temperature-dependent constraint theory to predict the compositional scaling of physical

properties and thus effectively explain the origin of the MNFE in phosphosilicate glasses. We note that the proposed structural and topological constraint models both differ significantly from the recent work of Zeng et al.[26,27] on the same topic. In detail, their approach do not take into account that modifying ions are required to charge-stabilize the Si^6 species, nor do they consider the modifying ion sub-network,[30,31] which is necessary to explain the physical properties of binary phosphate glasses.

II. EXPERIMENTAL

High purity Na_2CO_3, SiO_2, and P_2O_5 powders were batched to prepare a series of $0.3Na_2O$ $0.7[ySiO_2$ $(1\text{-}y)P_2O_5]$ compositions. The mixed powders were melted in platinum crucibles. Most of these melts gave opaque glasses when they were poured onto a stainless steel plate in air. However, clear glasses could be obtained by roller-quenching the melts for compositions containing up to 30 mole % of SiO_2 (y = 0.43). Two additional clear glasses were formed by mixing the y = 0.43 and y = 1 compositions, re-melting and roller-quenching, thereby yielding glasses with y = 0.54 and y = 0.89.

The amorphous nature of the clear samples was confirmed by X-ray diffraction (XRD), while the opaque silica-rich compositions were found to contain crystallized Na_3PO_4. The chemical compositions of the $0.3Na_2O$ $0.7[ySiO_2$ $(1\text{-}y)P_2O_5]$ glasses were determined by inductively coupled plasma atomic emission spectroscopy (ICP-AES). These analyzed compositions were found to be in good agreement with the batched ones, as seen in Table I. A notable exception was the phosphate-rich sample with y = 0, where the analyzed P_2O_5 content is lower than that batched, most likely due to the evaporation of P_2O_5 during melting.

The structure of the glasses were investigated by performing ^{29}Si and ^{31}P MAS NMR measurements on the $0.3Na_2O$ $0.7[ySiO_2$ $(1\text{-}y)P_2O_5]$ compositions with $y < 0.6$ and Raman spectroscopy measurements on all samples. The glass transition temperature (T_g) was measured as the onset of the glass transition by differential scanning calorimetry (DSC) at the standard heating rate of 10 K/min[32] (equal to the prior cooling rate). The isobaric heat capacity jump at T_g (ΔC_p) was also determined during the same measurement and it is considered to be a measure of thermodynamic fragility.[5,33,34] ΔC_p was measured by DSC as the difference between the liquid heat capacity (C_{pl}) and the glass heat capacity extrapolated to T_g (C_{pg}). The liquid fragility index (m) could not be determined directly from viscosity-temperature data for the roller-quenched glasses because the samples were too thin. Instead the values of m were inferred from the activation energy of the glass transition measured by DSC.[35] The activation energy was determined from six DSC cooling/heating rates between 2 and 40 K/min. Indentation hardness was measured on samples polished to a mirror-surface using a Vickers diamond with a load of 490 mN and a 10 s press time. The reported hardness value represents an average over 25 well separated indents.

III. STRUCTURE

Paper VI

The silicate network structure of phosphosilicate glasses at low y is dominated by the formation of the Si^6 network forming unit (NFU).[8,36] In general, the formation of Si^6 in phosphosilicate glasses can be understood by the concept of optical basicity.[37] Optical basicity is a measure of the effective negative charge on oxygen, and it is determined by the UV absorbance wavelength of probe ions such as Tl^+, Pb^{2+} or Bi^{3+}.[37] There is a higher effective negative charge on the oxygen in SiO_2 than P_2O_5, because the optical basicity of SiO_2 is higher than that of P_2O_5.[38] When a small amount of SiO_2 is added to P_2O_5, the positive charge on Si^{4+} must be balanced by oxygen with relatively low effective negative charge. Because more oxygen ions than the usual four are required to balance the positive charge on silicon, then silicon can assume a coordination number of six (Si^6) instead of the usual four (Si^4) in SiO_2.

Yamashita et al.[38] have investigated the correlation between optical basicity and the fraction of Si^6 in alkali phosphosilicate glasses and found that optical basicity alone cannot quantitatively predict the fraction of Si^6.[38] A quantitative relation between the Si^6 concentration and the P^3 concentration was observed by Jiang et al.[27] They found that the Si^6 concentration is approximately equal to one fourth of the expected P^3 concentration in a variety of phosphosilicate glasses. This result can be understood by the microscopic Si^6 formation mechanism suggested by Miyabe et al.[36], who found that a Si^4 NFU bound to four P NFUs can react with two P^2 NFUs to create a Si^6 with six P NFU neighbors. The two P^2 NFUs are converted to P^3 in this reaction, and the modifying cations that were charge balancing P^2 will instead charge balance the $[SiO_{6/2}]^{2-}$ (Si^6) NFU. Thus, Si^6 requires charge balancing by the modifying ions much like four-fold coordinated boron in borate and borophosphate glasses.[29,39] We suggest that Si^6 is formed by the scheme in Fig. 1, which agrees with the findings of both Miyabe et al.[36] and Jiang et al.[27]

Fig. 1 shows a Si^4 NFU having four P^3 NFU neighbors reacting with two P^2. The product is a Si^6 NFU with six P^3 NFU neighbors and charge balanced by two Na^+ ions. The P^3 NFUs stabilize the formation of Si^6, possibly by charge-delocalization, and can therefore only have a single Si^6 NFU neighbor. This explains why the Si^6 concentration is approximately one-sixth of the actual P^3 concentration, or one-fourth of the expected P^3 concentration if Si^6 was not charge compensated.

In summary, the formation of Si^6 is thus limited by the modifying oxide, silica, and P^3 concentrations. The Si^6 concentration in sodium phosphosilicate glasses with the generalized composition $x$$Na_2O$ (1-x)[$y$$SiO_2$ (1-y)P_2O_5] can be quantified as

$$\mathrm{Si}^6(x,y) = \min\left[x, (1-x)\times y, \frac{(1-x)\times(1-y)-x}{2}\right]. \quad (1)$$

Using Eq. (1) and the well-established knowledge about the chemistry of phosphate and silicate glasses, we propose a predictive structural model for phosphosilicate glasses. Si^6 is suggested to be the preferred charge-balancing species in these glasses, and other reactions will only occur when a higher concentration of Na_2O than what can be charge balanced by Si^6 is

present. Further modification occurs in the phosphate network, and the P NFU concentrations are determined by Van Wazer's depolymerization model.[20,40] When the phosphate network is fully depolymerized to P^0, the silicate network begins to become modified. The silicate network is also sequentially depolymerized from Si^4 to Si^0. As shown in Fig. 2, this structural model agrees well with the experimentally determined NFU fractions from the deconvoluted ^{29}Si and ^{31}P MAS NMR spectra of the $0.3Na_2O$ $0.7[ySiO_2$ $(1-y)P_2O_5]$ glasses.

As it will be explained in the following, the structural model is also backed up by the Raman spectra of the $0.3Na_2O$ $0.7[ySiO_2$ $(1-y)P_2O_5]$ glasses shown in Fig. 3. The Raman spectrum of the $y = 0$ composition contains three main peaks, and these are assigned to the symmetrical stretching of PO_2 (P^3) at 1310 cm^{-1}, symmetrical stretching of PO_2^- (P^2) at 1160 cm^{-1}, and symmetrical stretching of P−O−P at 667 cm^{-1}.[41] With increasing silica content several changes occur in the Raman spectra, most importantly a peak appears at 1200 cm^{-1}, which has previously been observed in Si^6-containing phosphosilicate glasses.[38] We assign this peak to the symmetrical PO_2 stretching of a P^3 unit with a Si^6 next-nearest neighbor. This assignment is based on the correlation between peak intensity and Si^6 and P^3 concentrations as determined from the ^{29}Si and ^{31}P MAS NMR data in Fig. 2. In addition, the band originally centered at 1310 cm^{-1} is split into two at about 1340 cm^{-1} and 1290 cm^{-1}. A similar splitting of this band has been observed for modifier-free phosphosilicate glasses, and the splitting was attributed to the PO_2 (P^3) vibrational frequency changing with P^3 having Si^4 next-nearest neighbors.[18] The Raman shift increases with a decreasing electron density in the P=O bond,[18] and as Si is less electronegative than P then the low frequency component is expected to correspond to P^3 with Si NFU neighbors. However, the 1290 cm^{-1} peak intensity increases with y, while the 1340 cm^{-1} component decreases in intensity, and therefore we hesitate to assign these peaks without more thorough investigation.

The P−O−P band at 667 cm^{-1} found in the $y = 0$ composition is shifted to about 700cm^{-1} upon silica addition. In sodium phosphate glasses the frequency of this band increases with the Na_2O content, and a frequency of 700cm^{-1} is reached for the metaphosphate ($x = 0.5$) composition.[41] We suggest that the blue-shift of this peak occurs because of the formation of P^3−O−Si bonds with low Raman intensity, which increases the P^2 contribution in the P−O−P bonding.

For the $y = 0.54$ composition a sharp peak assigned to the symmetrical stretching of PO_2^- (P^2) dominates the spectrum, which agrees with the ^{31}P MAS NMR measurements showing that the phosphorous speciation is dominated almost exclusively by P^2. The sharpness of the PO_2^- (P^2) peak could indicate that this composition is partially crystalline, although it is XRD amorphous. The same is the case for the $y = 0.89$ composition which is also XRD amorphous, but has a dominant sharp peak at 940 cm^{-1} due to asymmetrical stretching of PO_2^{3-} (P^0), and possibly contains Na_3PO_4 crystals.[42] A signature of P^1 units is found at 1000 cm^{-1}, which is the frequency of asymmetrical stretching of PO_2^{2-} (P^1).[42] In this composition it is also possible to see low intensity features of the silicate network. The peak at 1100 cm^{-1} is caused by the symmetrical stretching of SiO_2^- (Si^3), and the shoulder at about 1150 cm^{-1} is due to SiO_2 (Si^4).[42,43] The bands in the range of 430 to 600 cm^{-1} are

attributed to the symmetrical stretching of Si−O−Si with different numbers of bonding oxygen of the Si NFUs.[43] The Raman spectrum of the $y = 1$ composition almost exclusively shows Si^3 units and Si−O−Si bonding.

IV. TOPOLOGY

Topological constraint theory as applied to glasses was introduced in a series of seminal papers by Phillips and Thorpe,[44–52] and extended by Gupta and Mauro[29,28] to give a temperature dependent form that can quantitatively predict important glass properties such as T_g, fragility, and indentation hardness.[6,29,28,53] It has been successfully applied to explain the MNFE in borosilicate,[6] boroaluminosilicate,[54] and borophosphate[39] glasses. The theory links the short-range structures of the network formers[29] and network modifiers[30,31] to a number of constraints, which hinder the free movement of atoms. Generally only two types of constraints are considered, linear bond stretching constraints corresponding to chemical bonds, and angular bond bending constraints corresponding to bond angles. The number of linear and angular constraints around a network forming atom can be calculated as[50]

$$n_{c,linear} = \frac{1}{2}\mathrm{CN}\Big|_{\mathrm{CN}\geq 2}, \tag{2}$$

$$n_{c,angular} = (2\mathrm{CN}-3)\big|_{\mathrm{CN}\geq 2}, \tag{3}$$

where CN is the coordination number of the atom in question. In oxide glasses the network formers are exclusively coordinated by oxygen, and it is convenient to attribute all the linear constraints in a NFU to the oxygen atoms. There are two linear constraints per BO and one linear constraint per NBO when counting in this manner, corresponding to the Si−O or P−O bonds. The angular constraints are counted on O and Si or P, and are calculated by Eq. (3).

The procedure used to account for the constraints related to the modifying cations is debatable and not as straightforward as for the forming cations. The modifying cations form ionic bonds to NBOs and have high CN, but in spite of their high CN, modifying cations break up the network and lower the average number of constraints per atom. We have previously introduced the concept of a modifying ion sub-network to explain the effect of modifying ions on glass properties using temperature-dependent constraint theory.[30] In this approach, we assume that Eq. (3) is invalid for ionic bonding, as this type of bonding is non-directional.[30] Furthermore, because the individual ionic bonds are rather weak, they can easily be thermally activated, and a significant fraction of the linear constraints by Eq. (2) may not be intact.[31] This can be taken into account by utilizing the concept of constraint strength.[31,55]

We derive a topological model of sodium phosphosilicate glass by applying Eq. (2) and (3) to the network forming units (NFUs), while also using the theory of the modifying ion sub-network. In summary, we consider the following constraints:

- α: Si−O and P−O linear constraints. There are two at each BO and one at each NBO. None are counted at the double bonded terminal oxygen (TO) on P^3 as it is not considered to be a part of the network. The topological model is:

- β: O−Si−O and O−P−O angular constraints. There are nine for Si^6, five for Si^4, Si^3, Si^2, Si^1, Si^0, P^2, P^1, and P^0, but only three for P^3. P^3 is considered to be effectively three-fold coordinated because the TO is not part of the network.
- γ: Na^+−NBO linear constraints. The number of constraints is equal to the oxygen coordination number (CN) of Na^+ charge balancing NBO. There are no constraints for Na^+ charge balancing Si^6.
- δ: Si−O−Si, Si−O−P and P−O−P angular constraints. There is one for each BO. No angular constraints are counted for NBO.

The analytical expressions for the number of constraints (n_c) in phosphosilicate glasses with composition $x$$Na_2O$ (1-x)[$y$$SiO_2$ (1-y)P_2O_5] is derived from the speciation of the NFUs as described in Section III and given as

$$n_{c,\alpha}(x,y) = 2\times \mathrm{BO}(x,y) + 1\times \mathrm{NBO}(x,y), \tag{4a}$$

$$\begin{aligned} n_{c,\beta}(x,y) = {} & 9\times \mathrm{Si}^6(x,y) + 3\times \mathrm{P}^3(x,y) + 5\times\left[\mathrm{P}^2(x,y) + \mathrm{P}^1(x,y) + \mathrm{P}^0(x,y)\right] \\ & + 5\times\left[\mathrm{Si}^4(x,y) + \mathrm{Si}^3(x,y) + \mathrm{Si}^2(x,y) + \mathrm{Si}^1(x,y) + \mathrm{Si}^0(x,y)\right] \end{aligned}, \tag{4b}$$

$$n_{c,\gamma}(x,y) = \mathrm{CN}\times \mathrm{Na}^+_{\mathrm{NBO}}(x,y), \tag{4c}$$

$$n_{c,\delta}(x,y) = 1\times \mathrm{BO}(x,y). \tag{4d}$$

For convenience we consider the Si−O and P−O linear constraints equivalent and denote them as the strongest (α) constraint. The second strongest (β) constraint is the O−Si−O and O−P−O angular constraints. The Na^+–NBO linear γ constraint in sodium phosphate glasses is found to be only partially intact at T_g,[31] and we denote this as the third strongest constraints. The BO centered angular δ constraint is generally considered broken at T_g, even for low T_g compositions such as B_2O_3, and we consider this to be the weakest constraint.[6,29,30,39]

V. GLASS TRANSITION TEMPERATURE

The glass transition temperature is determined as the onset temperature of the glass transition by DSC with a heating/cooling rate of 10 K/min. The DSC scans of the 0.3Na_2O 0.7[$y$$SiO_2$ (1-y)P_2O_5] glasses are shown in Fig. 4, where the inset shows how T_g is determined. The T_g of the 0.36Na_2O 0.64P_2O_5 (y = 0) and 0.30Na_2O 0.70SiO_2 (y = 1) end-member compositions are close to those reported in the literature for anhydrous glasses.[30,31,56] The T_g is plotted vs. y in Fig. 5 and exhibits a MNFE as a sharp local maximum around the y = 0.29 composition, and a local minimum apparently around y = 0.54, which is at the edge of the glass-forming region. The trend of the MNFE in T_g closely matches the fraction of Si^6 from the structural model in Fig. 2b, and can be accounted for by temperature dependent constraint theory.[6,29,39,28]

The physical basis relating T_g to the number of network constraints is the Adam-Gibbs theory[57,58], linking viscosity and configurational entropy, and Naumis' result[59] of configurational entropy being largely due to the number floppy modes, i.e., degrees of freedom. With Angell's definition of T_g being the isokom temperature at which the viscosity is equal to 10^{12} Pa s,[60]

an equation can be derived which relates the T_g ratios of two compositions to the inverse ratio of the corresponding degrees of freedom. A detailed derivation and description can be found elsewhere,[29,28] but the result is

$$\frac{T_g(x,y)}{T_{g,ref}} = \frac{f\left[T_{g,ref}, x_{ref}, y_{ref}\right]}{f\left[T_g(x,y), x, y\right]} = \frac{3 - N_c\left[T_{g,ref}, x_{ref}, y_{ref}\right]}{3 - N_c\left[T_g(x,y), x, y\right]}, \tag{5}$$

where f is the number of degrees of freedom and N_c is the number of rigid constraints at T_g per network forming atom. Eq. (5) requires that $0 < f[T_g,x,y] < 3$.

For sodium phosphosilicate glasses with composition $x\mathrm{Na_2O}$ $(1\text{-}x)[y\mathrm{SiO_2}$ $(1\text{-}y)\mathrm{P_2O_5}]$, $N_c[T_g(x,y), x, y]$ is determined by the number of intact constraints in Eq. (4). Thus the average number of constraints per atom at T_g is

$$\begin{aligned} N_c(x,y,T_g) = {} & 2\times\mathrm{BO}(x,y) + 1\times\mathrm{NBO}(x,y) \\ & + 9\times\mathrm{Si}^6(x,y) + 3\times\mathrm{P}^3(x,y) + 5\times\left[\mathrm{P}^2(x,y) + \mathrm{P}^1(x,y) + \mathrm{P}^0(x,y)\right] \\ & + 5\times\left[\mathrm{Si}^4(x,y) + \mathrm{Si}^3(x,y) + \mathrm{Si}^2(x,y) + \mathrm{Si}^1(x,y) + \mathrm{Si}^0(x,y)\right] \\ & + q_\gamma(T_g)\times\mathrm{CN_{Na}}\times\mathrm{Na}^+_{\mathrm{NBO}}(x,y) \end{aligned} . \tag{6}$$

Here $q_\gamma(T_g)$ represents the constraints strength[31,55] for the γ constraint at T_g, and is used to reflect that the γ constraints are not fully intact. We find that $q_{\gamma,\mathrm{Na}}(T_g) = 0.4$ with $\mathrm{CN_{Na}} = 5$,[31] corresponding to 2 γ constraints per Na^+. This number of γ constraints is in good agreement with the results of a recent molecular dynamics simulation of soda lime silicate glasses.[61]

The structural model outlined in Section III is used to evaluate the concentrations of each network forming atom. We can then predict the composition dependence of T_g by inputting Eq. (6) into Eq. (5) and using the pure $\mathrm{P_2O_5}$ glass as reference with $T_{g,ref} = 590$ K[62] and $N_c(T_{g,ref}, x_{ref}, y_{ref}) = 2.4$.[30] The modeled composition dependence of T_g is plotted in Fig. 5 together with experimental values determined by DSC. The model and experiment differ up to ±50 K for the $0.3\mathrm{Na_2O}$ $0.7[y\mathrm{SiO_2}$ $(1\text{-}y)\mathrm{P_2O_5}]$ glass series, but the observed compositional trend is reproduced well by the model without any adjustable fitting parameters. We have also attempted to apply this model to the four glasses in the $0.1\mathrm{CaO}$ $0.2\mathrm{Na_2O}$ $0.7[y\mathrm{SiO_2}$ $(1\text{-}y)\mathrm{P_2O_5}]$ glass series, but a single constraint strength as in Eq. (6) cannot describe the experimental data well.

VI. FRAGILITY

The liquid fragility (m) of the glasses was determined indirectly by DSC measurements from the change in fictive temperature (T_f) with cooling rate (Q).[35]

$$\log\left(\frac{Q}{Q_{ref}}\right) = m - m\times\frac{T_{f,ref}}{T_f}. \tag{7}$$

Q is heating and previous cooling rate through the glass transition region, Q_{ref} is the reference heating and cooling rate taken as 10 K/min, and $T_{f,ref}$ is the fictive temperature corresponding to Q_{ref} and equivalent to our calorimetric definition of T_g.

Paper VI

In order to confirm the liquid fragility results obtained by DSC, the m of the $0.3Na_2O$ $0.7SiO_2$ (y = 0) composition was also determined from direct measurements of the temperature dependence of viscosity. The viscosity was measured with a rotational viscometer at low viscosities (approximately 10^0-10^2 Pa s) and ball penetration viscometer at high viscosities (10^{10}-10^{12} Pa s). The viscosity data was fitted with the Mauro-Yue-Ellison-Gupta-Allan (MYEGA) equation[63] and m was equivalent within the standard deviation to that determined by DSC with Eq. (7).

The m values of the $0.3Na_2O$ $0.7[ySiO_2\,(1\text{-}y)P_2O_5]$ glasses are plotted as a function of y in Fig. 6. In this figure the isobaric heat capacity jump at T_g (ΔC_p) is also plotted, and has a very similar trend as the m data. The y = 0.89 composition lower fragility than the compositional trend suggests. This could be caused by the P^0 units detected by Raman spectroscopy not participating in the glassy network. The fragility peaks at the y = 0.29 composition, which also has the largest T_g and Si^6 content.

The relation between liquid fragility and the network constraints was first suggested by Gupta and Mauro[29,28]. They suggested that the liquid fragility is related to the change in degrees of freedom per atom at T_g, and quantify it by

$$m(x,y) = m_0\left(1+\frac{\partial \ln f(x,y,T)}{\partial \ln T}\right)\Bigg|_{T=T_g(x)}, \tag{8}$$

where m_0 is the liquid fragility of a strong liquid such as silica and taken to be 17.[28] In order to take the temperature derivative of $\ln f(T,x)$, a continuous function is needed. The fraction of rigid constraints is estimated to depend on temperature as

$$q_i(T) = \left[1-\exp\left(-\frac{\Delta F_i^*}{k_B T}\right)\right]^{vt_{obs}}, \tag{9}$$

where ΔF_i^* is the activation energy for breaking constraint i and vt_{obs} is the product of the vibrational attempt frequency and observation time [28]. The activation energy is related to a characteristic constraint onset temperature by

$$\Delta F_i^* = -k_B T_i \ln\left(1-2^{-1/vt_{obs}}\right), \tag{10}$$

where T_i is the constraint onset temperature of constraint i, and can be considered to be the temperature at which the constraint goes from intact to broken.[29]

We model m by applying Eqs. (10)-(12) to the constraints of the topological model in Section IV. In our previous work on the topology of borosilicate glasses, we found that vt_{obs} = 60, and the oxygen bond stretching α constraint onset temperature T_α = 1600 K and $T_{\beta,Si}$ = 1425 K, and we use the same values here[6] The onset temperature of the bond bending β constraints around P ($T_{\beta,P}$) is taken from our analysis of the topology of alkali phosphate glasses where $T_{\beta,P}$ = 850 K.[30] The oxygen centered bond bending δ constraint onset temperature T_δ = 328 K is inferred from the Vogel temperature of B_2O_3.[29] This leaves only the onset temperature of the modifying ion bond stretching γ constraint as a fitting parameter. By fitting to the

experimental m values, the onset temperatures $T_{y,\mathrm{Na}}$ = 550 K is obtained, which agrees well with previous results on sodium phosphate.[30]

The modeled composition dependence of m by Eq. (8)-(10) is plotted in Fig. 6 together with the experimental m and ΔC_p values determined by DSC. The maximum in the experimental liquid and thermodynamic fragilities occurring at y = 0.29 is not replicated by the model, possibly because the α and β constraints related to the Si^6 units are taken to be the same strength as for other Si NFUs. Otherwise the model reproduces the compositional dependence of m and ΔC_p with reasonable accuracy.

VII. INDENTATION HARDNESS

The Vickers indentation hardness (H_V) is plotted as a function of y together with the T_g values in Fig. 5. The compositional trend of H_V and T_g are very similar, and they both exhibit a maximum close to at y = 0.2, which is the composition which has the maximum fraction of Si^6 in our structural model.

A relation between the indentation hardness and the network constraints was first proposed by Smedskjaer et al.[53], and has since been used to describe the compositional dependence of hardness in soda lime borate,[53] borosilicate,[6] boroaluminosilicate,[54] and borophosphate[39] glass compositions.

$$H_V(x,y) = \left(\frac{dH_V}{dN_c}\right) \times \left(N_c(x,y,T = 298\ \mathrm{K}) - N_{c,crit}\right). \tag{11}$$

Here $N_c(x,y,T = 298\ \mathrm{K})$ is the number of constraints per network forming atom at room temperature for composition x,y, dH_V/dN_c is a load-dependent proportionality constant found to be on the order of 10 GPa,[53] and $N_{c,crit}$ is the minimum number of constraints per atom necessary to significantly affect the hardness and was found to be approximately 2.5 (corresponding to rigidity in two dimensions).[53]

The intact constraints at room temperature can be enumerated by using the topological model in Section IV,

$$\begin{aligned} N_c(x,y,T = 298\ \mathrm{K}) = {} & 3\times \mathrm{BO}(x,y) + 1\times \mathrm{NBO}(x,y) \\ & + 9\times \mathrm{Si}^6(x,y) + 3\times \mathrm{P}^3(x,y) + 5\times\left[\mathrm{P}^2(x,y) + \mathrm{P}^1(x,y) + \mathrm{P}^0(x,y)\right] \\ & + 5\times\left[\mathrm{Si}^4(x,y) + \mathrm{Si}^3(x,y) + \mathrm{Si}^2(x,y) + \mathrm{Si}^1(x,y) + \mathrm{Si}^0(x,y)\right] \\ & + q_\gamma(T = 298\ \mathrm{K}) \times \mathrm{CN}_{\mathrm{Na}} \times \mathrm{Na}^+_{\mathrm{NBO}}(x,y) \end{aligned}. \tag{12}$$

The difference between Eqs. (12) and (6) is that the δ BO angular constraint is considered to be intact, and an increased rigidity of the γ constraints by $q_\gamma(T_g) < q_\gamma(T = 298\ \mathrm{K})$. We find that $q_{\gamma,\mathrm{Na}}(T = 298\ \mathrm{K}) = 0.6$ yielding 3 γ constraints per Na^+ at room temperature.

The modeled composition dependence of H_V by Eq. (7) with (dH_V/dN_c) = 7.5 GPa and $N_{c,crit}$ = 2.5 is plotted in Fig. 5 together with experimental values determined by Vickers microindentation. The model and experiment differ up to ±1 GPa for the $0.3Na_2O\ 0.7[y SiO_2\ (1\text{-}y)P_2O_5]$ glass series, but again the compositional trend is reproduced.

VIII. CONCLUSION

Paper VI

By combining structural and topological modeling with experimental studies, we have provided new insights into the structure-topology-property relations of sodium phosphosilicate glasses. The topological modeling approach is based on temperature-dependent constraint theory, which relies on accurate knowledge of the composition dependence of NFU speciation. We have therefore proposed a structural model of the NFU concentrations in these glasses, which is based on the formation mechanism of Si^6 suggested by Miyabe et al.[36]. An important aspect of the Si^6 formation mechanism is that the modifying sodium ions are needed to charge stabilize Si^6 and cannot modify the phosphate network simultaneously. Building on this structural model, we have derived a topological analysis of the glass system by associating temperature-dependent constraints with the various NFUs. This model successfully captures the MNFE for glass transition temperature, indentation hardness, and fragility of the investigated system.

FIGURES AND TABLES

Table I. The measured compositions and properties of the $0.3Na_2O$ $0.7[ySiO_2$ $(1-y)P_2O_5]$ glasses. The compositions of the two glasses with $y = 0.54$ and $y = 0.89$ were not measured, but these were prepared from mixing and re-melting appropriate amounts of the $y = 0.43$ and $y = 1$ compositions. Up to 0.4 mole % SnO_2 for $y = 1$ was additionally batched to improve fining. The experimental details of the measurements are given in the text.

	Analytical composition (mole %)			Properties			
y	Na_2O	SiO_2	P_2O_5	T_g (K)	H_V (GPa)	m (-)	ΔC_p (J × mol^{-1} × K^{-1})
0	36.4	0	63.6	549	2.0 ± 0.1	37 ± 2	7.9
0.14	31.5	11.3	57.2	630	3.0 ± 0.1	41 ± 2	9.2
0.29	29.3	20.5	50.2	650	3.0 ± 0.1	47 ± 3	10.9
0.43	29.6	29.2	41.2	615	2.7 ± 0.1	38 ± 2	8.8
0.54	-	-	-	581	2.1 ± 0.1	41 ± 1	7.8
0.89	-	-	-	712	3.9 ± 0.1	25 ± 1	4.1
1.00	29.8	70.2	0	739	4.3 ± 0.1	37 ± 1	5.8

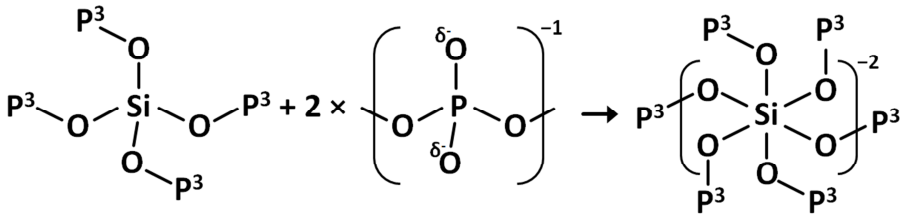

FIG. 1. The mechanism of Si^6 formation in phosphosilicate glasses is proposed to be: A Si^4 NFU with four P^3 NFU neighbors reacts with two P^2 NFU to form a Si^6 NFU with six P^3 NFU neighbors. In the process the two P^2 are converted to P^3, and the negative charge and charge stabilizing modifying ions are transferred to the Si^6 NFU.

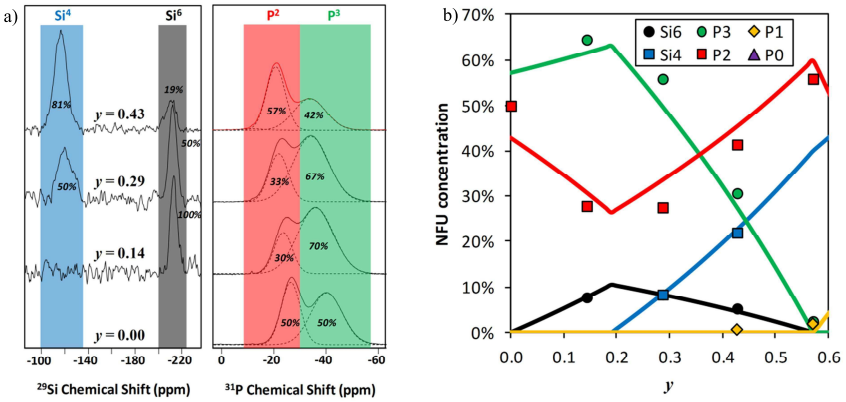

FIG. 2. a) ^{29}Si and ^{31}P MAS NMR spectra of the $0.3Na_2O$ $0.7[ySiO_2$ $(1-y)P_2O_5]$ glasses with $y \leq 0.43$. The chemical shift ranges belonging to each NFU are highlighted, and the area ratios obtained by deconvoluting the spectra are indicated. b) The network forming unit (NFU) fractions derived from the ^{29}Si and ^{31}P MAS-NMR spectra and the compositions of the $0.3Na_2O$ $0.7[ySiO_2$ $(1-y)P_2O_5]$ glasses. The solid lines represent the structural model from Section III.

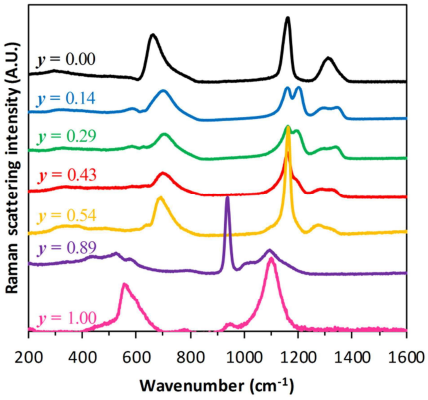

FIG. 3. Raman spectra of $0.3Na_2O$ $0.7[ySiO_2$ $(1-y)P_2O_5]$ glasses normalized by total scattering intensity. The Raman cross-section of P NFUs is much larger than for Si NFUs, and features of Si NFUs cannot be discerned in compositions with $0 \leq y \leq 0.54$. The band assignment is discussed in the text.

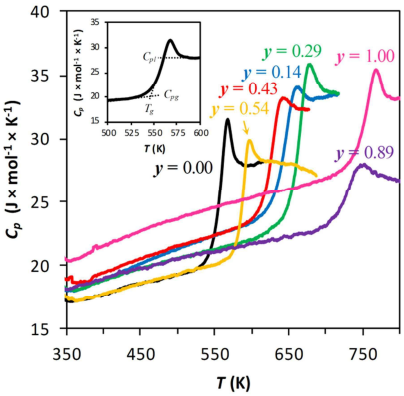

FIG. 4. Differential scanning calorimetry scans for the $0.3Na_2O$ $0.7[ySiO_2$ $(1-y)P_2O_5]$ glass compositions. C_p is given per mole of atoms in the glass. The inset shows how T_g, C_{pg} and C_{pl} are determined.

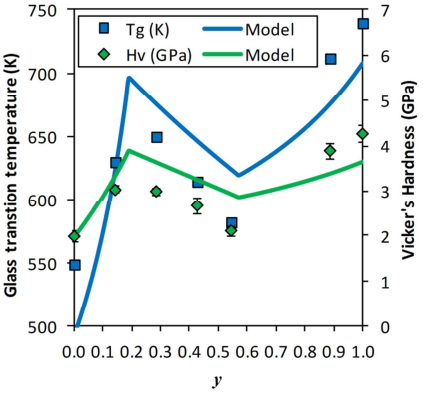

FIG. 5. Compositional dependence of the glass transition temperature and indentation hardness for a) the $0.3Na_2O$ $0.7[ySiO_2\ (1\text{-}y)P_2O_5]$ glass compositions. The squares represent experimental T_g determined by DSC, and the diamonds experimental H_V by Vickers microindentation. The solid lines represent the modeled properties by Eq. (5) and Eq. (11).

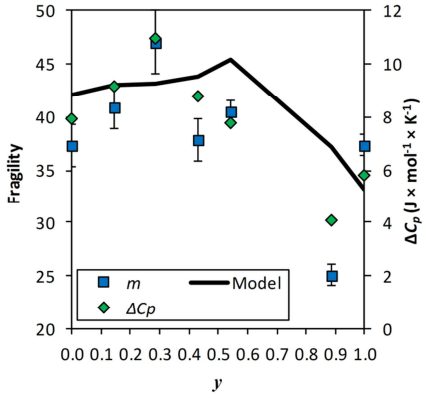

FIG. 6. Compositional dependence of the liquid fragility (m) and thermodynamic fragility (ΔC_p) for the $0.3Na_2O$ $0.7[ySiO_2\ (1\text{-}y)P_2O_5]$ glass compositions. The squares represent experimental m determined by DSC, and the diamonds experimental ΔC_p (equal to $C_{pl} - C_{pg}$). The solid lines represent the modeled properties by Eqs. (8)-(10).

REFERENCES

[1] D. Larink, H. Eckert, M. Reichert, and S.W. Martin, J. Phys. Chem. C **116**, 26162 (2012).

[2] M.T. Rinke and H. Eckert, Phys. Chem. Chem. Phys. **13**, 6552 (2011).

[3] R.B. Christensen, The Mixed Glass Former Effect in 0.35Na2O + 0.65[xB2O3 + (1-x)P2O5] Glasses, Iowa State University, 2012.

[4] C.M. Bischoff, The Mixed Glass Former Effect in 0.5Na2S + 0.5[xGeS2 + (1-x)PS5/2] Glasses, Iowa State University, 2013.

[5] Q. Zheng, M. Potuzak, J.C. Mauro, M.M. Smedskjaer, R.E. Youngman, and Y.-Z. Yue, J. Non. Cryst. Solids **358**, 993 (2012).

[6] M.M. Smedskjaer, J.C. Mauro, R.E. Youngman, C.L. Hogue, M. Potuzak, and Y.-Z. Yue, J. Phys. Chem. B **115**, 12930 (2011).

[7] A.K. Varshneya, *Fundamentals of Inorganic Glasses* (Gulf Professional Publishing, 1994), pp. 83–84.

[8] R. Dupree, D. Holland, M.G. Mortuza, J.A. Collins, and M.W.G. Lockyer, J. Non. Cryst. Solids **106**, 403 (1988).

[9] J.R. Jones, Acta Biomater. **9**, 4457 (2013).

[10] A. Tilocca and A.N. Cormack, J. Phys. Chem. B **111**, 14256 (2007).

[11] M.D.O. Donnell, S.J.J. Watts, R.V. V Law, R.G.G. Hill, and M.D. O'Donnell, J. Non. Cryst. Solids **354**, 3554 (2008).

[12] F. Fayon, C. Duée, T. Poumeyrol, M. Allix, and D. Massiot, J. Phys. Chem. C **117**, 2283 (2013).

[13] M. Sitarz, K. Bulat, a. Wajda, and M. Szumera, J. Therm. Anal. Calorim. **113**, 1363 (2013).

[14] S. Prabakar, K.J. Rao, and C.N.R. Rao, Mater. Res. Bull. **26**, 285 (1991).

[15] R.J. Kirkpatrick and R.K. Brow, Solid State Nucl. Magn. Reson. **5**, 9 (1995).

[16] M. Nogami, K. Miyamura, Y. Kawasaki, and Y. Abe, J. Non. Cryst. Solids **211**, 208 (1997).

[17] H. Yamashita, H. Yoshino, K. Nagata, H. Inoue, T. Nakajin, and T. Maekawa, J. Non. Cryst. Solids **270**, 48 (2000).

[18] V.G. Plotnichenko, V.O. Sokolov, V.V. Koltashev, and E.M. Dianov, J. Non. Cryst. Solids **306**, 209 (2002).

[19] J. Ide, K. Ozutsumi, H. Kageyama, K. Handa, and N. Umesaki, J. Non. Cryst. Solids **353**, 1966 (2007).

[20] R.K. Brow, J. Non. Cryst. Solids **263-264**, 1 (2000).

[21] M.G. Mortuza, J. a. Chudek, G. Hunter, and M.R. Ahsan, Chem. Commun. 2055 (2000).

[22] T.L. Weeding, B.H.W.S. de Jong, W.S. Veeman, and B.G. Aitken, Nature **318**, 352 (1985).

[23] R.E. Youngman, C.L. Hogue, and B.G. Aitken, MRS Proc. **984**, 0984 (2006).

[24] J.A. Duffy and D.E. Macphee, J. Phys. Chem. B **111**, 8740 (2007).

[25] W.H. Zachariasen, J. Am. Chem. Soc. **54**, 3841 (1932).

[26] H. Zeng, Q. Jiang, Z. Liu, X. Li, J. Ren, G. Chen, F. Liu, and S. Peng, J. Phys. Chem. B **118**, 5177 (2014).

[27] Q. Jiang, H. Zeng, X. Li, J. Ren, G. Chen, and F. Liu, J. Chem. Phys. **141**, 124506 (2014).

[28] P.K. Gupta and J.C. Mauro, J. Chem. Phys. **130**, 094503 (2009).

[29] J.C. Mauro, P.K. Gupta, and R.J. Loucks, J. Chem. Phys. **130**, 234503 (2009).

[30] C. Hermansen, J.C. Mauro, and Y.-Z. Yue, J. Chem. Phys. **140**, 154501 (2014).

[31] C. Hermansen, B. Rodrigues, L. Wondraczek, and Y.-Z. Yue, J. Chem. Phys. **Under revi**, (2014).

[32] Y.-Z. Yue, J. Non. Cryst. Solids **355**, 737 (2009).

[33] L.-M. Wang, V. Velikov, and C. a. Angell, J. Chem. Phys. **117**, 10184 (2002).

[34] L.M. Martinez and C.A. Angell, Nature **410**, 663 (2001).

[35] C.T. Moynihan, A.J. Easteal, M.A. DeBolt, and J. Tucker, J. Am. Ceram. Soc. **59**, 12 (1976).

[36] D. Miyabe, M. Takahashi, Y. Tokuda, T. Yoko, and T. Uchino, Phys. Rev. B **71**, 172202 (2005).

[37] J. a. Duffy, J. Chem. Educ. **73**, 1138 (1996).

[38] H. Yamashita, H. Yoshino, K. Nagata, I. Yamaguchi, M. Ookawa, and T. Maekawa, J. Ceram. Soc. Japan **106**, 539 (1998).

[39] C. Hermansen, R.E. Youngman, J. Wang, and Y.-Z. Yue, J. Chem. Phys. **Submitted**, (2014).

[40] J.R. Van Wazer, *Phosphorous and Its Compounds* (Interscience, New York, 1958).

[41] J.J. Hudgens, R.K. Brow, D.R. Tallant, and S.W. Martin, J. Non. Cryst. Solids **223**, 21 (1998).

[42] B. Mysen, Am. Mineral. **81**, 1531 (1996).

[43] P. McMillan, Am. Mineral. **69**, 622 (1984).

[44] J.C. Phillips, J. Non. Cryst. Solids **34**, 153 (1979).

[45] J.C. Phillips, J. Non. Cryst. Solids **43**, 37 (1981).

[46] J.C. Phillips, J. Non. Cryst. Solids **44**, 17 (1981).

[47] M.F. Thorpe, J. Non. Cryst. Solids **57**, 355 (1983).

[48] J.C. Phillips and M.F. Thorpe, Solid State Commun. **53**, 699 (1985).

[49] H. He and M.F. Thorpe, Phys. Rev. Lett. **54**, 2107 (1985).

[50] M.F. Thorpe, J. Non. Cryst. Solids **76**, 109 (1985).

[51] M.F. Thorpe and Y. Cai, Phys. Rev. B **40**, 10535 (1989).

[52] M.F. Thorpe, M. V Chubynsky, D.J. Jacobs, and J.C. Phillips, Glas. Phys. Chem. **27**, 160 (2001).

Paper VI

[53] M.M. Smedskjaer, J.C. Mauro, and Y.-Z. Yue, Phys. Rev. Lett. **105**, 115503 (2010).

[54] M.M. Smedskjaer, Front. Mater. **1**, 1 (2014).

[55] B.P. Rodrigues and L. Wondraczek, J. Chem. Phys. **140**, 214501 (2014).

[56] O. V Mazurin, M. V Streltsina, and T.P. Shvaiko-Shvaikovskaya, *Handbook of Glass Data* (Elsevier, Amsterdam, 1987).

[57] G. Adam and J.H. Gibbs, J. Chem. Phys. **43**, 139 (1965).

[58] Y. Bottinga and P. Richet, Chem. Geol. **128**, 129 (1996).

[59] G.G. Naumis, Phys. Rev. E **71**, 026114 (2005).

[60] C.A. Angell, Science (80-.). **267**, 1924 (1995).

[61] O. Laurent, B. Mantisi, and M. Micoulaut, J. Phys. Chem. B **118**, 12750 (2014).

[62] S.W. Martin and C.A. Angell, J. Phys. Chem. **90**, 6736 (1986).

[63] J.C. Mauro, Y.-Z. Yue, A.J. Ellison, P.K. Gupta, and D.C. Allan, Proc. Natl. Acad. Sci. U. S. A. **106**, 19780 (2009).

SUMMARY

The composition of glass can be varied continuously within their glass-forming regions. This compositional flexibility makes it possible to tailor the properties of a glass for a variety of specific uses. In the industry such tailoring is done on a trial-and-error basis with only the intuition of a glass scientist to suggest a way forward.

To a first approximation the intuition of the glass scientist boils down to two ideas: First, a higher degree of polymerization causes an increase in physical properties such as the glass transition temperature and hardness. Second, a higher oxygen bond strength also increases such properties. Yet, these rules are not strictly followed even for the simplest binary oxide glasses, such as alkali silicates, borates and phosphates.

In this thesis it is argued that the missing link between composition and properties is the glass structure. Structural models are proposed based on topological selection rules and experimentally verified. The relation between structure and properties is evaluated using topological constraint theory, which in its essence is a theory that quantifies the two intuitions of the glass scientist. The end result is a quantitative model capable of ab initio prediction of the oxide glass properties from composition.

ISSN: 2246-1248
ISBN: 978-87-7112-205-3

AALBORG UNIVERSITY PRESS